

NCAR-TN-52

The Microphysics and Dynamics of Convective Clouds -- A Colloquium

A Colloquium sponsored by the
NCAR Advanced Study Program
6 July to 18 August 1970

November 1970

NATIONAL CENTER FOR ATMOSPHERIC RESEARCH
Boulder, Colorado

Preface

For the past five years, the NCAR Advanced Study Program has organized, sponsored and cosponsored summer colloquia on a variety of special topics in the atmospheric sciences. These topics, chosen either for their importance or relevance to general scientific advance or for the interest engendered by new theoretical or technological developments, have included:

- Thermal convection in the earth's and planetary atmospheres.
- Physics of the solar corona.
- Generation, structure and propagation of acoustic-gravity waves.
- Solar magnetohydrodynamics.
- Microphysics and dynamics of convective clouds.

The subject of next summer's colloquium will be Planetary Magnetospheres and Aurorae.

The topic of this past summer's colloquium was specially selected for several reasons. First, it has long been recognized and deplored that the microphysical processes of vapor diffusion, heat conduction, droplet coalescence and electrification have been studied as if they were not strongly interactive with the dynamics and gross thermodynamics of convective clouds, and vice versa. Increasing attention and effort is being given to the integration of both microphysical and dynamical processes in simple mathematical models of the total precipitation process, but it is still important to understand the limitations, good points and defects of each ideal subprocess that comprises a part of the model. In this regard, we may safely say that the courtship between the two major branches of cloud physics is warm, but the marriage has not yet been consummated.

The second main basis for the choice of topic is simply that there has been mounting interest in the possibility of increasing or decreasing precipitation of various types by "tickling" convective clouds--i.e., by the introduction of artificial condensation or freezing nuclei. Without entering into the controversy about whether this is effective or not, the colloquium considered that such intervention into the natural process could not be dignified by the name of "control" until the natural process is understood--in the sense that it is more or less predictable. The complexity of the total precipitation process is much greater than that of simple chemical combustion (a frequently drawn analogy), in which enough heat supplied to a high enough concentration of combustibles will sustain an absolutely predictable reaction. But the analogy is not valid.

The pattern of this colloquium was much the same as in previous colloquia. Twelve strongly motivated graduate students were selected for summer appointments from a much larger group of applicants. Several additional graduate students came on their own initiative and with support from their own institutions. A number of postdoctoral participants took part at their own expense or with support from their own institutions. With participants from NCAR, ESSA and other agencies, the regular attendance was about 35 people.

The principal lectures were given by Professor Peter V. Hobbs of the University of Washington and Professor Richard S. Scorer of the Imperial College of Science and Technology. The notes that follow were prepared by the nominal "students" participating in the colloquium, and later revised and emended by the lecturers. It would have been valuable to have recorded or summarized some twenty special seminars that were presented in conjunction with the colloquium. It was evident at the very beginning, however, that the pace of question, answer, comment and repartee was too rapid and too disjointed to record in the proceedings.

We can only hope that these informal lecture notes will give the reader some feeling for the immensity and importance of the problem of cloud physics, and the direction in which its solution is to be sought. The students, despite being disabused of many widely accepted notions, are not discouraged. The effect, oddly enough, has not been merely to circumscribe more closely their limits of knowledge, but to challenge them to break out of the circumference.

Philip D. Thompson
Director
Advanced Study Program

CONTENTS

Prefaceiii
Participants.	vi
Special Seminars.	vii
Notes taken by Participants from Lectures by Professor Peter V. Hobbs:	
#1 <i>Condensation of Water Vapor in the Atmosphere; Cloud Condensation Nuclei</i>	1
#2 <i>Growth of Droplets and Precipitation in Warm Clouds.</i>	12
#3 <i>Nucleation of Ice and Properties of Ice Nuclei</i>	30
#4 <i>Properties and Distribution of Ice Nuclei in the Atmosphere.</i>	47
#5 <i>Growth of Ice Crystals</i>	62
#6 <i>Cloud Electrification.</i>	79
#7 <i>Artificial Modification of Clouds, Precipitation, Hailstorms, and Thunderstorms</i>	94
#8 <i>Numerical Modeling of Cumulus Clouds</i>	104
#9 <i>Unplanned Weather and Climate Modification</i>	113
Notes taken by Participants from Lectures by Professor Richard S. Scorer:	
#1 <i>Mechanics of Vorticity and the Generation of Streamwise Rotation.</i>	123
#2 <i>Comparison of Dynamic Instability in Rectilinear and Curved Flow with Static Instability.</i>	130
#3 <i>Billow Instability in the Atmosphere (Film of laboratory experiments)</i>	141
#4 <i>The Basic Properties of Thermals (Film of laboratory experiments)</i>	158
#5 <i>Plumes, Jets, and the Entrainment Coefficient.</i>	167
#6 <i>Vertical Eddy Transfer by Thermals, the Ratio K_M/K_H</i>	175
#7 <i>Horizontal Momentum Transport by Thermals; the Possibility of Cyclone Generation</i>	189
#8 <i>Distrails and Contrails in a Stable Atmosphere</i>	199
#9 <i>Density Currents, Mamma, Cells, and Streets. (Film of density currents)</i>	206

PARTICIPANTS

Predoctoral:

Miss Yun-Mei Chang
University of California
Los Angeles, California

Mr. William H. Mach
University of Washington
Seattle, Washington

Mr. James R. Miller
University of Maryland
College Park, Maryland

Mr. Robert F. D. Perret
Massachusetts Institute of
Technology
Cambridge, Massachusetts

Mr. John Presley
University of Nevada
Reno, Nevada

Mr. M. V. Ranga Rao
Florida State University
Tallahassee, Florida

Mr. John R. Travis
Purdue University
Lafayette, Indiana

Mr. Robert B. Wilhelmson
University of Illinois
Urbana, Illinois

UCAR Fellows:

Mr. Noah Chodes
University of Colorado
Boulder, Colorado

Mr. Robert M. DiCamillo
Drexel Institute of Technology
Philadelphia, Pennsylvania

Miss Janet E. Guin
University of Alabama
Huntsville, Alabama

Mr. Steven M. Platte
Iowa State University
Ames, Iowa

Postdoctoral:

Dr. Peter M. Caplan
State University of New York
Oswego, New York

Dr. Shu-Kwan Chan
Massachusetts Institute of
Technology
Cambridge, Massachusetts

Dr. Richard E. Forbes
Mississippi State University
State College, Mississippi

Dr. Ralph M. McGehee
New Mexico Institute of Mining
and Technology
Socorro, New Mexico

Dr. Michael J. Moore
Johns Hopkins University
Baltimore, Maryland

Dr. Michael S. Sher
University of Illinois
Urbana, Illinois

Dr. W.G.N. Slinn
Battelle Memorial Institute
Richland, Washington

SPECIAL SEMINARS

7 July	<i>Microstructure of Cumuli</i>	Professor Patrick Squires Desert Research Institute University of Nevada Reno, Nevada
9 July	<i>Models of Convective Clouds</i>	Professor Jack Warner Desert Research Institute University of Nevada Reno, Nevada
14 July	<i>The Aerodynamics and Mechanics of Droplets</i>	Professor Hans R. Pruppacher University of California Los Angeles, California
15 July	<i>Electricity and Rain</i>	Dr. Doyne J. Sartor National Center for Atmospheric Research Boulder, Colorado
16 July	(Continued from 14 July lecture)	Professor Hans R. Pruppacher
21 July	<i>Precipitation Particle Size Distribution by Doppler Radar</i>	Professor R. C. Srivastava University of Chicago Chicago, Illinois
23 July	<i>Hail Growth in One-Dimensional Models of Clouds</i>	Professor Roland List University of Toronto Toronto, Ontario, Canada
27 July	<i>Time Evolution of Droplet Size Spectra</i>	Dr. Ronald L. Drake National Center for Atmospheric Research Boulder, Colorado
28 July	<i>The Influence of Clouds on the Environment</i>	Professor Alistair B. Fraser University of Washington Seattle, Washington
29 July	(Continued from 27 July lecture)	Dr. Ronald L. Drake
30 July	<i>Meteorological Optical Phenomena</i>	Professor Alistair B. Fraser
31 July	<i>Numerical Simulation of Cloud Dynamics--in Two Dimensions or Three</i>	Dr. James W. Deardorff National Center for Atmospheric Research Boulder, Colorado
4 August	<i>The Life History of a Rain Shower</i>	Professor Harold D. Orville South Dakota School of Mines and Technology Rapid City, South Dakota

- | | | |
|-----------|--|--|
| 5 August | <i>Numerical Simulation of Three-Dimensional Thermals</i> | Dr. Douglas G. Fox
National Center for Atmospheric Research
Boulder, Colorado |
| 6 August | <i>The Ice Crystal Economy of Clouds and its Relation to Dynamical Processes</i> | Professor John Hallett
Desert Research Institute
University of Nevada
Reno, Nevada |
| 7 August | <i>Hail Growth in a Cumulus Model: its Size Distribution and Mie Scattering</i> | Dr. Edwin F. Danielson
National Center for Atmospheric Research
Boulder, Colorado |
| 11 August | <i>Dynamics and Flow Patterns of Particle Ensembles</i> | Professor Roland List |
| 12 August | <i>Characteristics of Hailstorms According to Hailstones</i> | Dr. Charles A. Knight
National Center for Atmospheric Research
Boulder, Colorado |
| 13 August | <i>Some Aspects of the Interaction Between the Microphysics and Dynamics of Clouds</i> | Professor Morris Neiburger
University of California
Los Angeles, California |
| 18 August | <i>Observation of Convective Storm Circulation by Dual Doppler Radar Techniques</i> | Dr. Roger M. Lhermitte
Environmental Science Services Administration
Boulder, Colorado |

I. CONDENSATION OF WATER VAPOR IN THE ATMOSPHERE; CLOUD CONDENSATION NUCLEI

A. Introduction

Clouds form because of the adiabatic expansion of moist air. During such an expansion, the relative humidity in the air increases to the point of supersaturation (i.e., larger than 100%). At a certain supersaturation, the water vapor condenses to form cloud droplets, the nucleation of which will be briefly reviewed here. At the outset, we shall distinguish two different types of nucleation and discuss them separately.

B. Homogeneous nucleation

This type of nucleation (also known as spontaneous nucleation) occurs in a system of pure water vapor. By raising the relative humidity of such a system (by either cooling it or isothermally compressing it) it can be brought to a state of supersaturation. To attain the state of lowest energy, the vapor should then condense to form small droplets. However, a small droplet is unstable to thermal agitations and will evaporate if the equilibrium vapor pressure over its surface exceeds that in the environment. In other words, condensation does not necessarily occur when the relative humidity exceeds 100%. As the degree of supersaturation increases, small droplets become less unstable. At a certain critical supersaturation, condensation of vapor occurs to form a dense fog. This is homogeneous nucleation.

In experiments with air carefully cleaned of particulates, C.T.R. Wilson found that spontaneous condensation in the form of a dense fog occurred at a supersaturation of about 800%. At this critical supersaturation small embryo droplets can form, by chance aggregation of water molecules, which are large enough to survive and to grow by condensation from the vapor phase.

C. Heterogeneous nucleation

Wilson also observed the formation of a less dense fog at super-

saturations of about 400%. The concentration of droplets in this fog did not increase with increasing supersaturation nor did it decrease by successive expansions. The nuclei responsible for the droplets could not be removed by filtering the air. However, a much denser fog formed when the air was radiated with X-rays. Wilson concluded that this fog was formed by heterogeneous nucleation on ions.

In air containing particulates, condensation occurs at much lower supersaturations than for homogeneous nucleation or heterogeneous nucleation on ions. This is due to the fact that the particulates act as nuclei for the condensation. In the atmosphere the air is never sufficiently clean for either homogeneous nucleation or for nucleation on ions to occur. Instead, condensation occurs at supersaturations of less than 1% on a certain fraction of the solid particles in the air. These are called cloud condensation nuclei (CCN). The efficiency of a particle as a CCN depends on three factors: (a) the size of the particle; (b) the contact angle of water on its surface; and (c) the solubility of the particle in water. These three factors are discussed in turn below.

The larger the size of the particle, the more effective it is as a CCN. This is a direct result of the decrease in the equilibrium vapor pressure over a curved surface with decrease in curvature (Kelvin's equation).

In order for a particle to be an effective CCN, the contact angle θ of water on the particle must be small. In the limiting case of $\theta = 180^\circ$, the drop merely sits on the surface of the particle and the latter is not effective as a CCN.

The effectiveness of a particle as a CCN increases as its solubility in water increases. This is because the equilibrium vapor pressure above

a solution droplet is less than that above a pure water droplet of the same size. This solubility effect works in the opposite direction to the curvature effect producing the results shown in Fig. 1 (see end of Lecture #1). When the radius of a droplet is small, the solubility effect is dominant. However, as the size of the droplet increases the effect of curvature dominates.

Most particles in the atmosphere appear to consist of an insoluble and a soluble component. For relative humidities less than 70%, the radius of the particle is constant (insoluble part). As the relative humidity increases above 70%, the mixed nucleus changes in size with humidity in much the same way as a wholly soluble nucleus of equivalent size.

D. Sources of condensation nuclei

There are two main processes by which CCN are produced in the atmosphere: dispersion and coagulation.

Dispersion involves the break-up of large particles to form smaller ones which remain suspended in the air. This process generally produces particles greater than 0.1μ in diameter.

Under the title coagulation, we include chemical reactions of gases in the atmosphere to produce particulates and the coagulation of smaller particles by Brownian motion. Particles produced by coagulation are generally less than about 0.1μ in diameter.

It has been thought for some time that salt particles from the ocean may be an important source of CCN. However, measurements made by Radke and Hobbs (1969a) indicate that even in maritime air masses the concentrations of sodium particles are only a small fraction of the concentrations of CCN in the air.

E. Measurement of CCN

The concentration of CCN in the air active at a given supersatur-

ation may be determined by counting the number of water droplets which form in a given volume of air raised to a known supersaturation. The Aitken expansion chamber is not a suitable device for this type of measurement since the supersaturations obtained in expansion chambers are generally several hundred per cent, rather than the fractions of one per cent at which we need to measure the concentrations of CCN. A much better device for measuring CCN is the thermal diffusion chamber in which a small vertical temperature difference is mounted between two horizontal plates which are wetted with water. The water vapor is distributed between the plates by mixing and diffusion. The water vapor pressure p at a given point in the chamber is linearly related to the temperature. However, the saturated vapor pressure p' is not a linear function of the temperature. The result is that at points between the two plates the chamber is supersaturated with respect to water. The maximum supersaturation in the thermal diffusion chamber is determined by the temperature difference between the plates and can be calculated.

An automatic CCN counter has recently been developed by Radke and Hobbs (1969b). In this counter the concentration of water droplets which form in a thermal diffusion chamber is determined by a light scattering technique and the number is recorded digitally (Fig. 2, see end of Lecture #1).

F. Some results of CCN measurements

The results of measurements of CCN in different air masses are shown in Fig. 3 (see end of Lecture #1). It can be seen that the concentrations of CCN in continental air masses are generally greater than those in maritime air masses.

Recent measurements at the University of Washington by Hobbs et al. (1968) and Radke (1970) have shown that when clouds evaporate, they can release

high concentrations of CCN. Some results obtained in wave clouds which show this effect are presented in Figs. 4 and 5 (see end of Lecture #1). One possible explanation for this effect is that droplets in clouds collect other particles by various diffusion processes and direct aerodynamic capture, etc. When the droplets evaporate, these captured particles will be released as bigger particles and therefore more efficient CCN. Another possible explanation is that gaseous reactions in cloud droplets may produce compounds (e.g. sulfates) which again will result in efficient CCN when the droplets evaporate.

Notes taken by:

S.-K. Chan

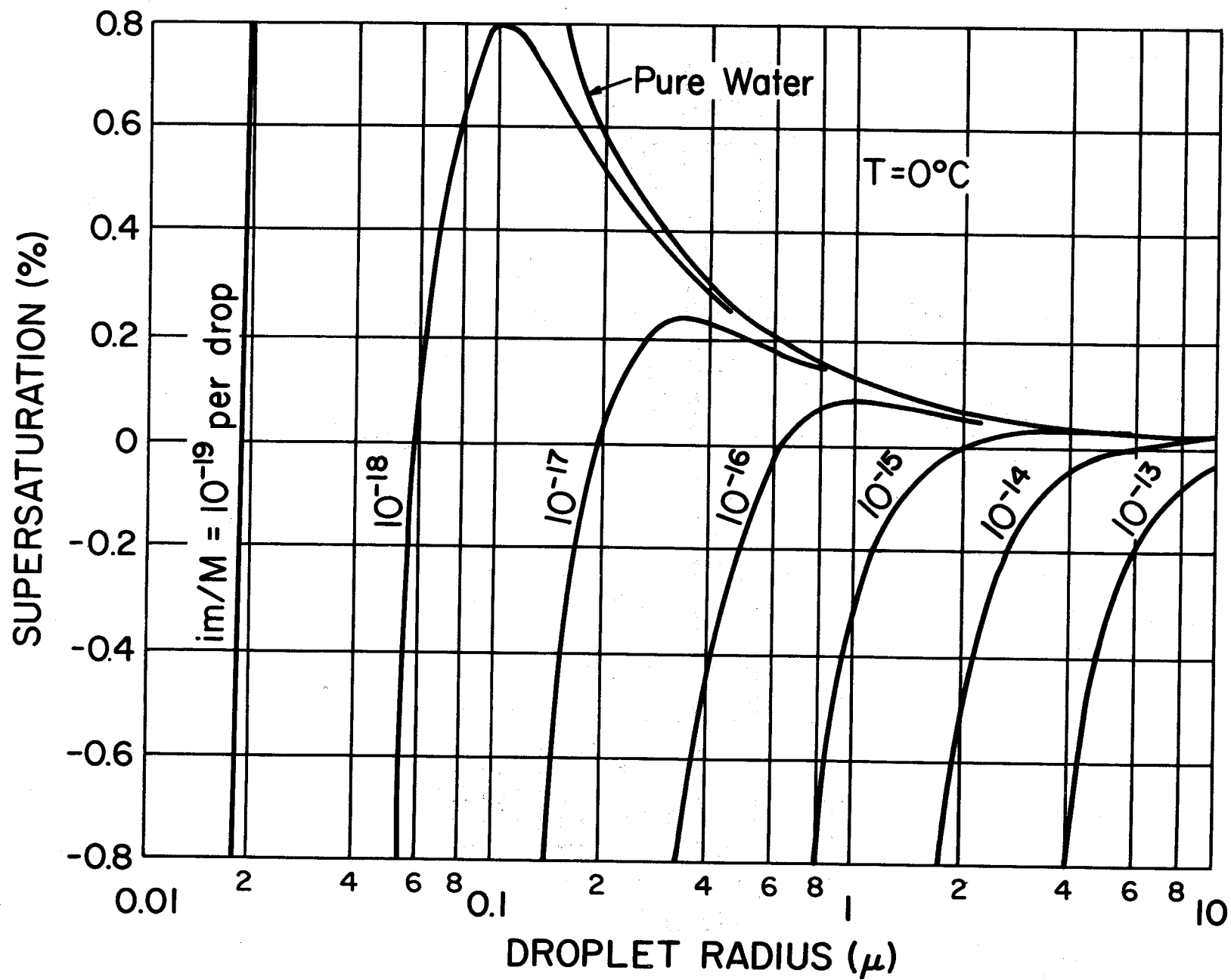
J. R. Travis

REFERENCES

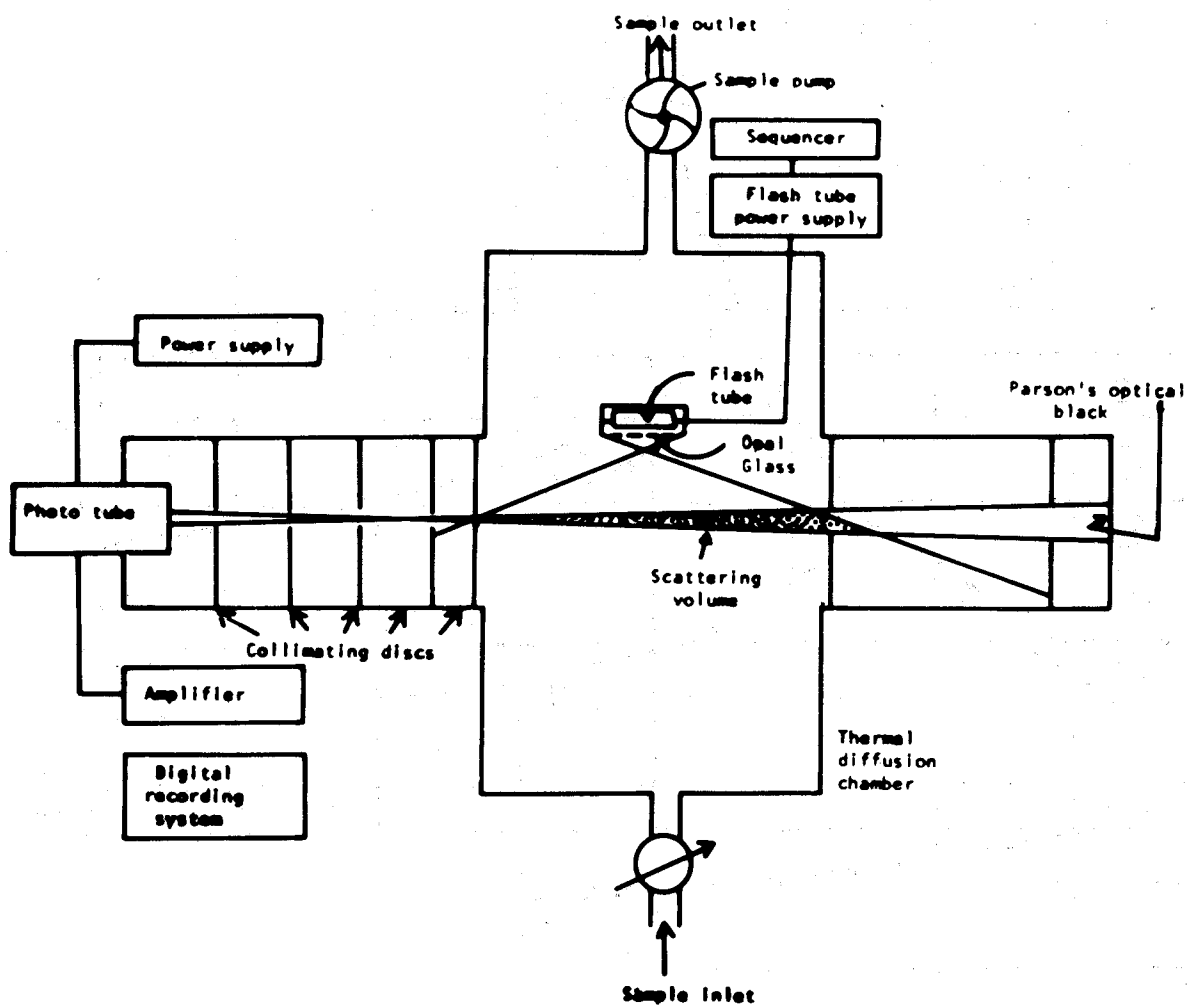
- Hobbs, P. V., Scott, W. D., Burrows, P. A., Radke, L. F., and Locatelli, J. D.,
Contributions from the Cloud Physics Lab., University of Washington,
September 1968.
- Radke, L. F. and Hobbs, P. V., J. Atmos. Sci., 26, 281, 1969a.
- _____ and _____, J. App. Met., 8, 105, 1969b.
- Radke, L. F., Proc. Cloud Physics Conf., Fort Collins, Colorado, 1970.

Figure Captions

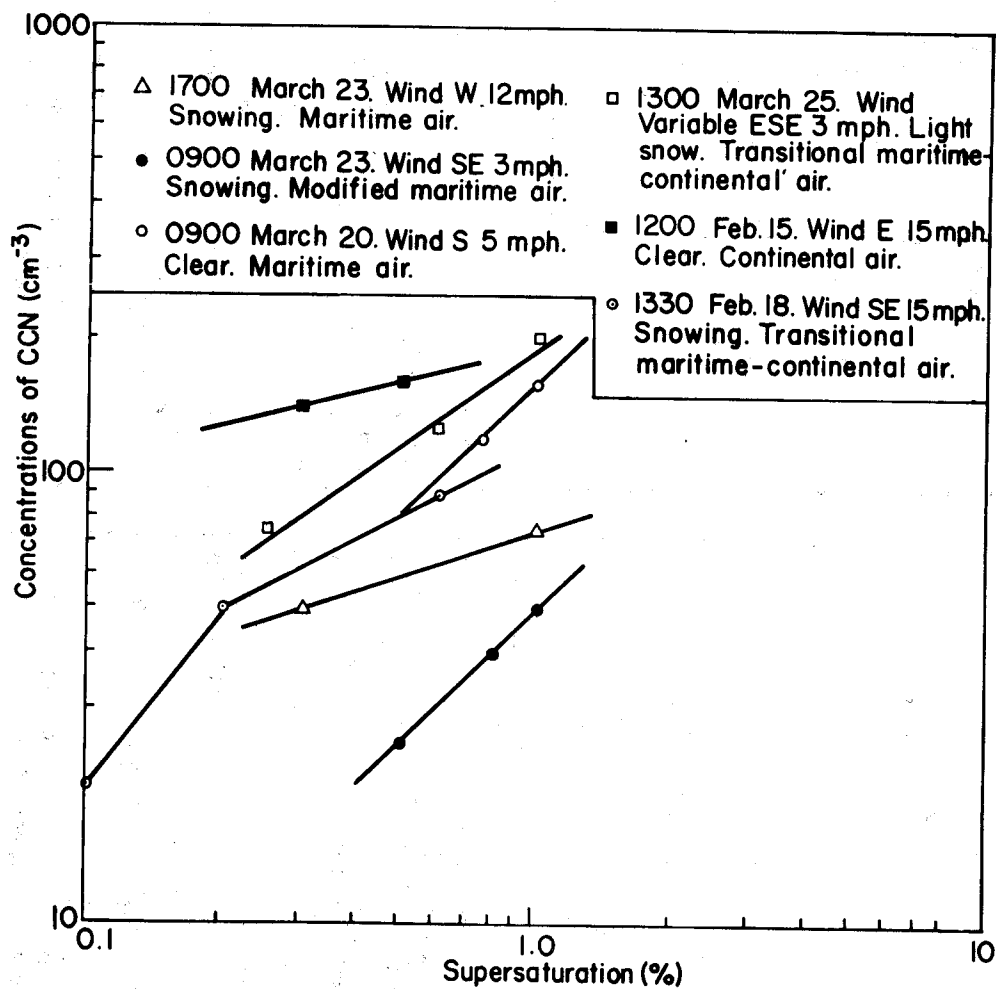
- Figure 1 - Equilibrium vapor pressures over droplets of a given radius
containing given masses of soluble salt
- Figure 2 - An automatic cloud condensation nucleus counter (From Radke and
Hobbs, 1968)
- Figure 3 - Concentrations of CCN as a function of supersaturation in different
air masses (From Radke and Hobbs, 1969)
- Figure 4 - Measurements of CCN in wave clouds (From Radke, 1970)
- Figure 5 - Measurements of CCN in wave clouds (From Radke, 1970)



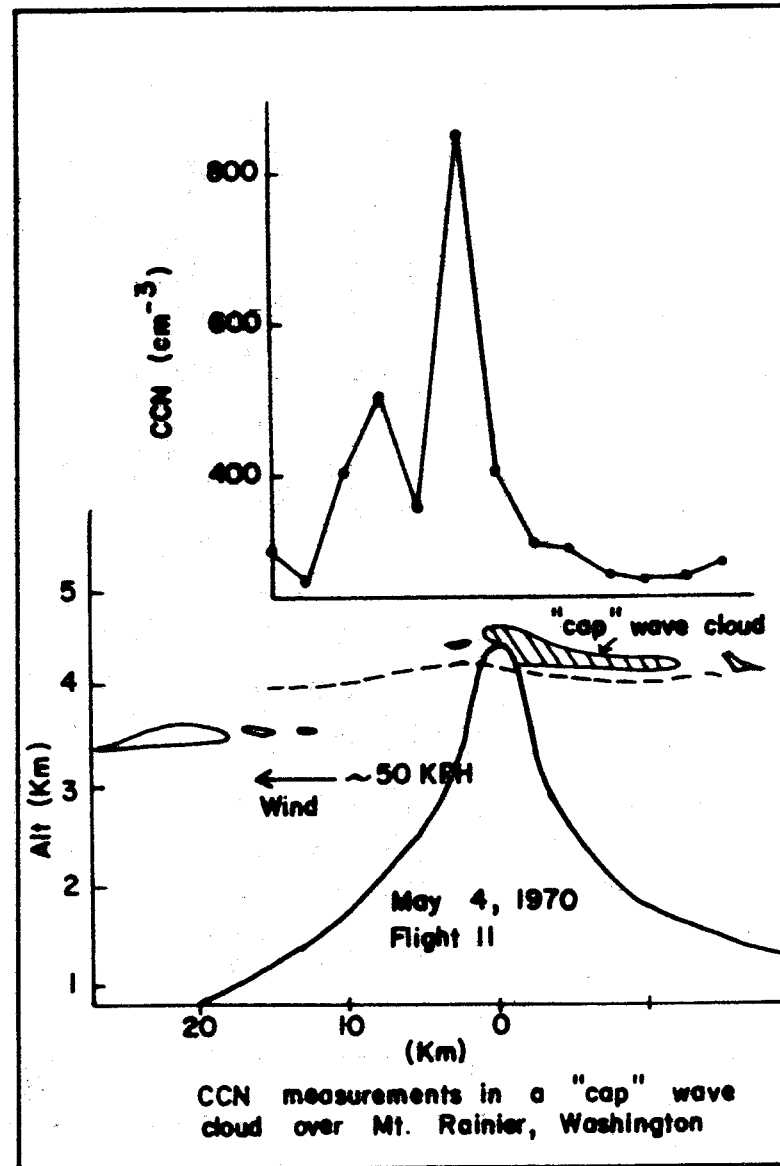
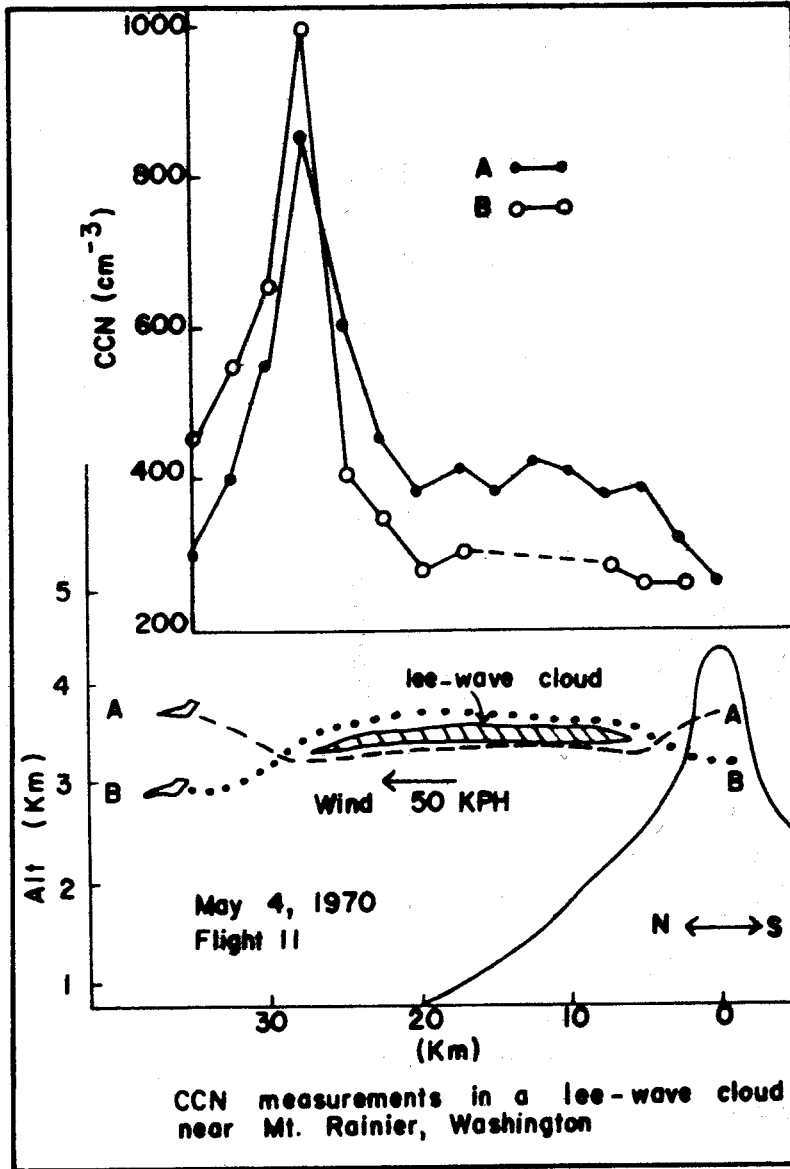
Lecture 1, Figure 1



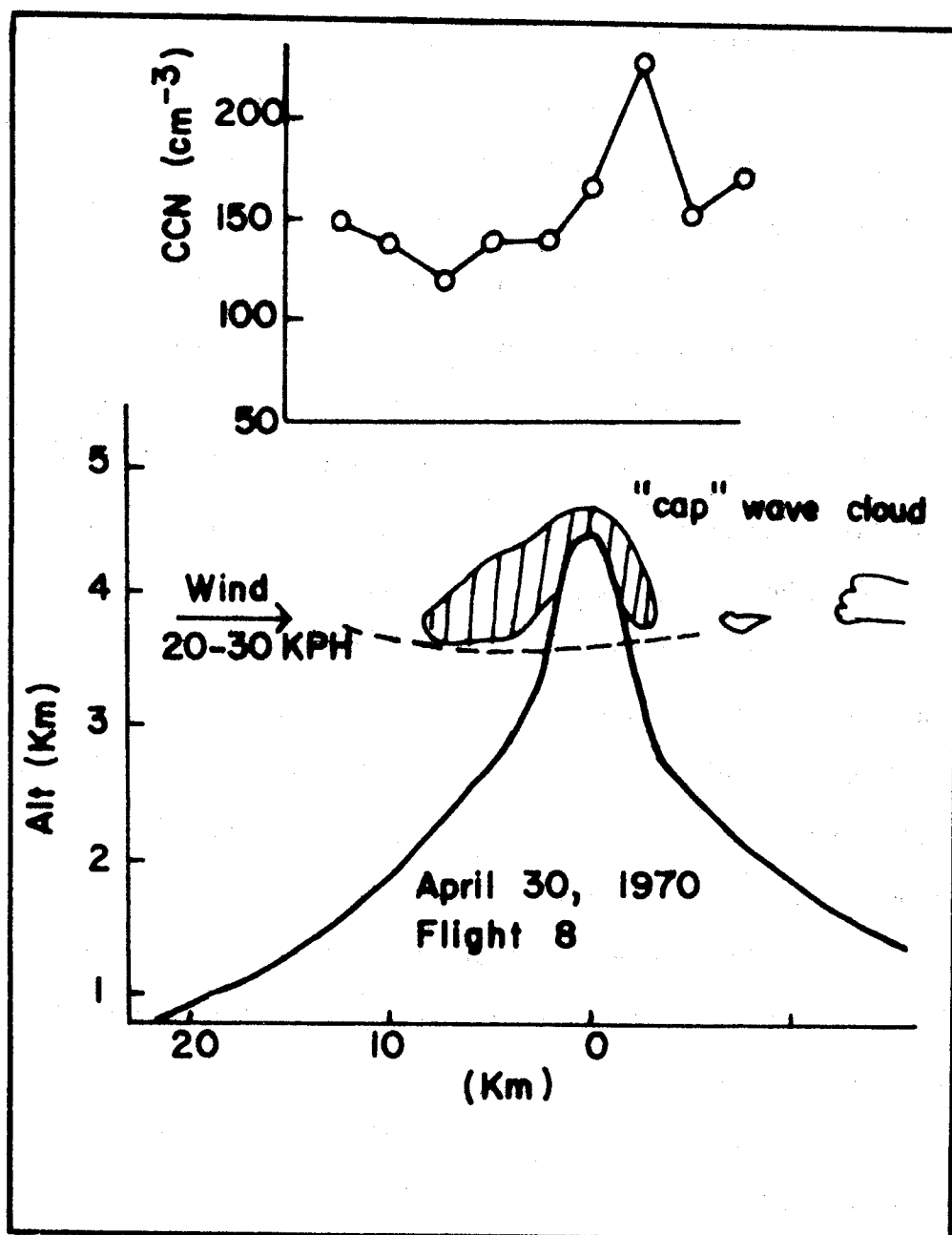
Lecture 1, Figure 2



Lecture 1, Figure 3



Lecture 1, Figure 4



Lecture 1, Figure 5

II. GROWTH OF DROPLETS AND PRECIPITATION IN WARM CLOUDS

A. Growth of cloud droplets by condensation

Following our consideration of the initial stages of condensation, we must consider the growth of cloud droplets. The rate of growth of isolated droplet of radius r by condensation from the vapor phase is given by $\frac{dr}{dt} \propto \frac{1}{r}$. Therefore, the droplets grow to a uniform size with time but the growth rate decreases (Fig. 1, see end of Lecture #2).

In a cloud we must consider the growth of a large population of droplets in a rising parcel of air. It may be assumed that the direct interactions between droplets is negligible. However, droplets influence each other by their combined influence on their environment. As the parcel of air rises, the saturation ratio increases. Once the saturation point is passed, condensation begins on the most efficient CCN. The supersaturation (SS) continues to rise and CCN increases. The rate of increase of SS is reduced because growing drops consume excess vapor. When the excess vapor is removed as quickly as it is being made available by condensation, the SS falls to zero.

Figure 2 (see end of Lecture #2) shows the growth of droplets by condensation onto various masses of salt for a lift rate of 60.4 cm sec^{-1} . We see from these calculations that:

(1) For first 10 sec, when the rate of condensation is negligible, the SS increases linearly with the time. The SS reaches a maximum of 0.35% in 25 sec, and then decreases.

(2) Above certain critical SS, the droplets increase rapidly in size and become uniform.

(3) As SS falls, the smaller droplets which have not been activated fall back to smaller sizes but larger drops continue to grow slowly.

(4) Growth by condensation becomes very slow after a few minutes and drops have only reached a radius about 20μ in 10 min or so.

B. Growth of precipitation particles by coalescence

The relative sizes of cloud and precipitation particles are shown in Fig. 3 (see end of Lecture #2). The volume of a typical cloud droplet (radius 10μ) has to increase by 10^6 in order to produce a precipitable particle of radius 1mm.

The growth of cloud drops from a radius of 10 or 20μ to raindrop size ($> 100\mu$) is an important problem in cloud physics. Condensation alone is too slow; in warm clouds precipitable drops can only form by the collision and coalescence of cloud droplets of different sizes.

We define the collision efficiency E as the fraction of drops lying within the geometrical cross-section of a collector drop which actually collide with the collector.

Then with reference to Fig. 4 (see end of Lecture #2)

$$E = \frac{y^2}{(a_1 + a_2)^2}$$

or, sometimes

$$E \equiv \frac{y^2}{a_1^2}$$

where y is the maximum impact parameter (Fig. 4). We may also define a linear collision efficiency as y/a_1 .

Figure 5 (see end of Lecture #2) shows calculated linear collision efficiencies. We see from these theoretical results that:

(1) The larger the collector drop the higher the collision efficiency.

(2) The collision efficiency is very small but still finite when the radius of the collector drop falls below 20μ .

Another question to be answered is: does coalescence always occur when two drops collide? We know from laboratory experiments that under certain conditions (not necessarily representative of those in the atmosphere) droplets can rebound after colliding with a water surface. However, it is generally assumed that in natural clouds the coalescence efficiency is unity.

C. Models for growth by coalescence

(1) Continuous model: In this model it is assumed that larger drops grow by continuously capturing smaller drops uniformly distributed in space (Fig. 6, see end of Lecture #2). This model predicts that drops of a given size grow at the same rate.

(2) Stochastic model: This is a statistical growth model. Consider those few drops which have made a coalescence collision after a rather short time. They are now in a more favorable position than their fellows to make a further collision because of their larger size. These second collisions are similarly statistically distributed giving a further widening of the spectrum (Fig. 7, see end of Lecture #2). The stochastic model predicts that the droplet spectrum is substantially determined by the first twenty captures. After this the statistical fluctuations are unimportant and the continuous growth equation may be used.

D. Growth by coalescence: The results of some model calculations

Droplets can grow to 20μ by condensation alone and droplets larger than 40μ can grow rapidly by coalescence. But what about the growth of the droplets from about 20μ to 40μ radius?

We will consider the growth from 20μ to 40μ by coalescence based on some model calculations by Bartlett (1966).

Figure 8 (see end of Lecture #2) shows a typical distribution of drop sizes in the early stages of growth of a cumulus cloud. The largest

drops have radius 26μ and are present in concentrations of 3/litre. The tail of the distribution at large sizes is most important for the production of precipitation.

Starting from the distribution shown in Fig. 8 Bartlett computes in a step-wise fashion the development of the spectrum due to growth by coalescence. Resulting drop-size distribution at various times are shown in Fig. 9 (see end of Lecture #2).

Figure 9 shows development of distribution shown in Fig. 8 with time. We see from Fig. 9 that:

- (1) Large drops develop with time.
- (2) There is little change in the distribution for drops with radius less than 10μ .
- (3) The concentration of 40μ drops exceeds 1/litre after 7 min and exceeds 10/litre after 16 min.
- (4) Most of the liquid water for the growth of the larger drops comes from drops with radius between 11 and 22μ . There must be a good supply of drops in this size range in order for larger drops to grow by coalescence. There is a significant amount of liquid water in drops greater than 40μ which, in this model, are assumed to fall out of the parcel. A convenient way to represent the development of precipitation is to plot this overflow as a fraction of the total liquid-water content. This is shown in Fig. 10 (see end of Lecture #2).

We see that initially there is no significant overflow, but after about 7 min the overflow begins to increase rapidly and after 14 min it increases at an almost constant rate. A rough calculation shows that this overflow can produce a precipitation rate of about 7 mm/hr. This is the right order of magnitude for moderate cumulus shower and indicates that coalescence is capable of producing precipitation.

Figure 11 (see end of Lecture #2) shows assumed initial drop size distributions.

Figure 12 (see end of Lecture #2) shows a table of characteristics of droplet spectra shown in Fig. 11.

A convenient way of comparing the development of precipitation for the different drop size distributions shown in Figs. 11 and 12 is to plot the overflow as a function of time. The results are shown in Fig. 13 (see end of Lecture #2). Figure 13 shows overflow as function of time for different initial distributions. We see from these results that:

(1) In maritime cumulus, if coalescence continued for 15 min, 25% of liquid water would be removed by drops larger than 40μ radius. Hence the coalescence mechanism could produce rain without difficulty in this case.

(2) The continental clouds need more time to get one droplet of 40μ than maritime clouds (since in maritime clouds there are initially some large drops).

(3) Maritime clouds are more efficient than continental clouds in producing precipitable particles by coalescence.

(4) An interesting case is spectrum IV which fails to produce 0.05% overflow in 30 min although it contains a few more large drops than II d. This is because in IV there is a deficiency of drops in the range 14 to 20 microns, which are needed to supply water for large drops.

Bartlett's calculations also show that the minimum collector size drop is the most important single parameter governing the onset of the coalescence mechanism, whereas, any changes which are equivalent to an increase of less than 10% in the collection efficiencies can be ignored.

Notes taken by:

Y. M. Chang

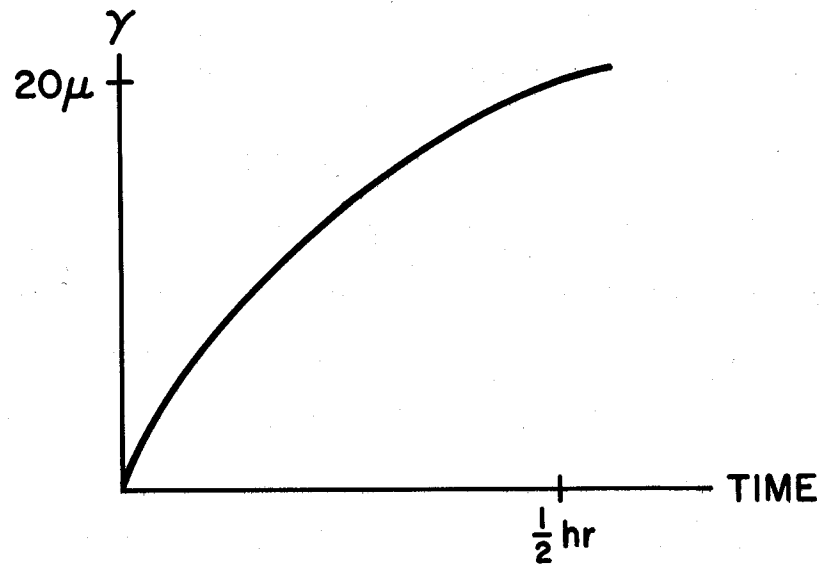
W. H. Mach

REFERENCES

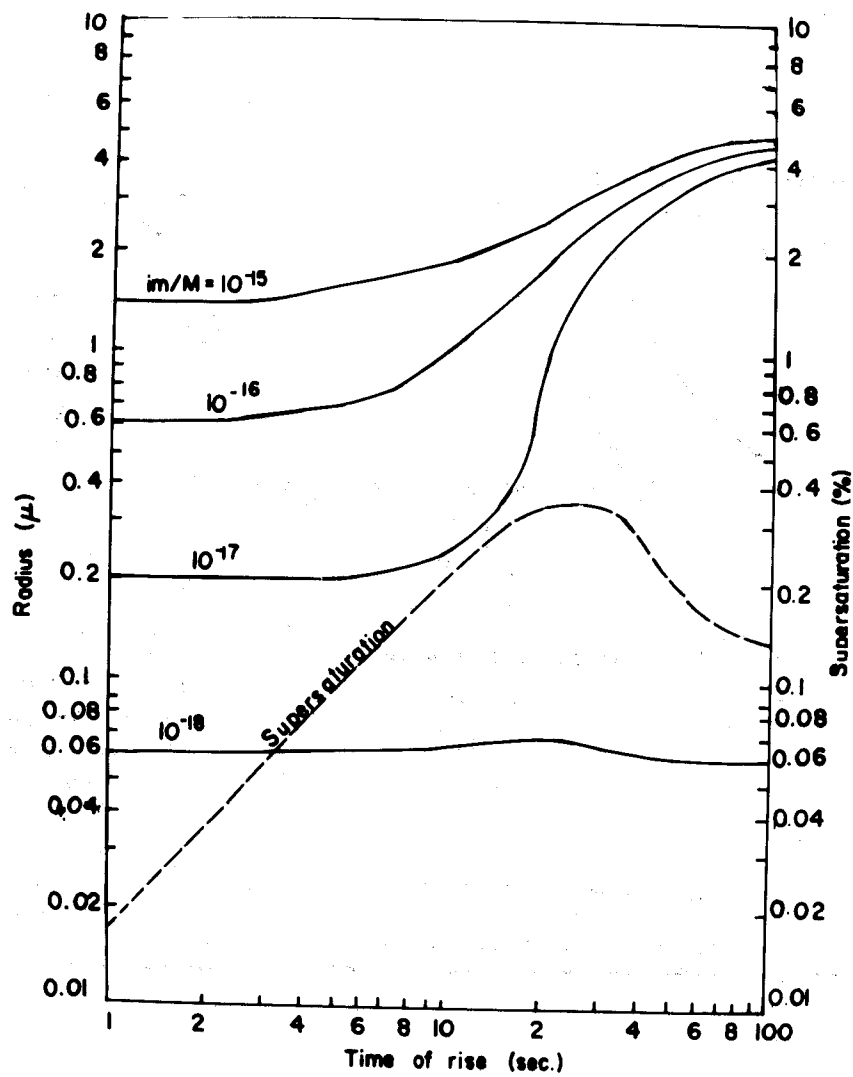
- Bartlett, J. T., Quart. J. Roy. Met. Soc., 92, 93, 1966.
- Berry, E. X., J. Atmos. Sci., 24, 688, 1967.
- Davis, M. H., Rand Corp. Memo. RM-5419-WSF, 1967.
- Howell, W. E., J. Met., 6, 134, 1949.
- McDonald, J., Advances in Geoph., 5, 223, 1958.

FIGURE CAPTIONS

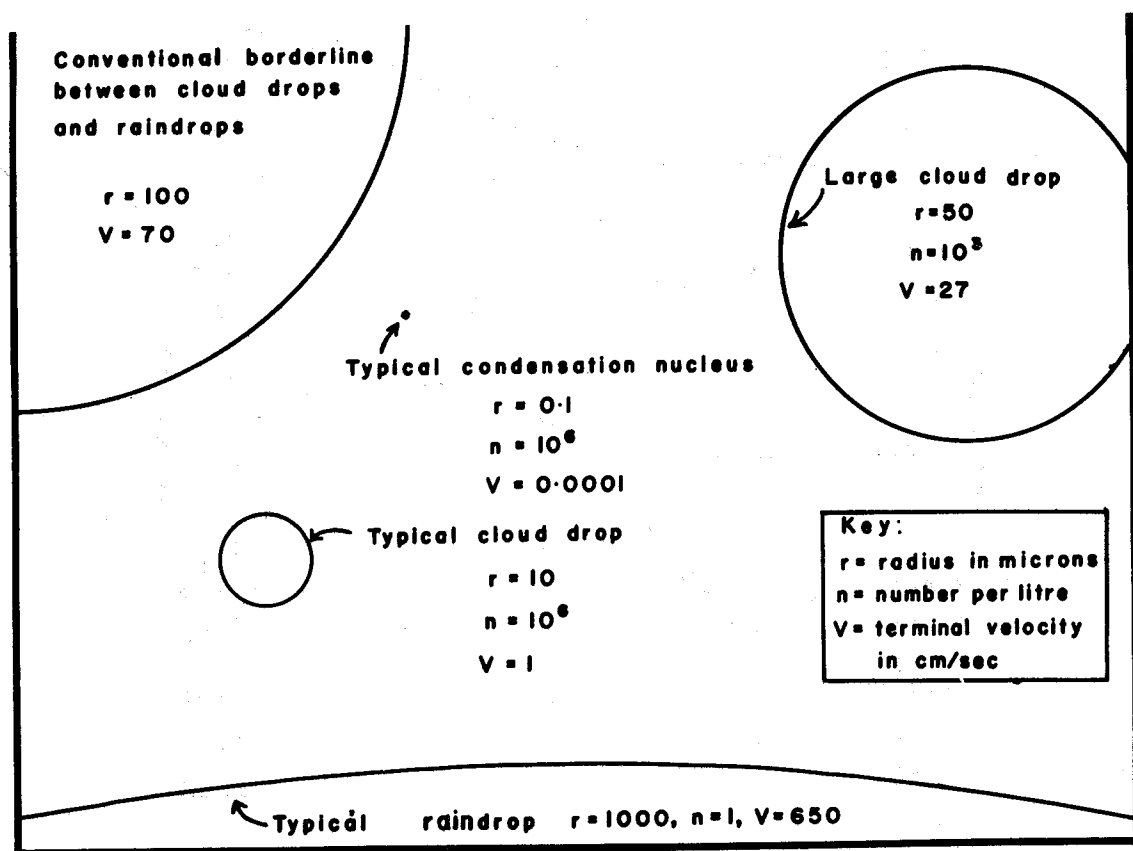
- Figure 1 Growth of a droplet by condensation.
- Figure 2 The growth of droplets by condensation onto various masses of salt for a lift rate of 60.4 cm sec^{-1} (from Howell, 1949).
- Figure 3 Relative sizes of cloud and precipitation particles (from McDonald, 1958).
- Figure 4 Definition of symbols.
- Figure 5 Calculated linear collision efficiencies (from Davis, 1967).
- Figure 6 Growth by coalescence according to continuous model.
- Figure 7 Growth by coalescence according to stochastic model (from Berry, 1967).
- Figure 8 A typical distribution of drop sizes in the early stages of a cumulus cloud. Inset: The same plotted on a logarithmic scale, (from Bartlett, 1966).
- Figure 9 Development of distribution shown in Fig. 8 with time (from Bartlett, 1966).
- Figure 10 Fraction of total liquid water content in drops with radius greater than 40 microns (from Bartlett, 1966).
- Figure 11 Assumed initial drop size distributions (from Bartlett, 1966).
- Figure 12 Table of characteristics of droplet spectra shown in Fig. 11 (from Bartlett, 1966).
- Figure 13 Overflow as function of time for different initial distributions (from Bartlett, 1966).



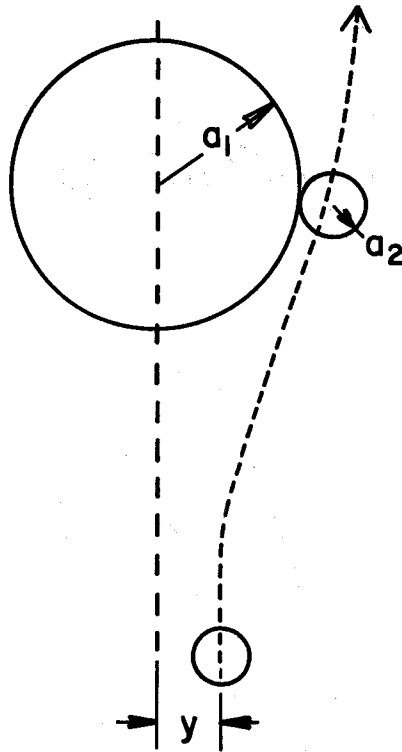
Lecture 2, Figure 1



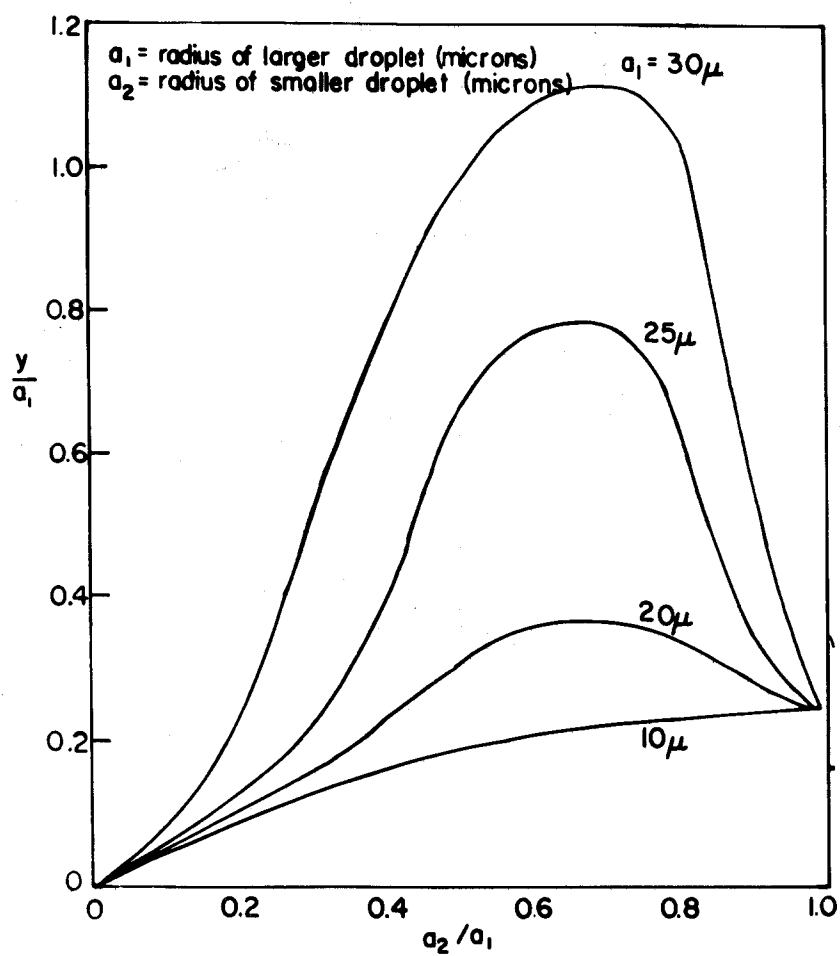
Lecture 2, Figure 2



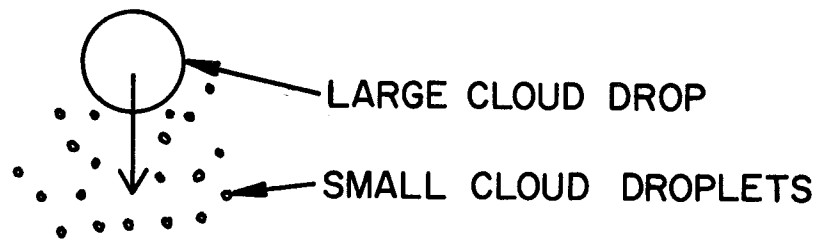
Lecture 2, Figure 3



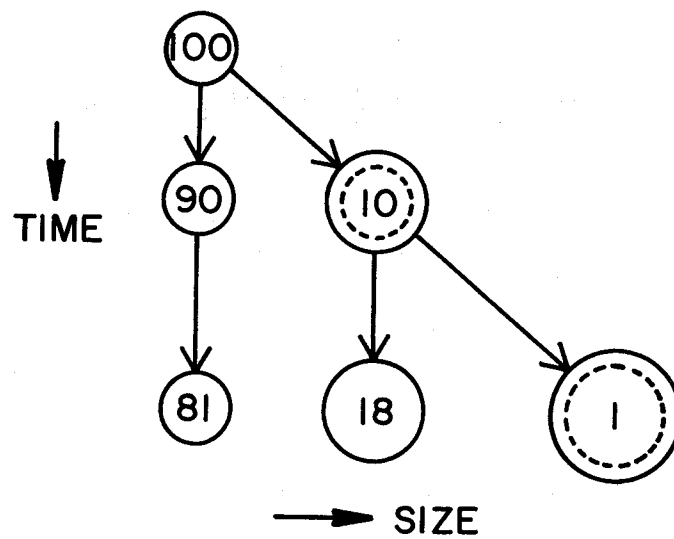
Lecture 2, Figure 4



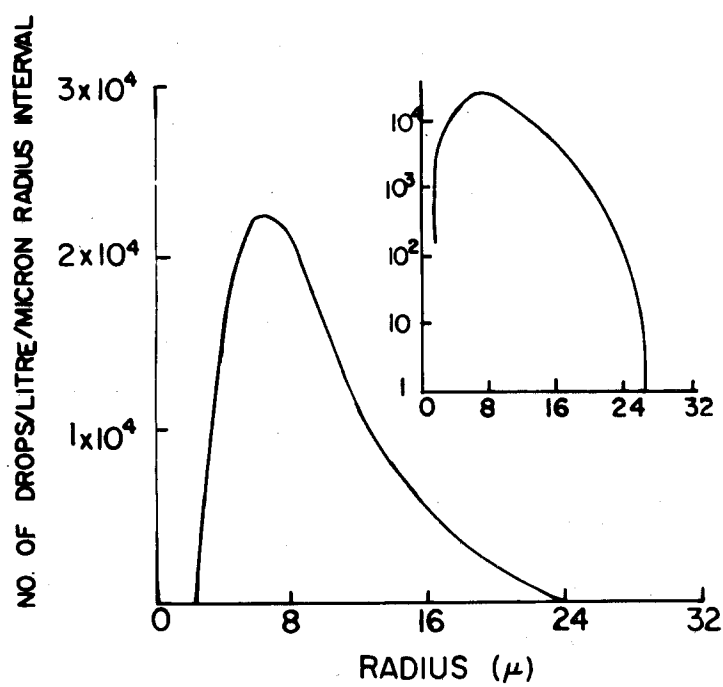
Lecture 2, Figure 5



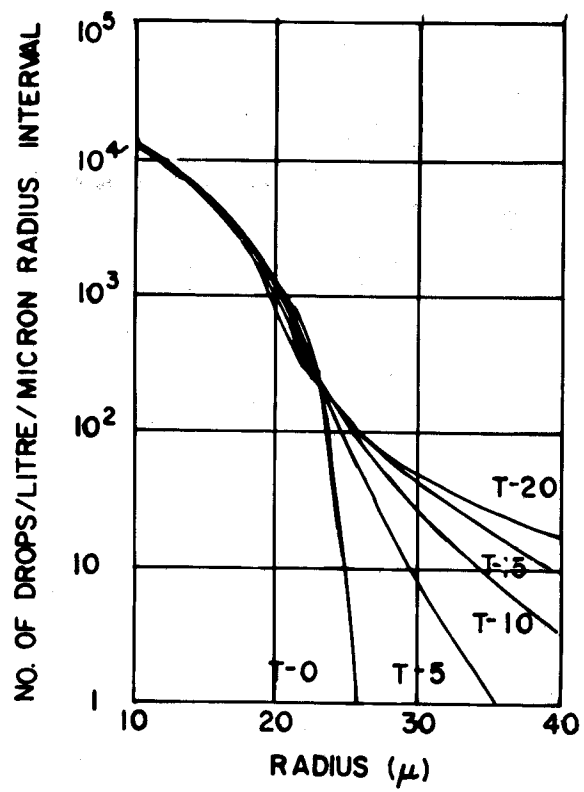
Lecture 2, Figure 6



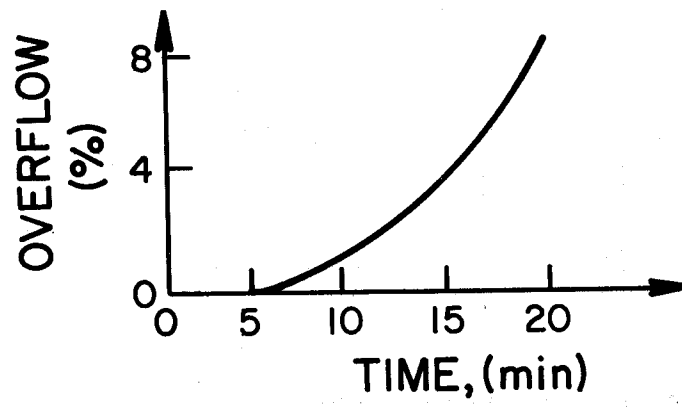
Lecture 2, Figure 7



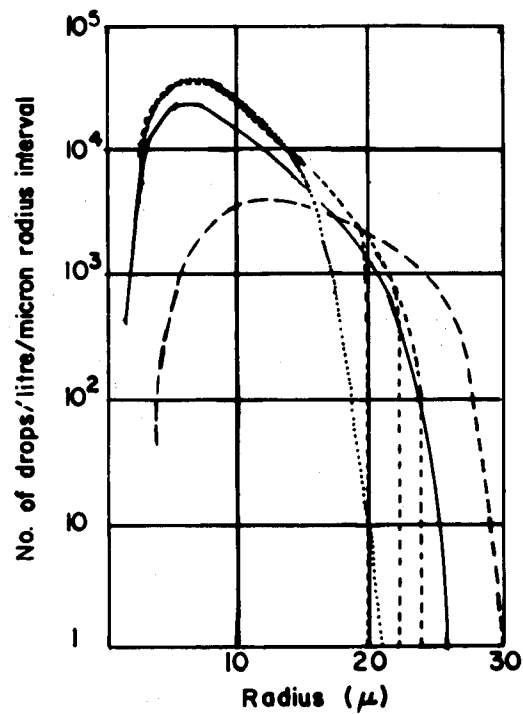
Lecture 2, Figure 8



Lecture 2, Figure 9



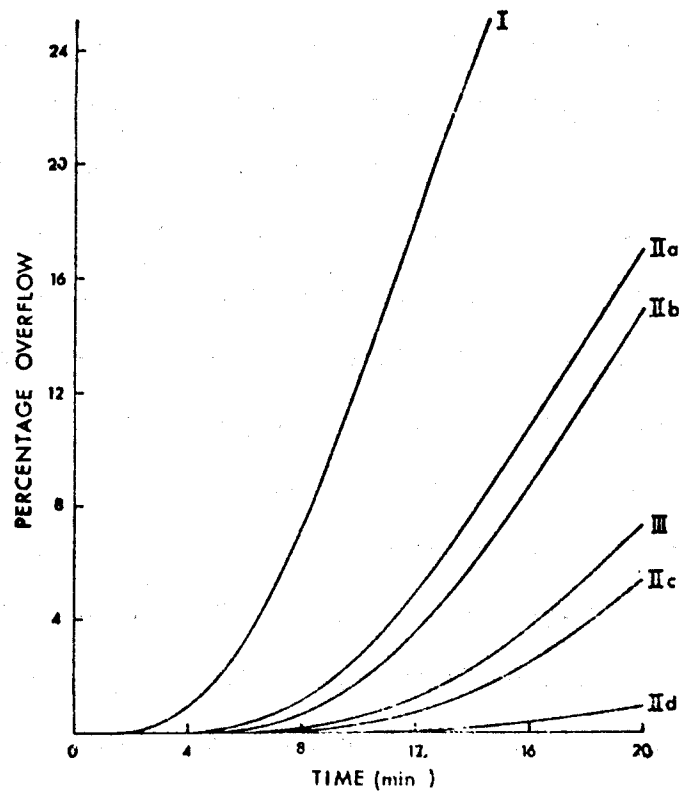
Lecture 2, Figure 10



- I TYPICAL OF MARITIME CUMULUS CLOUDS.
 - - - - - II A,B,C,D TYPICAL OF CONTINENTAL CUMULUS CLOUDS,
 CONTAINING DROPS WITH RADII UP TO 126,
 24, 22 AND 20 μ RESPECTIVELY.
 III SAME AS II WITH SMALLER WATER CONTENT.
 IV DISTRIBUTION DEFICIENT IN LARGE DROPS.

CHARACTERISTICS OF DROPLET SPECTRA

SPECTRUM	CLIMATIC TYPE	LIQUID-WATER CONTENT (GM ⁻³)	TOTAL DROPLET CONCENTRATION NO./CM ³	MAXIMUM DROP RADIUS (μ)	TIME TO GIVE ONE 40 μ DROP/LITRE (MINUTES)
I	MARITIME	1.00	58.8	30	2
IIA	CONTINENTAL	1.46	300.0	26	4
IIB	CONTINENTAL	1.45	299.8	24	5
IIC	CONTINENTAL	1.38	298.3	22	7 1/2
IID	CONTINENTAL	1.30	296.0	20	12 1/2
III	CONTINENTAL	1.00	205.1	26	6 1/2
IV	CONTINENTAL	1.00	305.7	21	>30



Overflow as a function of time for different initial distributions.

III. NUCLEATION OF ICE AND PROPERTIES OF ICE NUCLEI

A. Homogeneous and heterogeneous nucleation

Clouds frequently extend above the 0°C isotherm and may therefore contain ice particles. Ice can form either directly from the vapor phase or by the freezing of water droplets.

It has been found in the laboratory that very pure water drops, less than a few microns in size, will remain in the supercooled (or undercooled) liquid state to a temperature of about -40°C at which point they freeze spontaneously. This is called homogeneous nucleation. In an environment supersaturated with water vapor, it is also possible, in principle, for ice to be deposited directly from the vapor phase. This process will be in competition with condensation of vapor to liquid water.

Homogeneous nucleation of ice does not occur in the atmosphere because there are foreign particles which permit nucleation to occur at temperatures above -40°C . Nucleation of ice due to the presence of foreign particles is called heterogeneous nucleation. Two types of heterogeneous nucleation must be discussed. One is the direct deposition of ice from the vapor phase and the other is the nucleation of freezing in supercooled drops. For the direct deposition of ice from the vapor phase, the presence of foreign particles reduces the required supersaturation below that needed for homogeneous deposition. Similarly supercooled water containing solid particles will generally freeze at temperatures significantly higher than the homogeneous point.

A macroscopic theory of heterogeneous nucleation has been developed by Fletcher (1958). This approach is based on classical nucleation theory and does not consider in detail the microscopic mechanisms involved in nucleation. The theory consists of writing down an expression

for the change in free energy of a system when nucleation occurs on a substrate, then minimizing this expression to find the size of the critical free energy barrier and size of the critical ice embryo. As the ice embryo forms in the droplet the free energy of the system increases until the embryo reaches a critical radius after which the continued growth of the embryo results in a reduction of the free energy. This implies that if the embryo does grow to its critical radius, the droplet will continue to freeze to lower its free energy.

Figure 1 (see end of Lecture #3) shows the effect of the radius of a spherical particle on the temperature at which it can act as a deposition nucleus according to Fletcher's theory. The surface parameter m is the cosine of the contact angle of ice on the particle. The figure shows that the larger particles are more effective as ice nuclei, particularly for radii less than 1000 \AA . However, even for radii greater than 1μ the contact angle must be fairly small (less than 30°) if the substance is to be effective.

Figure 2 (see end of Lecture #3) shows the predictions of the theory when the nucleating particle is immersed in supercooled water. It shows the temperature at which freezing occurs in one second on a spherical particle of radius R in water. The size of the particle becomes important only below a radius of about 0.01μ . Again the surface parameter m has a large influence on the nucleating efficiency.

Since the above treatment is based entirely on thermodynamic considerations, it has a number of serious limitations. The main difficulty is that the chemical bonding and the crystallographic factors that need to be taken into account to calculate the interfacial energies (and hence m) are not well known.

B. Lattice misfit and entropy effects

The lattice misfit δ between a nucleating particle and ice is defined as

$$\delta = \left| \frac{a - a_o}{a_o} \right|$$

where a and a_o are the lattice parameters of the nucleating particle and ice respectively. This misfit causes a certain elastic strain in the ice which increases the energy barrier for nucleation thus lowering the temperature needed to achieve a given nucleation rate.

The value of the surface parameter m also depends upon the way in which the water molecules in ice are bound to the nucleating surface. Since water is polar, this bonding is mainly electrostatic, therefore, ice nucleation should be preferred on materials with intense ionic fields. The energy of the interface will be minimized if the dipole of each water molecule orients parallel to the direction of the electric field in its vicinity. But, this configuration of dipoles may produce a lower entropy and therefore higher free energy in the bulk of the ice well away from the interface. Fletcher (1959b) analyzed the manner in which the relations between interfacial energy and bulk entropy influence the nucleating ability of a material. His conclusion was that any substance which orients the ice dipoles at its surface parallel to one another would be a poor substance for nucleation.

C. Freezing versus deposition

Heterogeneous nucleation of ice by direct deposition and by freezing of droplets represent two competing processes. In practice, it may be impossible to distinguish between these two cases since

freezing may not involve a macroscopic droplet but merely a thin layer of water. However, the two processes are quite distinct theoretically. Figure 3 (see end of Lecture #3) demonstrates the situation for a typical nucleating material. The figure shows that for a completely insoluble particle in an environment just saturated with water vapor, condensation cannot occur. Sufficiently large particles (greater than 1μ) should act as deposition nuclei at slightly less than water saturation if the temperature is low enough. Figure 3 also shows that in the size range 0.01 to 0.1μ , particles wetted by water require considerable supersaturation to nucleate drops, but they might act as deposition nuclei at moderate supercoolings and saturation ratios near unity. Condensation should be more rapid than deposition at very small supercoolings and slight supersaturations with respect to water.

D. Experimental studies of heterogeneous nucleation

Studies of heterogeneous nucleation date back to 1724 when Fahrenheit slipped on stairs while carrying a flask of cold water and noticed that the water had become full of flakes of ice. Since then, there have been numerous and often conflicting reports on the means by which ice can be nucleated.

(1) Freezing of water drops

Fig. 4 Freezing temperature of water drops as a function of size (see end of Lecture #3).

From Fig. 4 it can be seen that an order of magnitude increase in the rate of cooling lowers the mean freezing temperature by about 2°C . (Biggs' results for drops $>30\mu$.) Displacements of the various lines in Fig. 4 is attributed to differing concentrations of ice nuclei in the samples of water used.

(2) Nucleation by particulates

In the belief that good ice-nucleating materials should have crystal properties similar to ice, Vonnegut (1947) searched through X-ray crystallographic data for materials which had cell dimensions and crystal symmetries as close as possible to those of ice. He found that AgI and PbI_2 had small lattice misfits (Fig. 5).

Fig. 5 Crystal structures of AgI, PbI_2 and ice (see end of Lecture #3). AgI and PbI_2 were introduced as powders into supercooled clouds of water droplets at -20°C . In the first trials, AgI had no effect but PbI_2 formed ice crystals. Later, Vonnegut attributed failure of AgI to act as ice nucleus to gross contamination by soluble salts. Cleaner samples of powdered AgI did form ice crystals. Vonnegut also found that electric discharges between Ag electrodes in the presence of iodine vapors produced many thousands of times more ice nuclei than AgI powders. Even more effective were the smokes produced by vaporizing AgI on a hot filament or by dispersing it in a flame. AgI smokes produced by burning an acetone solution of AgI and NH_4I in a hydrogen flame showed that at -20°C over 10^{16} ice nuclei were formed per gram of AgI.

Following Vonnegut's pioneering work, the ice-nucleating ability of a large number of materials was investigated. For example, Fukuta (1958) found 78 inorganic materials to be effective at temperatures above -20°C .

Fig. 6 Some effective artificial ice nuclei (see end of Lecture #3). Because of the widespread use of AgI in cloud seeding, this material has been studied in detail. Reynolds et al. (1951) found that when AgI particles in a container were exposed to strong sunlight, the concentration of active nuclei at -20°C decreased by a factor of about 100 per hour. This decrease

in efficiency is attributed to changes in the surface structure by photodecomposition. Corrin et al. (1967) found that "pure" AgI is less efficient than AgI containing hygroscopic impurities.

Fletcher's theory predicts the conditions under which a particle should act as a freezing nucleus or a deposition nucleus. Edwards and Evans (1960, 1968) determined ice-nucleating activity of a reproducible AgI under controlled temperature and humidity. They found:

(i) Almost all AgI particles of radius 75 \AA when exposed to water saturation are inactive as deposition nuclei down to at least -18.5°C . (According to Fletcher's theory, particles of this size should, at water saturation, act as deposition nuclei only below -30°C .)

(ii) AgI particles are much more active as freezing nuclei than as deposition nuclei.

(iii) AgI particles only act as freezing nuclei if the relative humidity with respect to water exceeds 110%. (Since the relative humidity in clouds seldom exceeds 101%, AgI particles should act only as relatively inefficient deposition nuclei unless they collide with cloud droplets.)

Is a particle more efficient as a freezing nucleus when it comes into contact with the surface of a supercooled drop or when it is imbedded in the drop? Gokhale (1965) concluded that nucleation by contact is much more effective than nucleation by particles imbedded in the drop. The difference in the nucleating temperature for these two cases may be 5° to 10°C , depending on the material.

E. Organic nuclei

Recent studies have revealed a large number of organic compounds which can act as ice nuclei at fairly high temperatures. The first organic

ice nucleus to be discovered was phloroglucinol (Bashkirova and Krasikov, 1957), effective at -8°C . In a study of more than 300 organics Fukuta (1963) found metaldehyde to be the most effective; this material nucleated ice at -1°C .

Mention should be made of the unusual ice-nucleating properties of urea. Due to the high endothermic heat of solution (-60.5 calories/gm) and high solubility, this organic produces strong local cooling when it dissolves in water and thus can cause ice nucleation when the air temperature is as high as $+6^{\circ}\text{C}$.

F. Nucleation of high pressure forms of ice

By using certain organic compounds as nucleators, Evans (1967) has crystallized most of the high pressure forms of ice from the liquid at pressures outside the range of thermodynamic stability. He also used the high pressure forms of ice to investigate the role of lattice misfit in ice nucleation.

Fig. 7 Portion of phase diagram for water substance (see end of Lecture #3).

Aqueous suspensions of AgI were frozen under pressures up to 3000 bars, which includes ice I and ice III phases. Now up to a pressure of 3000 bars, AgI has a hexagonal structure with a mismatch of not more than 2% with ice I. Ice III however has a tetragonal lattice in which none of the spacings correspond to the AgI lattice. For doubly-distilled water (without AgI suspension), ice I formed up to a pressure of 2060 bars while ice III formed above this pressure. Both phases nucleated at about 20°C below their respective melting curves. However, when an aqueous suspension of AgI was cooled, ice I nucleated at a supercooling of 4°C , (i.e. along curve EF) but nucleating temperature of ice III was the same as that for doubly distilled water. Drops containing AgI cooled at a pressure of 2500 bars nucleated at point X, on extrapolation of EF, as

ice I! These observations show that in cases where the nature of chemical bonding is the same, the phase which has the closest lattice fit with the nucleator is preferentially nucleated.

G. Summary of requirements of an ice nucleus

We have seen that the small mismatch between the crystal structure of AgI and ice led Vonnegut to test the ice-nucleating ability of AgI which was found to be very effective in this respect. Subsequently, it was widely held that a small mismatch with ice was the sole criterion for an effective ice nucleus. More recently, however, it has become evident that while lattice spacing does play an important role in determining the effectiveness of a material as an ice nucleus, it certainly is not the only factor involved.

AgI is essentially hydrophobic in nature and the surfaces of AgI and ice are probably energetically incompatible. Zettlemoyer et al. (1961) postulated that ice first develops on AgI at a few impurity sites which are hydrophilic in character. This hypothesis is supported by Corrin's work on impure and pure AgI.

To check this idea, Zettlemoyer et al. hydrophobed several types of silicas and determined their nucleating ability. They found that hydrophobing a silica surface significantly increased its ice-nucleating efficiency and some of these materials rivaled AgI. Studies of the absorption properties of these silicas showed that water was absorbed in clusters at high energy sites. A balance between hydrophilic and hydrophobic surface groups and proper distribution of sites were shown to be important for heterogeneous nucleation of ice. The relative inefficiency of pure AgI can be attributed to lack of impurity sites on which ice can form.

While the general requirements for an ice nucleus outlined above appear to be valid, it should not be assumed that the mechanism of heterogeneous nucleation is completely understood. Indeed, different materials probably nucleate ice in different ways.

Notes taken by:

R. M. McGehee

J. R. Miller

REFERENCES

- Bashkirova, G. M., and Krasikov, P. N., Trudy Glavnoi Geofiz. Obs., 72, 118, 1957.
- Corrin, M. L., Nelson, J. A., Cooley, B., and Rosenthal, B., J. Atmos. Sci., 24, 594, 1967.
- Edwards, G. R., and Evans, L. F., J. Met., 17, 627, 1960.
- _____ and _____, J. Atmos. Sci., 25, 249, 1968.
- Evans, L. F., J. App. Phys., 38, 4930, 1967.
- Fletcher, N. H., J. Chem. Phys., 29, 572, 1958.
- _____, J. Met. 16, 173, 1959a.
- _____, J. Chem. Phys., 30, 1476, 1959b.
- Fukuta, N., J. Met., 15, 17, 1958.
- _____, Nature, 199, 475, 1963.
- Gokhale, W. R., J. Atmos. Sci., 22, 212, 1965.
- Reynolds, S. E., Hume, W., Vonnegut, B., and Schaefer, V. J., Bull. Am. Met. Soc., 32, 47, 1951.
- Vonnegut, B., J. App. Phys., 18, 593, 1947.
- Zettlemoyer, A. C., Tcheurekdjean, N., and Chessick, J. J., Nature, 192, 653, 1961.

Figure Captions

Figure 1 - Temperature T at which a spherical particle of radius r and surface parameter m will nucleate an ice-crystal in 1 sec by sublimation from an environment at water saturation. The effect of elastic strain is not included (Fletcher, 1958).

Figure 2 - Temperature T at which a spherical particle of radius r and surface parameter m will nucleate an ice-crystal from water in one second by freezing. The effect of elastic strain is not included (Fletcher, 1958).

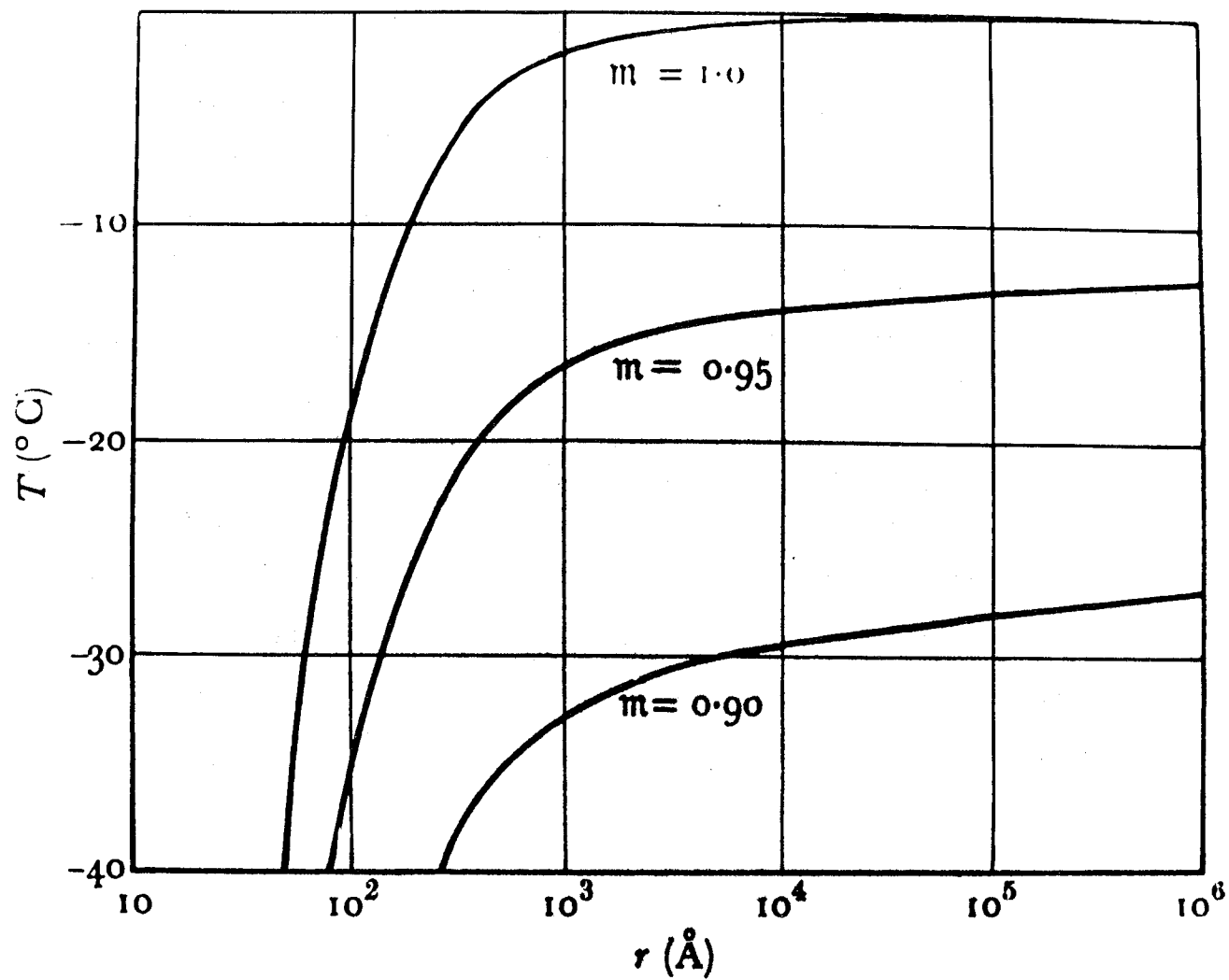
Figure 3 - Activity surfaces for a typical nucleating substance (Fletcher, 1959a).

Figure 4 - Freezing temperature of water drops as a function of size.

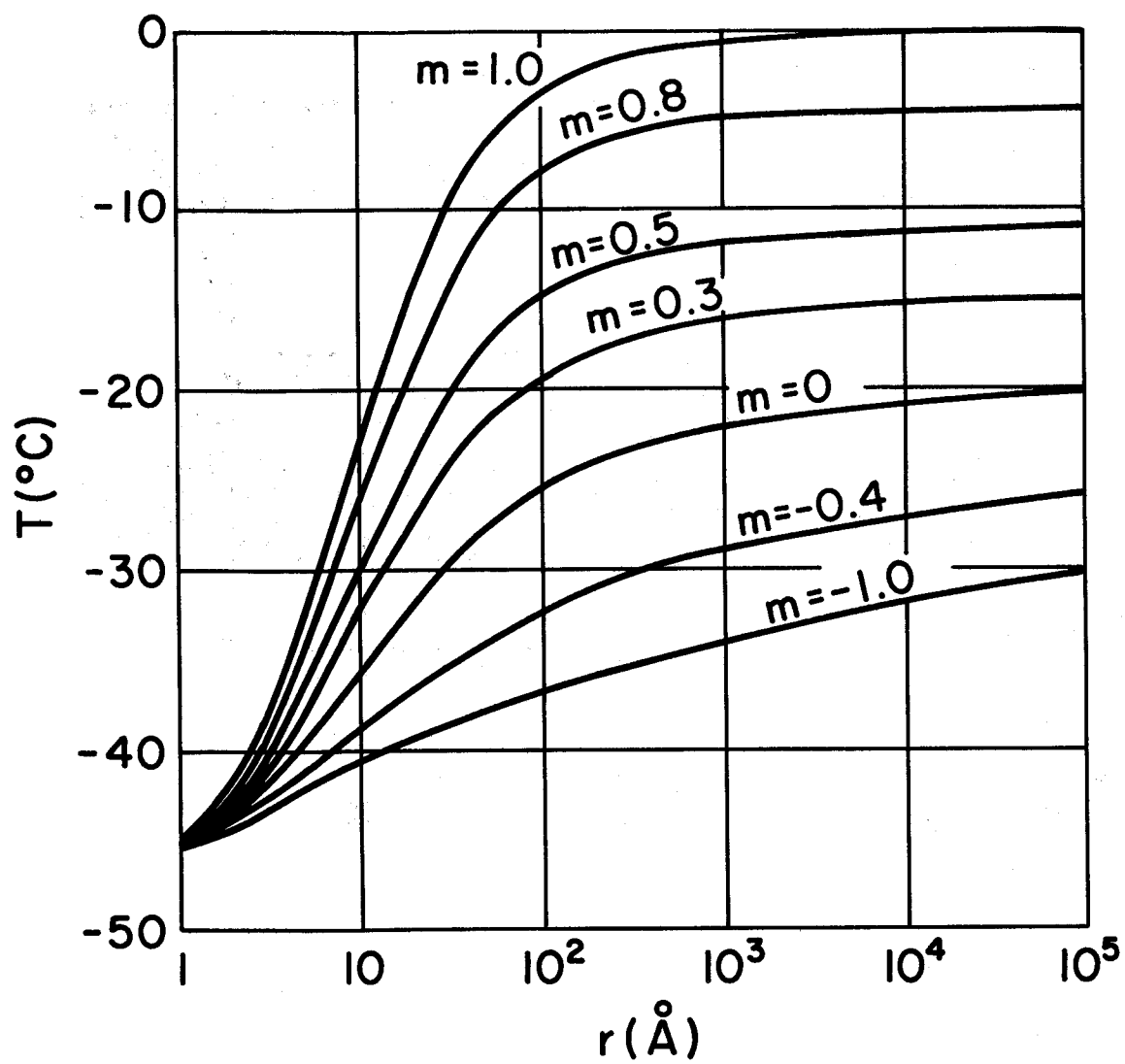
Figure 5 - Models of the crystal structures of ice, lead iodide and silver iodide. In the latter white spheres are iodide ions and black spheres metallic ions (Fletcher, 1959b).

Figure 6 - Some artificial ice nuclei.

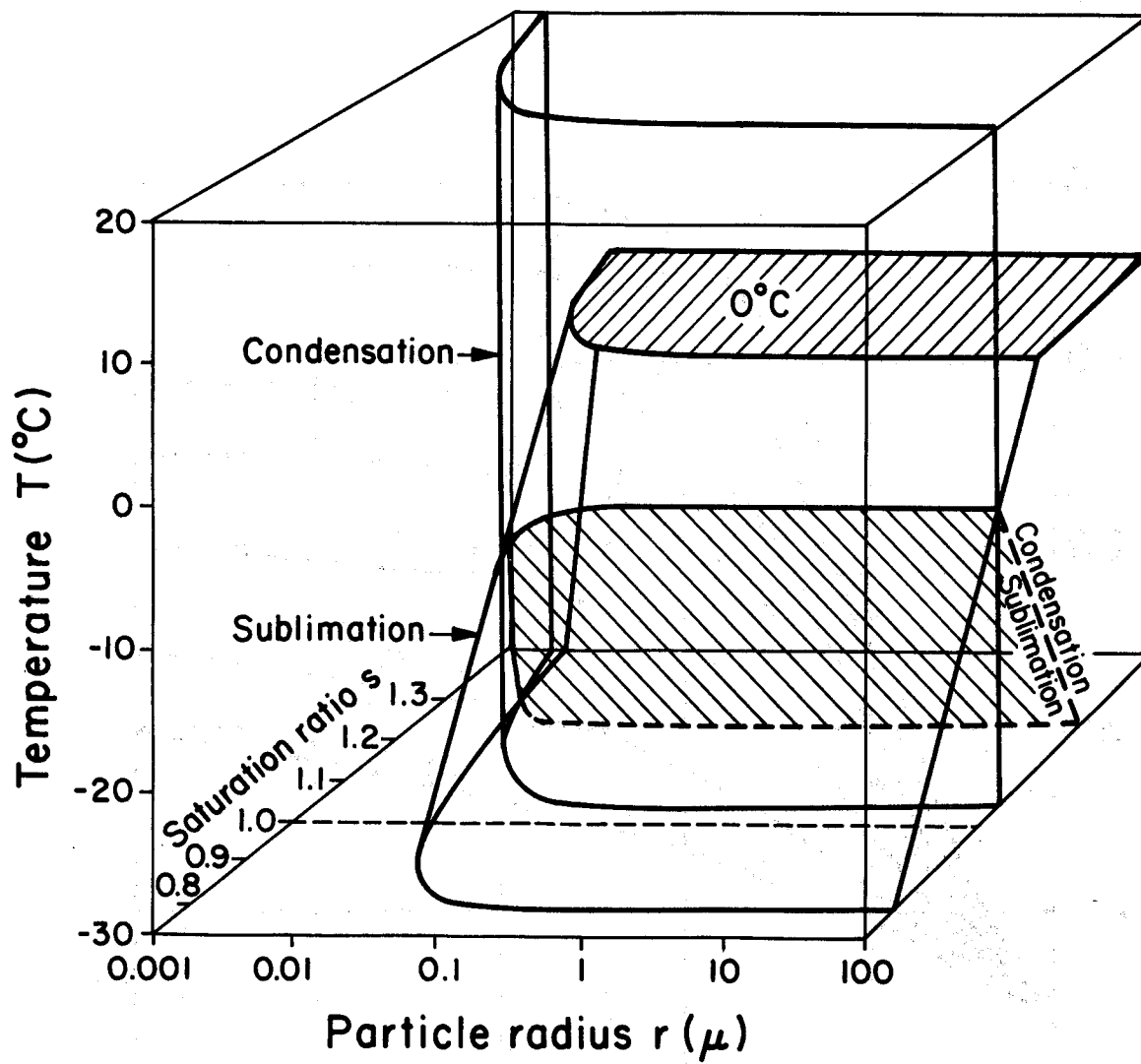
Figure 7 - Portion of phase diagram for water substance (Evans, 1967).



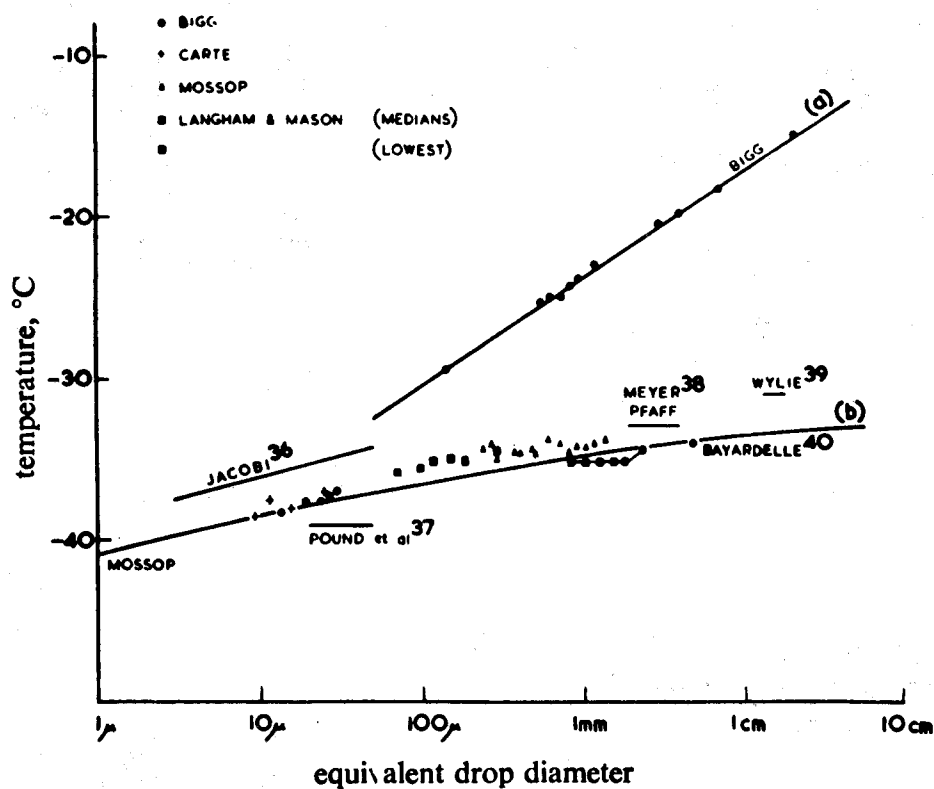
Lecture 3, Figure 1



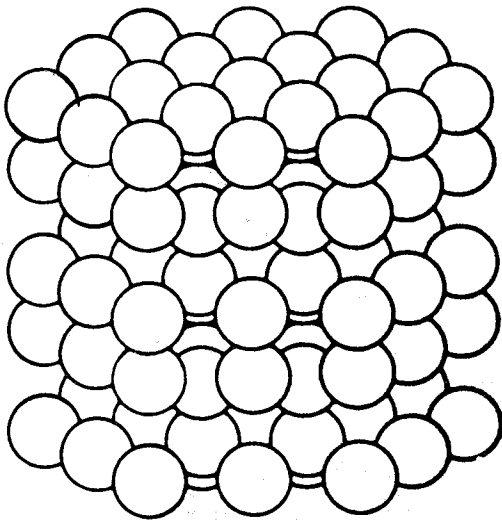
Lecture 3, Figure 2



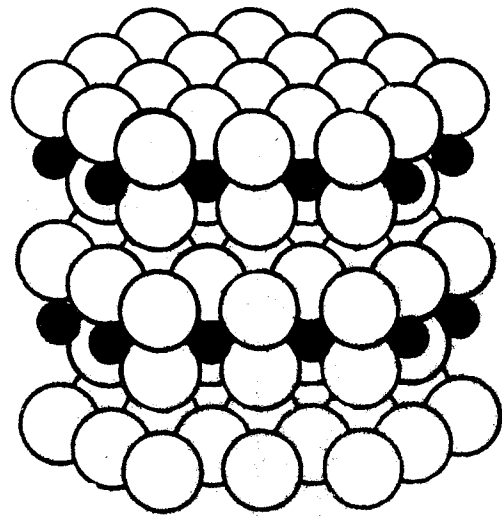
Lecture 3, Figure 3



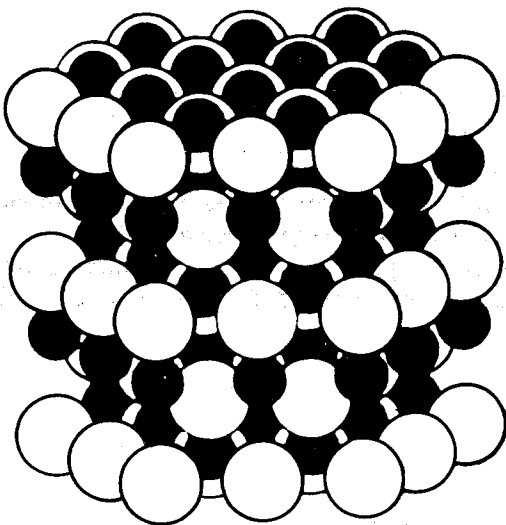
- (a).-- Bigg's relationship between the median freezing temperatures and the diameters of water drops containing foreign nuclei (heterogeneous nucleation).
- (b).—Median freezing temperatures for groups of droplets of very pure water having diameters $< 500\mu$ and the lowest freezing temperatures recorded for drops of $d > 500\mu$.



Ice

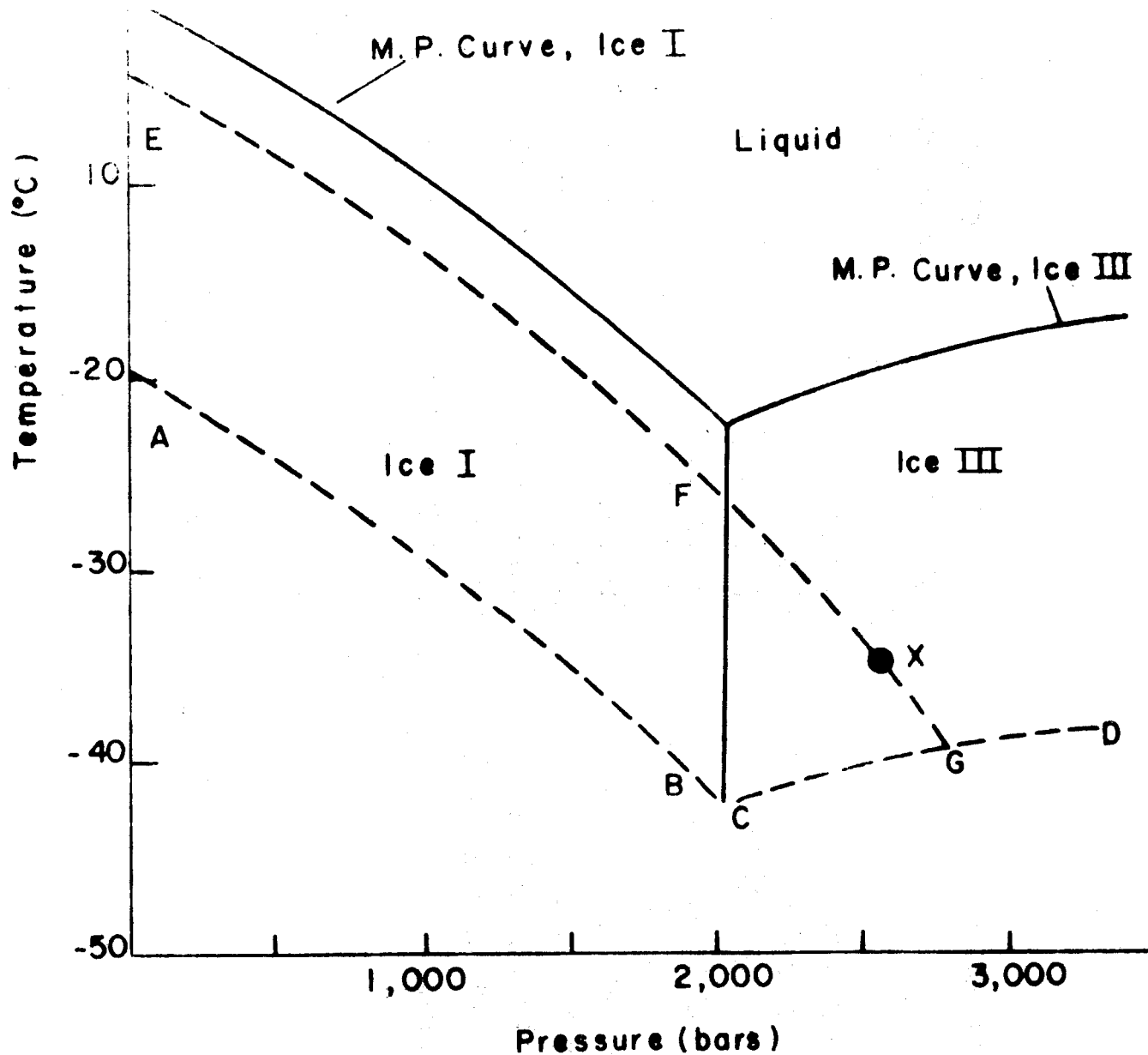


Lead iodide



Silver iodide

Substance	Crystal symmetry	Threshold temperature (°C)
Silver iodide	Hexagonal	— 4
Lead iodide	Hexagonal	— 6
Cupric sulphide	Hexagonal	— 6
Mercuric iodide	Tetragonal	— 8
Silver sulphide	Monoclinic	— 8
Ammonium fluoride	Hexagonal	— 9
Silver oxide	Cubic	— 11
Cadmium iodide	Hexagonal	— 12
Vanadium pentoxide	Orthorhombic	— 14
Iodine	Orthorhombic	— 14



Lecture 3, Figure 7

FULL LINES DENOTE PHASE BOUNDARIES BETWEEN ICE I, ICE III, AND THE LIQUID AS A FUNCTION OF TEMPERATURE AND PRESSURE. DASHED LINES DENOTE NUCLEATION LEVELS. AB, ICE I IN PURE WATER; CD, ICE III IN PURE WATER; EFG, ICE I IN SILVER IODIDE SUSPENSIONS.

IV. PROPERTIES AND DISTRIBUTION OF ICE NUCLEI IN THE ATMOSPHERE

A. Experimental techniques for investigating ice nuclei in the atmosphere

The accurate determination of the numbers and types of ice nuclei that will be activated in a natural cloud is inherently difficult for a variety of reasons. First the conditions under which ice nucleation can occur in the atmosphere are highly variable. The potential nuclei are exposed for various periods of time to different conditions of supersaturation and undercooling, depending on the particular synoptic, mesoscale and cloud conditions. Since nucleation is dependent to some extent on the past history of the particle, it is evident that nuclei which may not be activated in one situation may well be in another. Therefore, in order to use data obtained from measurements one should account for differences between the conditions to which the nuclei were exposed and the situation in which the data are to be applied. For example, the threshold temperature for activation by vapor deposition may differ considerably from that for ice nucleation from the liquid phase by a given nucleating agent.

Ice nuclei exist in the air both as free particles and embedded in cloud and precipitation particles. In the latter case, the particles may be collected and examined for ice nuclei. If the snow crystal is found to have a particle near its center this is usually assumed to be the ice nucleus on which the particle nucleated. The size and nature of the ice nucleus may be investigated by electron microscopy and micro-chemical analysis. The threshold temperature of the most efficient freezing nucleus in a snow crystal may be determined by melting the crystal, cooling it, and noting the temperature at which it nucleates.

Ice nuclei in suspension in the air have been studied using the following techniques:

(1) Isolating a quantity of air, cooling it below its dewpoint, and noting the freezing temperature of the condensation products.

(2) Allowing particles in the air in a cold box to settle onto a supercooled soap film (or sugar solution). The particles which act as freezing or contact nuclei at the temperature of the solution proceed to grow to visible ice crystals which can be counted.

(3) An air sample is introduced into an expansion chamber which is slowly pressurized and then suddenly expanded. The consequent cooling to temperature T activates those ice nuclei effective at temperature T or less. The ice particles which form in the chambers may be counted visually in a collimated light beam or allowed to settle out on a supercooled film.

(4) Using mixing chambers which are similar to the cold box technique with the major difference being found in the method of sampling the environmental air. The cold box uses a passive sampling system, in the sense that the box is open to the environment. The mixing chamber is a closed system into which the sample is drawn in, humidified and allowed to equilibrate. Nucleation detection is the same as those mentioned above.

(5) A known volume of air may be drawn through a millipore filter. The filter may subsequently be exposed to a known supersaturation and cooled to a given temperature and the number of ice crystals which form on the filter counted.

There are problems associated with each method of detection. For example, in the cold box, it is not known what proportion of the nucleating events occur as contact nucleation at the surface of the solution, and what proportion occur as vapor deposition nucleation in the air above the solution. The expansion chamber exposes the particles to the threshold temperature for only a short period; it is not known how long a nucleus should be exposed

before concluding that activation will not occur. The filter technique introduces the unknown influence of the filter base on the nucleation threshold.

B. Distribution and sources of ice nuclei in the atmosphere

The concentrations of natural ice nuclei show great variability in time and space. The nuclei count at a given temperature may vary by an order of magnitude during a period of one hour. Over longer periods of about a day the fluctuations in concentrations may be several orders of magnitude. During so-called ice nucleus "storms", ice nucleus concentrations an order of magnitude greater than normal may persist for many days.

On the average the local nucleus concentration can usually be fitted by a curve of the form $\ln N = a(T_1 - T)$ where N is the number of ice nuclei per liter of air activated at temperature T and " a " is a constant which varies between 0.3 and 0.8. T_1 is the temperature at which the concentration of ice nuclei is one per liter. Although T_1 varies with conditions, -20°C is a representative figure. Since there is normally a total of about 10^8 particles per liter in the air, only about one in 10^8 particles acts as an ice nucleus at -20°C . If " a " is given the value 0.6, the concentration of ice nuclei increases by an order of magnitude for each 4°C decrease in temperature.

Measurements of the concentrations of ice nuclei in the atmosphere in the vertical have given rather inconclusive results. Some show an increase with height, while others indicate no particular change with height. Results from measurements made in Australia indicate that the stratosphere acts as a source of ice nuclei, which observation, together with apparent correlations between periods of rainfall peaks and preceding meteor showers, led Bowen (1953) to suggest that meteoritic material might be an important source of ice nuclei in the earth's atmosphere.

Figure 1 (see end of Lecture #4) shows some measured ice nuclei concentrations against temperature for the northern and southern hemispheres using several different measuring techniques. There appears to be a real difference in the average concentration of nuclei in the two higher concentrations being observed in the northern hemisphere. The reason for this difference is probably the greater area of land in the northern hemisphere which is the most obvious source for ice nuclei in the atmosphere. The ice nucleating ability of various minerals have been tested in the laboratory. Some of the results of these measurements are shown in Figure 2 (see end of Lecture #4). It can be seen from these results that some silica and clay minerals are quite effective as ice nuclei and may be the primary sources of natural ice nuclei in the air. This conclusion receives support from the few observations which have been made on the composition of the central nuclei in snow crystals. In crystals collected in Michigan, Kumai (1961) found that 87% had clay mineral particles as the central nucleus. In Greenland 85% of the snow crystals had a clay particle as the central nucleus and one-half of these were kaolin. The diameters of the central nuclei ranged from 0.3 to 8 microns with a mean of 3 microns.

Figure 3 (see end of Lecture #4) shows the influence of wind direction on the concentration of ice nuclei at a site on the Pacific coast of Washington. The results support the hypothesis that the land is the major source of ice nuclei.

Some industries have been observed to emit ice nuclei into the atmosphere. Figure 4 (see end of Lecture #4) shows a wind rose of ice nucleus concentrations for Seattle, Washington, and two locations remote from urban industrial areas. The concentrations of ice nuclei in the city were much greater than those in the non-urban areas and reached maximum values when the wind was from the city center (SW of sampling site).

C. Effects of synoptic conditions on ice nuclei

The concentrations of ice nuclei in the air can vary rapidly with changing synoptic conditions. Figure 5 (see end of Lecture #4) shows an increase in ice nucleus concentrations by a factor of 50 during a rain shower. Figure 6 (see end of Lecture #4) shows increase in ice nucleus concentrations during the evaporation of fogs. The increase in ice nucleus count in a rain shower might be due to the release of ice nuclei by evaporating drops. In order for fogs to increase the concentrations of ice nuclei in the air during evaporation they would have to act as a sink for ice nuclei during formation.

As previously mentioned, increases in the concentrations of ice nuclei which exist for several days are termed ice nucleus "storms". An example of ice nucleus storms in Alaska and Washington are shown in Fig. 7 (see end of Lecture #4). Analysis of air trajectories coincident with this event showed that the particles were carried along in the air mass from Alaska to Washington. Significantly, the Japanese investigation of materials in these storms showed increases of nuclei of earth materials (Isono, et al., 1970). One such storm was traced back to a dust storm in the Mongolian desert. It is hypothesized the particles were carried on strong winds from Asia across the Pacific Ocean to the west coast of the United States.

D. Comparison of concentrations of ice nuclei and ice particles in natural clouds

Following Bergeron's suggestion on the role of ice crystals in producing precipitation in clouds, it was generally accepted that each ice particle in a cloud originates on an ice nucleus. However, recently several field observations have indicated that this is not always the case. Figure 8 (see end of Lecture #4) shows measurements of the concentrations of ice

particles and ice nuclei in natural clouds. It can be seen that there are many more ice crystals than ice nuclei for cloud top temperatures higher than about -20°C . However, as the temperature of cloud top decreases, the ratio of ice crystals to ice nuclei approaches unity. In regions of clouds where this ratio is greater than unity ice multiplication mechanisms may be occurring. One possible mechanism by which the number of ice particles in a cloud may increase without the action of ice nuclei is by the explosion or fragmentation of droplets during freezing. Such fragmentation produce a number of tiny ice splinters, each of which is capable of nucleating freezing in another droplet which can subsequently shatter, and so on. Recent experiments (Hobbs and Alkezweeny, 1968) suggest that a small fraction of cloud droplets might fragment during freezing. Other mechanisms of propagating ice in clouds are the mechanical breaking-up of ice crystals due to collisions and thermal shock when supercooled drops collide with and are nucleated by delicate ice crystals. It has also been suggested that cloud drops might shatter or fragment during freezing after colliding with ice particles in clouds. However, this seems unlikely since in this case freezing occurs from the ice substrate outwards and the stresses necessary for explosion and fragmentation are unlikely to build up.

Notes taken by:

M. J. Moore

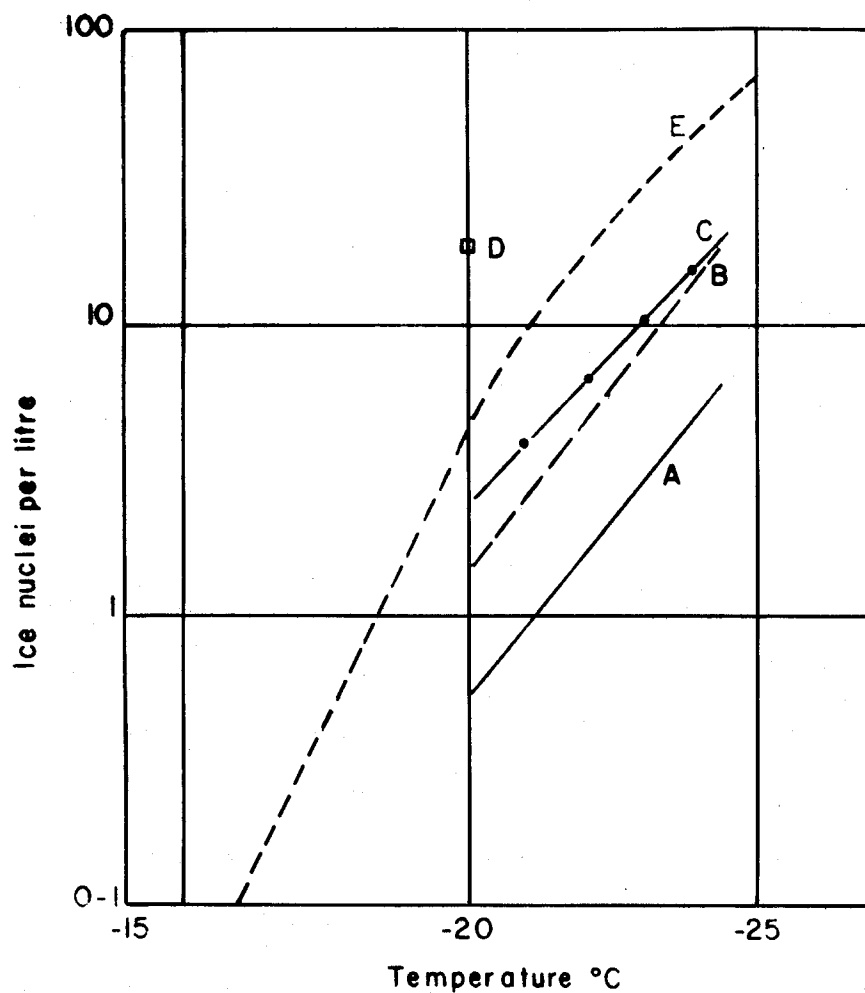
R. F. Perret

REFERENCES

- Bigg, E. K., Bull. Obs. Puy de Dome, 3, 89, 1960.
- _____ and Hopwood, S. C., J. Atmos. Sci., 20, 185, 1963.
- Bowen, E. G., Austr. J. Phys., 6, 490, 1953.
- Hobbs, P. V., J. Atmos. Sci., 26, 315, 1969.
- _____ and Alkezweeny, A. J., J. Atmos. Sci., 25, 881, 1968.
- _____, Bluhm, G. C., and Ohtake, T., Tellus 1970: in print.
- _____, and Locatelli, J. O., J. Atmos. Sci., 27, 90, 1970.
- Isono, K., Komabayasi, M., Takeda, T., Tanaka, T., and Iwai, K., Tellus 1970:
in print.
- Kumai, M., J. Met., 18, 139, 1961.
- Mossop, S. C., Z. Angew. Math. Phys., 14, 456, 1963.

Figure Captions

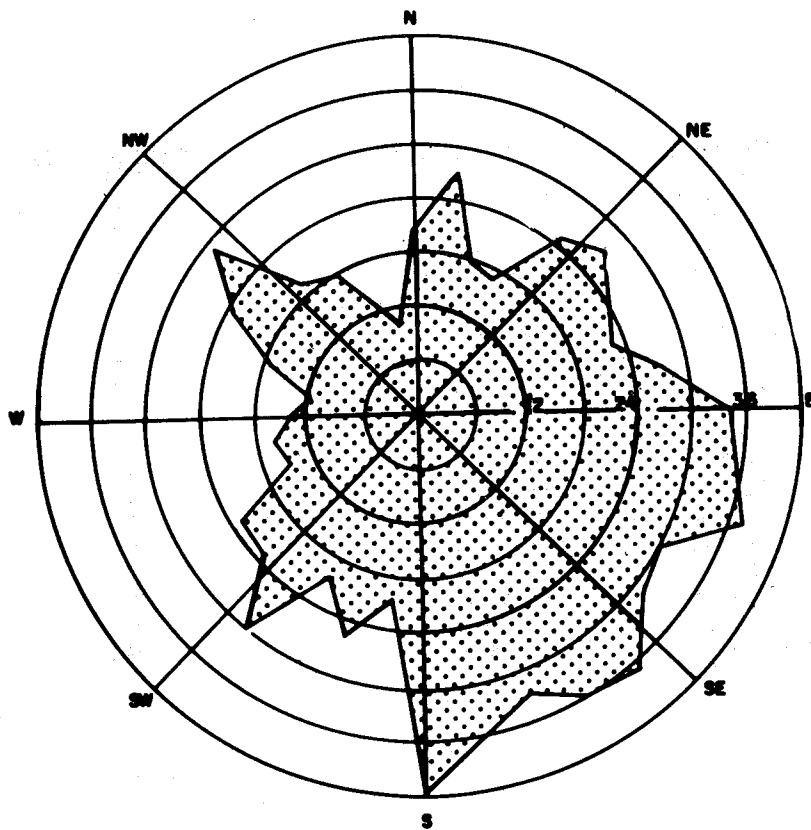
- Figure 1 - World-wide measurements of ice nuclei made during 1956-1960.
- Figure 2 - Threshold temperatures for ice nucleation of some earth minerals.
- Figure 3 - Wind rose of ice nucleus concentrations measured at a site on the
Pacific Coast of Washington (from Hobbs and Locatelli, 1970).
- Figure 4 - Wind rose of ice nucleus concentrations measured in a city (Seattle)
and two non-urban sites (from Hobbs and Locattelli, 1970).
- Figure 5 - Variations in ice nucleus concentrations with weather conditions
(from Hobbs and Locattelli, 1970).
- Figure 6 - Variations in ice nucleus concentrations during the evaporations
of fogs (from Hobbs and Locattelli, 1970).
- Figure 7 - Ice nucleus storms in Alaska and Washington (from Hobbs et al., 1970).
- Figure 8 - Measurements of the concentrations of ice particles and ice nuclei in
natural clouds (from Hobbs, 1969).



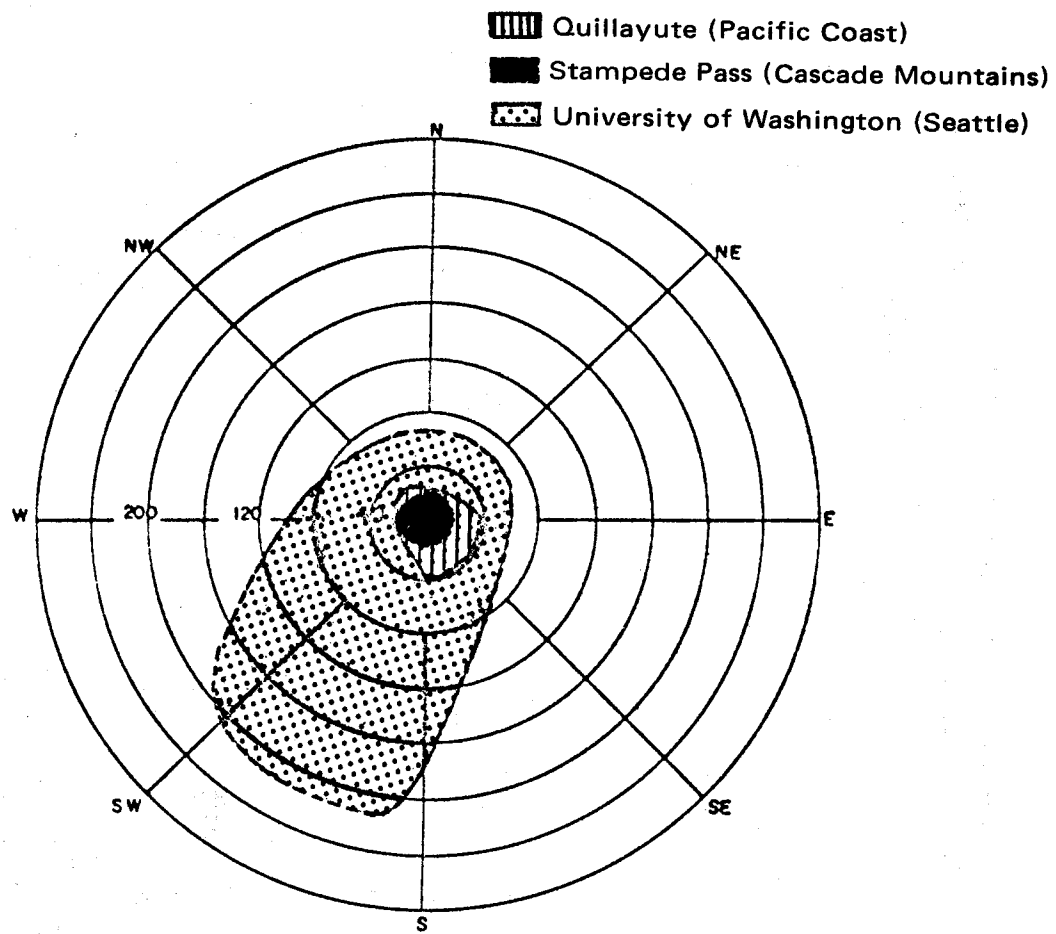
AVERAGE ICE NUCLEUS CONCENTRATIONS IN THE
NORTHERN AND SOUTHERN HEMISPHERES (FROM MOSSOP, 1963).
A SOUTHERN HEMISPHERE, EXPANSION CHAMBER, BIGG (1960).
B SOUTHERN HEMISPHERE, MIXING CHAMBER, BIGG (1960).
C NORTHERN HEMISPHERE, EXPANSION CHAMBER, BIGG (1960).
D NORTHERN HEMISPHERE, MIXING CHAMBER, BIGG (1960).
E ANTARCTICA, MIXING CHAMBER, BIGG AND HOPWOOD (1963).

Lecture 4, Figure 1

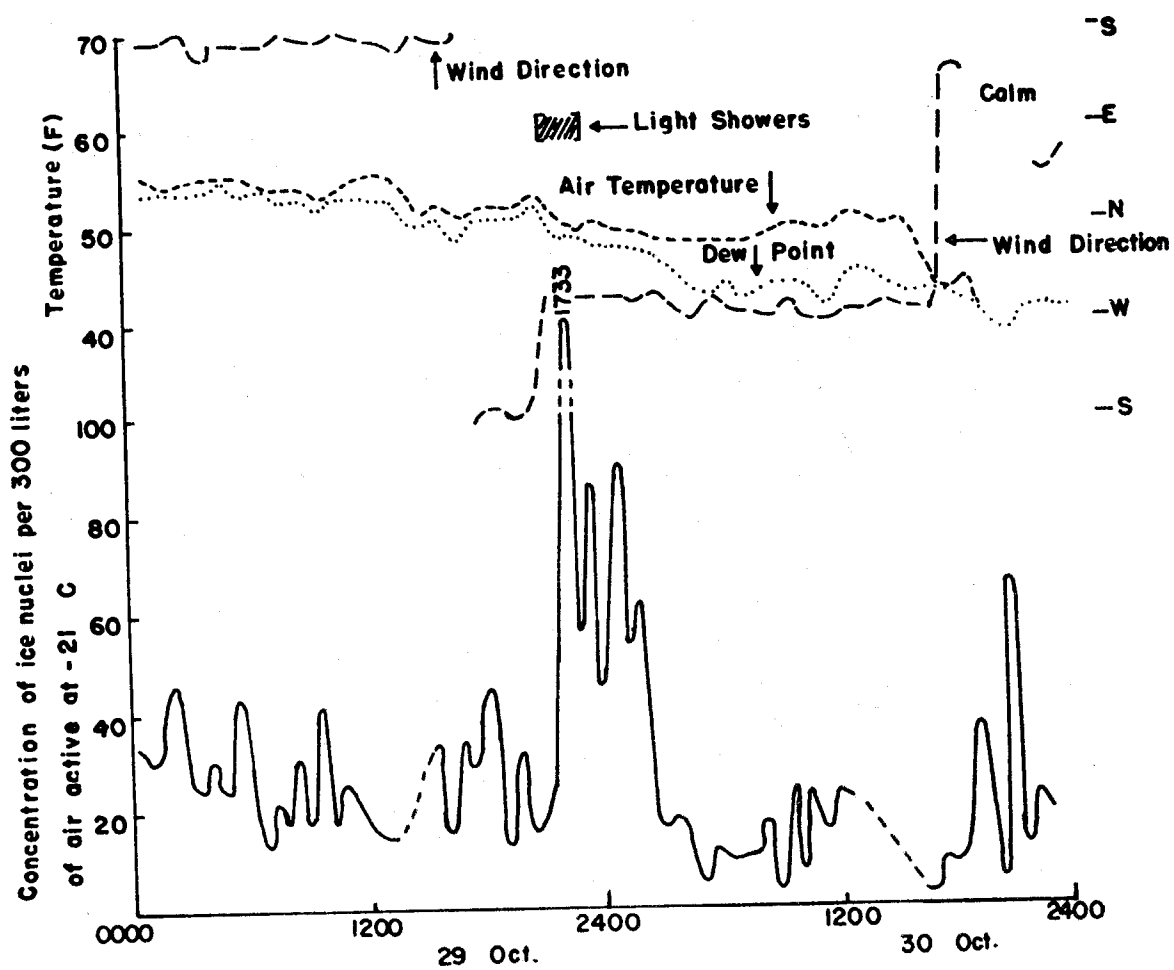
<u>Substance</u>	<u>Crystal Symmetry</u>	<u>Threshold Temperature</u> (°C)
Ice crystal	Hexagonal	0
Covellite	Hexagonal	- 5
Vaterite	Hexagonal	- 7
Beta tridymite	Hexagonal	- 7
Magnetite	Cubic	- 8
Anauxite	Monoclinic	- 9
Kaolinite	Triclinic	- 9
Illite	Monoclinic	- 9
Glacial debris		-10
Hematite	Hexagonal	-10
Brucite	Hexagonal	-11
Gibbsite	Monoclinic	- 11
Halloysite	Monoclinic	- 12
Volcanic ash	--	- 13
Biotite	--	- 14
Vermiculite	Monoclinic	- 15
Phlogopite	--	- 15
Nontronite	Monoclinic	- 15



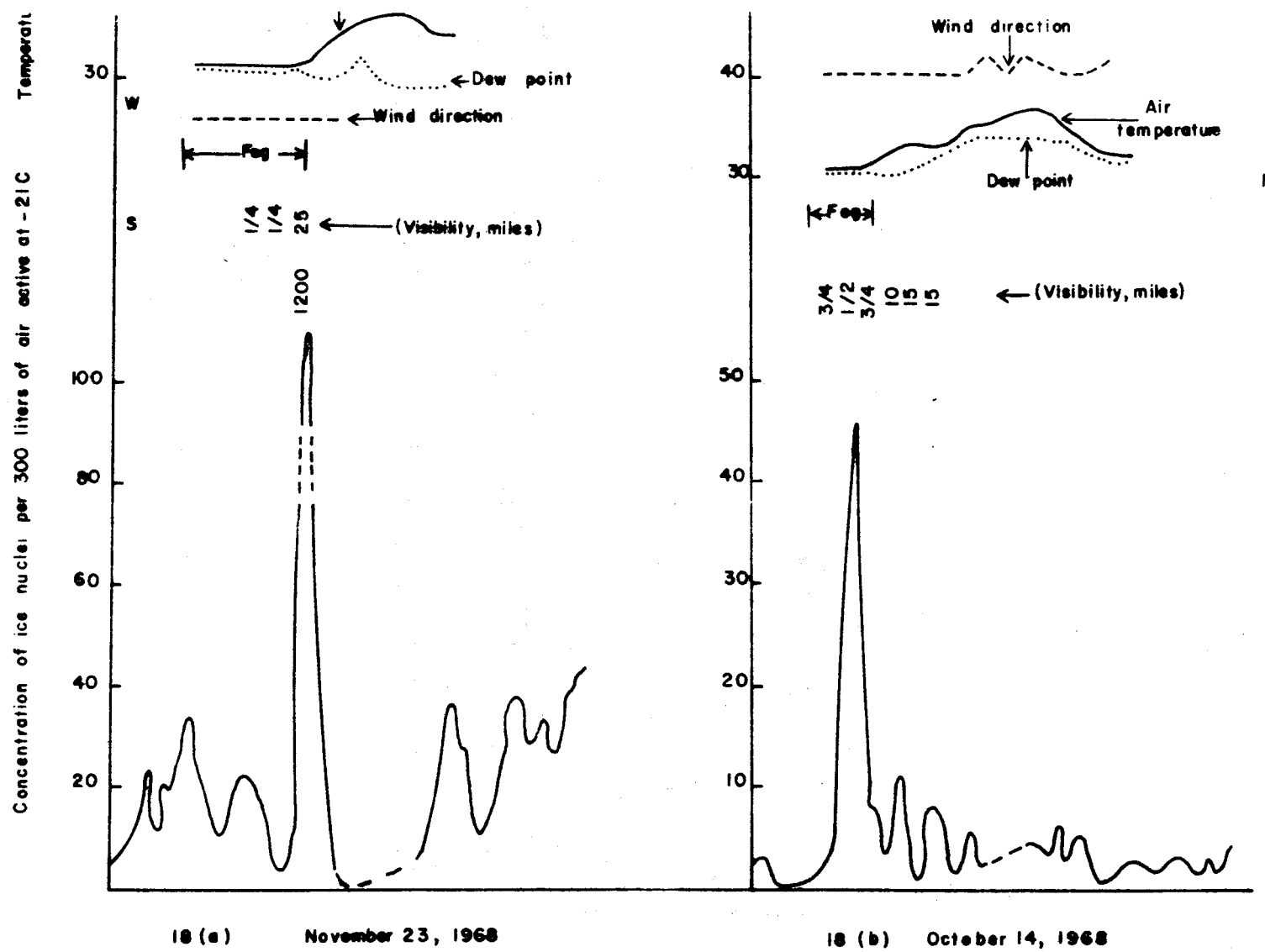
Lecture 4, Figure 3



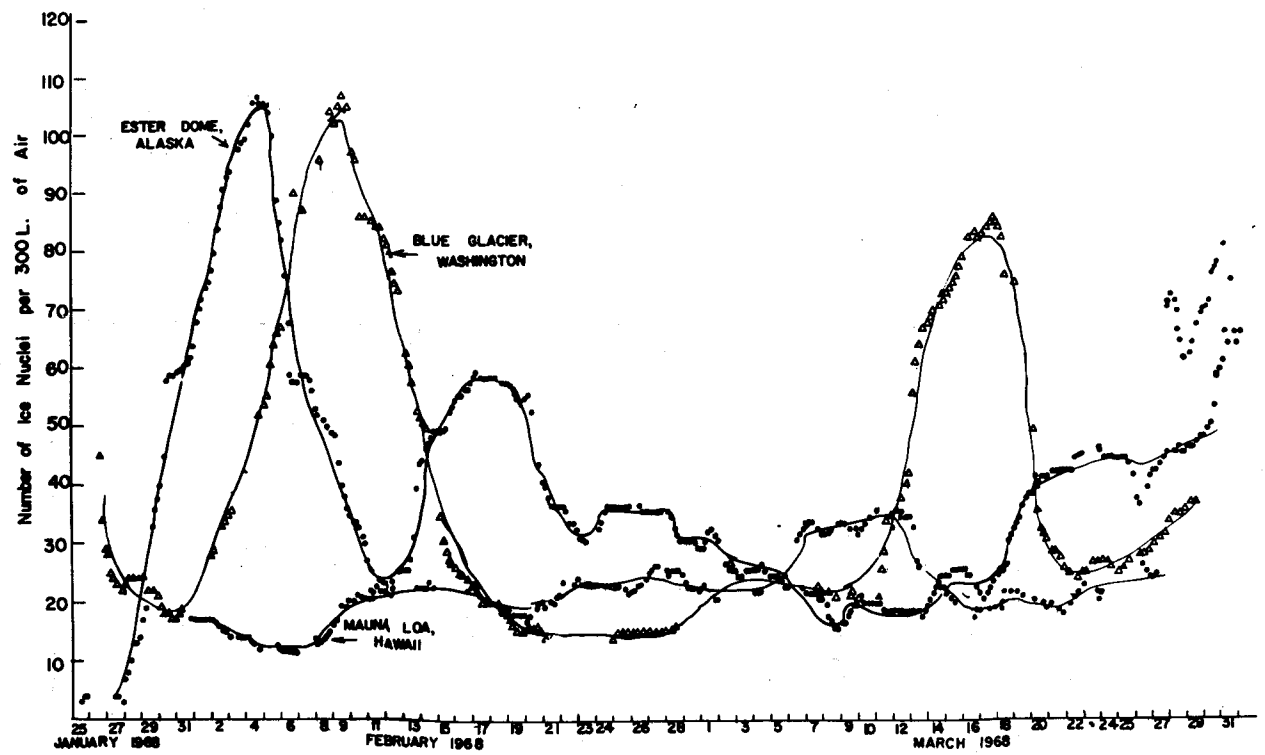
Lecture 4, Figure 4



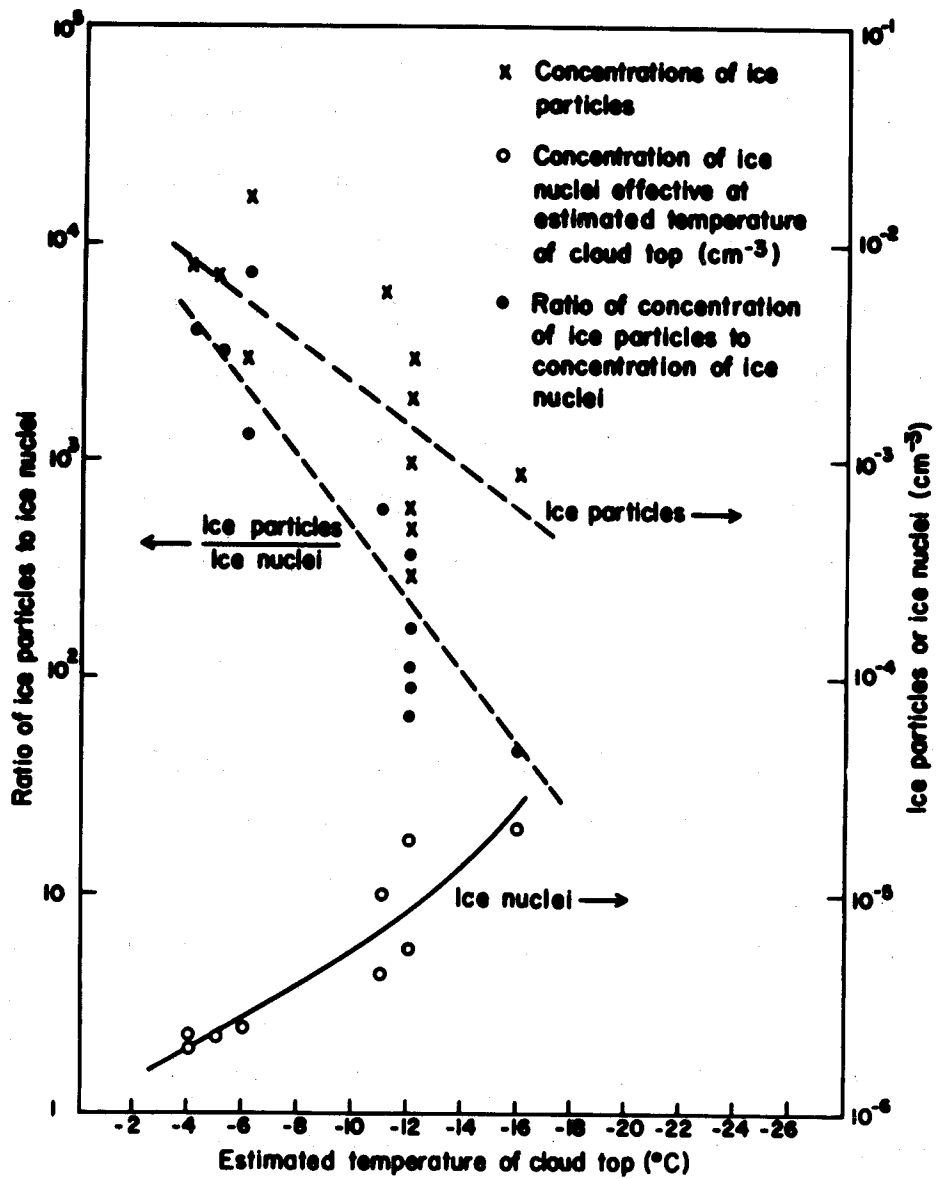
Lecture 4, Figure 5



Lecture 4, Figure 6



Lecture 4, Figure 7



Lecture 4, Figure 8

V. GROWTH OF ICE CRYSTALS

A. Role of ice crystals in clouds

One of the most important aspects of cloud physics that needs detailed study is the physical processes that produce precipitation. We now consider the suggestion first put forward by Franklin (1789), and developed by Wegener (1911) and Bergeron (1935), that most of the precipitation reaching the ground originates as ice crystals in supercooled clouds. This process is probably dominant in the formation of precipitation in temperate latitudes and in the interior of continents where the growth of precipitable particles by coalescence may be limited (see Lecture 2).

To understand the Wegener-Bergeron mechanism, it is necessary to study in detail the germination and the growth of ice crystals in clouds. In the previous lecture we discussed the origin of the ice crystals; in this lecture we will consider the mechanisms by which they may increase in size.

Ice crystals can grow by the direct condensation of water from the vapor phase, by aggregation, and by the accretion of water droplets. Each of these processes is considered in turn below.

B. Growth of ice crystals by condensation from the vapor phase

We may assume that ice crystals in subfreezing clouds are initially formed by condensation and freezing (or by deposition) on to active ice nuclei, or as somewhat larger crystals by the freezing of cloud droplets. At temperatures just below 0°C the concentrations of ice crystals in clouds is comparatively low; also the difference between the saturation vapor pressure over ice and liquid water is small so that the growth rate of an ice crystal at these temperatures is little different from that of a cloud droplet. However, as the temperature is lowered the number of ice particles in a cloud

will increase and they will grow more rapidly than the cloud droplets since the saturation vapor pressure over ice is less than that over liquid water at the same temperature. For example, at -10°C air that is saturated with respect to liquid water is supersaturated relative to ice by 10% and at -20°C by 21%.

The rate of growth of an ice crystal by deposition from the vapor phase is given by $dM/dt = 4\pi CGS$ where, M is the mass of the ice crystal, S the supersaturation of the environment with respect to ice, C the electrostatic capacity of the crystal, and G is a temperature dependent function. The rates of growth of ice crystals by deposition in an environment at water saturation calculated from this equation are shown in Fig. 1 (see end of Lecture #5).

The curves in Fig. 1 show that by growing by deposition alone an ice crystal may reach a mass of a few tens of micrograms at -5°C (or, assuming the crystal to be a dendritic plate, it will grow to a diameter of about 2mm) in about 30 minutes. Such a crystal has a terminal velocity of about 30cm/sec and would be unable to fall toward the ground in the vigorous updrafts which exist in active cumulus clouds. In less active clouds such a crystal might reach ground level as precipitation. Therefore, growth of ice crystals by condensation alone is insufficient to explain precipitation in active cumulus clouds.

C. Growth by aggregation of ice crystals

Rough calculations show that a plate having an initial diameter of 1mm can grow by collecting other crystals (in concentration of $1\text{gm}/\text{m}^3$) to a diameter of 1 cm in about 20 minutes. Such a crystal has a fall velocity of about 150 cm/sec and can therefore fall out in moderate updrafts. Hence, with updrafts of about 100 cm/sec, cloud depths of about 1500 m, and fairly

high concentrations of ice particles, particles can grow to precipitable size in about 40 minutes by a combination of deposition and aggregation.

The mechanism by which ice particles adhere together is of interest. It is observed that when two ice particles are kept in contact for a few minutes, they stick together and some force is required to separate them. The force that is required to separate two ice spheres at ice saturation is shown as a function of temperature in Fig. 2 (see end of Lecture #5). It is clear from the figure that the force of adhesion decreases with decreasing temperature. The explanation for this adhesion of ice particles and its variation with temperature has been given by Hobbs and Mason (1964).

If two spheres are kept in contact for a few minutes a solid neck of ice forms between them due to sintering. This neck grows with time as shown in Figs. 3 and 4 (see end of Lecture #5) and it welds the particles into contact.

D. Accretion of droplets

In a supercooled cloud we must also consider the growth of ice particles due to the accretion of supercooled droplets. Rough calculations indicate that the collision efficiency of an ice crystal 1mm in diameter for droplets greater than 10μ diameter is reasonably high. With a collection efficiency of about 0.5, it can be shown that an ice crystal can grow to a spherical shape of about 1mm in radius in about 30 minutes. This will have a terminal velocity of about 100 cm/sec, and will be able to fall through moderate updrafts in clouds to reach the ground as precipitation.

E. Ice crystal habits

Observations both in the field and the laboratory have shown that ice crystals may grow in a variety of habits, the basic shapes of which are determined mainly by temperature (Nakaya, 1951). This fact is demonstrated

by growing ice crystals in a diffusion chamber. The crystals are grown on a thin fiber which hangs vertically in a chamber in which the gradients of temperature and supersaturation are accurately controlled. (see Fig.5 at the end of Lecture #5).

The crystal habit varies along the length of the fiber in the following manner (Hallett and Mason, 1958):

0 to -3°C	Thin hexagonal plates
-3 to -5°C	Needles
-5 to -8°C	Hollow prismatic columns
-8 to -12°C	Hexagonal plates
-12 to -16°C	Dendritic, fern-like crystals
-16 to -25°C	Hexagonal plates
-25 to -50°C	Hollow prisms

Some photographs of different ice crystals in the diffusion cloud chamber are shown in Figs. 6,7 and 8. (see end of Lecture #5).

The effect of suddenly changing the temperature and supersaturation on the growth habit of a particular crystal may be observed simply by raising or lowering the fiber in the chamber. When a crystal is transferred to a new environment, the continued growth assumes a new habit characteristic of the temperature of the environment. For example, Fig. 7 shows a case where needles were grown at -5°C and were then lowered in the chamber to where the temperature was about -14°C , stars then grew on the ends of the needles.

If a crystal grows under thermodynamic equilibrium the shape of the crystal can be predicted from Wulff's theorem which states that in equilibrium the distance of any crystal face from the center of the crystal is proportional to the surface energy of the face. Exact values of the surface energies for different faces of ice are not known. However, approximate

values can be calculated by assuming that the molecules in ice interact only with their nearest neighbors. Using these values it may be shown from Wulff's theorem that ice crystals should grow in the form of rather thick hexagonal plates in which the ratio (ℓ/r) of the thickness of the plate to the radius of the circumscribed circle about the hexagonal end is 0.82. Some ice crystals are in the shape of hexagonal prisms but at different temperatures ℓ/r takes on values from less than 0.1 to greater than 10. We conclude, therefore, that ice crystals do not grow under equilibrium conditions but are probably controlled by surface kinetic effects. Considerable insight into the mechanism by which ice crystals grow has been obtained from studies of the epitaxial growth of ice crystals using the apparatus shown in Fig. 9 (see end of Lecture #5).

Hallett (1961) found that when ice crystals grew epitaxially on the basal plane of cupric sulfide (CuS) the crystals thicken in a direction normal to the basal plane by steps of ice (a few 100 Å in height) sweeping across the basal plane. The velocity of these steps varied with temperature in the manner shown in Fig. 10 (see end of Lecture #5). It is believed that the relative growth velocities of such steps on the basal and on the prism faces determine the habit of ice crystals growing from the vapor phase. Thus, if at a particular temperature the velocity on the basal plane were greater than that on the prism face prisms would form, and if the reverse were true plates would form. The velocities of steps on the prism face of ice have not been measured. However, if we postulate that this velocity varies with temperature in the manner indicated by the dotted line in Fig. 9, then the basic changes in ice crystal habit with temperature would be explained. For example, between about -3 and -8°C the velocity of steps on the basal plane would exceed that on the prism face and the ice crystals would grow prism-like

as observed experimentally. However, this theory does not explain the more complicated habits such as dendrites.

Notes taken by:

J. Presley

M. R. Rao

REFERENCES

- Bergenson, T., 1935. Proc. 5th Assembly U.G.G.I., Lisbon, 2, 156.
- Franklin, B., 1789. Memo. Manch. Lit. and Phil. Soc., 2, 374.
- Hallett, J., 1961. Phil. Mag., 6, 1073.
- _____ and B. J. Mason, 1958. Proc. Roy. Soc., A247, 440.
- Hobbs, P. V. and B. J. Mason, 1964. Phil. Mag., 9, 181.
- Houghton, H. G., 1950. J. Met., 7, 363.
- Jensen, D. C., 1956. M.Sc. Thesis, Penn. State Univ.
- Mason, B. J., 1962. Clouds, Rain and Rainmaking, Cambridge Univ. Press.
- Nakaya, U., 1951. Compendium of Met., 207.
- Shaw, D. and B. J. Mason, 1955. Phil Mag., 46, 249.
- Wegener, A., 1911. Thermodynamik der Atmosphere. Barth (Leipzig).

FIGURE CAPTIONS

Figure 1 - Growth of ice crystals by deposition in a cloud at water saturation
(A) plane dendritic crystal at -15°C (B) hexagonal plate at -5°C (from Houghton 1950).

Figure 2 - Force required to separate ice spheres at ice saturation against temperature (from Jensen, 1956).

Figure 3 - Two ice spheres placed in contact at -6°C .

Figure 4 - Same two ice spheres as in Fig. 3 sometime later.

Figure 5 - Diffusion cloud chamber.

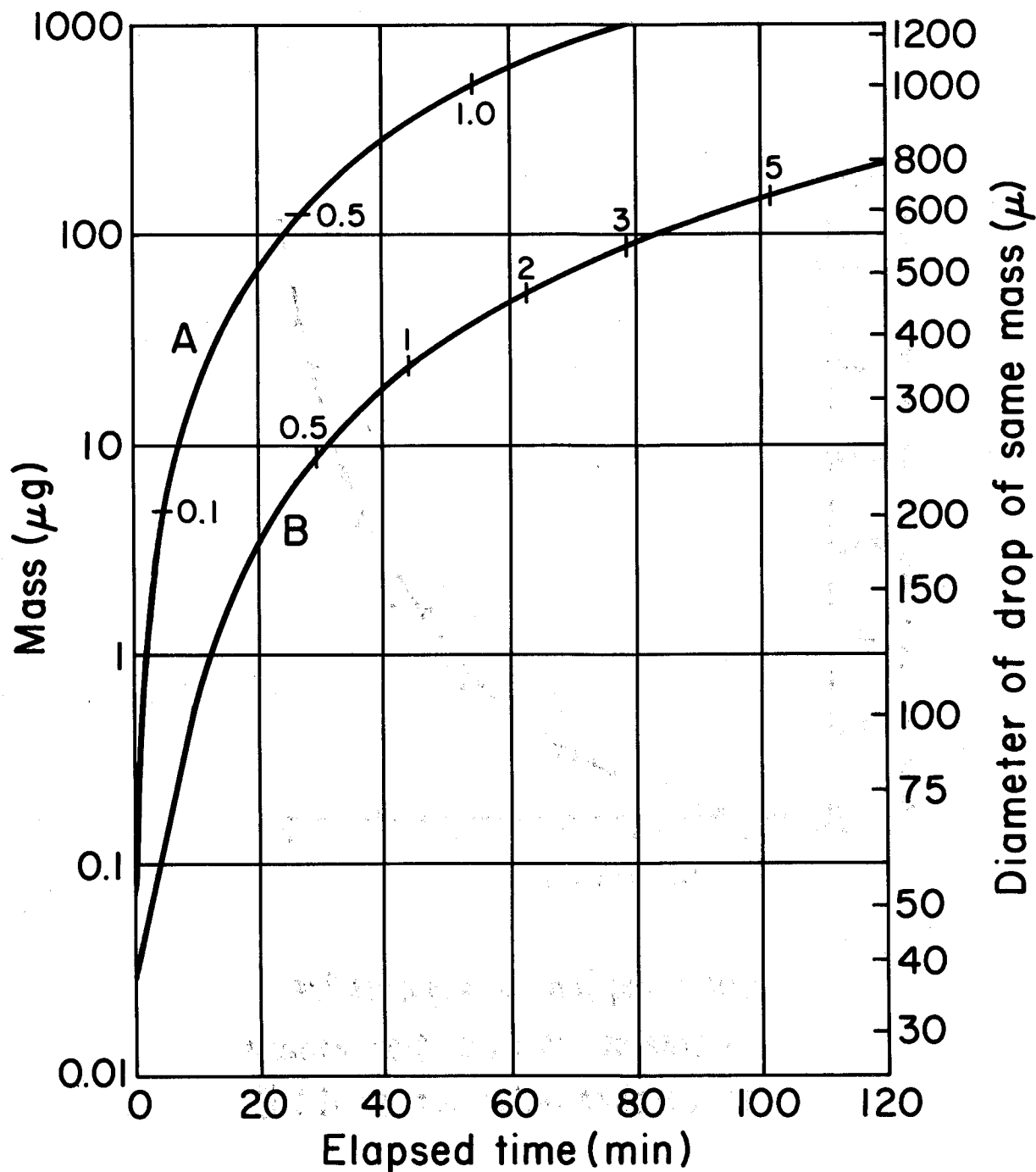
Figure 6 - Ice crystals of differing shapes growing on a filament suspended in a diffusion chamber with controlled temperature gradient. The crystals take characteristic forms at different temperatures as indicated along the right edge of the photograph. Reading from the top, the symbols represent: thin hexagonal plates, needles, hollow prismatic columns, hexagonal plates, branched fern-like crystals (or dendrites), and hexagonal plates. At temperatures below -25°C , prisms appear again (from Mason, 1962).

Figure 7 - Hollow prismatic columns (from Mason, 1962).

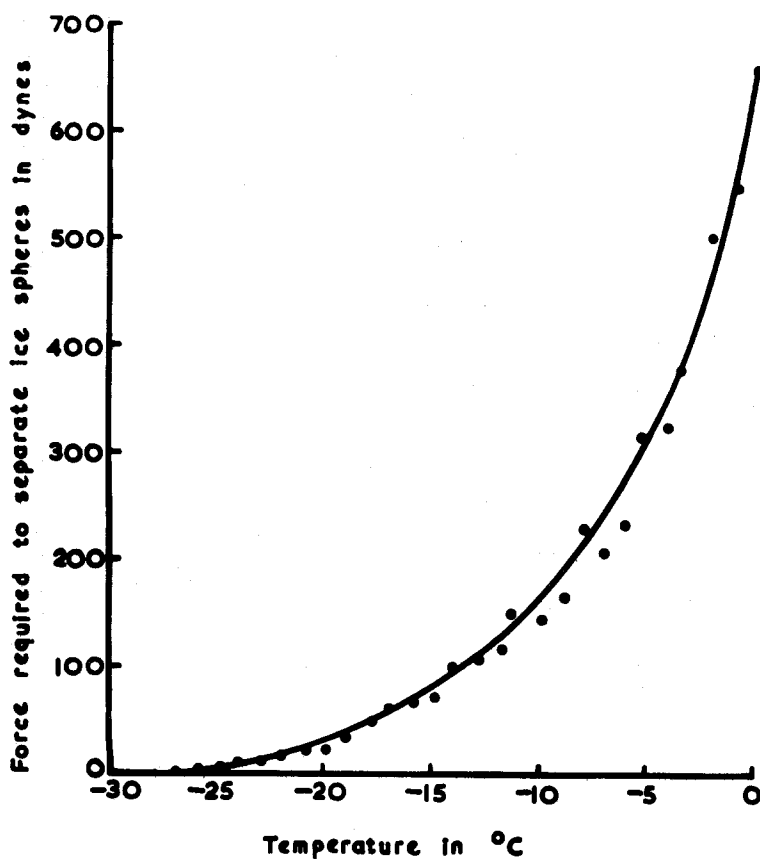
Figure 8 - Crystal hybrids showing how the form is dictated by temperature. Needles grown at -5°C developed stars on the ends when shifted to a temperature of -14°C (from Mason, 1962).

Figure 9 - Apparatus for studying epitaxial growth of ice crystals (from Shaw and Mason, 1955).

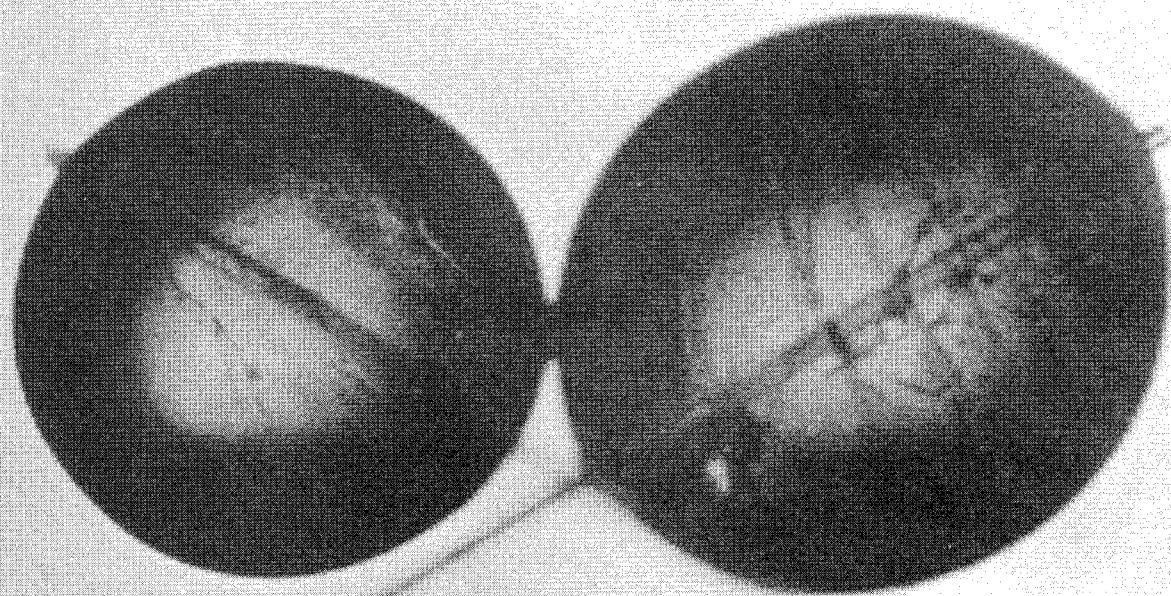
Figure 10 - Velocity of steps on ice as a function of temperature. _____ Basal plane (measured); - - - - - Prism face (postulated).



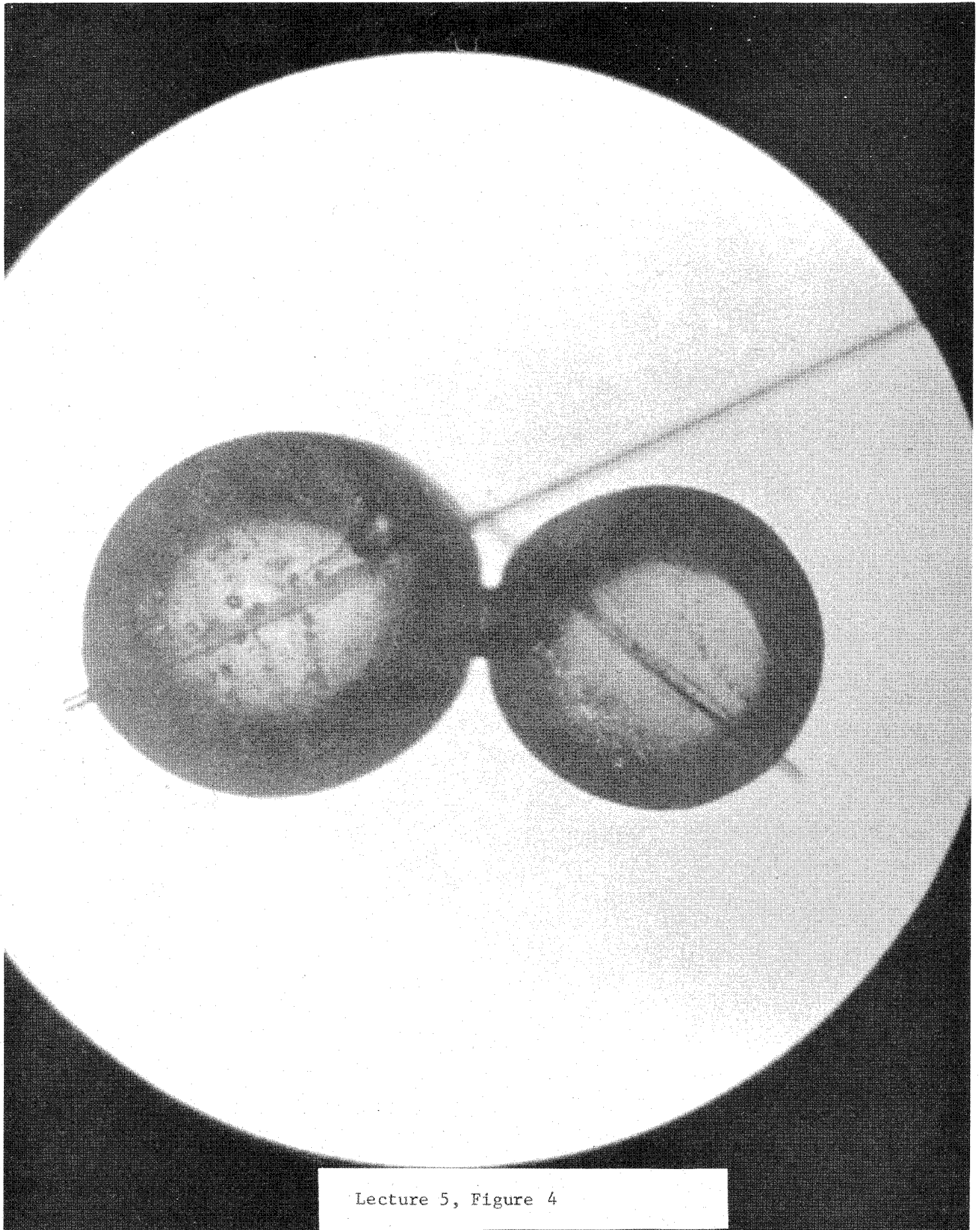
Growth of ice-crystals by sublimation in a cloud at water saturation. A: plane dendritic crystal at -15 C; B: hexagonal plate at -5 C. Figures entered at intervals along curves give fall distances in kilometres(after Houghton, 1950).



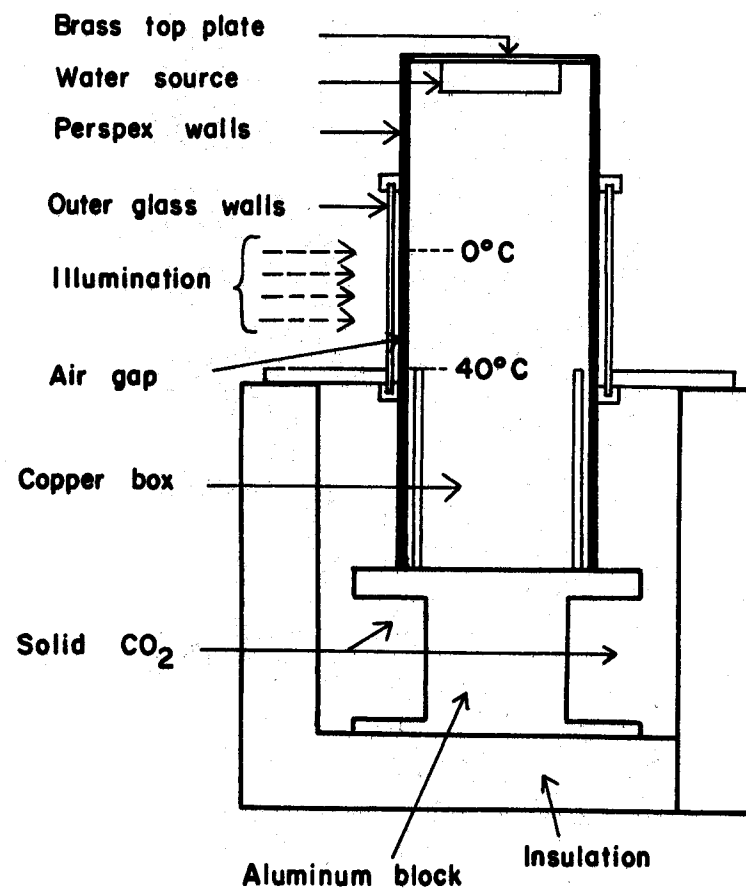
**Force required to separate ice
spheres at ice saturation against
temperature (after Jensen, 1956)**



Lecture 5, Figure 3

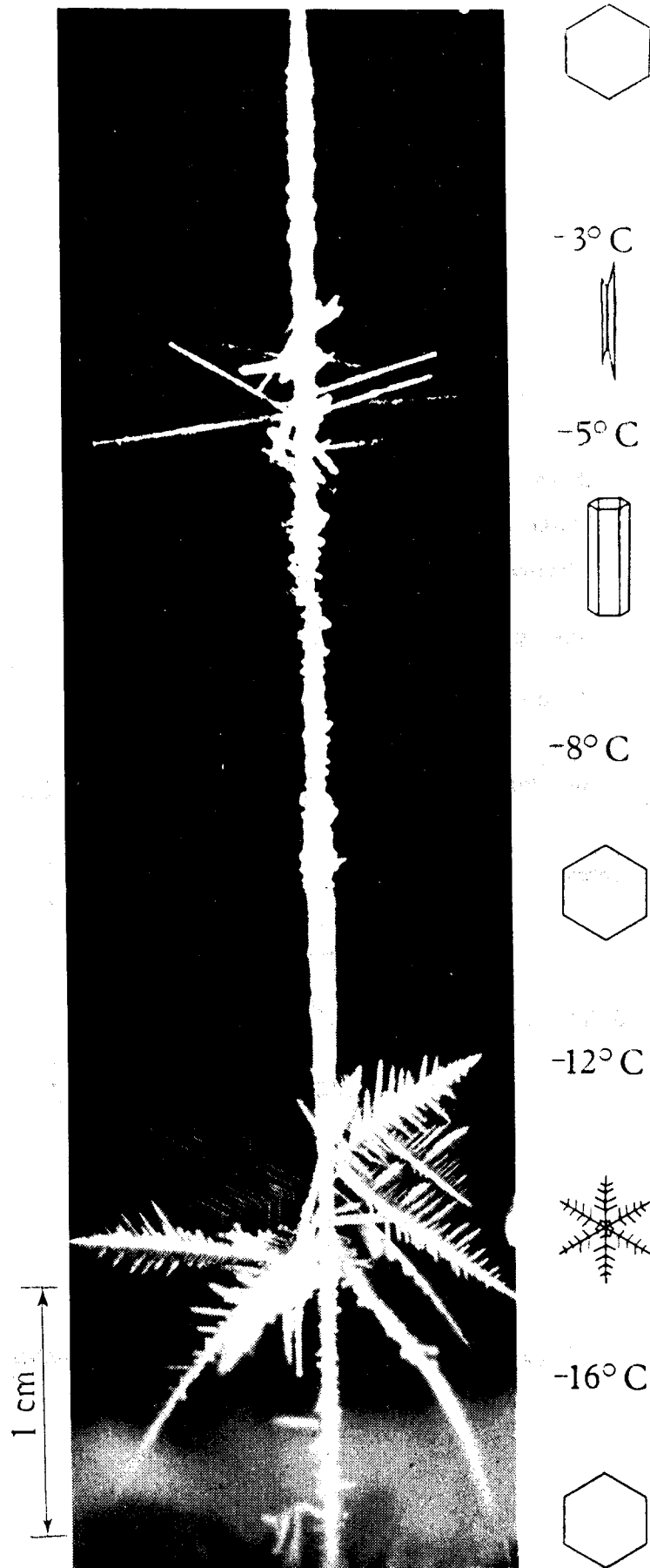


Lecture 5, Figure 4



Lecture 5, Figure 5

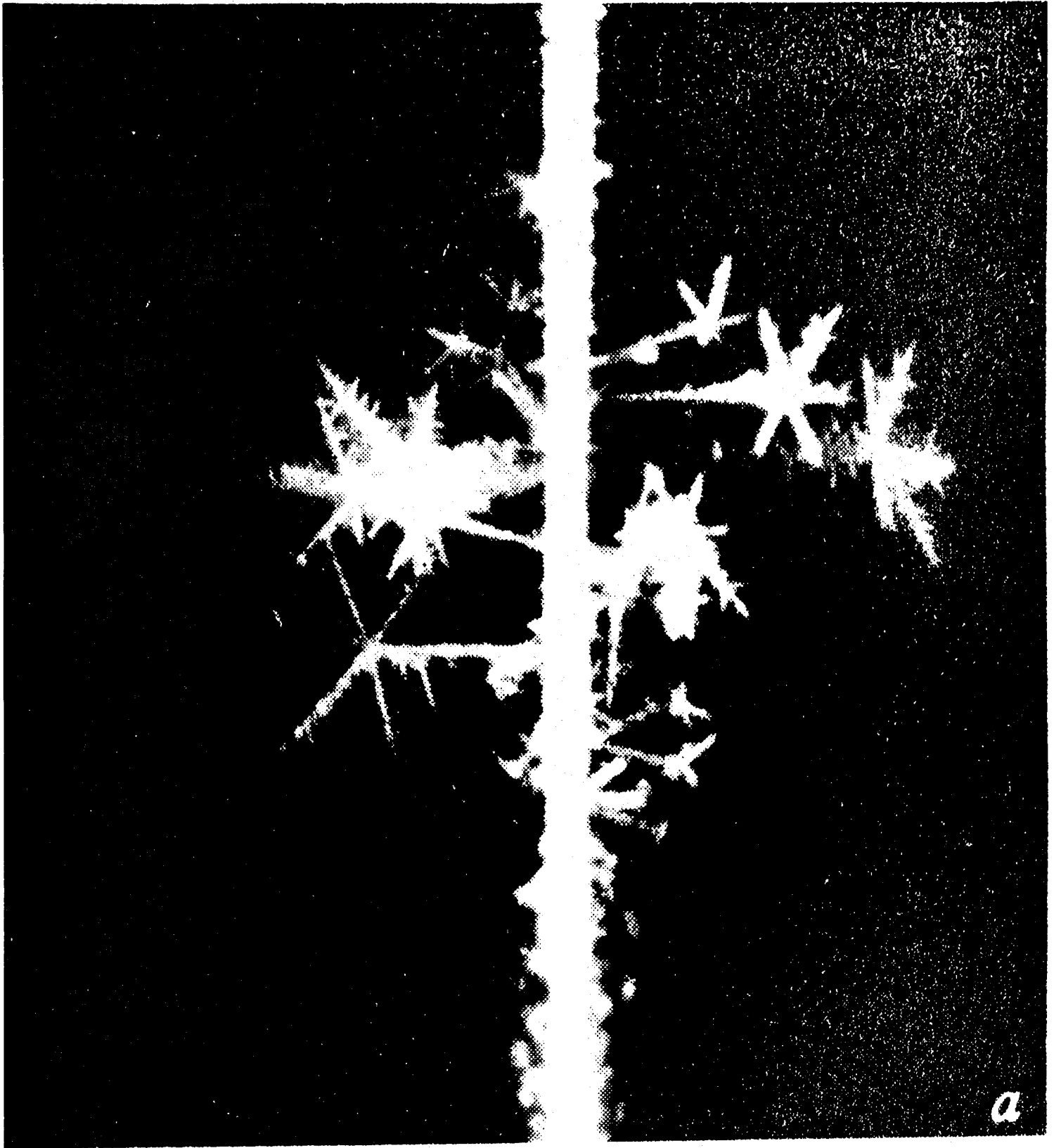
The diffusion cloud chamber



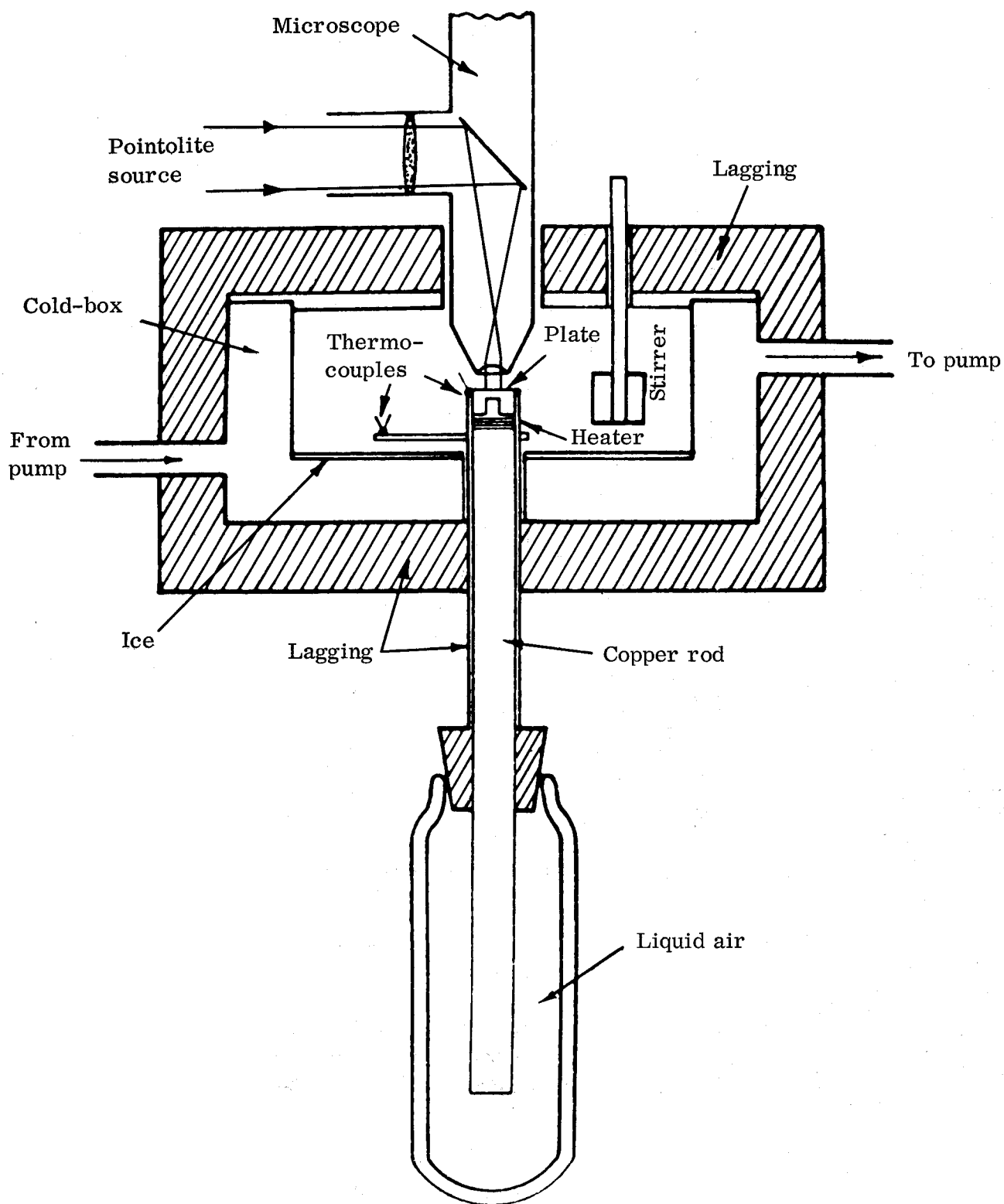
Lecture 5, Figure 6



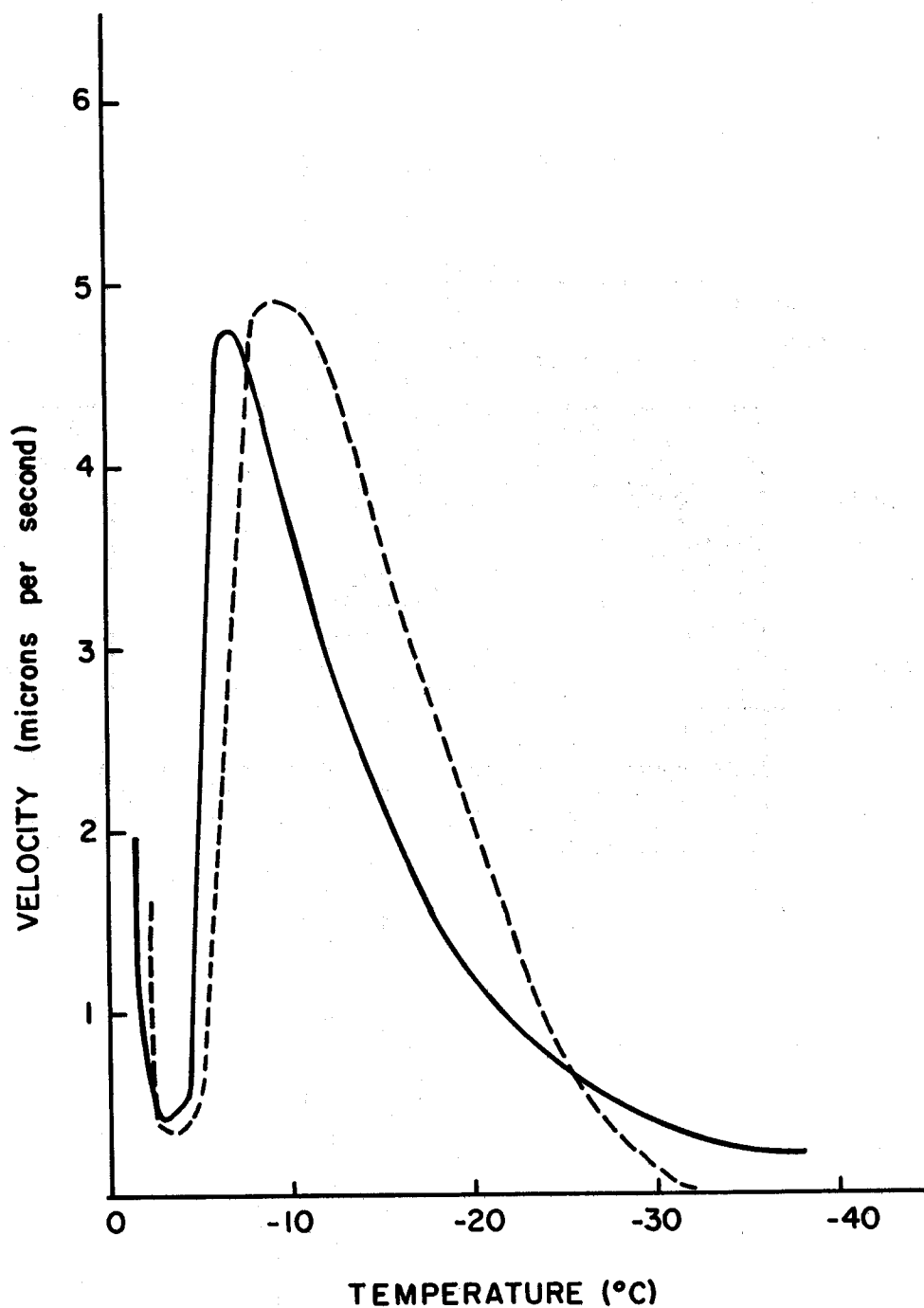
Lecture 5, Figure 7



Lecture 5, Figure 8



Lecture 5, Figure 9



Velocity of steps on ice as a function of temperature. — Basal plane (measured); - - - - Prism face (postulated).

VI. CLOUD ELECTRIFICATION

In this lecture an outline is given of several theoretical models which have been proposed to explain the generation and separation of electrical charges in clouds and thunderstorms and some experimental evidence for and against these models is presented.

A. Requirements of a satisfactory theory of thunderstorm charge generation

Mason (1953) has listed the conditions which a satisfactory theory of thunderstorm electrification must meet. They are:

1. The average duration of precipitation and lightning from a single-cell thunderstorm is about 1/2 hour.
2. The average electric moment destroyed in a lightning flash is about 110 coulomb km. Corresponding charge is 20 to 30 coulombs.
3. The magnitude of the charge being separated immediately after a flash, by virtue of the fall speed v of the precipitation elements, is of the order of $(8000/v)$ coulombs, where v is in m/sec.
4. In a large extensive thundercloud this charge is generated and separated in a volume bounded by the -5 and -40°C levels and has a radius of about 2 km.
5. The negative charge is centered near the -5°C level while the main positive charge is situated some kilometers higher up, near the -20°C level.
6. Charge generation and separation processes are closely associated with the development of precipitation in the ice phase (probably soft hail). These precipitation particles must be capable of falling through upcurrents of several meters per second.
7. Sufficient charge must be generated and separated to supply the first lightning flash within 12 to 20 mins. after the appearance of precipitation particles of radar-detectable size.

8. Rate of generation of charge is about $1 \text{ C km}^{-3} \text{ min}^{-1}$ (1000 C in 50 km^3 in 20 min).

Some workers might question these requirements on two grounds, namely, that lightning sometimes occurs in warm clouds and that convective activity and not precipitation may be the prerequisite for charging.

An adequate theory of thunderstorm electrification based on the hypothesis that precipitation is responsible for generation and separation of the charge must explain how the heavier precipitation elements acquire a negative charge and the smaller cloud particles (which are assumed to be carried along by the updrafts) acquire positive charges.

B. Outline of a simple theory for charge separation by interaction of cloud and precipitation particles.

Suppose that the electrification is produced by collision between cloud particles (ice crystals or water droplets) present in number density n and hailstones of radius R present in number density n_h . The number of collisions per cc per second between hailstones and cloud particles is given by

$\frac{dN}{dt} = E\pi R^2 n_h n V$ where V is the full speed of the hailstone and the E the collision efficiency. The precipitation rate p due to the hailstones is $p = \frac{4}{3} \pi R^3 \rho n_h V$ when ρ is the density of the hail. If each collision, on the average, results in a charge transfer q , the rate of production of charge per unit volume of cloud is $\frac{dQ}{dt} = \frac{3}{4} q \frac{E n p}{R \rho}$.

If we take $dQ/dt = 1 \text{ C km}^{-3} \text{ min}^{-1}$, $p = 5 \text{ cm/hr}$, $R = 0.2 \text{ cm}$, $\rho = 0.5 \text{ gm/cc}$ and $E = 1$. Then for ice crystals $n = n_c = 0.1/\text{cc}$ (diam. $> 80\mu$) yields $q = q_c = 5 \times 10^{-5} \text{ esu/collision}$. For water droplets, $n = n_d = 1/\text{cc}$ (diam. $> 30\mu$) so that $q = q_d = 5 \times 10^{-6} \text{ esu/collision}$.

C. Ice crystal - hailstone charge transfer theory of Reynolds, Brook and Gourley (1957).

Laboratory measurements by Reynolds et al. (1957) found in laboratory experiments that the charge separated during the collision of ice crystals with an ice surface was of the order 5×10^{-4} esu per collision. If the hailstone was warmer than the crystal, it received a negative charge. In a natural cloud hailstones growing by collecting supercooled water drops might be expected to be warmer than ice crystals which collide with them. Thus the hailstones would acquire negative charges which would be carried to the lower levels of the cloud.

However, rather similar laboratory measurements made by Latham and Mason (1961) yielded a value for q_c of 5×10^{-9} esu/collision. This would produce a negligible dQ/dt .

D. Drop-splintering theory of Latham and Mason (1961).

Laboratory experiments carried out by Latham and Mason indicated that when supercooled drops collided with an ice surface a charge $q_d = 5 \times 10^{-6}$ esu/collision was separated, the ice surface becoming negatively charged. They explained this charging on the basis of the explosion or fragmentation of supercooled droplets during freezing onto the ice surface. As we have shown above, if this amount of charge is separated when supercooled cloud droplets collide with natural hailstones it would be a powerful enough mechanism to explain the generation of charges in thunderstorms. However, the laboratory observations of Latham and Mason are open to criticism on a number of points:

1. Reynolds et al. observed negligible charging when supercooled droplets alone collided with ice (they observed charging only with mixture of droplets and ice crystals).
2. Field measurements by Hobbs and Burrows (1966) agreed with the laboratory measurements of Reynolds et al.

3. Supercooled drops are unlikely to explode or fragment after colliding with a hailstone (see Lecture #4).

E. Recent observations on charging resulting from ice particle interactions

A detailed study of the charging of ice surfaces due to collisions with natural ice particles has been carried out by a group at the University of Washington during the past few years. A brief summary of the results of these measurements will now be given.

Shown in Fig. 1 (see end of Lecture #6) are four cases of the spectrum of charges transferred to an ice surface due to natural ice crystals colliding with it. The magnitude of the charges received by individual collisions range from -10^{-2} to $+10^2$ esu/collision.

Results fall into two types of distributions:

(1) Symmetrical distributions for positive and negative charges.

This is generally observed for graupel and rimed particle. For graupel at warm temperatures, net charge is generally positive or zero. For rimed spatial dendrites the net charge is negative or zero at -8°C . Figure 2 (see end of Lecture #6) shows examples of symmetrical distribution for rimed spatial dendrites at -8°C . (In two cases, the median charge is zero and in one case it is -5×10^{-4} esu/collision).

(2) Asymmetrical distribution in which charges of one sign dominate.

This is observed with most other types of ice crystals. Charges follow a log-normal distribution. Figure 3 (see end of Lecture #6) shows a log-probability plot for the charging events when stellar crystals collided with an ice surface at -12°C . Net charge may be positive or negative but this appears to be temperature dependent as summarized in Fig. 4 (see end of Lecture #6) which shows the temperature dependence of the net charge acquired by an ice sphere per cm of path length due to collisions with ice particles (values below dotted

line, i.e., between -2 and -8°C , are more than sufficient to give $dQ/dt = 1$ coulomb/ km^3/min).

The observed charging when ice particles collide is probably due to two basically different mechanisms, (see, for example, Loeb, 1958).

(a) Symmetrical charging which occurs on the basis of pure statistics whenever two surfaces come into contact across a small area in which, by chance, more ions of one sign diffuse across the boundary in one direction than the other. In this case the direction of charge transfer can go both ways.

(b) Asymmetrical charging which leads to the transfer of a series of charges predominately of one sign. This may be due to direct transfer of existing charges on particles, thermoelectric effect, impurities, etc.

F. Effect of a polarizing electric field on charging

In the work described so far, we have neglected the effects of electric fields on the charging of interacting particles. Such fields can polarize the particles and enhance the transfer of charges between colliding particles. It may be shown that the charge transferred by contact and separation between conducting spheres of radii R and r , whose line of centers is at an angle θ to field F , is given by (Davis, 1964).

$$q = \left(\gamma_1 F \cos \theta + \gamma_2 \frac{q_R}{R^2} \right) r^2$$

where q_R is the charge carried by the sphere of radius R and γ_1 and γ_2 are functions of r/R . If $R \gg r$,

$$q = \left(\frac{\pi^2}{2} F \cos \theta + \frac{\pi^2}{6} \frac{q_R}{R^2} \right) r^2.$$

Due to this polarizing effect, if the electric field is directed towards the ground, the hailstone will receive a negative charge and the

cloud particle a positive charge. The field builds up as charge separation by this process continues until the downward force acting on the cloud particles due to the electric field gives them a downward velocity comparable to the fall velocity of the hailstones. The probability of collisions between cloud and precipitation particles is then reduced.

Figure 5(see end of Lecture #6) shows some experimental measurements of the charges transferred to a sphere by the collision of stellar ice crystals as a function of the applied electric field. We see from these results that the charge transfer increases rapidly with increasing fields; even fair weather electric fields of 1 volt/cm give a charge per collision of 10^{-5} esu. For fields up to about 50 volt/cm, the results agree well with Davis's theory based on the collisions of conducting spheres in an electric field. For higher fields the experimental results increase more rapidly with the applied field than the theory predicts.

G. Some possible effects of electrical forces on cloud physical processes

1. Collisions and coalescence of droplets.

Recent calculations show that for highly charged droplets interacting in fields approaching the dielectric breakdown of air, the collision efficiencies are drastically affected (generally increased). The effects are most pronounced for smaller drops. Fields below about 1000 V/cm have insignificant effects on collisions. Thus in many clouds, electrical fields will have little effect.

There is evidence that electrical forces can modify coalescence efficiency. Woods (1965) found that the coalescence rate for drops of radius less than 40μ , increases linearly with applied charge above a threshold value of 5×10^{-5} esu. If the drops carried charges of the same sign, then coalescence could be totally inhibited.

Moore et al. (1964) observed intense rainfall from highly electrified clouds within a very short time of the detection of the radar echo. The estimated collection efficiencies must have been 4 to 10 times greater than normal values. They have suggested that gushes of rain or hail which sometimes follow lightning are caused by drops capturing ions and then travelling at high velocities in intense local fields, colliding and coalescing with numerous oppositely charged droplets.

2. Collisions and aggregation of ice crystals

Figure 6 (see end of Lecture #6) shows the increase in mass acquired by an ice sphere exposed to a stream of ice particles as function of applied electric field.

3. Nucleation of ice

The role of electrical charges and fields on the action of ice nuclei is unknown. There is some experimental evidence that electric fields can cause nucleation of supercooled droplets. It has been suggested that freezing occurs if electrical forces are of sufficient strength to disrupt the surface of the drop, drawing it out in a liquid filament of thickness around 10^{-6} cm. Molecular aggregates of water of these dimensions, possibly orientated by the field, take the form of minute crystallites which could cause the drop to nucleate. Recent experiments by Abbas and Latham (1969) lend support to this idea.

Notes taken by:

M. S. Sher

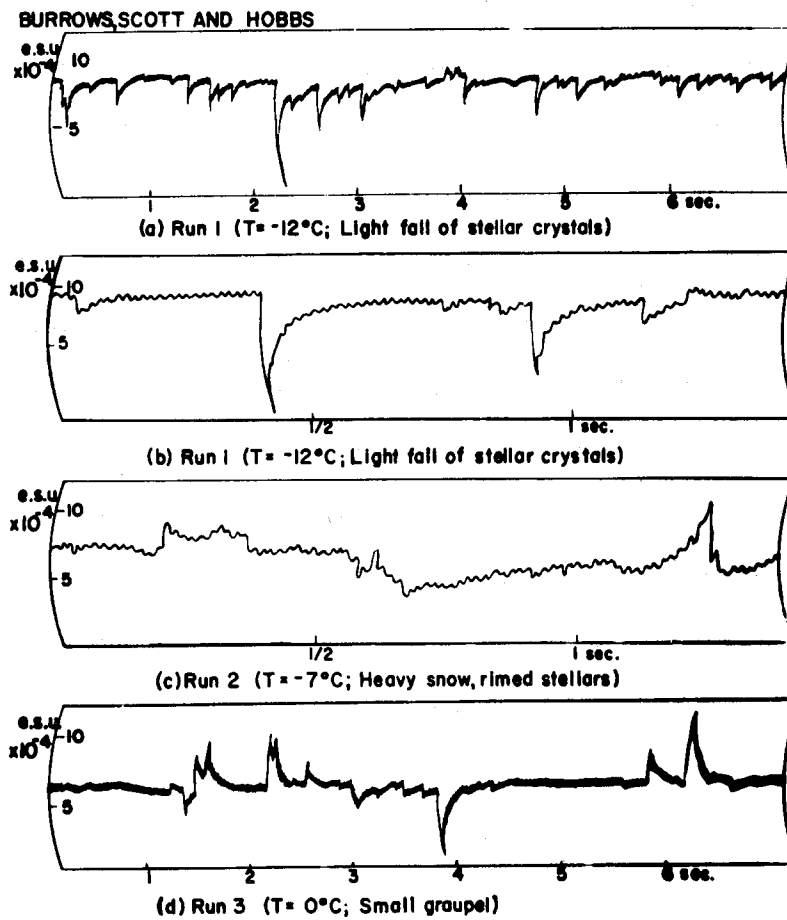
W. G. Slinn

REFERENCES

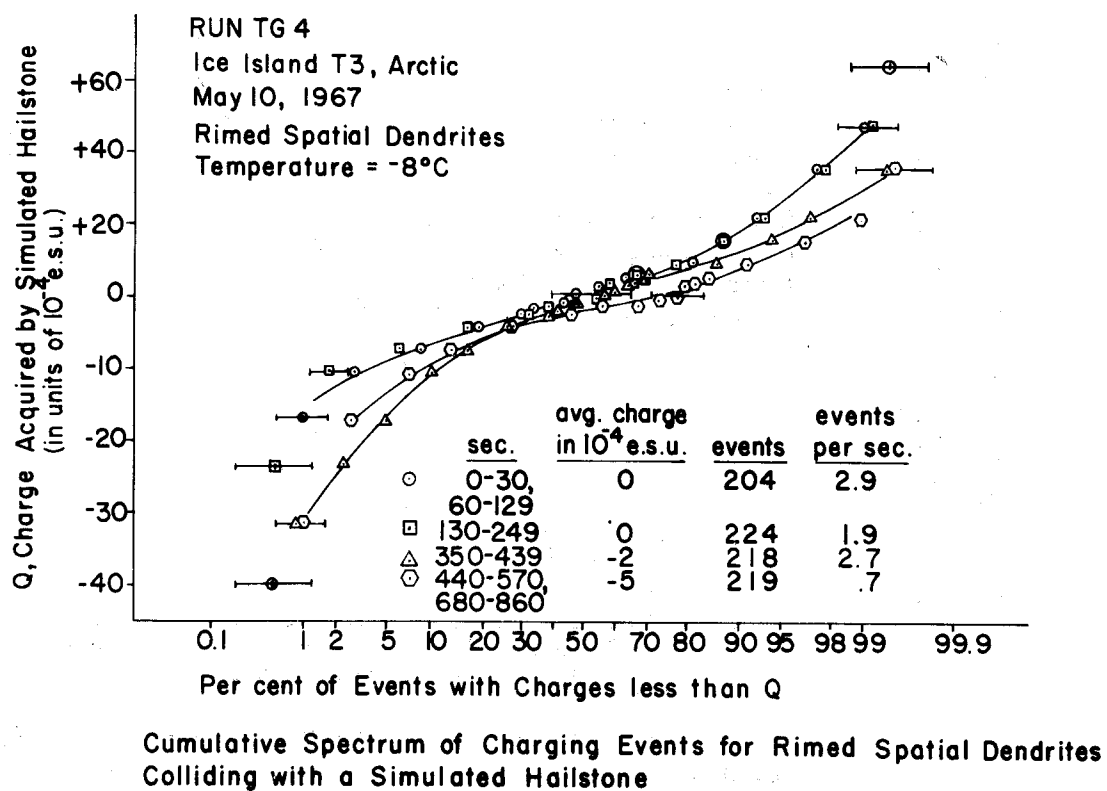
- Abbas, M.A., and Latham, J., J. Met. Soc., Japan, 47, 65, 1969.
- Burrows, D.A., and Hobbs, P.V., J. Atmos. Sci., 26, 560, 1969.
- Davis, M.H., Quart. J. Mech. and App. Math., 17, 499, 1964.
- Hobbs, P.V., and Burrows, D.A., J. Atmos. Sci. 23, 757, 1966.
- Latham, J., and Mason, B.J., Proc. Roy. Soc., A260, 523, 1961.
- Loeb, L.B., Static Electrification, Springer-Verlog, 1958.
- Mason, B.J. Tellus, 5, 446, 1953.
- Moore, C.B., Vonnegut, B., Vrablik, E.A., and McCaig, D.A., J. Atmos. Sci., 21, 646, 1964.
- Reynolds, S.E., Brook, M., and Gourley, M.F., J. Met., 14, 426, 1957.
- Saunders, C.P.R., Proc. Int. Conf. on Cloud Physics, Toronto, Canada, 1968.
- Scott, W.D., and Hobbs, P.V., Quart. J. Roy. Met. Soc., 94, 510, 1968.
- _____ and Levin, Z., J. Atmos. Sci., 27, 463, 1970.
- Woods, J.D., Quart. J. Roy. Met. Soc., 91, 353, 1965.

Figure Captions

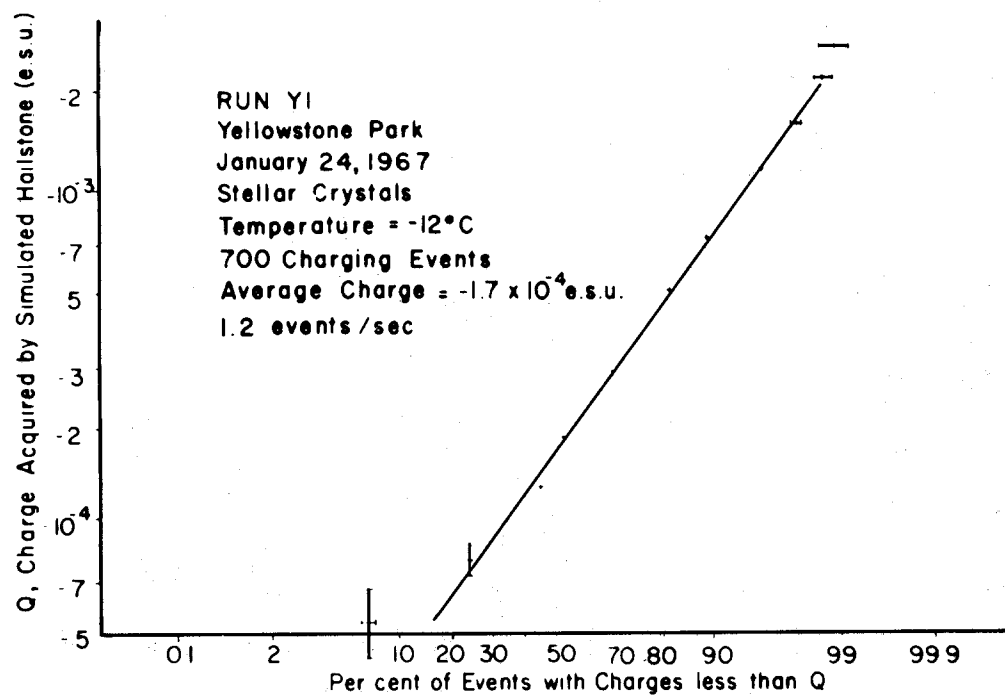
- Figure 1: Spectra of charges received by an ice surface exposed to natural ice crystals. (From Scott and Hobbs, 1968).
- Figure 2: Example of a symmetrical distribution of charging events for rimed spatial dendrites colliding with ice at -8°C . (From Scott and Hobbs, 1968).
- Figure 3: Log-probability plot for charges received by an ice surface exposed to natural stellar crystals at -12°C . (From Scott and Hobbs, 1968).
- Figure 4: Temperature dependence of net charge acquired by an ice sphere for cm of path length as it moves through a cloud of natural ice crystals (From Burrows and Hobbs, 1969).
- Figure 5: Measurements of the charges transferred to a sphere by the collision of natural ice crystals (From Scott and Levin, 1970).
- Figure 6: Increase in the mass of ice acquired by an ice sphere exposed to a stream of ice particles as a function of the applied electric field (From Saunders, 1968).



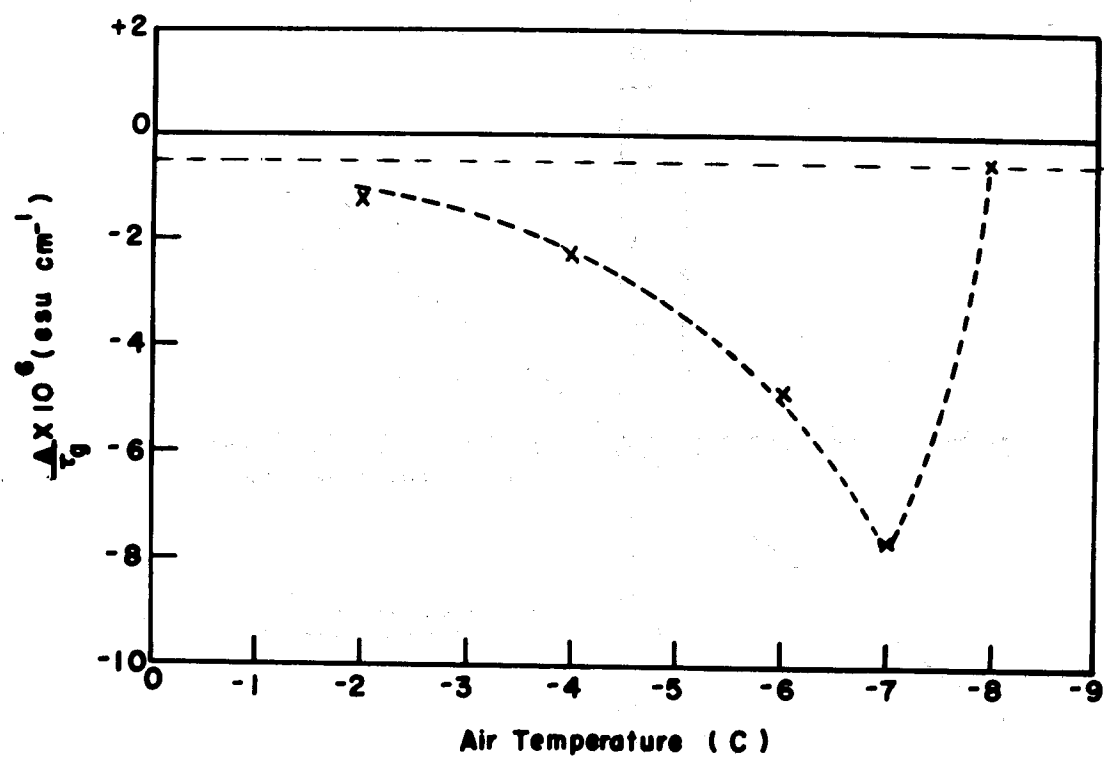
The charging of an ice sphere exposed to a stream of snowflakes.
(Upward deflections correspond to the ice surface receiving a positive charge and vice versa.)



Lecture 6, Figure 2

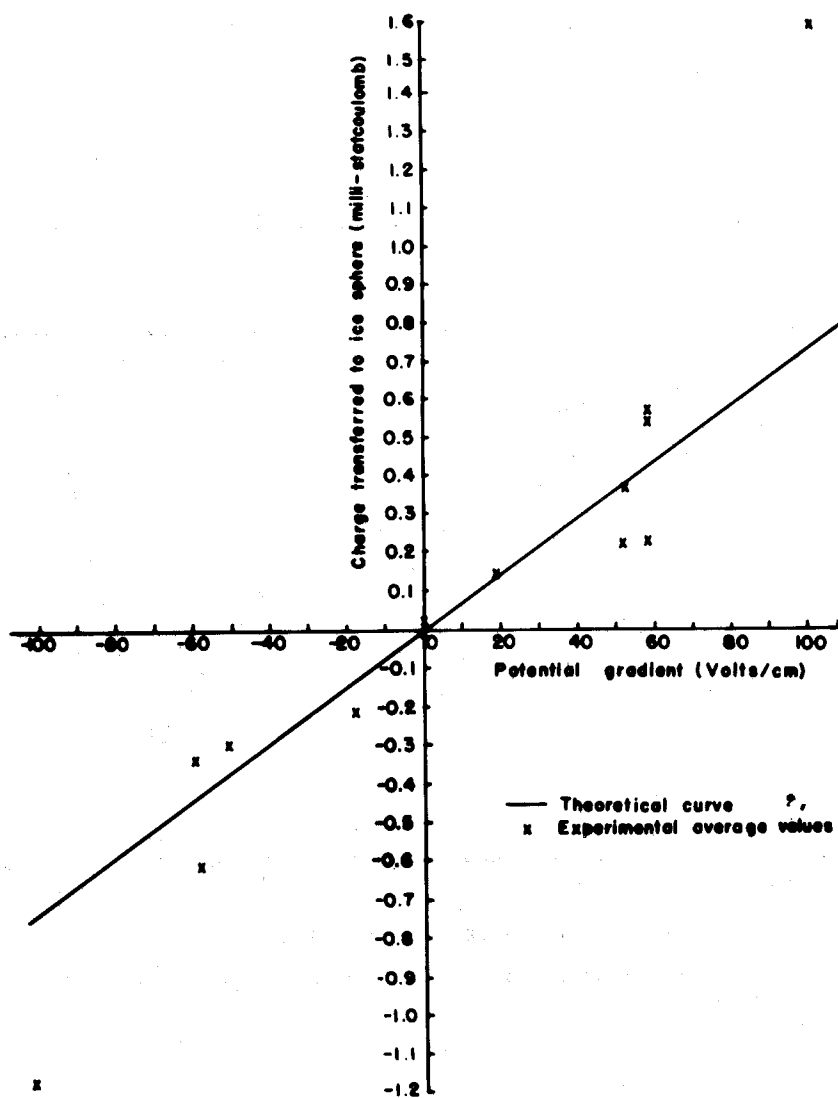


Cumulative Spectrum of Charging Events for Stellar Crystals Colliding with a Simulated Hailstone.

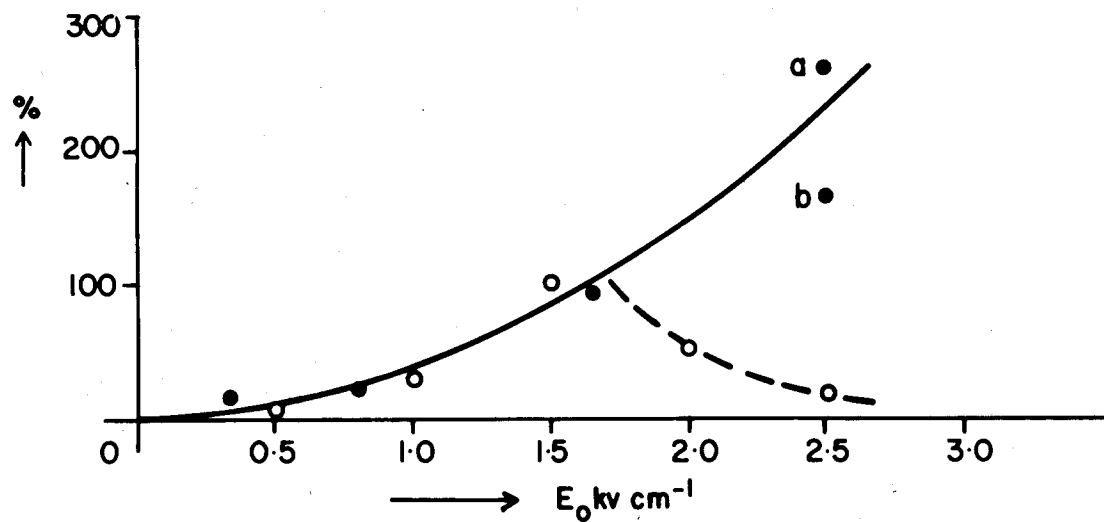


Charge acquired by an ice sphere per cm of path length due to collisions with ice particles in the air.

Lecture 6, Figure 4



Lecture 6, Figure 5



% Increase in aggregation at -7°C due to an electric field.

● Volume increase determination

○ Mass increase determination

(a) 20 cm sec⁻¹ (b) 800 cm sec⁻¹

VII. ARTIFICIAL MODIFICATION OF CLOUDS, PRECIPITATION, HAILSTORMS, AND THUNDERSTORMS

In this lecture a brief review is given of work which has been carried out in the past twenty years or so on the artificial modification of clouds, precipitation, hailstorms and the electrical properties of clouds.

A. Early history of artificial modification of clouds and precipitation

In 1938 the German cloud physicist Findeisen suggested that the introduction of artificial ice nuclei into supercooled clouds might enhance the formation of rain. In July 1946 Schaefer (1946) accidentally discovered that a tiny piece of dry ice when dropped into a cold box filled with a supercooled cloud resulted in the formation of millions of tiny ice crystals. (N.B. Dry ice forms ice crystals by homogeneous nucleation.) On November 13, 1946, Schaefer made the first field tests using 3 pounds of crushed dry ice which was dropped into a layer of supercooled altocumulus cloud. Observers on the ground saw snow fall out of the cloud for about 2000 feet before it evaporated.

In November 1946 Vonnegut (1947) discovered that silver iodide particles acted as ice nuclei at about -5°C . These particles could be produced in large numbers (about $10^{15}/\text{gm}$ of AgI) by vaporizing an acetone solution of AgI in a hot flame. This suggested that if large quantities of the particles were released from the ground that they might be carried in updraughts to cloud levels. On December 21, 1948, Vonnegut dropped lumps of burning charcoal impregnated with silver iodide from an aircraft into 6 square miles of supercooled stratus about 1000 feet thick. The cloud was converted into ice crystals using less than 1 ounce of AgI!

B. Experimental seeding of cumulus clouds

Kraus and Squires (1947) seeded large supercooled cumulus clouds with dry ice. They observed that in some cases the clouds showed "explosive"

vertical growth following seeding. In one spectacular case a cloud with a base at 11,000 feet and summit at 23,000 feet was seeded with 150 pounds of dry ice. In 13 minutes it grew to an elevation of 29,000 feet and after 21 minutes heavy rain fell while radar echoes within a 100 miles showed no other precipitation activity. The explosive growth can be explained by the liberation of latent heat as the supercooled droplets freeze, but this only occurs under certain environmental conditions. This has led in recent years to fairly detailed studies of the dynamics of cumulus clouds using the latent heat released by seeding to check certain aspects of theoretical models.

C. Artificial seeding to increase rainfall

(1) Warm clouds

We have seen in a previous lecture that the presence of fairly large water droplets is necessary in order to initiate the growth of precipitable drops by coalescence, and that these large droplets probably form by condensation onto large cloud condensation nuclei. Hence, the introduction of hygroscopic particles into a cloud might initiate the coalescence mechanism. A few experiments of this type were carried out in the 1950's and appeared to be partially successful.

A recent experiment carried out in India in which clouds were seeded with salt particles has been reported by Biswas, et al. (1967). Ground based salt seeding was carried out in three climatologically similar regions surrounding Delhi, Agra, and Jaipur in northwest India. Control and target areas for each seeding day were defined as the 90° sectors upwind and downwind, respectively, of the central seeding location. Hygroscopic particles were introduced by the spraying of a known concentration of salt solution or by compressed air dusting of a finely powdered salt solution. In spraying, particles having dry masses of 4×10^{-10} to 10^{-8} grams and diameters of 7 to 25μ were spread with a generation rate of 10^9 /sec. In dusting the particles

were about 10^{-9} grams with a radius of 5μ and were dispersed at a rate of 2×10^{10} /sec.

The experiments were carried out for eight seasons in Delhi, six seasons in Agra, and four in Jaipur. Comparisons were made between target and control areas for seeded and nonseeded days. In 16 out of the total 18 seasons an average increase of rain of 41.9% occurred in the target area.

(2) Cold clouds

It takes about a million cloud droplets 10μ in radius to form a raindrop 1000μ in radius. One possible way to achieve this is to introduce into the cloud about 1 ice nucleus per million supercooled droplets. Since there are about 100 cloud droplets per cubic centimeter of air, this means introducing about 1 ice nucleus per 10 liters of air. An average isolated cumulus cloud might contain 10^{12} liters of air and therefore about 10^{11} ice nuclei are needed to remove all the droplets. To achieve this number only a few grams of AgI are needed as one gram yields about 10^{13} nuclei.

In some early Australian experiments about 10 grams of AgI were introduced into isolated supercooled cumulus clouds. These clouds had summit temperatures ranging from -2.5 to -10°C and depths of 4000 to 17,000 feet. The results indicated that 72% of the clouds which were seeded precipitated within 20 to 25 minutes, 21% evaporated, and 7% showed no change.

In large-scale experiments where AgI is dispersed into stratiform or layer cloud systems (warm fronts, occlusions, orographic clouds) by either aircraft or from the ground, statistical evaluations of the results of seeding become mandatory. A number of such well-conducted experiments have been carried out and the results indicate that precipitation may be increased, decreased, or be unaffected by artificial seeding. A summary of the results

obtained in a few projects of this kind is given below.

Israel Experiment

This experiment is based on a randomized cross-over design with a north and a center target area separated by a buffer zone. Seeding is done from aircraft just below the cloud base and upwind of the target area at a rate of 800 to 900 grams of AgI per hour resulting in about 10^{12} nuclei at -10°C . The clouds are assumed to be convective and seeding is started only when the cloud tops have reached the -5°C level. Six seasons of data have been evaluated since 1967. The results indicate an average increase of 15.2% over both target areas with individual yearly increments ranging from 1.2 to 65%. These results are significant at the 5% level (i.e. there is a 5% probability that the results are merely chance). The study of seeding effects versus temperature at the 700 mb level (as a substitute for cloud top temperature) indicate that the largest ratios of rain increase occurred for cloud tops in the -5° to -6°C range.

Project Whitetop

This experiment, which was rather similar in design to the Israel experiment, was carried out in summertime in Missouri over a period of 6 years. Seeding was carried out from aircraft along 10 mile tracks upwind from the test area during a 6 hour period (1100-1700 CST) at or below the cloud base. The three aircraft involved, each with two acetone burners, dispersed about 2700 grams of AgI per hour into afternoon convective clouds, neither single thunderstorm or stratus clouds were included. This resulted in about 10^{14} to 10^{16} nuclei per gram at -17°C .

Many different statistical evaluations of the results of Project Whitetop have been made by different groups. Rainfall amounts inside and outside the target area were considered on seeded and non-seeded days. It was found that the largest average rainfall occurred in the seeded areas on the nonseeded

days (Decker and Schickendanz, 1967). Neyman et al. (1969) extended the analyses up to distances of 180 miles from the seeded area and found that the average precipitation on 102 seeded days was less than on the 96 experimental days without seeding. For distances less than 30 miles there was 32% less rain on seeded days. Estimated average rainfall over the whole region of about 100,000 square miles was 21% less on seeded days.

Climax Project

This project is being carried out in orographic cloud systems in one of the Colorado River watersheds. Silver iodide ground generators are placed at distances of 13, 20, 22, 30, 47, and 59 km from the target area. These produced 20 grams of AgI per hour resulting in about 10^{14} nuclei per gram of AgI at -12°C . The normal concentrations of freezing nuclei in the target area is 1 per liter and this is increased to between 10 and 100 per liter at -20°C during seeding. The criterion used in choosing the experimental days is that Leadville (located upwind from the target area) be forecast to have over 0.01 inches of precipitation within the 24 hour period.

A simple theoretical model has been developed which equates the diffusional growth of ice crystals to the rate of formation of condensate in an orographic cloud. Riming is not considered to be important. Computations have been made for various cloud temperatures and updraft velocities to determine the concentrations of ice crystals needed in order for all the water vapor released in the updraft to be accumulated as snow. This concentration of crystals is called the optimum concentration.

The results so far have shown that nearly 100% more precipitation has fallen on seeding days when the temperature at the 500 mb level was -11 to -20°C (significant at the 5% level). However, when the 500 mb temperature was less than or equal to -26°C there was a 30% decrease in precipitation in the target area (significant at the 1% level). These results are in

agreement with the predictions of the theoretical model. At lower temperatures there are sufficient natural nuclei to effectively release precipitation, and the artificial nuclei cause overseeding and therefore a reduction in precipitation.

King's River Watershed

This project was begun in California in 1955 and is still continuing. Ground based AgI-acetone burners (supplemented recently by pyrotechnic AgI flares) consume 12 grams of AgI per hour. The target area is about 3000 km^2 . The evaluation is based on the streamflow in the King's river and two nearby watersheds are used as controls. The results over 13 years suggest an average annual increase in runoff from the King's river of approximately 6% as a result of the artificial seeding.

Lake Almanor

This project was carried out in the watersheds of Lake Almanor in northeast California to determine the effects of seeding on wintertime Pacific storms. An area of about 500 square miles was divided into control and target areas which varied with the wind direction. Six AgI generators were used at or near mountain tops and the outputs were 27 grams of AgI per hour. Fifty-one raingauges were spaced at 2 mile intervals on the watershed. Operations were carried out from January to May of 1963 and included 76 randomized seeding events. The results for these winter orographic clouds indicate 80% more rain on seeded days in a westerly wind and a 10% decrease in precipitation on seeded days when the winds were from the south.

D. Targeting of Snowfall by Seeding

Two projects are currently underway, one carried out by the University of Washington in winter storms over the Cascade Mountains of Washington State and the other by ESSA in the Lake Erie area. The main purpose of these projects is to investigate the feasibility of targeting snowfall by seeding

with ice nuclei. For example, in winter orographic storms over the Cascade mountains the concentrations of natural ice nuclei are quite low (about 1 per 10 liters at -21°C). The ice crystals which form in these clouds increase in mass mainly by riming and attain fall velocities of the order of 1 m/sec. If these clouds are completely glaciated by overseeding with artificial ice nuclei so that all of the supercooled water droplets are removed, the ice crystals will grow only by condensation from the vapor phase. Such crystals have fall velocities of about 0.5 m/sec. Therefore, if these crystals fall out in a westerly airstream they will be carried further east than will the rimed crystals which form under natural conditions.

E. Hail Suppression

The principle here is that if the number of ice embryos is increased the size of the hailstones will be correspondingly reduced, since

$$\frac{4\pi}{3} R_s^3 N_s = \frac{4\pi}{3} R_I^3 N_I$$

or,

$$R_s = R_I \left(\frac{N_I}{N_s} \right)^{1/3}$$

where the subscripts s and I indicate after-seeding and before-seeding respectively, N the number of ice embryos and R the radius of the hailstones. Theoretical work indicates that the water content of a hail cloud becomes effectively depleted by a small number of hailstones (about 10 per m^3), so that even modest increases of their concentration of two orders of magnitude can be expected to decrease their size sufficiently to prevent damage.

Hail modification experiments are currently being carried out in the USSR. Seeding agents are delivered by guns and shells or by rockets. Guns have greater range and altitude and can deliver 100 to 200 grams of AgI or PbI. Rockets can carry larger quantities (3.2 kg of pyrotechnic material). In 1966 more than one million hectars (3900 square miles) were "protected" by artificial

seeding. Hail damage in the protected areas was 3 to 5 times smaller than in the unprotected areas. The cost of protection amounted to about 2 or 3% of the value of the crops saved. However, these experiments were not randomized therefore statistical evaluation is not possible.

F. Modification of Electrical Behavior of Clouds

Lightning is the greatest single cause of forest fires in the Western United States. The U. S. Forest Service has developed a program on lightning research known as Project Skyfire.

The attempts at modifying lightning have centered around experiments in which silver iodide seeding is employed to produce an abundance of ice crystals in that part of a supercooled thundercloud in which most ground strokes are thought to originate (i.e., between the -10 and -15°C isotherms). It is postulated that the increased number of ice crystals produced by the seeding will provide additional corona points; these should increase the leakage current between the charge centers in the form of a corona current and thereby suppress the formation of a stepped leader.

A two-year pilot experiment of the kind outlined above was carried out during the summers of 1960 and 1961 in Western Montana. Seeding was done from aircraft and ground-based generators, and lightning within a selected area was recorded. It was found that there were 30 percent fewer ground discharges on those days when the clouds were seeded than on those days when seeding was not carried out. Intracloud and total lightning discharges showed decreases of 8 and 21 percent, respectively, for seeded clouds during the two-year period. However, statistical analysis of the data showed that the probability of this distribution occurring by chance was as high as 1 in 4.

A new series of seeding experiments were carried out during the summers of 1965 and 1967 using more efficient silver iodide generators, new instruments for identifying the lightning flashes, and an improved physical

and statistical design. Analysis of data on the basis of the life cycle of individual storms showed 66 percent fewer cloud-to-ground discharges, 50 percent fewer intracloud discharges, and 54 percent less total storm lightning occurred during seeded storms than during unseeded storms.

It should be noted here that the physical explanation of the results obtained in Project Skyfire is complicated by the fact that although artificial seeding might cause an increase in the leakage current in a cloud, and therefore tend to decrease lightning activity, it may also affect the electrical behavior of the cloud in other ways. For example, several workers have found that the collision of ice particles can produce significant generation and separation of electric charge and this could be the mechanism for charge generation in thunderstorms (Reynolds, Brook and Gourley, 1957; Hobbs and Burrows, 1966; Burrows and Hobbs, 1969). If this is the case, the artificial glaciation of a cloud might lead to an increase in electrical activity. Moreover, the vigor of a cloud may be significantly increased as a result of the latent heat released by seeding and this might also increase the electrical activity of a cloud.

Chaff Seeding

If leakage currents in a cloud can be increased by the ice crystals produced by artificial seeding, the dispersal of long chaff needles into a thundercloud should have the same effect. Moreover, in the latter case, the experiment is not complicated by an increase in the concentrations of ice in the cloud.

Experiments of this kind were started by the U. S. Army Atmospheric Sciences Laboratory (Kasemir and Weickmann, 1965) and are now being continued in the APCL of ESSA. Laboratory experiments have shown that the onset of corona discharge on a 10 cm long chaff fiber is about 30 KV/m which is about twenty times lower than the field necessary to initiate lightning discharges

in clouds. If such chaff were dispersed in a large column of cloud about five pounds of it, containing 10^7 fibers, would produce a 10 ampere corona current in a field of 70 KV/m. This current would be adequate to counter-balance the current output from an average thunderstorm (approx. 3 ampere) and should therefore suppress lightning.

Carefully controlled field experiments to test this idea have yet to be carried out.

REFERENCES

- Biswas, K. R., Kapoor, P. K., Nanuga, K. K. and Ramana Murty, Bh.V., 1967, J. App. Met. 5, 914.
- Burrows, D. A., and Hobbs, P. V., 1969, J. Atmos. Sci. 26, 560.
- Decker, W. L., and Schickedany, 1967, Project Whitetop Part IV, Univ. of Chicago - Univ. of Missouri Report.
- Hobbs, P. V., and Burrows, D. A., 1966, J. Atmos. Sci. 23, 757.
- Kasemir, H. W., and Weickmann, H. K., 1965, Proc. Intern. Conf. on Cloud Physics, Tokyo.
- Kraus, E. B., and Squires, P., 1947, Nature, 159, 489.
- Neyman, J., Scott, E. L., and Smith, J. A., 1969, Science, 163, 1445.
- Reynolds, S. E., Brook, M. and Gourley, M. F., 1957, J. Met. 14, 426.
- Schaefer, V., 1946, Science, 104, 457.
- Vonnegut, B., 1947, J. App. Phys., 18, 593.

Notes taken by:

B. Wilhelmson

R. E. Forbes

VIII. NUMERICAL MODELING OF CUMULUS CLOUDS

A. Early work and ideas

Early models of cumulus dynamics neglected the interactions between the rising cloud and the environment. Thus, they generally overpredicted cloud height, liquid water content, vertical velocity, and temperature excess. Stommel (1947) showed how entrainment or mixing could be included if the rising air is represented by a conical steady-state jet, and thereby laid the foundation for the present one-dimensional models of cumulus convection.

If a steady-state jet spread angle of the jet is α (Fig. 1, see end of Lecture #8), the rate of entrainment μ of air into the jet is given by $\mu = 1/M \cdot dM/dz = 2\alpha/R \approx 0.2/R$. The important point here is the inverse dependence of μ upon the radius R .

Scorer and Ludlam (1953) proposed a different model for cumulus convection called "bubble" model in which the convective element is likened to a hot bubble whose top is continuously being eroded away and entrained into the wake. They found that in this case $\mu = 1/M \cdot dM/dz = 9/32 \cdot K/D$ where D is the diameter of the jet in kilometers. The value of K can range from 0.5 to 0.8. (Color slides are shown, illustrating the development and decay of a cumulus tower).

Turner (1962) proposed a "starting plume" model which combines the jet and bubble models. A steady-state jet is topped by a bubble-type cap. In this case μ is the same as for the steady-state jet, i.e., $\mu = 0.2/R$.

B. The model of Weinstein and Davis

In the one dimensional, steady-state cumulus model by Weinstein and Davis (1967), it is assumed that at cloud base, the rising thermal is just saturated and has the temperature and pressure of its environment,

as well as a prescribed upward velocity and radius. A parcel of air is initially lifted moist adiabatically through one grid interval (usually 200m) to the next level where its temperature is T_2'' and its mixing ratio q_2'' (Fig. 2, see end of Lecture #8). The environment at this level is cooler and drier than the cloud, and the mixing that is now assumed to take place at this point cools the parcel to a temperature T_2' and lowers its mixing ratio to q_2' given by

$$T_2' = \frac{T_2'' + \mu dz T_e}{1 + \mu dz} \quad \text{and} \quad q_2' = \frac{q_2'' + \mu dz q_e}{1 + \mu dz}$$

where T_e and q_e refer to the environment. These expressions are weighted means of the mass M of the parcel mixed with an amount dM of environmental air. The parcel is now undersaturated, but since it contains some liquid drops these must be allowed to evaporate until the parcel is once more saturated, which will further cool it. This adjustment can be accomplished graphically by lifting the parcel dry adiabatically to saturation and bringing it back moist adiabatically to its original level. The final result, T_2 and q_2 , is that which would have resulted from the evaporation of enough water to saturate the air. The resulting lapse rate of the parcel γ_c shown in Fig. 2, is greater than γ_m , the pseudo-adiabatic lapse rate. The process is then repeated for higher levels.

The principal source of energy for the buoyancy of cloudy air is the latent heat of condensation. A second important source is available if freezing occurs, namely, the latent heat of freezing. After freezing occurs

it is assumed that vapor condenses directly from the vapor to the solid phase so that the ice adiabatic lapse rate is then used before mixing is allowed to occur. Glaciation is assumed to take place at one particular level, where all of the latent heat of freezing is released.

The model assumes that water in the cloud consists of two components, cloud droplets of mixing ratio Q_c and hydrometeor water having a mixing ratio Q_h . The droplets are formed by condensation and removed by three processes: evaporation (due to mixing with the environment), conversion to hydrometeor water, and collection by hydrometeor water. The hydrometeor water can be created only by conversion and collection and is the only water that goes into precipitation.

Details of the conversion process are not taken into account; rather the process is parameterized in the manner suggested by Kessler (1965). Conversion is not allowed to occur until Q_c reaches a critical value a ; after this, conversion is assumed to take place at a constant rate given by $dQ_h/dt = K_1(Q_c - a)$ where $a = 0.5 \text{ g/m}^3$.

Collection is treated on the assumption of a Marshall-Palmer drop size distribution for the hydrometeor water, namely, $N = N_0 e^{-\lambda D}$ where N is the concentration of drops of diameter D . All drops are given a fall velocity appropriate to the volume mean diameter and coalescence growth is considered to be continuous.

C. Applications of the model

The model has been used in connection with field experiments involving the artificial seeding of isolated cumulus clouds. Inputs that are needed include an environmental vertical sounding of temperature and relative humidity, the height of the cloud base, and certain microphysical parameters

such as K , a and the ice nucleation temperature. Some of the outputs of the model are shown schematically in Fig. 3 (see end of Lecture #8). They include vertical profiles of temperature, vertical velocity, Q_c and Q_h . The temperature at which ice is nucleated can be varied to model a natural cloud say (-25°C) or a seeded cloud say (-8°C) and the effects of cloud seeding upon the physical properties of the cloud can be assessed. The results are sensitive to environmental stability, ice nucleation temperature, and the radius R .

The field procedure consists of taking an early morning sounding, using this as input for the model, comparing unseeded computations with seeded computations, and looking at the range of initial cloud radii that will yield a maximum difference between growth with and without seeding. Then an aircraft is taken up to look only at clouds in the size range of interest. Randomly selected clouds in this range are seeded and their changes in height are noted. Another sounding is taken by the plane and this is once again run on the computer with two ice nucleation temperatures for verification. Also radar reflectivity observations give a measure of rainfall produced by the cloud.

Figure 4 (see end of Lecture #8) shows a comparison between observed and predicted changes in cloud top height for seeded and unseeded clouds. It can be seen that the model exhibits considerable skill in its predictions for both kinds of clouds. However, the model may be somewhat unrealistic in that its predictions of liquid water do not correspond to those usually observed; this may be a serious defect because latent heat of condensation is the main driving force for the cloud.

Notes taken by:

P. M. Caplan

S. K. Chan

REFERENCES

Kessler, E., *Geofisica Intern.*, 5, 79, 1965.

Scorer, R. S., and Ludlam, F. H., *Quart. J. Roy. Met. Soc.*, 79, 96, 1953.

Stommel, H., *J. Met.*, 4, 91, 1947.

Turner, J. S., *J. Fluid Mech.*, 13, 356, 1962.

Weinstein, A. I., and Davis, L. G., Rept. No. 11 to NSF, Dept. of Meteor.,
Penn. St. Univ., 1967.

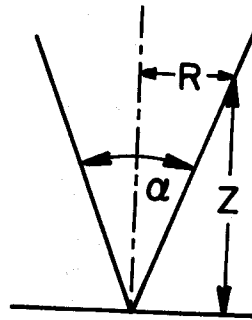
Figure Captions

Figure 1 - Illustration of the angle of a divergent jet.

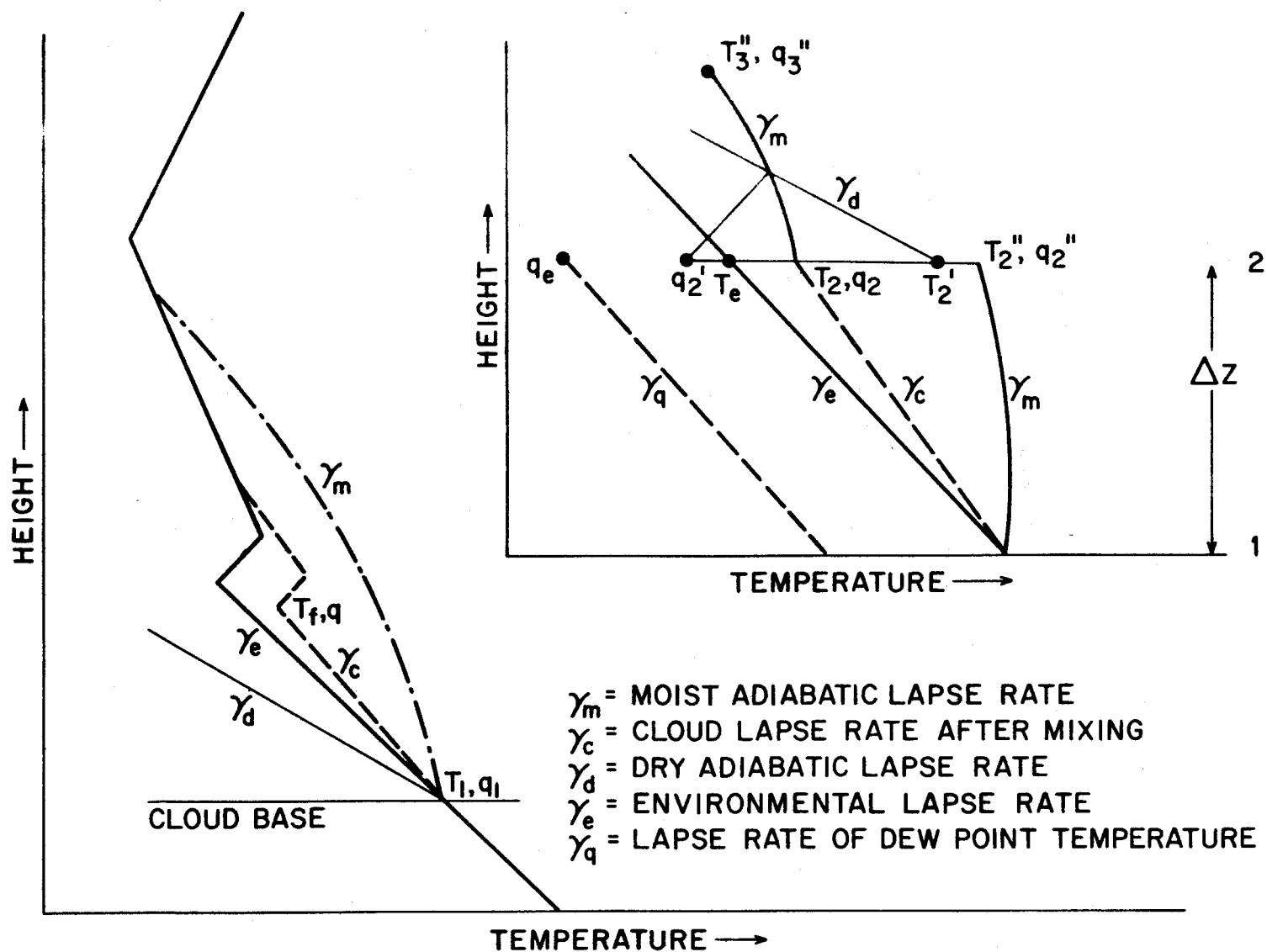
Figure 2 - Graphical description of thermodynamical calculations (From
Weinstein and Davis, 1967).

Figure 3 - Steady-state outputs of the model (From Weinstein and Davis, 1967).

Figure 4 - Predicted versus observed cloud top heights for 19 clouds in
Arizona (From Weinstein and Davis, 1967).

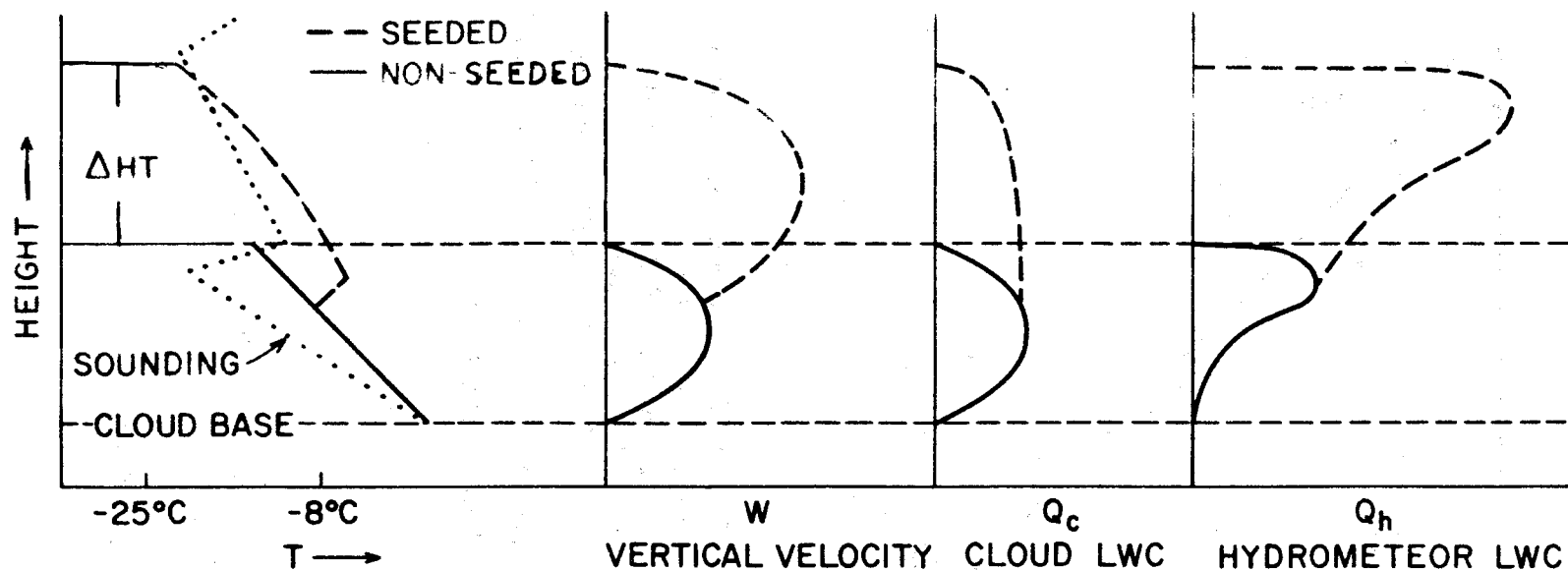


Lecture 8, Figure 1



Graphical Description of Thermodynamic Calculations.

Lecture 8, Figure 2



ADDITIONAL RESULTS: HEIGHT INCREASE FROM SEEDING (ΔHT)

TOTAL PRECIPITATION ($\int_{\text{BASE}}^{\text{TOP}} Q_h$) SEEDED OR NON-SEEDED

DURATION OF PRECIPITATION, SEEDED AND NON-SEEDED

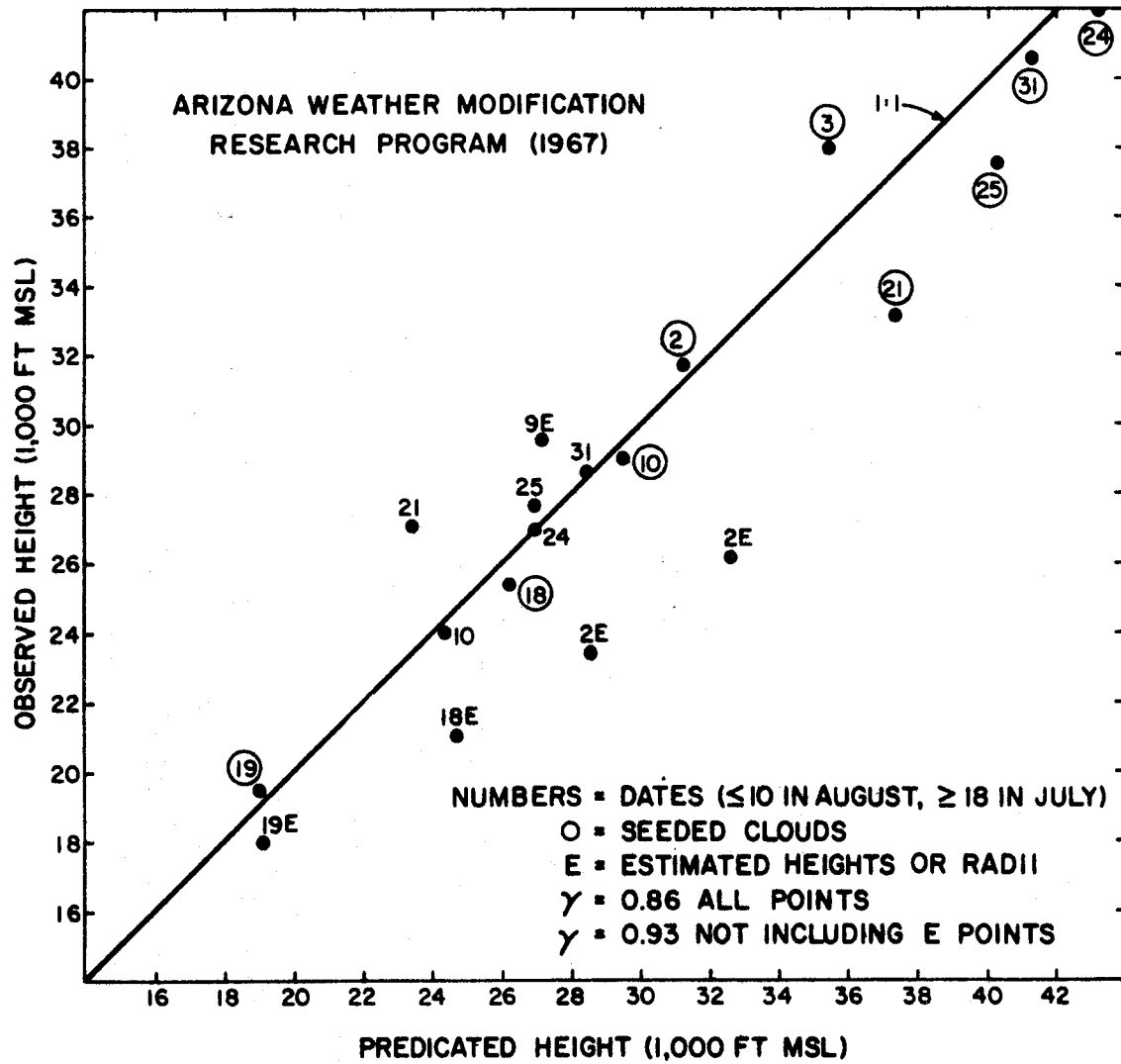
NOTE: CLOUD DYNAMICS RESULTS PARTICULARLY SENSITIVE TO:

- (1) ENVIRONMENTAL STABILITY (STRENGTH AND ALTITUDE OF INVERSIONS).
- (2) ICE NUCLEATION TEMPERATURE.
- (3) UPDRAFT RADIUS, MIXING PARAMETER μ .

Q_c , Q_h , TOTAL PRECIPITATION AMOUNT AND DURATION, ARE IN ADDITION SENSITIVE TO K_1 , K_2 , α .

STEADY STATE MODEL OUTPUT

Lecture 8, Figure 3



Predicted Vs Observed Cloud Top Heights for
19 Clouds in Arizona.

IX. UNPLANNED WEATHER AND CLIMATE MODIFICATION

We have long known that cities can have an effect on certain aspects of the weather. Thus the temperatures in large cities are generally several degrees higher than those in areas just outside of the cities. However, in recent years there has been a growing body of evidence that cities and certain industrial activities may be influencing precipitation.

A. A study of precipitation by day-of-the-week over the eastern United States

Frederick (1970) analyzed fifty years of daily precipitation data from twenty-two Weather Bureau stations in the eastern United States to see if the precipitation on week days (Monday through Friday) differed from that on week-end days. The results are shown in Figs. 1 and 2.

(See end of Lecture #9).

It can be seen from these figures that during the cool season (October through March) Sundays, Saturdays and Mondays had, on an average, less than $1/7$ (14.3%) of the total weekly precipitation while on Tuesday through Thursday this daily precipitation was greater than $1/7$. However, during the warm season (April through September) the precipitation on each day was within 0.2% of 14.3%.

These results show that the precipitation during the cool season in urban areas of the United States is not randomly distributed but is less on weekends and greater on weekdays. Since there is not a natural seven-day cycle, the implication is that this difference in precipitation is due to the "higher level" of man's activities on weekdays than on weekends.

B. The La Porte weather anomaly

La Porte, Indiana, is a small town situated about 30 miles east of the industrial complex of East Chicago and Gary. Changnon (1968)

has pointed out that during the period 1920 to 1945 there was an apparent pronounced increase in precipitation at La Porte, but during the same period nearby stations experienced little precipitation change.

The indicated increases in precipitation at La Porte occurred during the warm season of the year. The increases in summer rainfall were accompanied by an increase in the number of thunderstorm days. The suggestion is that these changes were brought about by the increasing industrial activities in the Chicago area. However, since 1945 there has been a general downward trend in the precipitation at La Porte although the industrial activity in Chicago has continued to increase.

C. Cloud condensation nuclei from industrial sources and their apparent effects on precipitation in Washington State

Hobbs, et al. (1970) have reported on survey measurements of cloud condensation nuclei (CCN) in Washington State. These measurements showed that certain industries are prolific sources of CCN. Some of the more important sources identified were:

<u>Source</u>	<u>Output per sec of CCN active at 1% supersaturation</u>
Large paper mills (Kraft process)	$10^{17} - 10^{19}$
Small paper mills (Kraft process)	$10^{14} - 10^{15}$
Small paper mills (Sulfite process)	$10^{14} - 10^{15}$
Large sawmills with wood-waste burners	10^{18}
Aluminum smelters	$10^{14} - 10^{16}$

All of the above sources produced sufficient numbers of CCN to cause appreciable changes in the concentrations of CCN in the air for distances extending up to 100 km downwind. Many of the major sources of general air pollution are not appreciable sources of CCN. Thus the

exhaust from automobiles, oil refineries and oil-fired power plants produce relatively few CCN. Consequently, the city of Everett, Washington, which has four large paper mills and a sawmill produces more CCN than Seattle, although Seattle has a population ten times greater than Everett. The locations of some of the principal sources of CCN in Washington State are shown in Fig. 3. (See end of Lecture #9.)

The effluents from industrial sources of CCN can have an appreciable influence on the visible structure of clouds and precipitation. Clouds forming downwind of these sources (proposed name: "fumulus") have been observed to produce precipitable particles very efficiently. In addition to emitting CCN these industries emit varying amounts of heat and water vapor into the air which also aid the formation of clouds and precipitation.

D. Comparison of precipitation in Washington State for the periods 1929 - 1946 and 1946 - 1966.

An analysis has been made of the precipitation and streamflow records in Washington State for the periods 1929 to 1946 and 1946 to 1966. Figure 4 (see end of Lecture #9) shows values of the Student "t" statistic when a comparison is made between the mean annual precipitations and streamflows for the period 1929 to 1946 with those for the period 1946 to 1966. Positive values of "t" indicate that the mean annual precipitation was greater in the second period than in the first period. "t" values of 2.0, 2.7 and 3.0 are significant at the 0.05, 0.01 and 0.001 levels respectively.

The principal conclusions to be drawn from the results shown in Fig. 3 are:

1) Over most of the State of Washington the mean annual precipitation during the period 1946 - 1966 was higher than in the period 1929 - 1946. The increases in precipitation were generally more pronounced over higher elevations than lower. This conclusion is substantiated by high "t" values for streamflow from those rivers fed by high elevation watersheds.

2) Contrary to the general trend described above, there are two lowland pockets in the Puget Sound Basin which have highly significant positive values of "t". One of these is centered south of Pt. Townsend at Chimicum and the other just N.E. of Victoria. Also, the North Fork of the Stillaguamish River (NFS) which has a low elevation watershed shows the most significant "t" value (3.18) of all the rivers in the Puget Sound. The "t" values of 5.6 at Chimicum and Victoria reflect the fact that the mean annual precipitations at these locations during the period 1946-1966 were 33.7% greater than during the period 1929-1946. The mean annual runoff from the NFS was 20.8% greater during 1946-1966 than 1929-1946.

3) The two regions west of the Cascade Mountains which have the highest "t" values (Chimicum and Victoria) are both in the vicinity of large sources of CCN from paper mills (see Fig. 3). Also, the NFS is directly N.E. and therefore generally downwind of paper mills at Everett, Pt. Townsend and Port Angeles.

4) There is a region in the S.W. corner of the Olympic Peninsula (located at Raymond) where the "t" value is 3. This is also adjacent to a source of CCN associated with the burning of woodwastes in open furnaces (Fig. 3).

Several industrial sources of CCN along the Columbia River may be associated with fairly high "t" values.

5) Several high "t" values are found in the eastern part of the area shown in Fig. 4 (see end of Lecture #9). The largest of these ($t = 6.03$) is at Trail, Canada, where the largest non-ferrous smelter in the world is located. Near the center of the "t" value of 4.31 at Newport is a large wood-burning match factory. At Kellogg, Idaho, where the "t" value is 4.29, there is a large non-ferrous smelter.

It appears from these results that there is a high correlation between industrial sources of CCN and areas which have experienced anomalously high precipitation in the past twenty years.

E. Climate modification

We turn now to the possible effects of man's activities on worldwide climate.

From 1880 to 1940 the mean temperature over the earth's surface averaged for one year increased by 0.6°C while in the last 25 years it has decreased by 0.3°C . These apparently small changes in temperature caused dramatic changes in the position of frost and ice boundaries over the earth. The question must be asked: Were these changes in temperature caused by man's activities on this planet? We consider below several possible ways in which man's activities might cause a change in world climate.

The radiation balance of the earth is very sensitive to the amount of CO_2 in the air. In the nineteenth century the concentration of CO_2 in the air was about 290 parts per million and in 1970 it was 330 parts per million. This increase in CO_2 in the air is probably due to the burning of fossil fuels by man.

Calculations by Manabe and Wetherald (1967) show that for a period of relative humidity a 5% increase in CO_2 would lead to an increase in the mean temperature of the earth of 0.1°C . Hence, the warming trend up to 1940 may have been due in part to the increase in CO_2 in the atmosphere. However, since 1940 the CO_2 content has continued to increase while the temperatures have decreased.

The thermal balance of the earth is also affected by particulates. Bryson (1968) estimates that a decrease in atmospheric transparency, due to increased particulates, of 3% would reduce the surface temperature by 0.4°C . As we have seen above, particulates can also affect cloud cover. At present, about 31% of the earth's surface is covered by low cloud. If this increased to 36% the average temperature over the earth's surface would fall by 4°C ! The transparency of the atmosphere is certainly decreasing and this is in part due to man's activities.

Manabe and Wetherald (1967) estimate that a unit increase in the average albedo over the earth's surface would result in a decrease in average surface temperature of 1°C . The albedo of the earth is being changed by cultivation, de-forestation and urbanization. However, the net magnitude (and even the direction) of the change in albedo is unknown.

It is clear from these brief remarks that the changes in the environment caused by man's activities might be producing modifications in world climate. However, at the present time we are unable to predict the direction of these changes let alone their magnitude.

Notes taken by:

J. R. Travis

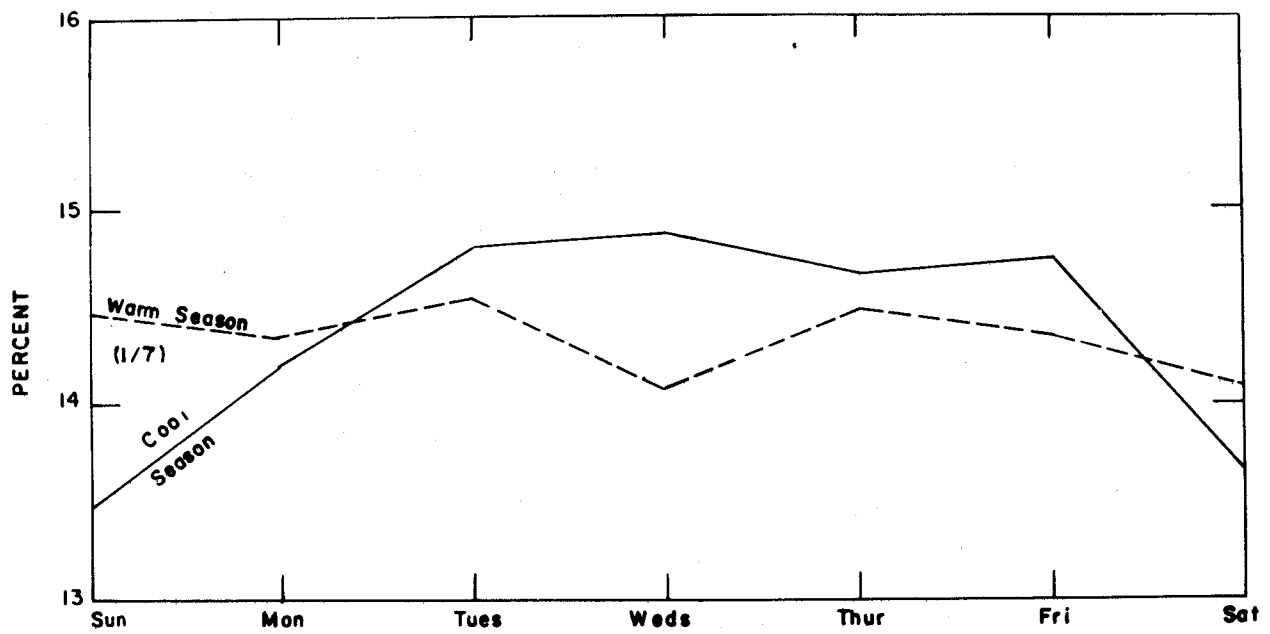
Y. M. Chang

REFERENCES

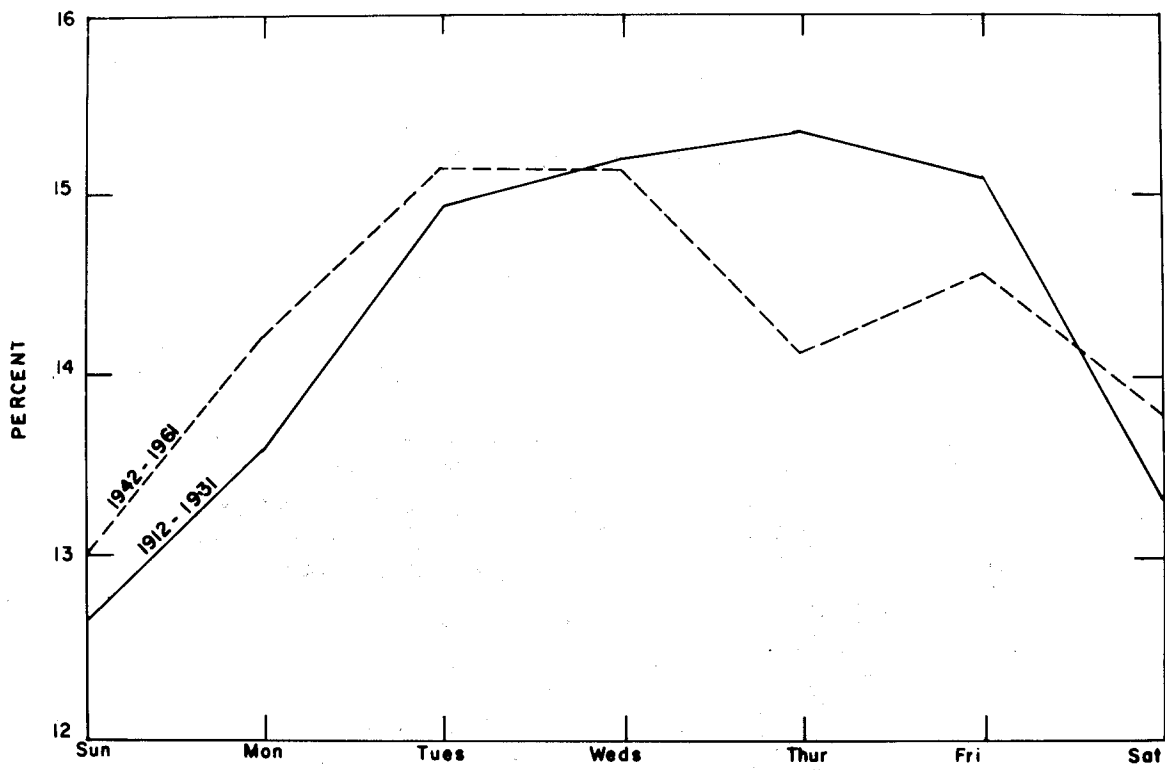
- Bryson, R. A., 1968: Seminar for the Amer. Meteor. Soc., Boston.
- Changnon, S. A., 1968: Bull. Amer. Met. Soc., 49, 4.
- Frederick, R. H., 1970: Proc. 2nd National Conf. on Weather Modification, Santa Barbara, Calif.
- Hobbs, P. V., L. F. Radke and S. E. Shumway, 1970: J. Atmos. Sci., 27, 81.
- Manabe, S. and R. T. Wetherald, 1967: J. Atmos. Sci., 24, 241.

Figure Captions

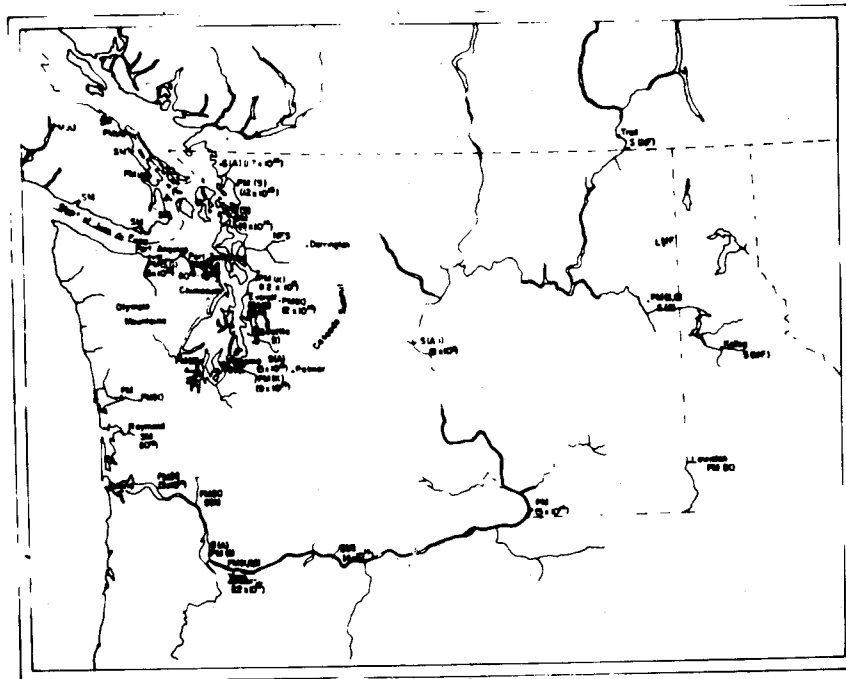
- Figure 1 - Per cent of total precipitation by day-of-the-week for 22 stations in the Eastern United States for the period 1912 - 1961 (From Frederick, 1970)
- Figure 2 - Per cent of total cool-season precipitation by day-of-the-week for 22 stations in the Eastern United States for the periods 1942 - 1961 and 1912 - 1931 (From Frederick, 1970)
- Figure 3 - Locations of some industrial sources of CCN in Washington State
- Figure 4 - Values of Student "t" statistic for comparison of mean annual precipitations and streamflows for period 1929 - 1946 with 1946 - 1966.



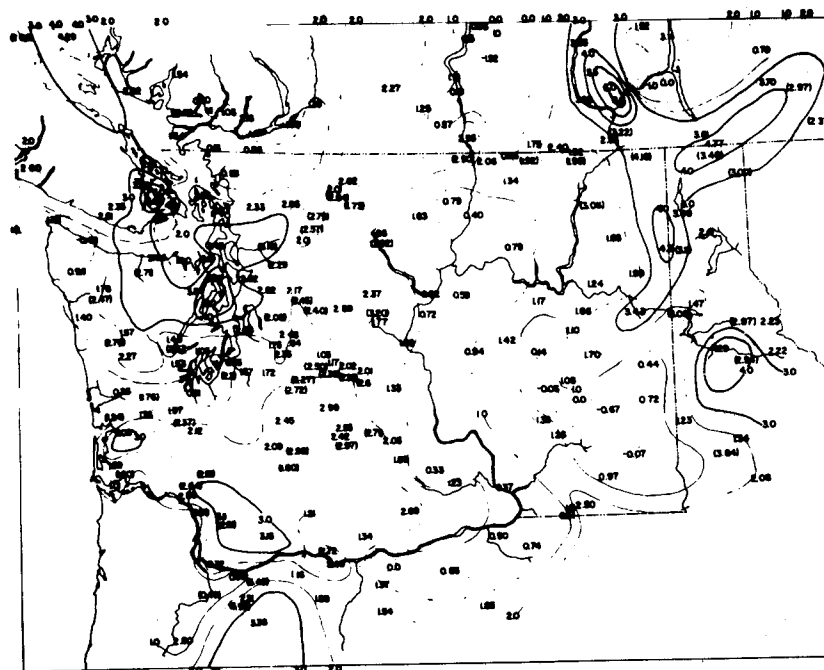
Lecture 9, Figure 1



Lecture 9, Figure 2



Lecture 9, Figure 3



Lecture 9, Figure 4

I. MECHANICS OF VORTICITY AND THE GENERATION OF STREAMWISE ROTATION

In this series of lectures we shall talk about some dynamical motions of the atmosphere. To get a basic view of fluid motion, let us examine the vorticity equation, since we see that many motions of the atmosphere are chaotic vorticity, that is vorticity all tangled up. First some notation and definitions.

1.0 Notation and fundamental relations

Velocity

$$\underline{v}$$

Speed

$$q = |\underline{v}|$$

Vorticity

$$\underline{\omega} = \text{curl } \underline{v} = \nabla \times \underline{v}$$

$$\omega = |\underline{\omega}|$$

Gravity

$$\underline{g} = \text{grad } gz = \nabla gz$$

z = vertical coordinate

Material Derivative

in Time

$$\frac{D}{Dt} = \frac{\partial}{\partial t} + \underline{v} \cdot \text{grad}$$

Material Derivative

in Space

$$\frac{D}{Ds} = \underline{v} \cdot \text{grad}$$

in steady flow where s is measured along a streamline. Material rate of change along the path of the particle

Acceleration

$$\underline{f} = \frac{D\underline{v}}{Dt} = \frac{\partial \underline{v}}{\partial t} + (\underline{v} \cdot \text{grad}) \underline{v}$$

$$\underline{f} = \frac{\partial \underline{v}}{\partial t} + \text{grad} \left(\frac{q^2}{2} \right) - \underline{v} \times \underline{\omega}$$

Some Vector Identity Formulas

$$\text{div } \sigma \underline{v} = \nabla \cdot \sigma \underline{v} = \sigma \text{div } \underline{v} + \underline{v} \cdot \text{grad } \sigma$$

$$\text{curl } \sigma \underline{v} = \nabla \times \sigma \underline{v} = \sigma \text{curl } \underline{v} + \text{grad } \sigma \times \underline{v}$$

$$\begin{aligned} \text{curl curl } \underline{v} &= \nabla \times (\nabla \times \underline{v}) \\ &= \text{grad div } \underline{v} - \nabla^2 \underline{v} \\ &= \nabla (\nabla \cdot \underline{v}) - \nabla^2 \underline{v} \end{aligned}$$

$$\nabla^2 \underline{v} = (\text{div grad}) \underline{v} = (\underline{\nabla} \cdot \underline{\nabla}) \underline{v}$$

$$\text{div} (\underline{v} \times \underline{w}) = \underline{w} \cdot \underline{\text{curl}} \underline{v} - \underline{v} \cdot \underline{\text{curl}} \underline{w}$$

$$\underline{\text{curl}} (\underline{v} \times \underline{w}) = \underline{v} \text{ div } \underline{w} - \underline{w} \text{ div } \underline{v} + (\underline{w} \cdot \underline{\text{grad}}) \underline{v} - (\underline{v} \cdot \underline{\text{grad}}) \underline{w}$$

$$\text{div} (\underline{\text{curl}} \underline{v}) = 0$$

$$\underline{\text{curl}} (\underline{\text{grad}} \sigma) = 0$$

2.0 The Equations of Fluid Motion (Navier-Stokes)

Several assumptions are made in deriving the Navier-Stokes equations:

- (1) The stress is instantaneously and linearly related through a physical coefficient of viscosity to the rate of strain.
- (2) The fluid properties are isotropic and uniform.
- (3) The normal pressure in a fluid is the same as the mean pressure (which is 1/3 times the sum of 3 mutual perpendicular normal components of stress) in a fluid in motion.

Then for a unit mass of fluid the Navier-Stokes Equation is:

$$\frac{D\underline{v}}{Dt} = \underline{g} - \frac{1}{\rho} \underline{\text{grad}} p + \nu \nabla^2 \underline{v} + \frac{1}{3} \nu \underline{\text{grad}} \text{div } \underline{v}$$

acceleration = gravity + pressure + viscous terms

where

gradient
force

$$\nu = \frac{\mu}{\rho} \quad \mu = \text{viscosity}$$

$$\rho = \text{density}$$

The viscous forces arise in two ways:

$$(1) \text{ Terms like } \nu \frac{\partial}{\partial x} \frac{\partial \underline{v}}{\partial x} \quad \text{when } \underline{v} = (u, v, w),$$

arise from $\frac{1}{\rho} \frac{\partial}{\partial x} \left(\mu \frac{\partial v}{\partial x} \right)$ and $\mu \frac{\partial v}{\partial y}$ and is the shear stress due to a change in the x direction of the y velocity. If v varies in the x direction it produces a body force in the y direction.

(2) Terms involving $\frac{\partial}{\partial x} \mu \frac{\partial u}{\partial x}$ arise from the first viscous term and the whole of the second viscous term arise from the work needed to deform the fluid when it is stretched ($\frac{\partial u}{\partial x} \neq 0$) or otherwise deformed due to non-uniformity of expansion ($\frac{\partial}{\partial x} \frac{\partial u}{\partial y} \neq 0$). In practice the only terms which matter to us are those related to the shearing; those related to the deformation are usually negligible in meteorology, even in the case of turbulent stresses, because the velocity gradients are usually greatest in a direction normal to the velocity.

3.0 The Vorticity Equation

Assuming μ is uniform, multiply the Navier-Stokes Equation by ρ and take the curl so that

$$\underline{\text{curl}} \left(\rho \frac{D\underline{v}}{Dt} \right) = \underline{\text{curl}} \rho \underline{g} + \mu \underline{\text{curl}} \nabla^2 \underline{v} + \underline{\text{curl}} \left(\frac{\underline{v}}{3} \text{grad div } \underline{v} \right)$$

$$\underline{\text{curl}} \left(\rho \frac{D\underline{v}}{Dt} \right) = \rho \underline{\text{curl}} \frac{D\underline{v}}{Dt} + \text{grad } \rho \times \frac{D\underline{v}}{Dt}$$

$$\underline{\text{curl}} \left(\rho \frac{D\underline{v}}{Dt} \right) = \rho \underline{\text{curl}} \left\{ \frac{\partial \underline{v}}{\partial t} + \cancel{\text{grad} \left(\frac{\underline{v}^2}{2} \right)} - \underline{v} \times \underline{\omega} \right\} + \text{grad } \rho \times \underline{f} \quad \text{where } \underline{f} = \frac{D\underline{v}}{Dt}$$

$$\underline{\text{curl}} \left(\rho \frac{D\underline{v}}{Dt} \right) = \rho \left\{ \frac{\partial \underline{\omega}}{\partial t} - \underline{v} \text{div} \cancel{\underline{\omega}} + \underline{\omega} \text{div } \underline{v} - (\underline{\omega} \cdot \text{grad}) \underline{v} + (\underline{v} \cdot \text{grad}) \underline{\omega} \right\} + \text{grad } \rho \times \underline{f}$$

$$\text{also } \underline{\text{curl}} \rho \underline{g} = \rho \cancel{\underline{\text{curl}} \underline{g}} + \text{grad } \rho \times \underline{g}$$

$$\underline{\text{curl}} \nabla^2 \underline{v} = \underline{\text{curl}} \left\{ \cancel{\text{grad div } \underline{v}} - \underline{\text{curl}} \underline{\text{curl}} \underline{v} \right\} = \text{grad } \cancel{\text{div } \underline{\omega}} - \nabla^2 \underline{\omega}$$

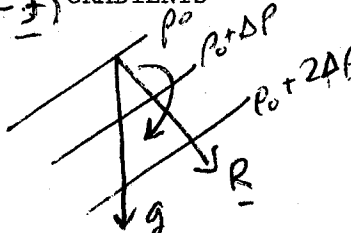
So collecting terms, dividing by ρ , and defining $\underline{R} = \frac{1}{\rho} \text{grad } \rho$, the vorticity equation is

$$\frac{D\underline{\omega}}{Dt} = -\underline{\omega} \text{div } \underline{v} + (\underline{\omega} \cdot \text{grad}) \underline{v} + \underline{R} \times (\underline{g} - \underline{f}) + \nu^2 \nabla^2 \underline{\omega}$$

Now let us examine each term for its physical meaning:

$$(1) \frac{D\omega}{Dt} = \nu^2 \nabla^2 \omega \quad \text{VISCOSITY}$$

This is the diffusion equation, in which the vorticity ω is diffused by the viscosity, such that for uniform ν , gradients of ω become uniform throughout the fluid. This equation applies to each component of ω separately and there is no conversion between components. Also there is no vorticity production, and so if ω is zero initially, it will remain zero in a viscous fluid without boundaries.

$$(2) \frac{D\omega}{Dt} = R \times (g - f) \quad \text{GRADIENTS}$$


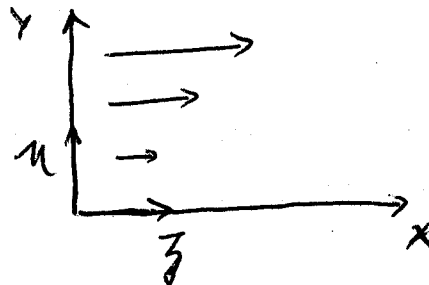
The diagram shows a fluid element in a pressure field. Three parallel lines represent pressure surfaces labeled p_0 , $p_0 + \delta p$, and $p_0 + 2\delta p$ from top to bottom. A downward arrow labeled g represents gravity. A vector labeled R points from the $p_0 + \delta p$ surface towards the $p_0 + 2\delta p$ surface, perpendicular to the pressure surfaces.

This equation says that the fluid acceleration and gravity act in the same way so as to produce a rotation of the fluid in the direction that makes R and $(g - f)$ parallel. In the atmosphere the dominant accelerations are gravity g and centrifugal. The fluid accelerations f are of minor importance.

$$(3) \frac{D\omega}{Dt} = (\omega \cdot \text{grad}) \underline{v} \quad \text{ADVECTION BY THE FLUID}$$

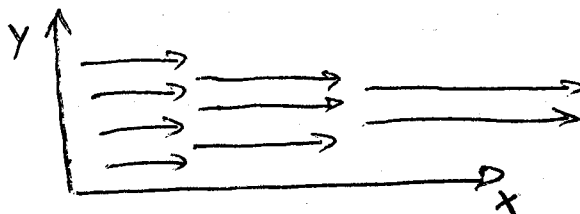
To understand this term, $\text{div } \underline{v} = 0$, otherwise the other term $\omega \text{ div } \underline{v}$ will be important in the interpretation. In the component equations, where $\omega = (\xi, \eta, \zeta)$ and $\underline{v} = (u, v, w)$ are terms like

$$\frac{D\xi}{Dt} = \eta \frac{\partial u}{\partial y} + \zeta \frac{\partial u}{\partial z}$$



which represent the tilting over of η or ζ to become ξ , and terms like

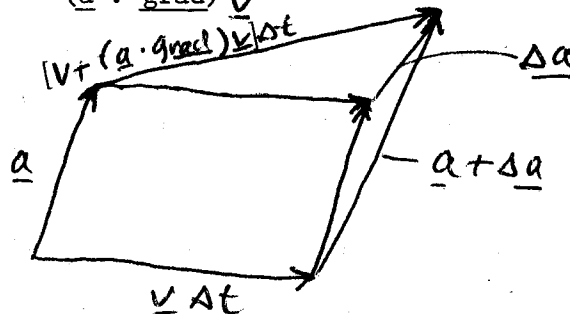
$$\frac{D\xi}{Dt} = \xi \frac{\partial u}{\partial x}$$



which represent an increase of ξ by a stretching of the fluid in the x direction, which must be accompanied by a contraction in the y z plane and a decrease in the moment of inertia in the x direction. This term represents the conservation of local angular momentum.

A non-divergent vector field may be represented by either the density of lines or by the magnitude and direction of elemental vectors embedded in the fluid. If \underline{a} is an elemental vector marked in the fluid, then after a time

Δt , \underline{a} becomes $\underline{a} + \Delta \underline{a}$ and it is evident that, to first order in small quantities, $\Delta \underline{a} = (\underline{a} \cdot \text{grad}) \underline{v} \Delta t$ so the material vector \underline{a} changes at a rate $\frac{\Delta \underline{a}}{\Delta t} = (\underline{a} \cdot \text{grad}) \underline{v}$



In order to preserve the relationship between the vector field as represented by the \underline{a} lines and the field represented by the elemental vectors \underline{a} , we must have $\text{div } \underline{a} = \text{div } \underline{v} = 0$. Thus in incompressible flow

$$\frac{D\omega}{Dt} = (\underline{\omega} \cdot \text{grad}) \underline{v}$$

states that the vortex lines are advected with the fluid.

$$(4) \quad \frac{D\omega}{Dt} = -\underline{\omega} \text{ div } \underline{v} \quad \text{FLUID EXPANSION}$$

If the fluid expansion is along the x direction only, that is $\frac{D\xi}{Dt} = -\xi \frac{\partial u}{\partial x}$

we have to note that the following term in the equation supplies the term

$$\frac{D\zeta}{Dt} = \zeta \frac{\partial u}{\partial x}$$

which cancels the first. Therefore stretching along the vortex lines does not alter the vorticity unless it is accompanied by a contraction in the plane perpendicular to the stretching. But the other terms, such as $\frac{D\zeta}{Dt} = -\zeta \left(\frac{\partial v}{\partial y} + \frac{\partial w}{\partial z} \right)$ represent the conservation of angular momentum about the x axis. As the area perpendicular to the x direction decreases the rotation is correspondingly increased.

4.0 The Atmospheric Version of the Equations

Two definitions are needed:

$$\theta = \text{potential temperature} = \frac{1}{\gamma} = T \left(\frac{P_1}{P} \right)^{\frac{\gamma-1}{\gamma}}$$

$$\theta = \frac{\gamma R}{\gamma-1} \left(\frac{P}{P_1} \right)^{\frac{\gamma-1}{\gamma}}$$

Now with the assumption that the motion is adiabatic, that is,

$p = k_0 \rho^\gamma$ where k_0 is a constant for a particle and is constant in the material surfaces of the fluid, then $\frac{1}{\rho} \text{grad } p = \frac{1}{\gamma} \text{grad } \theta$ and in the equations above we may replace p and ρ by ζ and θ . The vorticity equation is unaltered except that $R = \frac{1}{\gamma} \text{grad } \zeta$ and we can think of the reciprocal of potential temperature instead of gradients of density. This really means that we should think in terms of gradients of ζ , instead of gradients of p , when we are determining the motion. In a saturated cloudy atmosphere it is θ_{wet} that we use. Incidentally

$$R = \frac{1}{\gamma k_0} \text{grad } k_0$$

5.0 The Isopycnic Vorticity Theorem

In an inviscid fluid we have

$$\frac{D\omega}{Dt} = -\omega \operatorname{div} \underline{v} + (\underline{\omega} \cdot \underline{\operatorname{grad}}) \underline{v} + R \times (\underline{g} - \underline{f})$$

This adds vorticity

This moves vortex

This creates

in the same direction

lines with the fluid

vorticity \perp to \underline{g} ,

as existing vorticity

i.e., in the

isopycnic surfaces

So the theorem states that if vortex lines are at any moment in the surfaces of constant density (or θ) they will remain in those surfaces. Gravity produced vorticity is always perpendicular to \underline{g} , and is therefore always horizontal, and is generated along the horizontal contours of the isopycnic surfaces.

Notes taken by:

W. H. Mach

R. M. McGehee

I. BERNOULLI'S EQUATION

For the case of steady, inviscid, isentropic flow the equation of motion is

$$\underline{\text{grad}} \frac{1}{2} q^2 - \underline{v} \times \underline{\omega} = - \underline{\text{grad}} g z - \frac{1}{\rho} \underline{\text{grad}} p$$

where the z-axis is vertical. If we now put $\frac{1}{\rho} \underline{\text{grad}} p = \underline{\text{grad}} \frac{p}{\rho} -$

$$p \underline{\text{grad}} \frac{1}{\rho}$$

$$\text{and} \quad \frac{1}{\sigma} \underline{\text{grad}} \omega = \underline{\text{grad}} \frac{\omega}{\sigma} - \omega \underline{\text{grad}} \frac{1}{\sigma}$$

then the equation of motion becomes

$$\underline{\text{grad}} \left(\frac{1}{2} q^2 + \frac{\omega}{\sigma} + g z \right) - \omega \underline{\text{grad}} \frac{1}{\sigma} = \underline{v} \times \underline{\omega}$$

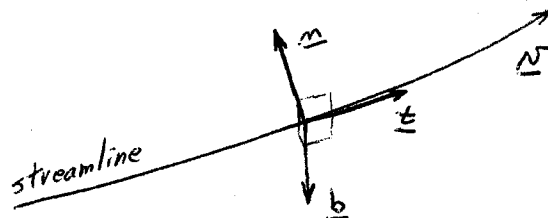
If we let $gH = \frac{1}{2} q^2 + \frac{\omega}{\sigma} + g z$, we would like to determine along what surface gH is constant ($\underline{\text{grad}} gH = 0$). Suppose there is an isentropic surface containing streamlines and vortex lines; then

$$\underline{v} \cdot \underline{\text{grad}}(gH) = \underline{\omega} \cdot \underline{\text{grad}}(gH) = 0, \text{ and } H \text{ is always}$$

constant in these "Bernoulli surfaces" which are the surfaces of constant θ (or ρ for an incompressible fluid). The streamlines and vortex lines lie in the Bernoulli surface. If the vortex lines do not initially lie in an isentropic surface, Bernoulli's theorem is not very useful.

II. STREAMWISE VORTICITY

Streamwise or "secondary" vorticity does not exist in basic flows because it is not usually produced by viscosity as most basic vorticity is. To establish a coordinate system, first consider the unit vector, \underline{t} , tangent to a streamline. Then $\underline{t} = \frac{\underline{v}}{q}$. Let s be the arc length along particle paths; hence $\underline{t} \cdot \underline{\text{grad}} = \frac{\partial}{\partial s}$. Since



\underline{t} is a unit vector, it must be normal to its derivative (i.e. $\frac{\partial \underline{t}}{\partial s} \cdot \underline{t} = 0$), and we can define \underline{n} , the principal unit normal, perpendicular to \underline{t} , such that

$$\frac{\partial \underline{t}}{\partial s} = \kappa \underline{n} \quad (1)$$

where κ is the curvature of the particle path ($\kappa = \frac{\partial \underline{t}}{\partial s} \cdot \underline{n} = \left| \frac{\partial \underline{t}}{\partial s} \right|$).

The normal \underline{n} lies in the osculating plane which contains successive positions

of \underline{t} . Differentiating $\underline{t} \cdot \underline{n} = 0$, we obtain $\frac{\partial \underline{t}}{\partial s} \cdot \underline{n} = -\underline{t} \cdot \frac{\partial \underline{n}}{\partial s} = \kappa$.

Defining \underline{b} as $\underline{t} \times \underline{n}$ and using the result that $\underline{n} \cdot \frac{\partial \underline{n}}{\partial s} = 0$, we obtain

$$\frac{\partial \underline{n}}{\partial s} = -\kappa \underline{t} + \tau \underline{b} \quad (2)$$

where τ is the torsion (not to be confused with $\frac{1}{\rho}$). Since $\underline{t} \cdot \underline{b} = 0$,

differentiating implies that $\underline{t} \cdot \frac{\partial \underline{b}}{\partial s} = -\underline{b} \cdot \frac{\partial \underline{t}}{\partial s} = 0$, and

$$\frac{\partial \underline{b}}{\partial s} = -\tau \underline{n}. \quad (3)$$

Equations (1), (2), and (3) are Frenet's formulae. The vectors \underline{t} , \underline{b} , and \underline{n} define a coordinate system.

The acceleration is in the plane of \underline{t} and \underline{n} , so for steady flow

$$\underline{f} = \frac{D\underline{v}}{Dt} = (\underline{v} \cdot \underline{\text{grad}}) \underline{v} = \underline{\text{grad}} \frac{1}{2} q^2 - \underline{v} \times \underline{\omega}$$

$$\underline{f} = (\underline{f} \cdot \underline{t}) \underline{t} + (\underline{f} \cdot \underline{n}) \underline{n}$$

$$\underline{f} = q(\underline{t} \cdot \underline{\text{grad}})(\underline{t}) = q^2(\underline{t} \cdot \underline{\text{grad}}) \underline{t} + q \underline{t} (\underline{t} \cdot \underline{\text{grad}} q)$$

$$= \kappa q^2 \underline{n} + a \underline{t} \quad \text{where "a" is}$$

the tangential acceleration given by $\underline{v} \cdot \underline{\text{grad}} q$. Thus,

$$\underline{f} \cdot \underline{t} = \underline{t} \cdot \underline{\text{grad}} \frac{1}{2} g^2,$$

$$\underline{f} \cdot \underline{m} = \kappa g^2 \quad (\text{the centrifugal force per unit mass}),$$

$$\underline{f} \cdot \underline{b} = 0 \quad (\text{by definition of } \underline{b}),$$

$$\underline{f} \times \underline{t} = (\underline{f} \cdot \underline{m}) \underline{m} \times \underline{t} = -\kappa g^2 \underline{b}, \quad \text{and}$$

$$\underline{\omega} \cdot \underline{f} = \underline{\omega} \cdot \underline{\text{grad}} \frac{1}{2} g^2 = \underline{\omega} \cdot \underline{\text{grad}} \frac{1}{2} (\underline{v} \cdot \underline{v}) = \underline{v} \cdot (\underline{\omega} \cdot \underline{\text{grad}}) \underline{v}.$$

The secondary vorticity is $\omega_s = \underline{\omega} \cdot \underline{t} = \frac{1}{g} \underline{\omega} \cdot \underline{v}$. The vorticity represents the rotation in unit time, but the effects of secondary vorticity are better represented as rotation in unit distance; therefore the relevant quantity is $\frac{\omega_s}{g}$. In steady motion the vorticity equation is

$$(\underline{v} \cdot \underline{\text{grad}}) \underline{\omega} = -\underline{\omega} \operatorname{div} \underline{v} + (\underline{\omega} \cdot \underline{\text{grad}}) \underline{v} + \underline{R} \times (\underline{g} - \underline{f}) - \nu \nabla^2 \underline{\omega}.$$

Thus,

$$(\underline{v} \cdot \underline{\text{grad}}) \frac{\underline{\omega} \cdot \underline{t}}{g} = \underline{\omega} \cdot \left\{ \frac{1}{g} (\underline{v} \cdot \underline{\text{grad}}) \underline{t} + \underline{t} (\underline{v} \cdot \underline{\text{grad}} \frac{1}{g}) \right\} + \frac{\underline{t}}{g} \cdot (\underline{v} \cdot \underline{\text{grad}}) \underline{\omega}$$

$$= \underline{\omega} \cdot \left\{ \kappa \underline{m} - \frac{1}{g^3} \underline{t} (\underline{v} \cdot \underline{\text{grad}} \frac{1}{2} g^2) \right\} + \frac{\underline{t}}{g} \cdot \left\{ -\underline{\omega} \operatorname{div} \underline{v} + \right.$$

$$(\underline{\omega} \cdot \underline{\text{grad}}) \underline{v} + \underline{R} \times (\underline{g} - \underline{f}) + \nu \nabla^2 \underline{\omega} \left. \right\}$$

$$= \underline{\omega} \cdot \left\{ \kappa \underline{m} - \frac{1}{g^2} \underline{t} (\underline{f} \cdot \underline{t}) \right\} - \frac{\underline{\omega} \cdot \underline{t}}{g} \operatorname{div} \underline{v} + \frac{1}{g^2} \underline{\omega} \cdot \underline{f} +$$

$$\frac{\underline{t}}{g} \cdot \left\{ \underline{R} \times (\underline{g} - \underline{f}) + \nu \nabla^2 \underline{\omega} \right\}$$

$$= \underline{\omega} \cdot \left\{ \kappa \underline{m} + \frac{1}{g^2} \underline{m} (\underline{f} \cdot \underline{m}) \right\} - \frac{\underline{\omega} \cdot \underline{t}}{g} \operatorname{div} \underline{v} - \frac{1}{g} \underline{R} \cdot \underline{f} \times \underline{t} +$$

$$\frac{1}{g} \underline{R} \times \underline{g} \cdot \underline{t} + \frac{\nu \underline{t}}{g} \cdot \nabla^2 \underline{\omega}.$$

Using $\frac{1}{g^2} \underline{\omega} \cdot \underline{n} (\underline{f} \cdot \underline{n}) = \kappa \underline{\omega} \cdot \underline{n}$ and $-\frac{1}{g} \underline{R} \cdot \underline{f} \times \underline{t} = \kappa_g \underline{R} \cdot \underline{b}$,

we obtain

$$(\underline{n} \cdot \underline{\text{grad}}) \frac{\underline{\omega} \cdot \underline{t}}{g} = 2\kappa \underline{\omega} \cdot \underline{n} + \kappa_g \underline{R} \cdot \underline{b} + \frac{1}{g} \underline{R} \times \underline{g} \cdot \underline{t} - \frac{\underline{\omega} \cdot \underline{t}}{g} \underline{\text{div}} \underline{n} + \frac{1}{g} \underline{t} \cdot \nabla^2 \underline{\omega}.$$

In the ensuing discussion the $\underline{\text{div}} \underline{n}$ term and the viscosity term are of small importance and will be ignored. $\kappa \underline{\omega} \cdot \underline{n}$ represents the change in the direction of \underline{t} due to κ and the effect of the conservation of the component $\underline{\omega} \cdot \underline{b}$, hence the factor of 2 in $\kappa \underline{\omega} \cdot \underline{n}$. $\kappa_g \underline{R} \cdot \underline{b}$ represents the effect of centrifugal forces on the \underline{b} component of density gradient, and $\frac{1}{g} \underline{R} \times \underline{g} \cdot \underline{t}$ represents the effect of gravity on the density gradient resolved along \underline{t} .

Alternatively we note that

$$\begin{aligned} \underline{\omega} \cdot \underline{n} &= \underline{\omega} \cdot \underline{b} \times \underline{t} = \underline{t} \times \underline{\omega} \cdot \underline{b} = \frac{1}{g} (\underline{n} \times \underline{\omega}) \cdot \underline{b} \\ &= \frac{1}{g} (\underline{\text{grad}} \frac{1}{2} g^2 - \underline{f}) \cdot \underline{b} = \frac{1}{g} \underline{\text{grad}} \frac{1}{2} g^2 \cdot \underline{b}. \end{aligned}$$

Thus

$$\begin{aligned} 2\kappa \underline{\omega} \cdot \underline{n} + \kappa_g \underline{R} \cdot \underline{b} &= \kappa_g \left\{ \frac{1}{g^2 \rho} \rho \underline{\text{grad}} \frac{1}{2} g^2 + \frac{2}{g^2 \rho} \frac{1}{2} g^2 \underline{\text{grad}} \rho \right\} \cdot \underline{b} \\ &= \kappa_g \underline{\text{grad}} \log \frac{1}{2} \rho g^2 \cdot \underline{b}. \end{aligned}$$

Thus the effect of curvature is to produce a rotation around the tangent if there is a gradient of $\frac{1}{2} \rho g^2$ in the direction of \underline{b} . For this purpose the inertial effect depends on gradients of $\frac{1}{2} \rho g^2$, not simply of ρ .

III. STABLE AND UNSTABLE OSCILLATIONS IN CURVED FLOW (GRAVITY NEGLECTED)

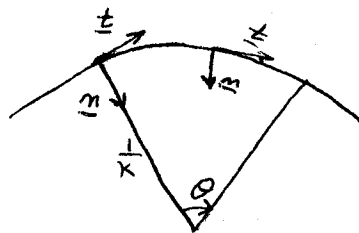
Suppose ϕ measures the angle rotated by the Bernoulli surfaces around the streamline, then if the fluid on a streamline is in locally solid rotation around it,

$$\omega_s = 2g \frac{\partial \phi}{\partial s}, \quad \underline{N} \cdot \underline{\text{grad}} \frac{\omega_s}{g} = g \frac{\partial}{\partial s} 2 \left(\frac{\partial \phi}{\partial s} \right) =$$

$$= 2g \frac{\partial^2 \phi}{\partial s^2} = \kappa g \underline{\text{grad}} \log \frac{1}{2} \rho g^2 \cdot b,$$

$$\frac{\partial^2 \phi}{\partial s^2} = \frac{\kappa}{2} \underline{\text{grad}} (\log \frac{1}{2} \rho g^2) \sin \phi.$$

If θ is the angle turned through by the tangent (or normal), then $\kappa ds = d\theta$ and $\frac{\partial^2 \phi}{\partial \theta^2} = \frac{1}{2\kappa} \underline{\text{grad}} (\log \frac{1}{2} \rho g^2) \sin \phi$, which is the pendulum equation with period of oscillation $2\pi \left(\frac{2\kappa}{\underline{\text{grad}} \log \frac{1}{2} \rho g^2} \right)^{1/2}$ in θ .



$b = \text{constant}$

For this to be important in the atmosphere the terms considered here must exceed the gravitational term, which can occur if q is large enough. In the atmosphere the effect of curvature on density gradients is usually negligible because $f \ll g$, but in curved pipes this is not the case.

Combining the above,

$$\underline{N} \cdot \underline{\text{grad}} \left(\frac{\omega \cdot \underline{t}}{g} \right) = 2\kappa \underline{\omega} \cdot \underline{m} + \kappa g \underline{R} \cdot \underline{b} + \frac{1}{g} \underline{R} \times \underline{g} \cdot \underline{t}$$

$$= \kappa g \underline{\text{grad}} \lambda \cdot \underline{b} + \frac{1}{g} \underline{R} \times \underline{g} \cdot \underline{t} = 2g \frac{\partial^2 \phi}{\partial s^2}$$

where $\lambda = \ln(\frac{1}{2} \rho g^2)$, or in the usual atmospheric case,
 $\lambda = \ln(\frac{1}{2} \tau g^2)$.

Let us consider motion in a vertical plane. If the tangent is inclined at an angle ψ to the horizontal,

$$\underline{g} \times \underline{t} = g \cos \psi \underline{b}.$$

Then

$$\begin{aligned} \frac{1}{g} \underline{R} \cdot \underline{g} \times \underline{t} &= \frac{1}{g} g \cos \psi \underline{R} \cdot \underline{b} \\ &= \frac{g R}{g^2} \cos \psi \sin \phi, \end{aligned}$$

and

$$\begin{aligned} \frac{\partial^2 \phi}{\partial s^2} &= \frac{1}{2g} \left[\kappa g \text{grad } \lambda \cdot \underline{b} + \frac{1}{g} \underline{R} \times \underline{g} \cdot \underline{t} \right] \\ &= \left[\frac{\kappa}{2} \frac{\partial \lambda}{\partial n} - \frac{g R}{2 g^2} \cos \psi \right] \sin \phi. \end{aligned}$$

n is measured in the direction normal \underline{n} , in the vertical plane. Stability is determined by the sign of the coefficient of $\sin \phi$.

To relate this to the Richardson number $Ri = \frac{g R}{(\partial g / \partial n)^2}$, examine the stability of a horizontal flow ($\psi = 0$). The sign of the coefficient of $\sin \phi$ is determined by the ratio

$$S = \frac{g R}{\kappa g^2 \frac{\partial \lambda}{\partial n}}.$$

Ignoring variation in ρ as too small,

$$\begin{aligned} \frac{\partial \lambda}{\partial n} &= \frac{1}{g^2} \frac{\partial}{\partial n} g^2 = \frac{2}{g} \frac{\partial g}{\partial n} \\ S &= \frac{g R}{2 \kappa g (\partial g / \partial n)} = \frac{(\partial g / \partial n)}{2 \kappa g} Ri = \frac{\omega}{2 \kappa g} Ri. \end{aligned}$$

The motion is stable if $S > 1$, that is, if $Ri > \frac{2kq}{\omega}$. So no matter how large Ri , the motion can be destabilized by a large enough curvature k . Physically, R stabilizes while ω and kq destabilize.

Next, consider the validity of this when the motion is not steady, and look for a criterion for dynamic stability analogous to the criterion for static stability.

IV. STATIC STABILITY

As alternative to the familiar displaced particle method of deriving a criterion of stability, we can use the vorticity equation. In absence of motion, we can write

$$\frac{D\omega}{Dt} = R \times g$$

or

$$\frac{D\xi}{Dt} = gR \sin\phi,$$

where ξ is the x-component of vorticity (assumed horizontal), and ϕ is the angular displacement about the x-axis of a local tube of fluid. Then from the definition of vorticity,

$$\xi = 2 \frac{D^2\phi}{Dt^2}$$

and we can write

$$\begin{aligned} \frac{D^2\phi}{Dt^2} &= \frac{\xi}{2} = \frac{g}{2\tau} \frac{\partial\tau}{\partial z} \sin\phi \\ &\approx \frac{g}{2\tau} \frac{\partial\tau}{\partial z} \phi \quad \text{for } \phi \ll 1. \end{aligned}$$

This predicts exponential growth of ϕ if $\frac{\partial\tau}{\partial z} > 0$, that is, if potential temperature increases downward. (Recall $\frac{1}{\tau} \frac{\partial\tau}{\partial z} = -\frac{1}{\theta} \frac{\partial\theta}{\partial z}$). We can apply the same analysis to a fluid in motion to obtain a local criterion of instability due to centrifugal forces.

We shall use an analysis which deals with the possibility of an unsteady motion, as distinguished from motion in unstable equilibrium. Use the unit vectors \underline{t} , \underline{n} , \underline{b} , relative to the path of a particle. Then

$$\underline{f} \cdot \underline{b} = 0$$

$$\begin{aligned}\underline{f} &= \frac{D\underline{v}}{Dt} = a\underline{t} + \kappa g^2 \underline{n} \\ &= \text{grad} \frac{g^2}{2} - \underline{v} \times \underline{\omega} + \underline{\dot{v}}\end{aligned}$$

where $\underline{\dot{v}} = \frac{\partial \underline{v}}{\partial t}$.

$$\underline{f} \cdot \underline{t} = a = \frac{Dg}{Dt} = \dot{g} + g\underline{t} \cdot \text{grad} g.$$

Define

$$\underline{I} = (\underline{t} \cdot \text{grad}) \underline{v} = \text{grad} g - \underline{t} \times \underline{\omega} = \frac{1}{g} (\underline{f} - \underline{\dot{v}})$$

$$\begin{aligned}\underline{N} &= (\underline{n} \cdot \text{grad}) \underline{v} \\ &= \text{grad}(\underline{v} \cdot \underline{n}) - (\underline{v} \cdot \text{grad}) \underline{n} - \underline{n} \times \text{curl} \underline{v} - \underline{v} \times \text{curl} \underline{n} \\ &= -g(\kappa \underline{t} + \tau \underline{b}) + \dot{\underline{n}} - \underline{n} \times \underline{\omega} - \underline{v} \times \text{curl} \underline{n}\end{aligned}$$

$$\begin{aligned}\underline{B} &= (\underline{b} \cdot \text{grad}) \underline{v} \\ &= \text{grad}(\underline{v} \cdot \underline{b}) - (\underline{v} \cdot \text{grad}) \underline{b} - \underline{b} \times \text{curl} \underline{v} - \underline{v} \times \text{curl} \underline{b} \\ &= g\tau \underline{n} + \dot{\underline{b}} - \underline{b} \times \underline{\omega} - \underline{v} \times \text{curl} \underline{b}\end{aligned}$$

Using this basis,

$$(\underline{\omega} \cdot \text{grad}) \underline{v} = (\underline{\omega} \cdot \underline{t}) \underline{I} + (\underline{\omega} \cdot \underline{n}) \underline{N} + (\underline{\omega} \cdot \underline{b}) \underline{B}.$$

For the streamwise vorticity,

$$\frac{D}{Dt} \left(\frac{\underline{\omega} \cdot \underline{t}}{\rho} \right) = \frac{1}{\rho} \left\{ \underline{t} \cdot \frac{D\underline{\omega}}{Dt} + \underline{\omega} \cdot \frac{D\underline{t}}{Dt} \right\} - \frac{1}{\rho^2} \underline{\omega} \cdot \underline{t} \frac{D\rho}{Dt}$$

recalling that \underline{t} is the tangent unit vector, and the scalar t is the time.

$$\begin{aligned} \frac{D}{Dt} \left(\frac{\underline{\omega} \cdot \underline{t}}{\rho} \right) &= \frac{1}{\rho} \left\{ \underline{t} \cdot [(\underline{\omega} \cdot \underline{\text{grad}}) \underline{v} - \underline{R} \times \underline{f}] + \underline{\omega} \cdot \rho \underline{\kappa} \underline{n} \right\} - \frac{\rho \underline{\omega} \cdot \underline{t}}{\rho^2} \\ &= \frac{1}{\rho} \left\{ \underline{t} \cdot [(\underline{\omega} \cdot \underline{t}) \underline{T} + (\underline{\omega} \cdot \underline{n}) \underline{N} + (\underline{\omega} \cdot \underline{b}) \underline{B}] - \underline{t} \cdot \underline{R} \times (a \underline{t} + \rho \underline{\kappa} \underline{n}) \right\} \\ &\quad + \kappa \underline{\omega} \cdot \underline{n} - \frac{a}{\rho^2} \underline{\omega} \cdot \underline{t} \\ &= \frac{(\underline{\omega} \cdot \underline{t})}{\rho} \underline{t} \cdot \underline{\text{grad}} \rho + \frac{\underline{\omega} \cdot \underline{n}}{\rho} (\kappa \rho + \dot{n} \cdot \underline{t} - \underline{\omega} \cdot \underline{b}) \\ &\quad + \frac{(\underline{\omega} \cdot \underline{b})}{\rho} (\dot{b} \cdot \underline{t} + \underline{\omega} \cdot \underline{n}) + \kappa \rho \underline{R} \cdot \underline{b} \\ &\quad + \kappa \underline{\omega} \cdot \underline{n} - \frac{a}{\rho^2} \underline{\omega} \cdot \underline{t} \end{aligned}$$

$$\begin{aligned} \frac{D}{Dt} \frac{\underline{\omega} \cdot \underline{t}}{\rho} &= \frac{2\kappa \underline{\omega} \cdot \underline{n} + \kappa \rho \underline{R} \cdot \underline{b}}{\rho} \\ &\quad + \frac{1}{\rho} \underline{t} \cdot \left\{ -\frac{\dot{\rho}}{\rho} (\underline{\omega} \cdot \underline{t}) + \dot{n} (\underline{\omega} \cdot \underline{n}) + \dot{b} (\underline{\omega} \cdot \underline{b}) \right\} \end{aligned}$$

where we used

$$a = \underline{t} \cdot \rho \underline{\text{grad}} \rho + \dot{\rho} \cdot \underline{t}.$$

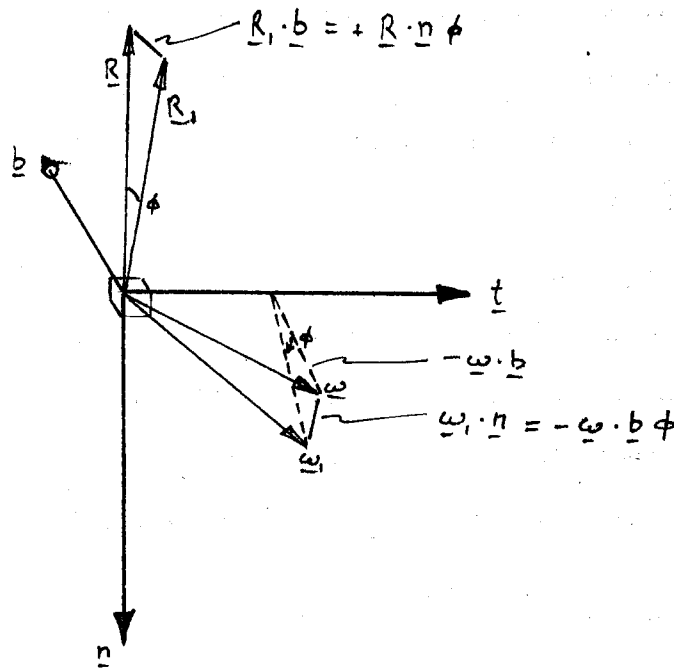
If we take the form (justified later)

$$\frac{D}{Dt} \frac{\underline{\omega} \cdot \underline{t}}{\rho} = 2\kappa \underline{\omega} \cdot \underline{n} + \kappa \rho \underline{R} \cdot \underline{b}.$$

This represents the way streamwise vorticity changes in an equilibrium motion.

If we subtract out the equilibrium motion, effectively assuming $\underline{\omega} \cdot \underline{n} = 0 = \underline{R} \cdot \underline{b}$ in the steady state, we are looking at a perturbation in the form of a rotation ϕ about \underline{t} .

In such a rotation, the vorticity and the density structure move with the fluid, so that \underline{R} and $\underline{\omega}$



become \underline{R}_1 and $\underline{\omega}_1$, and

$$\underline{\omega}_1 \cdot \underline{n} = - \underline{\omega} \cdot \underline{b} \phi$$

$$\underline{R}_1 \cdot \underline{b} = \underline{R} \cdot \underline{n} \phi$$

and the equation for streamwise vorticity is transformed to

$$\begin{aligned} \frac{D}{Dt} \frac{\underline{\omega} \cdot \underline{t}}{\rho} &= \rho \frac{D}{Ds} \left(\frac{1}{\rho} 2\rho \frac{D\phi}{Ds} \right) \\ &= -2\kappa \underline{\omega} \cdot \underline{b} \phi + \kappa \rho \underline{R} \cdot \underline{n} \phi \end{aligned}$$

or,

$$\frac{D^2 \phi}{Ds^2} = \left(-\frac{\kappa}{\rho} \underline{\omega} \cdot \underline{b} + \frac{\kappa}{2} \underline{R} \cdot \underline{n} \right) \phi$$

This pendulum equation indicates unstable motion if

$$-\frac{\kappa}{g} \underline{\omega} \cdot \underline{b} + g \underline{R} \cdot \underline{n} > 0.$$

$\underline{R} \cdot \underline{n} > 0$ implies, obviously, that density increases toward the center of curvature; centrifugal force would tend to overturn the structure. We shall interpret the condition $\underline{\omega} \cdot \underline{b} < 0$ later; in the meantime, notice it compares the sense of the vorticity with the direction the stream is turning.

Now consider the equation above, for $\frac{D}{Dt} \frac{\underline{\omega} \cdot \underline{b}}{g}$. When we are discussing rotational perturbations about \underline{b} , we can ignore the terms $\underline{b} \cdot \{ \dots \}$ and $\frac{a}{g^2} \underline{\omega} \cdot \underline{b}$.

The term $\underline{R} \cdot \underline{n}$ is large, and when $a \neq 0$, produces rotation around \underline{b} . Although this could be simply subtracted from the equation as equilibrium flow was in the streamwise vorticity case, if we were studying instabilities due to tangential accelerations, we are here interested in rotational perturbations. So we ignore terms in a , and simplify to

$$\frac{D}{Dt} \frac{\underline{\omega} \cdot \underline{b}}{g} = -2\tau \underline{\omega} \cdot \underline{n} - \kappa g \underline{R} \cdot \underline{t}.$$

Notes taken by:

J. D. Presley

J. R. Miller

STATIC STABILITY (Continued from Lecture #2)

By analogous treatment we also obtain

$$\frac{D}{Dt} \frac{\underline{\omega} \cdot \underline{b}}{g} = -2\zeta \underline{\omega} \cdot \underline{n} - K_g \underline{R} \cdot \underline{t} - \frac{a}{g^2} (\underline{\omega} \cdot \underline{b} + g \underline{R} \cdot \underline{n}) \\ + \frac{1}{g} \underline{b} \cdot \{ (\underline{\omega} \cdot \underline{t}) \text{grad } g + (\underline{\omega} \cdot \underline{n}) (\underline{n} - \underline{v} \times \text{Curl } \underline{n}) - (\underline{\omega} \cdot \underline{b}) \underline{v} \times \text{Curl } \underline{b} \}$$

By the argument given below we ignore the last term when considering the effects of rotational displacements about \underline{b} . Likewise we ignore $\frac{a}{g^2} \underline{\omega} \cdot \underline{b}$. The term in $\underline{R} \cdot \underline{n}$ is large anyway and produces rotation around \underline{b} if $a \neq 0$. This term cannot be subtracted from the equation as for the case of equilibrium flow (given above), although it could be if we were studying instabilities due to tangential accelerations (but then we would be concerned with $\underline{R} \cdot \underline{t}$).

So we ignore terms in a and get

$$\frac{D}{Dt} \frac{\underline{\omega} \cdot \underline{b}}{g} = -2\zeta \underline{\omega} \cdot \underline{n} - K_g \underline{R} \cdot \underline{t}$$

The full equations are

$$\frac{D}{Dt} \frac{\underline{\omega} \cdot \underline{t}}{g} = 2K \underline{\omega} \cdot \underline{n} + K_g \underline{R} \cdot \underline{b} \\ + \frac{1}{g} \underline{t} \cdot \left\{ -\frac{\underline{v}}{g} (\underline{\omega} \cdot \underline{t}) + \underline{n} (\underline{\omega} \cdot \underline{n}) + \underline{b} (\underline{\omega} \cdot \underline{b}) \right\} \quad (1)$$

$$\frac{D}{Dt} \frac{\underline{\omega} \cdot \underline{n}}{g} = (\underline{\omega} \cdot \underline{t}) \left\{ \frac{1}{g} \underline{n} \cdot \text{grad } g - K \right\} + (\underline{\omega} \cdot \underline{b}) \{ 2\zeta - \underline{n} \cdot \underline{t} \times \text{Curl } \underline{b} \} \\ + \underline{n} \cdot \{ (\underline{\omega} \cdot \underline{n}) \underline{t} \times \text{Curl } \underline{n} - \frac{1}{g} (\underline{\omega} \cdot \underline{b}) \underline{b} \} - \frac{a}{g} \underline{R} \cdot \underline{b} - \frac{a}{g^2} \underline{\omega} \cdot \underline{n} \quad (2)$$

$$\frac{D}{Dt} \frac{\underline{\omega} \cdot \underline{b}}{g} = 2\zeta \underline{\omega} \cdot \underline{n} - K_g \underline{R} \cdot \underline{t} \\ + \frac{1}{g} \underline{b} \cdot \{ \text{grad } g (\underline{\omega} \cdot \underline{t}) + (\underline{n} - \underline{v} \times \text{Curl } \underline{n}) \underline{\omega} \cdot \underline{n} - \underline{v} \times \text{Curl } \underline{b} (\underline{\omega} \cdot \underline{b}) \} \\ - \frac{a}{g} \underline{R} \cdot \underline{n} - \frac{a}{g^2} \underline{\omega} \cdot \underline{b} \quad (3)$$

The terms underlined are the only ones retained in the above argument, in considering terms of order ϕ for angular displacement ϕ around the 3 directions. The terms in "a" in (3) do not have corresponding terms in (1), although we showed that for helical flow the terms underlined are equivalent. This means that the terms in $\dot{\underline{y}}$, $\dot{\underline{n}}$, $\dot{\underline{b}}$ in (1) represent physical mechanisms which are the same ones as those which are tangential accelerations in (3), because the terms we retained do not represent such mechanisms even in the non-helical case (they do not include time derivatives or longitudinal gradients of q).

The justification given in the published paper for ignoring the last term in (1) is wrong because it does not justify getting rid of $a/q(\underline{R} \cdot \underline{n})$ in (3). It is wrong because although $\dot{\underline{n}} \cdot \underline{t}$ is not altered by a rotation of fluid around \underline{t} , (to first order) its coefficient ($\underline{\omega} \cdot \underline{n}$) is altered. The justification for omitting that term must be based on the assumption that $1/q \underline{t} \cdot \dot{\underline{u}} \ll 2K$, which is the coefficient of $\underline{\omega} \cdot \underline{n}$ in the first term we retained.

This comparison is between (I) changes in direction of a particle motion and (II) changes in direction of the motion at a fixed point. If the eddies pass at a rate such that these two rates of change are comparable then we already have a situation which is, for practical purposes, turbulent, and our study of the local instability is not very worthwhile. In restricting our considerations to those situations in which all the neglected terms are in fact negligible we are concentrating our attention on the most important cases.

There is no watertight justification for our choice, and in fact there cannot be without a rigid restriction of our considerations. In choosing the helical cases we are allowing K , ϕ , $\frac{\partial \theta}{\partial r}$, $\frac{\partial v}{\partial r}$, $\frac{\partial w}{\partial r}$ and $\underline{\omega}$ to take arbitrary values and we move the coordinate system along with the biggest local eddy so as to reduce all the terms in \underline{a} and $\frac{\partial}{\partial t}$.

Finally, by similar treatment, we get

$$\begin{aligned} \frac{D}{Dt} \frac{\underline{\omega} \cdot \underline{n}}{\rho} &= \underline{\omega} \cdot \underline{t} \left(\frac{1}{\rho} \underline{n} \cdot \text{grad } g - K \right) + \underline{\omega} \cdot \underline{b} (2\tau - \underline{n} \cdot \underline{t} \times \text{Curl } \underline{b}) \\ &+ \frac{a}{\rho} \underline{R} \cdot \underline{b} - \frac{a}{\rho^2} \underline{\omega} \cdot \underline{n} \\ &+ \underline{n} \cdot \left\{ (\underline{\omega} \cdot \underline{n}) \underline{t} \times \text{Curl } \underline{n} - \frac{1}{\rho} (\underline{\omega} \cdot \underline{b}) \underline{b} \right\} \end{aligned}$$

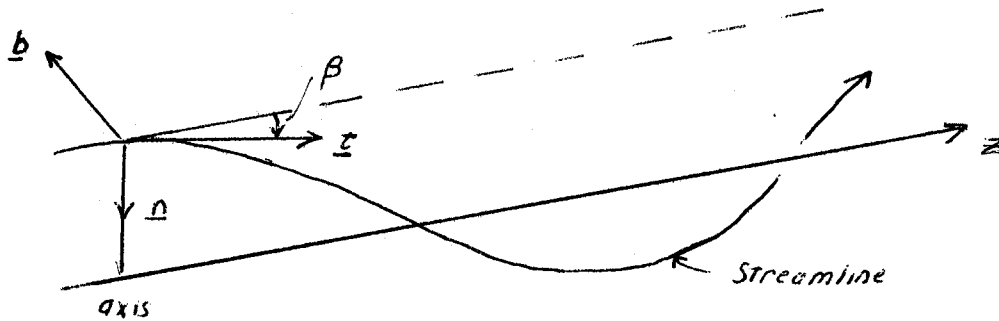
We neglect the last term because it is of the form $\underline{n} \cdot$ and is of second order for rotations around \underline{n} ; we also neglect the terms in "a" for the same reason as before (i.e. we are not studying the effects of tangential accelerations). Thus

$$\begin{aligned} \frac{D}{Dt} \frac{\underline{\omega} \cdot \underline{n}}{\rho} &= \underline{\omega} \cdot \underline{t} \left(\frac{1}{\rho} \underline{n} \cdot \text{grad } g - K \right) \\ &+ \underline{\omega} \cdot \underline{b} (2\tau + \underline{n} \cdot \underline{t} \times \text{Curl } \underline{b}) \end{aligned}$$

The three equations, by the very nature of the situation, involve the velocity, vorticity, curvature, and torsion and the density gradient \underline{R} . When we take them in perturbation form (in terms of angle ϕ) they only involve $\underline{R} \cdot \underline{n}$ because we are not concerning ourselves with the terms in a. Consequently, everything is expressible in terms of the local helix, namely the helix which has the same properties as the flow at the point where we are discussing the stability.

THE LOCAL HELIX

This is a cylindrical flow pattern in which the only direction in which quantities have gradients is the radial one.

Velocity

$$\underline{v} = (0, v, w) = (0, q \sin \beta, q \cos \beta)$$

Position

$$\underline{x} = (r, \theta, z)$$

(cylindrical polar)

$$= (r, \cos \theta, r \sin \theta, z)$$

(cartesian)

$$\underline{t} = (0, \sin \beta, \cos \beta)$$

(cylindrical polar)

$$= (-\sin \beta \sin \theta, \sin \beta \cos \theta, \cos \beta)$$

(cartesian)

$$\frac{d\underline{t}}{ds} = (-\sin \beta \cos \theta \frac{\partial \theta}{\partial s}, -\sin \beta \sin \theta \frac{\partial \theta}{\partial s}, 0)$$

$$= \frac{1}{r} \sin^2 \beta (-\cos \theta, -\sin \theta, 0)$$

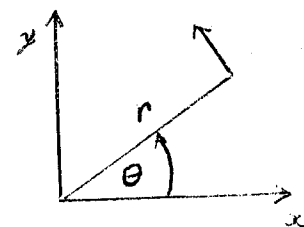
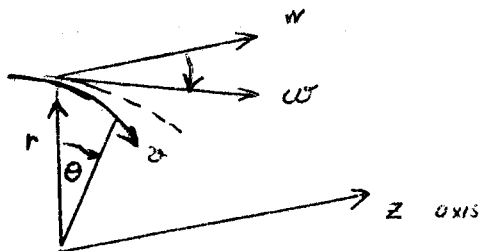
$$= K \underline{n}$$

$$= K(-\cos \theta, -\sin \theta, 0)$$

(cartesian)

$$= K(-1, 0, 0)$$

(cylindrical polar)

Cylindrical coordinates (r, θ, z) Velocity $(0, v, w)$ Vorticity $(0, \omega \sin \gamma, \omega \cos \gamma)$ Plane $z = 0$

In the above derivation we have used

$$\frac{\partial \underline{x}}{\partial \theta} = \left(-r \sin \theta \frac{\partial \theta}{\partial \theta} \quad r \cos \theta \frac{\partial \theta}{\partial \theta} \quad \frac{\partial z}{\partial \theta} \right) = \underline{t}$$

so that $r \frac{\partial \theta}{\partial s} = \sin \beta \quad \frac{\partial z}{\partial s} = \cos \beta$

Thus $K = \frac{1}{r} \sin^2 \beta = \frac{v^2}{g^2 r}$

$$\underline{b} = (0, -\cos \beta, \sin \beta) \quad (\text{in cylindrical polar})$$

$$= (\cos \beta \sin \theta, -\cos \beta \cos \theta, \sin \beta) \quad (\text{in cartesian})$$

$$\frac{\partial \underline{b}}{\partial s} = \left(\cos \beta \cos \theta \frac{\partial \theta}{\partial s}, \cos \beta \sin \theta \frac{\partial \theta}{\partial s}, 0 \right)$$

$$= \frac{1}{r} \sin \beta \cos \beta (\cos \theta, \sin \theta, 0)$$

$$= -\underline{\tau} \underline{n}$$

so that $\underline{\tau} = \frac{1}{r} \sin \beta \cos \beta = K \cot \beta = \frac{v^2 w}{g^2 r}$

With cylindrical symmetry, i.e. a situation in which quantities vary with r , but not with θ or z , a vector \underline{c} satisfies

$$\text{Curl } \underline{c} = \left\{ 0, -\frac{\partial c_z}{\partial r}, \frac{1}{r} \frac{\partial}{\partial r} (r c_z) \right\}$$

where c_z is the z component of c (the axial component) and the components of $\text{curl } \underline{c}$ are in cylindrical coordinates.

Thus

$$\text{curl } \underline{n} = 0$$

$$\text{curl } \underline{b} = \text{curl } (0, -\cos \beta, \sin \beta)$$

$$= (0, \cos \beta \frac{\partial \beta}{\partial r}, \sin \beta \frac{\partial \beta}{\partial r} - \frac{1}{r} \cos \beta)$$

$$\underline{\omega} = \text{Curl } \underline{v} = \left(0, -\frac{\partial w}{\partial r}, \frac{1}{r} \frac{\partial(vr)}{\partial r} \right)$$

Using

$$\sin \beta = \frac{v}{g}$$

$$\cos \beta = \frac{w}{g}$$

$$\sec^2 \beta = \frac{g^2}{w^2}$$

$$\sec^2 \beta \frac{\partial \beta}{\partial r} = \frac{\partial}{\partial r} (\tan \beta) = \frac{\partial}{\partial r} \left(\frac{v}{w} \right)$$

$$= -\frac{v}{w^2} \frac{\partial w}{\partial r} + \frac{1}{w} \frac{\partial v}{\partial r}$$

$$= \frac{g^2}{w^2} \frac{1}{g} \left(-\sin \beta \frac{\partial w}{\partial r} + \cos \beta \frac{\partial v}{\partial r} \right)$$

$$\frac{v \cos \beta}{r} = \frac{v}{g r}$$

we can find

$$\underline{t} \times \text{Curl } \underline{b} = (0, \sin \beta \cos \beta) \times \text{Curl } \underline{b}$$

$$= \left(\frac{1}{r} \sin \beta \cos \beta - \frac{\partial \beta}{\partial r} \right) \underline{n}$$

$$= \left(\tau - \frac{\partial \beta}{\partial r} \right) \underline{n}$$

$$\underline{n} \cdot \underline{t} \times \text{Curl } \underline{b} = \tau - \frac{\partial \beta}{\partial r}$$

$$\underline{\omega} \cdot \underline{t} = -\sin \beta \frac{\partial w}{\partial r} + \frac{1}{r} \cos \beta \frac{\partial(vr)}{\partial r}$$

$$= g \left(\frac{\partial \beta}{\partial r} + \tau \right)$$

$$\underline{\omega} \cdot \underline{b} = \frac{\partial w}{\partial r} \cos \beta + \frac{1}{r} \sin \beta \frac{\partial(vr)}{\partial r}$$

$$= \frac{\partial w}{\partial r} \cos \beta + \frac{\partial v}{\partial r} \sin \beta + \frac{v}{r} \sin \beta$$

$$\begin{aligned}
 \text{i.e. } \underline{\omega} \cdot \underline{b} &= \frac{\partial g}{\partial r} + \frac{v}{r} \sin \beta \\
 &= -\underline{n} \cdot \text{grad } g + K g
 \end{aligned}$$

Consequently

$$\begin{aligned}
 (\underline{\omega} \cdot \underline{t}) \left\{ \frac{1}{g} \underline{n} \cdot \text{grad } g - K \right\} + (\underline{\omega} \cdot \underline{b}) \{ 2\gamma - \underline{n} \cdot \underline{t} \times \text{curl } \underline{b} \} \\
 = (\underline{\omega} \cdot \underline{t}) (-\underline{\omega} \cdot \underline{b}) \frac{1}{g} + (\underline{\omega} \cdot \underline{b}) (\underline{\omega} \cdot \underline{t}) \frac{1}{g} \equiv 0
 \end{aligned}$$

These are the terms in $\frac{D}{Dt} \frac{\underline{\omega} \cdot \underline{n}}{g}$ which we proposed not to neglect.

Thus we have

$$\frac{D}{Dt} \frac{\underline{\omega} \cdot \underline{n}}{g} = 0$$

and so the motion is neutral for rotations around the normal.

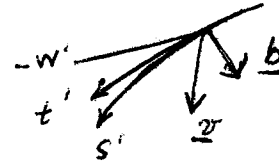
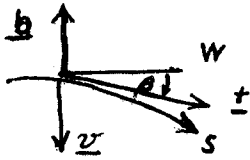
The final step in our argument to reduce the complexity of our mathematical problem is to note that, having defined our helix, which has the same stability properties as our local piece of fluid, it must follow that the equations for

$\frac{D}{Dt} \frac{\underline{\omega} \cdot \underline{t}}{g}$ and $\frac{D}{Dt} \frac{\underline{\omega} \cdot \underline{b}}{g}$ mean the same thing because we can add an arbitrary constant to w without changing anything. To demonstrate this result we replace

w by w' so that $\underline{t}' = -\underline{b}$, $\underline{b}' = \underline{t}$, $\beta' = \beta + \frac{\pi}{2}$

$$t = t' \text{ (time) }, \quad r = r', \quad v' = v$$

$$\frac{v}{w} = \tan \beta, \quad \frac{v'}{w'} = \tan \beta' = -\cot \beta$$



$$w' = -v \tan \beta$$

$$g' = \frac{v}{\cos \beta} = g \tan \beta$$

$$k' = \frac{1}{r'} \sin^2 \beta = \frac{1}{r} \cos^2 \beta = k \cot^2 \beta = v \cot \beta$$

$$\underline{\omega} = \underline{\omega}' \quad \underline{R} = \underline{R}' \quad \underline{n} = \underline{n}'$$

$$\tau' = k' \cot \beta' = -k \cot^2 \beta \tan \beta = -k \cot \beta$$

$$\begin{aligned} \left(\frac{D}{Dt} \right)' \left(\frac{\underline{\omega}' \cdot \underline{b}'}{g'} \right) &= -2\tau' \underline{\omega}' \cdot \underline{n}' - k' g' \underline{R}' \cdot \underline{t}' \\ &= 2k \cot \beta \underline{\omega} \cdot \underline{n} - \tau \cot \beta g \tan \beta \underline{R} \cdot (-\underline{b}) \\ &= \cot \beta (2k \underline{\omega} \cdot \underline{n} + k g \underline{R} \cdot \underline{b}) \\ &= \frac{g}{g'} \frac{D}{Dt} \frac{\underline{\omega} \cdot \underline{t}}{g} \end{aligned}$$

$$\text{i.e.} \quad \frac{D}{Dt} \underline{\omega}' \cdot \underline{t}' = \frac{D}{Dt} \underline{\omega} \cdot \underline{t}$$

and so from an outside observers viewpoint the information is the same.

$$\frac{D}{Dt} \frac{\underline{\omega} \cdot \underline{t}}{g} = 2k \underline{\omega} \cdot \underline{n} + k g \underline{R} \cdot \underline{b}$$

in displacement ϕ we have from above

$$\begin{aligned}
 \frac{D^2 \phi}{Ds^2} &= \left(-\frac{K}{g} \underline{\omega} \underline{b} + \frac{K}{2} \underline{R} \underline{\Omega} \right) \phi \\
 &= \frac{2}{g} \nu^2 \phi \\
 \nu^2 &= -gK \left(\underline{\omega} \underline{b} - \frac{g}{2} \underline{R} \underline{\Omega} \right) \\
 &= -gK \left(\frac{\partial g}{\partial r} + Kg + \frac{g}{2\rho} \frac{\partial \rho}{\partial r} \right) \\
 &= -Kg \left(\frac{\partial g}{\partial r} + \frac{v^2}{gr} + \frac{g}{2\rho} \frac{\partial \rho}{\partial r} \right)
 \end{aligned}$$

But in equilibrium flow

$$\frac{v^2}{r} = \frac{1}{\rho} \frac{\partial p}{\partial r}$$

So

$$\begin{aligned}
 \nu^2 &= -\frac{K}{\rho} \frac{\partial}{\partial r} \left(p + \frac{1}{2} \rho g^2 \right) \\
 &= -\frac{K}{\rho} \frac{\partial p_0}{\partial r}
 \end{aligned}$$

where p_0 is the stagnation pressure measured by a fixed pitot tube directed into the flow.

When

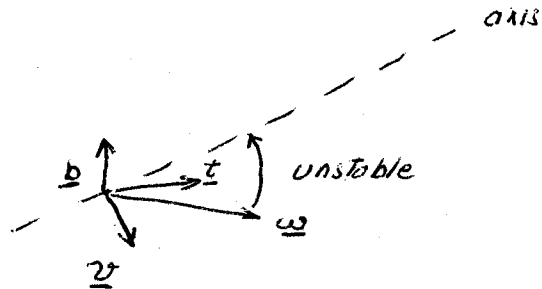
$$\begin{aligned}
 \underline{R} = 0, \quad \nu^2 &= -Kg \underline{\omega} \underline{b} \\
 &= \frac{v\omega}{r} \sin \beta \sin (\gamma - \beta)
 \end{aligned}$$

which as a max when $\beta = \frac{1}{2} \gamma$ and

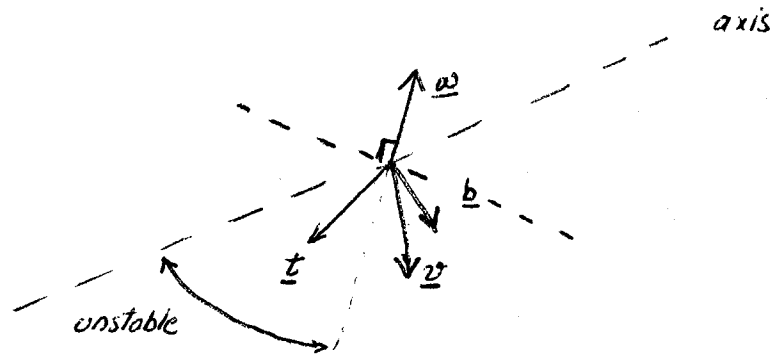
$$\mu_{\max}^2 = \frac{v\omega}{r} \sin^2 \frac{\gamma}{2}$$

Cases

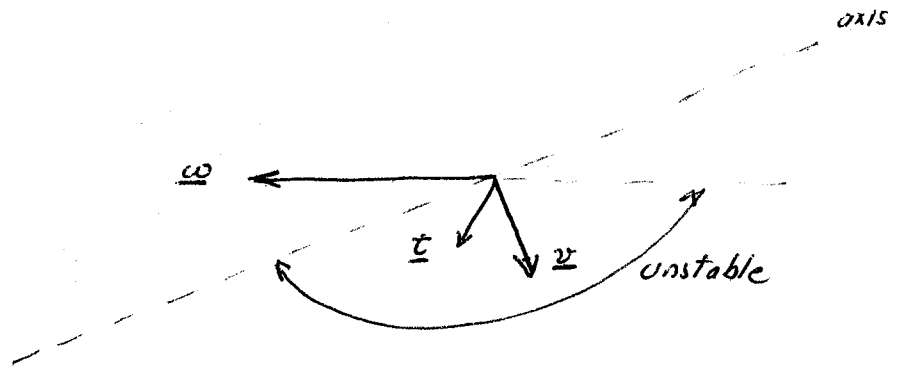
(1)



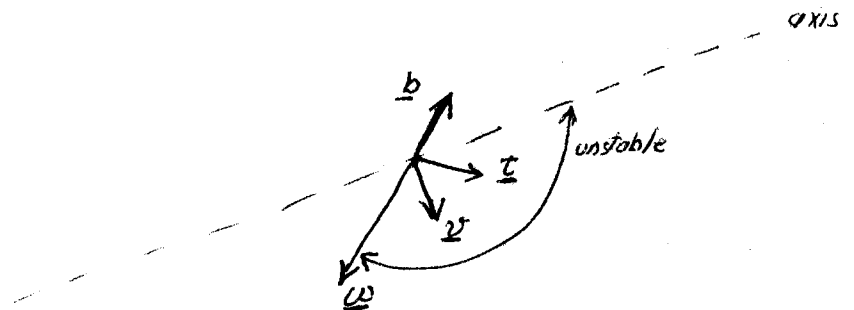
(2)



(3)

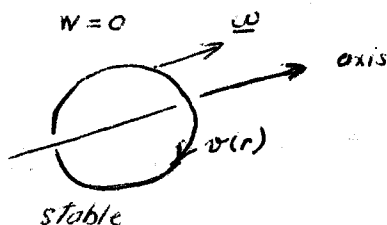


(4)

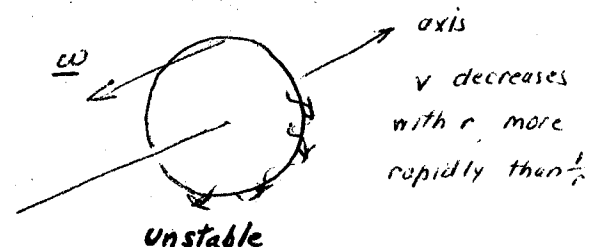


The results of the above treatment can be briefly summarized as follows: Disturbances which correspond to rotational displacements around directions which lie between the direction of the vorticity vector and the direction of the axis of the local helix are unstable. Having determined the direction of the axis of the local helix by reference to \underline{y} , K , and \underline{v} for the particle path, if $\underline{\omega}$ lies off the direction of the axes there are always some disturbances which are unstable. The most unstable are those pointing in the direction bisecting the angle between the vorticity and the helical axis, the growth rate being proportional to $\frac{v\omega}{r} \sin^2 \frac{\chi}{2}$.

The special case of $w = 0$ everywhere reduces the motion to plane flow in circles. If the vorticity is directed in the same direction as the angular velocity the motion is stable, if it is in the opposite direction it is unstable and the most unstable disturbances are toroidal (i.e. rotations of the fluid around the streamlines, which are plane circles).



v decreases with r , more slowly than $\frac{1}{r}$. If $v < \frac{1}{r}$, $\underline{\omega} = 0$



Instability takes the form of spiral motion around the streamlines.

Eddies produced by curvature are necessarily 3D.



Note that "billow" type motion in unstable case is not an unstable disturbance but is neutral having zero growth rate--this is a 2D type of disturbance that might occur.

BILLOW MECHANICS

There are no grounds for the assumption that "turbulence" has anything like a steady state anywhere in the atmosphere except close to the ground in a wind. For the free atmosphere clear air turbulence exists and is intermittent, localized, and, as far as radio observations reveal its structure at all, it appears to occur in horizontal layers and is often dominated by a wavelength.

Clouds act as tracers of the motion when other forces are dominant over buoyancy forces, and the only common cloud form is billows. Dynamic instability is most likely to be billows, i.e. Helmholtz instability and we now examine how it operates, what the turbulence does, and how we can produce a situation in which it will occur. The classical theory to be found in any good hydrodynamics textbook is as follows. Waves between two fluids, each of uniform speed and density, grow like $e^{i\sigma t}$ with wavelength $\frac{2\pi}{k}$, the motion being 2D, where

$$i\sigma_c = \frac{k}{\rho_1 + \rho_2} \left\{ \rho_1 \rho_2 (u_1 - u_2)^2 - \frac{g}{k} (\rho_1 + \rho_2) (\rho_1 - \rho_2) \right\}^{\frac{1}{2}}$$

$\rightarrow u_1, \rho_1$
 $\rightarrow u_2, \rho_2$

provided that $k > k_c$ (otherwise the waves don't grow), where

$$k_{c0} = \frac{(\rho_1 - \rho_2)(\rho_1 + \rho_2)}{\rho_1 \rho_2 (u_1 - u_2)^2} g \approx \frac{2g \Delta\rho}{U^2 \rho}$$

if

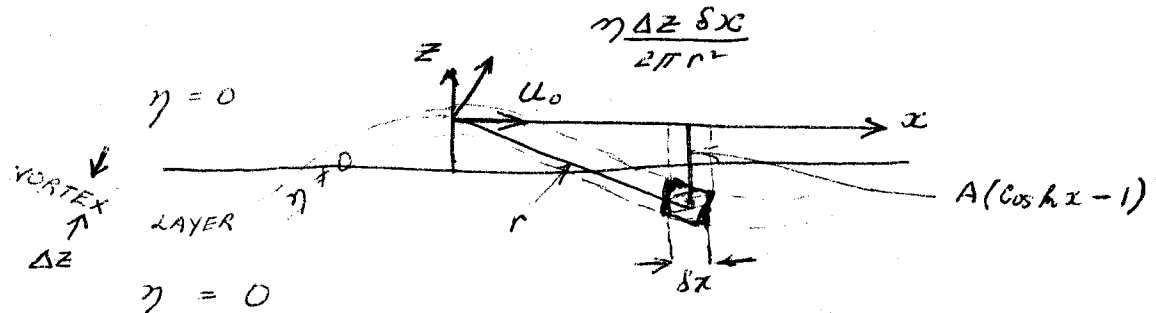
$$\Delta\rho = \rho_2 - \rho_1 \ll \rho$$

If η is the velocity gradient in a thin layer with which we replace the discontinuity, and $\beta = \frac{1}{\rho} \frac{\partial \rho}{\partial z}$, and Δz is the larger thickness we

have instability if

$$h > h_c = \frac{2g\beta}{\eta^2 \Delta z}$$

This is the classical result, but the growth mechanism remains unrevealed by the analysis. This is illustrated by a physical derivation of this result:



The velocity of any particle in the fluid in 2D motion can be thought of as produced by the integrated effect of all the vorticity present. At the wave crest the vorticity containing fluid has horizontal velocity

$$\begin{aligned}
 u_c &= \int_{-\infty}^{\infty} \frac{\eta \Delta z A (1 - \cos hx)}{2\pi r^2} dx \\
 &= \frac{\eta \Delta z A}{\pi} \int_{-\infty}^{\infty} \frac{\sin^2 \frac{1}{2} kx}{x^2} dx \\
 &= \frac{\eta \Delta z A}{\pi} \left\{ \left[\frac{1}{x} \sin^2 \frac{1}{2} kx \right]_{-\infty}^{\infty} - \frac{k}{2} \int_{-\infty}^{\infty} \frac{\sin kx}{x} dx \right\} \\
 &\quad \equiv 0, \left\{ \begin{array}{l} \text{Integral of} \\ \text{odd function} \end{array} \right\} = \frac{\pi k}{2} \\
 &= \frac{1}{2} \eta \Delta z A k.
 \end{aligned}$$

So in a periodic small amplitude disturbance, at other points

$$u = \frac{1}{2} \eta \Delta z A k \cos hx.$$

This gives the rate of horizontal advection by the vorticity containing fluid. The rate of increase of vorticity by advection at a point x , which is equal to $-\eta \Delta z \frac{\partial u}{\partial x}$, is therefore $-\frac{1}{2} (\eta \Delta z)^2 A k^2 \sin kx$

The slope of the density "discontinuity" (the vortex layer, also being a layer of large density gradient) is such that the rate of generation of vorticity is

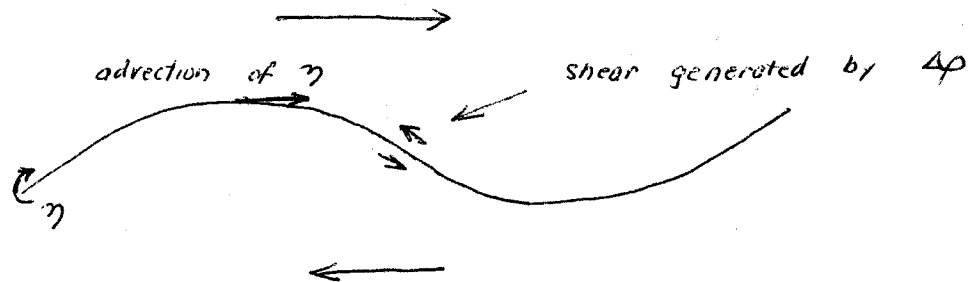
$$-g \beta \Delta z \frac{\partial}{\partial x} (A \cos kx) = g \beta \Delta z A k \sin kx$$

If the sum of these two expressions is positive where $\sin kx$ is negative there will be a total accumulation of vorticity at the downward sloping nodes, towards which the crest and trough fluid will be advected, and so the disturbance will grow if

$$\frac{1}{2} (\eta \Delta z)^2 k > g \beta \Delta z$$

$$\text{i.e. } k > \frac{2g\beta}{\Delta z \eta^2}$$

the classical result:

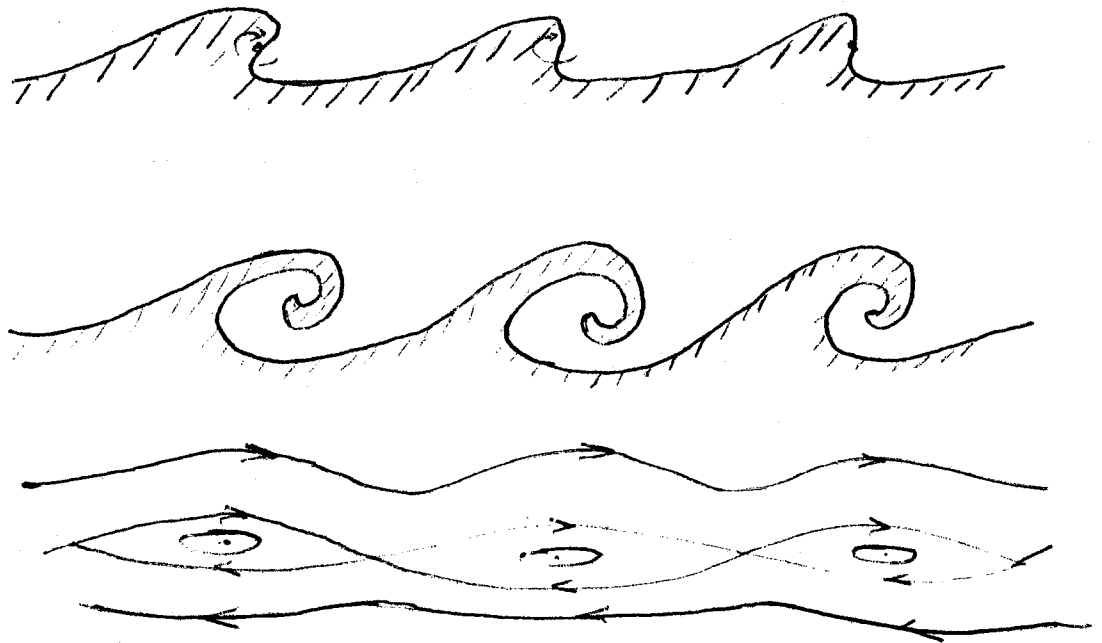


Thus the mechanism of instability is the excess of advection of vorticity over the destruction of it by the sloping density gradient. The vorticity accumulates at the downward sloping nodes (the direction being that in the upper fluid).

The vortex layer is stretched at the upward sloping nodes, and thickened at the downward ones:



These latter then become the vortex centres in the billows, and the motion soon takes on the cats eyes pattern;



The curved flow produces a lowering of pressure in the vortices and so the fluid flow is accelerated, and some of the particles therefore get an excess of K. E., and energy is concentrated in the vortices.

Note that it is the original concentration of vorticity that makes this possible, not the vorticity alone. (Uniformly distributed vorticity does not produce instability.) The final result is that the vorticity sheets become rolled up.

Wavelengths small compared with the thickness of the layer are not unstable, and so there is a second critical wave number for a uniform layer of thickness h , vorticity γ , static stability β , which is given by

$$F\left(\frac{g\beta}{\gamma^2}, k_c h\right) = 0 \quad \text{for largest unstable wavelength}$$

$$F\left(\frac{g\beta}{\gamma^2}, k_c h\right) = 0 \quad \text{" smallest " "}$$

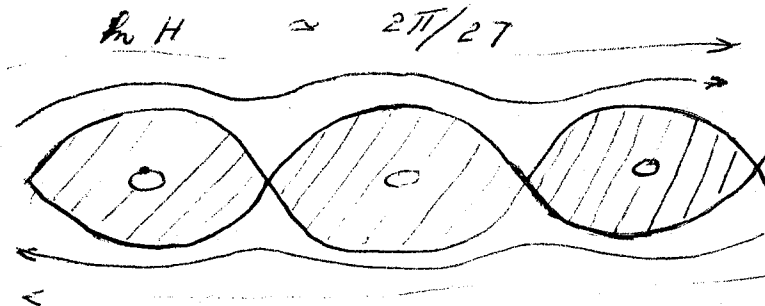
Now $k_c = \frac{2g\beta}{\gamma^2 h}$

So $Ri = \frac{1}{2} k_c h = \frac{g\beta}{\gamma^2} = \text{constant for the critical case,}$

i.e. there exists a critical Ri for a finite thickness layer above which it is not unstable. Also $k_c h = \text{constant}$ for any specified condition, in particular when $k_c = k_c$, $Ri \approx \frac{1}{4}$ according to many investigations of particular cases. Also it implies that as h increases k_c decreases, so that a thickening of the layer increases the smallest unstable wavelength. The most unstable wavelength or the one that sets in first is likely to be close to $\frac{2\pi}{k_c}$ rather than $\frac{2\pi}{k_c}$. Therefore we will assume

$$\frac{1}{2} k_c h \approx \frac{1}{4}$$

When the cats eyes pattern is set up the region inside the eyes has an area corresponding to a layer of uniform thickness H , where



Equating this k with k_c we have $\frac{H}{h} = \frac{4\pi}{27} = 5$ approximately.

Thus the layer is thickened by a factor of about 5.

THE GENERATION OF THE SMALL RICHARDSON NUMBER

The relevant terms in the vorticity equation are

$$\frac{D\omega}{Dt} = (\omega \cdot \text{grad}) \underline{v} + \underline{R} \times \underline{g}$$

(the first term is negligible in 2D flow). For steady 2D flow

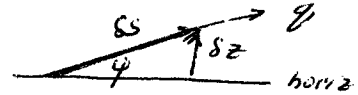
$$\frac{g}{\beta} = \text{constant} = \frac{g}{\beta_0} \quad \text{where } |\underline{R}| = \beta.$$

Where the streamline is tilted at ψ to horizontal

$$\frac{D\eta}{Dt} = g \frac{D\eta}{Ds} = g\beta \sin \psi$$

$$\delta \eta = \frac{g\beta}{g} \delta s \sin \psi$$

$$= g \frac{\beta_0}{g_0} \delta z$$



$$R_i = \frac{g\beta}{\eta^2} = \frac{g\beta}{(g_0 + \delta \eta)^2}$$

$$= \frac{g\beta}{(g_0 + g \frac{\beta_0}{g_0} \delta z)^2}$$

Thus we need to have large β_0 to get a good change in R_i . If initially

$R_i = \infty$, i.e. $\eta_0 = 0$ then later on,

$$R_i = \frac{\beta g_0^2}{g \beta_0^2 (\delta z)^2} = \frac{g^2}{g \beta (\delta z)^2}$$

Thus the most unstable vortex layers will be produced by a vertical displacement (up a wave or front) in layers of large β .

Notes taken by:

M. J. Moore

R. F. Perret

I. THE BASIC PROPERTIES OF THERMALS

Thermals are isolated masses of fluid rising by buoyancy forces into and mixing with the surrounding fluid. Here we will consider only those thermals that are produced by very small buoyancy forces. In other words we assume that the difference between the densities of the interior and exterior fluid is only a very small fraction of the density of the exterior fluid ($\Delta\rho/\rho_0 \ll 1$). We will also assume that if the initial volume is sufficiently small compared with the subsequent volume then the subsequent growth of a thermal is independent of the initial shape. These thermals are different from the vortex rings. Thermals have a turbulent region at the front and vorticity distributed throughout the buoyant fluid whereas in a vortex ring the vorticity is concentrated along a ring, the velocity being maximum at the inner surface of the ring and the flow is laminar. Also the vortex ring possesses circulation initially and it remains constant (in the absence of viscosity) as it moves because the buoyant fluid does not extend to the center. Whereas thermal does not possess any circulation or kinetic energy initially. The circulation is generated by the buoyancy force in the early stages of its growth.

II. THE CHARACTERISTICS OF A THERMAL

As shown in Fig. (1) (see end of Lecture #4 for figures), the thermal has a turbulent region over its ascending front. In this region it mixes with the surrounding fluid. As a result of mixing its volume grows gradually and the buoyancy force decreases. Half (approximately) the entrainment is by mixing over the upper surface but the other half is by orderly (laminar) entrainment at the rear. Inside and at the rear of the thermal the fluid circulation is relatively smooth. Velocities in different regions of a standard thermal are shown in Fig. (2).

The motion in a thermal can be observed in a laboratory by injecting a colored dye at the advancing front. Figure (3) shows successive positions of the colored column of fluid. It is clear from the figure that at the rear and

near the axis the colored column of the fluid is elongated indicating relatively smoothness of the flow in these regions.

If we assume the viscous forces are negligible then the width $2R$ and the velocity w of a thermal can be shown from the dimensional analysis to be independent of Reynolds number and it depends only upon a Froude number.

III. DIMENSIONAL ANALYSIS

Since we are considering only those thermals that are grown by buoyancy forces and if we neglect the viscous force then

$$R = R(Z, gB)$$

$$\text{and } w = w(Z, gB)$$

where $gB = g \frac{\Delta \rho}{\rho_0}$ is the buoyancy force, $2R$ the width of the thermal and Z is the distance traveled by the thermal. Applying the dimensional analysis,

$$R = \frac{Z}{n} \tag{1}$$

$$\text{and } w = C(gBR)^{\frac{1}{2}} \tag{2}$$

where c and n are constants yet to be determined. (According to the Boussinesq approximation $\frac{\Delta \rho}{\rho}$ only appears in the analysis when multiplied by g . The point is that $\frac{\Delta \rho}{\rho}$ is a non-dimensional number and the dimensional analysis would be impossible if B were not tied to g). (c^2 is a Froude number, being a ratio between the inertial and buoyancy forces, n on the other hand represents an angle or shape and is not dynamical.) If the laboratory experiments are performed at the Froude number of the atmosphere at which these thermals are observed, then we can assume that the constants will have the same value for the thermals in the atmosphere and in the laboratory provided that the Reynolds number is already large enough. In the atmosphere c measured from time lapse pictures

and it was about $(8/9)^{\frac{1}{2}}$ for clouds analysed by Malkus and Scorer. The laboratory experiments which we will describe later have value of c about 1.2. We can therefore assume the laboratory experiments are prototypes of thermals in the atmosphere.

IV. LABORATORY EXPERIMENTS

The thermals were released at the center of a large tank from a thin hemispherical cup. The level of the fluid inside the cup is made the same as that of the fluid outside and then it is released by rotating the cup. Colored dye or white precipitate is added to the fluid inside the cup before being released, to make the buoyant fluid visible. Immediately after release the front surface of the thermal becomes covered with protuberances and the volume begins to increase as shown in Fig. 4. The width, $2R$ and the distance traveled by the thermal, Z , are measured with time. Substituting these values of R and Z in Eq. (1), it was found that the value of n is approximately between 2 and 8, although it was very constant for an individual thermal. Since the buoyancy force, gB , changed with time, therefore, mean B is taken instead of B in Eq. (2) and it was found that $c = 1.2$.

$$v = \text{volume of the standard thermal} = mR^3 \quad (3)$$

where m is a constant to be determined from the experiment. The total buoyancy of the thermal is constant, so that if $g\bar{B}$ denotes the buoyancy force at the moment of release,

$$g\bar{B} m R^3 = gB \quad (4)$$

where \bar{B} is the average buoyancy in a thermal at any arbitrary time. Writing

$$W = \frac{dz}{dt} \text{ and integrating (2), we obtain}$$

$$K Z^2 = t \quad (5)$$

where

$$K = m^{\frac{1}{2}} / 2nc(g\beta)^{\frac{1}{2}} \quad (6)$$

The values of Z^2 and t are plotted on a graph and the value of K is obtained by fitting a straight line to these values. Using this value of K we can obtain the value of m to be approximately 3 (which fits a flattened roughly spherical shape well).

(At this point, films were shown of Scorer's 1954 experiments on thermals.)

Thus, the Reynolds number, $Re = \frac{wR}{\nu}$, is proportional to $wZ = \text{constant}$. This means that once the thermal motion is turbulent, it will remain turbulent and the eddies will grow larger as the thermal enlarges.

Circulation along a curve enclosing one-half of the thermal
 $= \oint \underline{z} \cdot d\underline{s} \propto wR = \text{constant}$

This says that when thermal reaches the standard stage, the circulation is constant. Hence, the eddy viscosity is slowing circulation at the same rate as buoyancy is speeding it up. n is not a true constant, it varies over a large range from one thermal to another.

Scorer tried $C n^{\frac{1}{2}} = \text{constant}$ ($2.9 \leq n \leq 5.0$). Richards improved it $C_1 = 0.73$ ($1.7 \leq n \leq 7.3$) where $w = \frac{1}{2} C_1 n^{\frac{3}{2}} (m\beta g z)^{\frac{1}{2}}$

$$\text{and } C = \frac{1}{2} C_1 n^{\frac{1}{2}} m^{\frac{1}{2}}.$$

REFERENCES

Malkus and Scorer, 1955, The erosion of cumulus towers, J. Met., 12, 43.

Scorer and Ronne, 1956, Experiments with convection bubbles, Weather, 11, 5, 151.

_____, 1957, Experiments on convection of isolated masses of buoyant fluid, J. Fluid Mech., 2, pt. 6, 583.

Richards, 1961, Experiments on the penetration of an interface by buoyant thermals, J. Fluid Mech., 11, pt. 3, 369.

_____, 1965, Puff motions in unstratified surroundings, J. Fluid Mech., 21, pt. 1, 97.

Woodward, 1959, The motion in and around isolated thermals, Quart. J. Roy. Met. Soc., 85, 144.

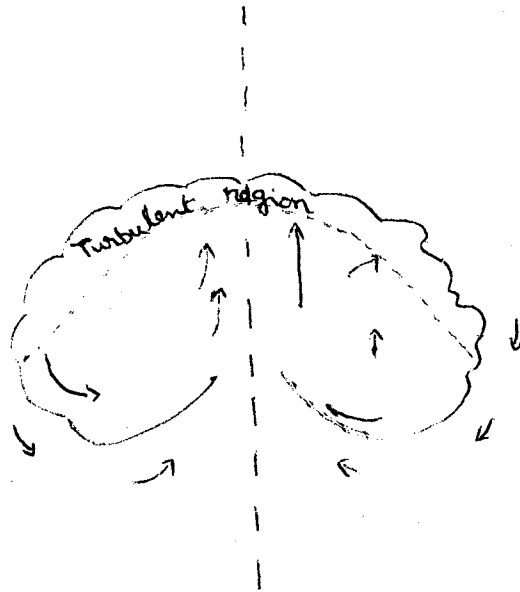


Figure 1. Different regions of a standard thermal

Lecture #4

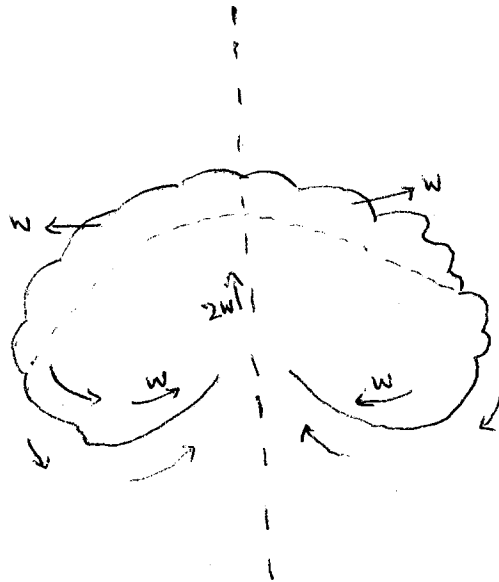


Figure 2. Velocity of the fluid in different regions of a standard thermal

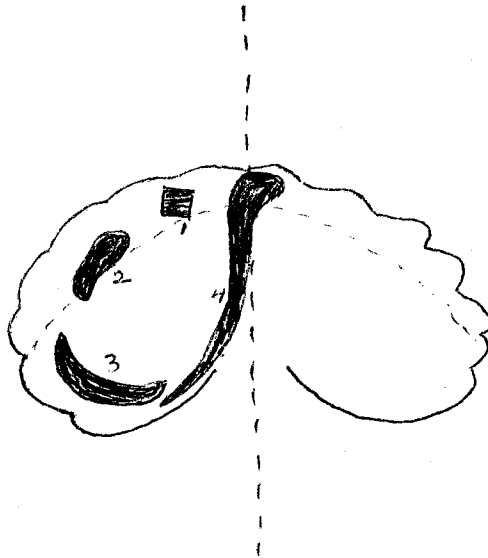


Figure 3. Successive positions of colored column of fluid

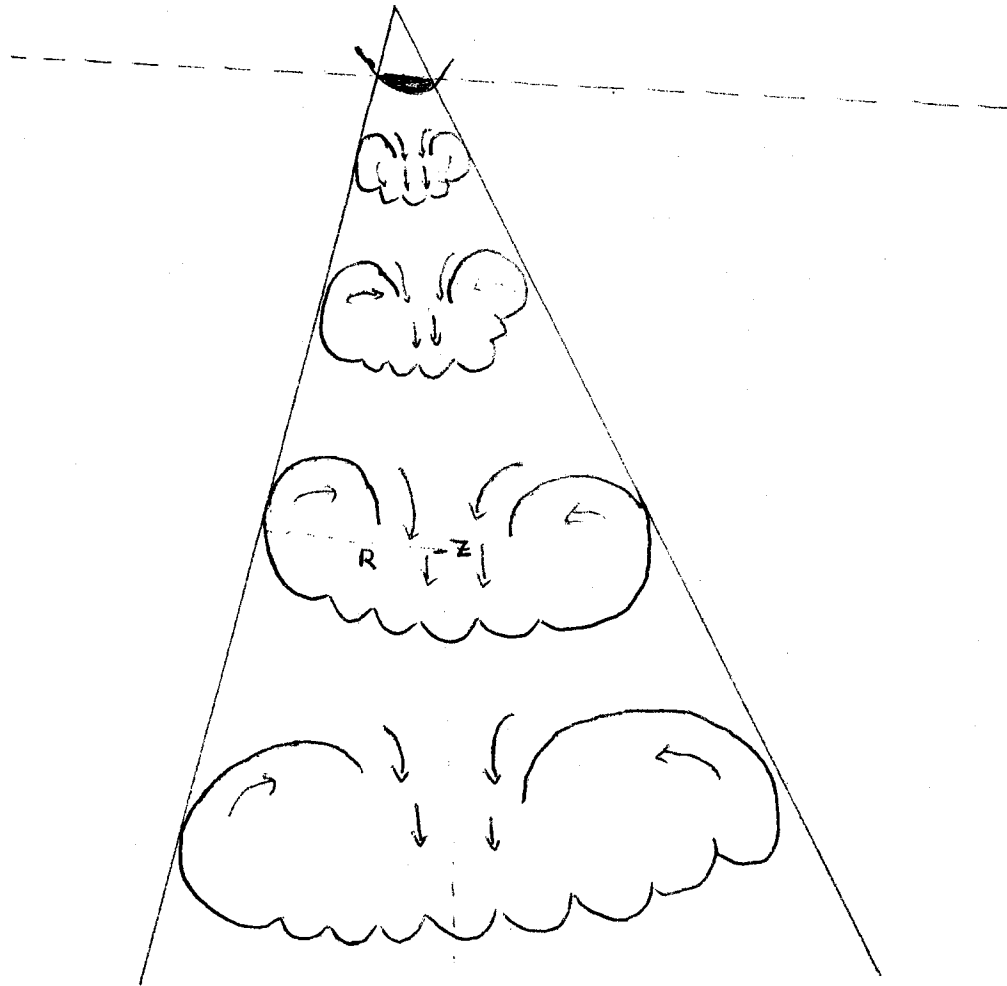


Figure 4. Growth of a thermal

Lecture #4

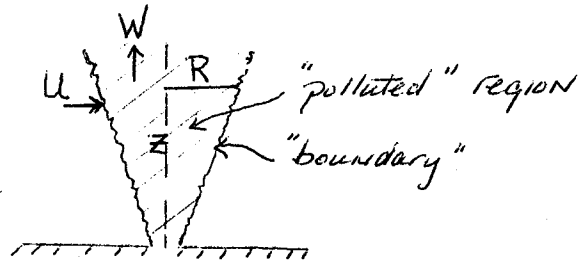
Notes taken by:

M. V. Ranga Rao

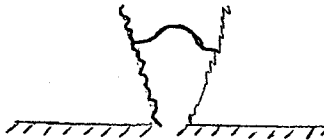
Michael S. Sher

I. NON-BUOYANT JETS

A jet can be considered as a cone of radius R in which the momentum and pollution can be studied as follows. The jet discussed is non-buoyant and is of uniform density.



The mean velocity has a profile in the turbulent region which dominates the



motion for z greater than about 5 times the diameter of the orifice. The mean velocity over an area $2\pi R^2$ is W .

The volume flux as given by

$$\text{volume flux} = \pi R^2 W$$

from which we see that the momentum flux which is constant is

$$\text{momentum flux} = \dot{M} = k\pi R^2 W^2 = \text{constant.}$$

where k is a constant defined by this relation. Thus $R^2 W^2 = \text{constant} = R_0^2 W_0^2$. The radius $R = R(\dot{M}, z)$, and by dimensional analysis

this means that

$$R = z/\eta$$

where η is a universal constant. From experiments we find that $\eta \approx 5$. This means that W/z is a constant or that $W/z = W_0/z_0$.

The pollution flux is given by pollution flux = $\ell \pi R^2 W \sigma$

where ℓ is a constant taken to be 1 since σ can be adjusted to incorporate a non-one factor. Here σ is a mean of the concentration of material emitted from the orifice. The Reynolds number is another constant of the

jet since

$$\text{Reynolds number} = \frac{Wz}{\nu} = \text{constant}$$

This constant value implies that if the jet is turbulent to begin with it will remain turbulent.

The entrainment of the jet can also be considered by beginning with the continuity equation, $\text{inflow} = 2\pi R U = \frac{d}{dz} (\text{vol. flux}) = \frac{d}{dz} (\pi R^2 W)$ where U is the inflow velocity at the boundary. So

$$2RU = \frac{d}{dz} \left(\frac{z^2}{n^2} \cdot \frac{W_0 z_0}{z} \right) = \frac{W_0 z_0}{n^2} \quad \text{or} \quad U = \frac{W_0 z_0}{2nz} = \frac{W}{2n} = \alpha W$$

where $\alpha = \frac{1}{2n} \approx 0.1$ is the entrainment coefficient. Note that the value of α depends on the definition of W . Furthermore, if the flow outside the jet is to be strictly horizontal this implies that the radial pressure gradients must be the same at all heights. Thus for r and U outside the jet

$$2\pi r u = 2\pi R U$$



independent of height. From the continuity equation and the relation of R to z the velocity at the jet boundary to such that $U \propto \frac{1}{R} \propto \frac{1}{z}$. It follows directly then that u is a function only of r independent of z outside the jet boundary as was implied by the assumption on which the theory was based.

II. BUOYANT VERTICAL PLUME

A plume can be considered as a cone of radius R in which the buoyancy and pollution are proportional as they are carried with the fluid. Again a sufficient distance from the source or orifice is assumed to be turbulent and also the buoyancy is considered small, i.e., $B = \frac{4\rho}{\sigma} \ll 1$.

The buoyancy flux is considered constant as expressed by $BWR^2 = B_0 W_0 R_0^2$.

The buoyancy itself is given by

$$\pi R^2 B = \frac{d}{dz} (\text{momentum flux}) = \frac{d}{dz} (k_p \pi R^2 W^2)$$

where k_p is the constant, which is a property of plumes, which gives us equality in this equation. It depends on the space and time fluctuations of the vertical velocity from the mean value W . B is defined as the mean area buoyancy. As for the jet $r_p R = z$. From these relationships

$$\frac{d}{dz} (k_p R^2 W^2) = \frac{k_p}{r_p^2} \frac{d}{dz} (z^2 W^2) = R^2 B = \frac{B_0 W_0 R_0^2}{W} = \frac{B_0 W_0 z_0^2}{r_p^2 W}$$

which has a power solution in z for W and B such that $W = W_0 \left(\frac{z_0}{z}\right)^{1/3}$ and $B = B_0 \left(\frac{z_0}{z}\right)^{5/3}$ can be considered solutions. One also notes from dimensional analysis that W can be represented as $W = C(gBR)^{1/2}$ as the motion is dominated by buoyancy; this relationship holds for all buoyancy dominated motion, with different constants (C) for different geometrical configurations.

Again an equation of continuity yields

$$2\pi R U = \frac{d}{dz} (2\pi R^2 W)$$

where W is thus the mean velocity over the area $2\pi R^2$. It follows that

$$\frac{2zU}{r_p} = \frac{d}{dz} \left(\frac{z^2}{r_p^2} \cdot \frac{W_0 z_0^{1/3}}{z^{1/3}} \right) = \frac{W_0 z_0^{1/3}}{r_p^2} \cdot \frac{5}{3} z^{2/3}$$

and

$$U = \frac{1}{z r_p} \cdot \frac{5}{6} z W = \frac{5}{6 r_p} W.$$

From observation $\eta = \eta_p$ to within 2% or so and thus the entrainment coefficient $\alpha = \frac{5}{6\eta_p} \approx 0.16$. It should be noted that $u \propto W \propto z^{-1/3}$ implies that the pressure field is not strictly the same at all levels and so the flow cannot be strictly horizontal. However, the deviation is small so that the theory is correct for practical purposes.

Finally the Reynolds number is

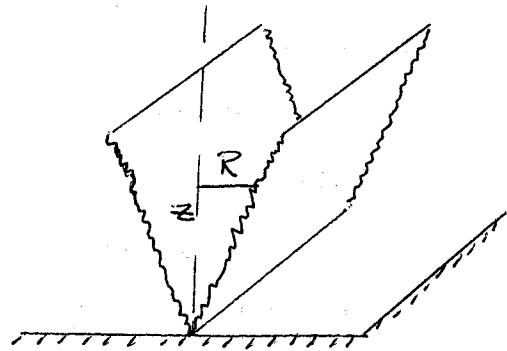
$$Re = \frac{WR}{\nu} \propto z^{2/3}$$

This indicates that a buoyant source always produces a turbulent plume if z is high enough.

III. 2D PLUME (LINE SOURCE OF BUOYANCY)

This case was studied by G.I. Taylor during the war, in a problem associated with airport fog dispersal.

By dimensional arguments, similar to the above, the "radius" must satisfy $R = z/n$. If B is the mean linear buoyancy (per unit length) at height z , then for constant flux of buoyancy per unit length, we have



$$BRW = B_0 R_0 W_0 \quad (1)$$

To obtain W , dynamics gives us that the buoyancy forces changes the momentum flux:

$$BR = \frac{d}{dz} (kRW^2) \quad (2)$$

where k is characteristic of this configuration.

The simplest way to solve equations (1) and (2) is to recognize that if there is a unique solution it will be in powers of z . This follows from the dimensional analysis. If it was not true then the solution would not be uniquely determined, that is, the solution is some power series. Such non-unique solutions are not useful. Thus try

$$W \propto z^{\beta} \quad \text{and} \quad B \propto z^{\gamma}$$

Then (1) gives $\gamma + \beta + 1 = 0$

and (2) gives $\gamma + 1 = -1 + 1 + 2\beta$, which yields

$\beta = 0$ and $\gamma = -1$. Consequently, $W \propto z^0$, is independent of the height and the mean velocity profile

might look something like the sketch.

To obtain the entrainment, look at the continuity equation

$$U = \frac{d}{dz} (WR)$$

(3)

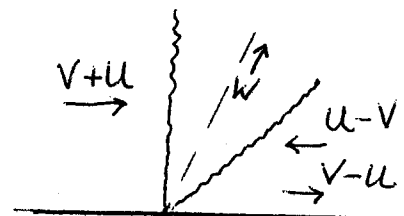
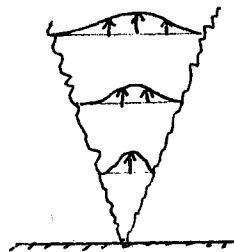
where W is now defined as the mean areal value.

Since $R = z/n$, (3) gives $U = \frac{W_0}{n}$ so that the entrainment coefficient is $1/n$ which, typically, is larger than for the jet and about the same as for the buoyant plume.

The Reynolds number for this case is $\frac{WR}{\nu} \approx z \rightarrow \infty$

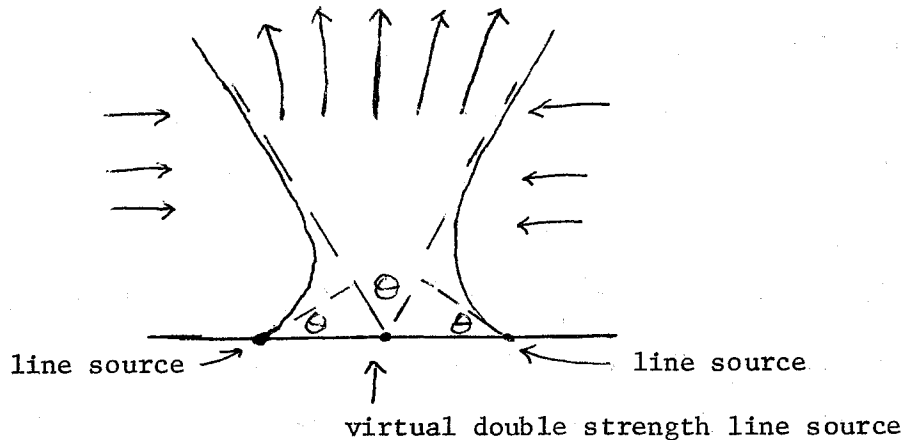
and thus so long as the model remains valid, the flow necessarily becomes turbulent at sufficient height.

Perhaps the most interesting aspect of this type of flow is that $U = \text{const.} = w/n$. This means that if a wind blows, then to a first approximation (i.e., assuming the buoyancy force is still along the plume axis) then the wind



simply tilts the plume over.

Further, two plumes, for example, one on either side of a runway, would attract each other and merge. Thus the total effect would be as if there were a single line source (in the middle of the runway!) whose strength is twice the strength of each.



In this figure the line sources and runway are perpendicular to the page.

In Taylor's simple theory the angles θ are all equal. This double plume technique is useful for lifting fog off runways.

Two other simple configurations are the puff (like the "puff" when one says the word!) and the "starting" or "new" plume.

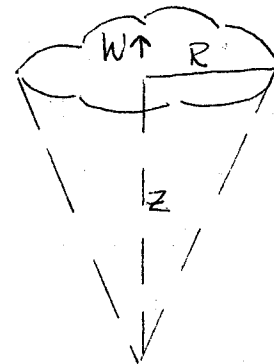
Puff (Axisymmetric)

The puff is similar to a thermal but has constant total momentum:

$$WR^3 = \text{const.}$$

If it's turbulent (and sometimes it's not),

then $nR = z$



with $n \approx 4$, so that $W \propto z^{-3}$. The Reynolds number is $\frac{RW}{z} \approx \frac{1}{z^3} \rightarrow 0$,

so that the puff always becomes dominated

by viscous stresses at large enough z . The

turbulent motion is then smoothed out and the puff degenerates.

Richards (1965) determined that the velocity distribution inside and outside a puff is similar to that for a thermal. In both cases, the turbulence appears to be a result mainly of the mean motion, rather than the buoyancy, although, in the case of a thermal the buoyancy produces the mean or orderly part of the motion.

New Plume

This is like a thermal, at the top, and a plume, down below. About half of the total entrainment occurs in each part.

The volume is mR^3 , where m is a shape factor, and, once again, $nR=z$. The total upward momentum for a unit mass is $\ell R^3 W$ and the total buoyancy increases with time according to $\dot{B}t$, where \dot{B} is the constant source strength.

To obtain W , Newton's law gives

$$\dot{B}t = \frac{d}{dt}(\ell R^3 W),$$

so

$$\frac{1}{2} \dot{B}t^2 = \ell R^3 W,$$

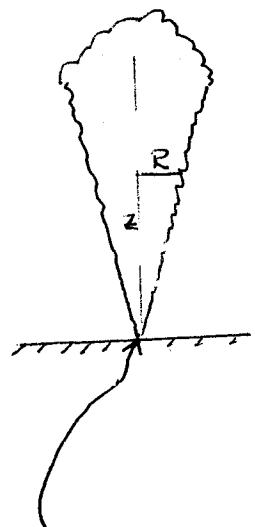
or

$$\frac{1}{2} \dot{B}t^2 = \ell \frac{z^3}{n^3} \frac{dz}{dt}.$$

Thus $z \propto t^{3/4}$ and $W \propto t^{-1/4}$ which are confirmed by observation.

The flow is always turbulent, since

$$Re = \frac{WR}{\nu} \propto Wz \propto t^{1/2}$$



Continuous source of buoyant material

In summary, these simple dimensional arguments work well but one must recognize their limitations. Namely, if it is desired to bring in other effects, such as viscosity or wind shear, or, for example, to study the transition region between a jet and a buoyant plume, then there may be ambiguities in the length scale and one won't be able to proceed to a unique solution in terms of a single power law. The simplicity in the cases studied here has been $R^{-1/2}$. Further, there seems to be no significant advantage in the theory by choosing other velocity profiles than the mean velocity profile used.

Notes taken by:

W. G. Slinn

B. Wilhelmson

Lecture #6

Dr. Richard S. Scorer

3 August 1970

VERTICAL EDDY TRANSFER BY THERMALS,

THE RATIO K_M/K_H

The following material was taken from a reprint by Dr. R. S. Scorer, entitled, "The Ratio of the Momentum and Material Vertical Eddy Transfer Coefficients in Buoyancy Driven Turbulence" Arch. Met. Geoph. Biokl. Ser. A, 18, 249-265, 1969.

Summary

The eddy coefficients for vertical transfer are calculated for a hypothetical pattern of thermal convection possessing certain similarity properties and their ratio is found to be given by

$$\frac{K_M}{K_H} = \frac{\sigma}{1-\sigma} \frac{C^2}{3n}$$

where σ is the fraction of the area occupied by thermals, C is a constant giving the velocity of a thermal in terms of its buoyancy and size, and n represents its angle of spread. Typical values of this ratio are thought to be in the range 10^{-1} to 10^{-3} . A value correspondingly larger than unity can be expected in a stably stratified fluid.

The phenomenon is explained in terms of the elastic properties of the tangled vortex tubes which compose the turbulence: vertically oriented ones are well placed to produce a Reynolds stress, but transfer no material; horizontal ones produce no stress but transfer material effectively. Only the latter are generated by the buoyancy forces directly in thermal convection.

1. Choice of a Case for the Estimation of K_M/K_H

Actual convection in the atmosphere is complicated by variations in time, and from place to place, of the heat flux near the surface, by the presence of a condensation level and a stable stratification of the environment of the convection clouds above it and by considerable fluxes of heat except near the surface through larger scale convergence than thermals. The purpose of this paper is to examine a very special and simple kind of thermal convection to see how its effectiveness for the transfer of heat and momentum compare with one another.

Because of the great variety of factors with physical dimensions affecting the motion, each with a region of the atmosphere in which it is more dominant, we cannot expect similarity. The argument we shall use depends very much on the motion being similar over a fair height range but the conclusions are not really restricted to that case so long as the convection is composed of thermals; they merely need rather careful interpretation.

In order to obtain similarity we envisage the motion of a body of buoyant fluid to be determined solely by its size and buoyancy (total weight deficiency). The motion as a whole is so turbulent that molecular transfer is negligible. The smaller eddies are generated by, and are proportional to the larger buoyancy produced motions namely the thermals or whatever they may be, and we study the motion at a sufficient distance from the boundary for radiative transfer and the details of the surface features to be of little importance. The eddies are essentially buoyancy driven, which means that

Ratio of Momentum and Material Vertical Eddy Transfer 251

we must be above the layer in which the eddies are predominantly generated by flow over a rough boundary.

The convection must not have a top near at hand, otherwise its presence will exert a complicating influence on the thermal size and there will be no similarity. Thermals must therefore grow indefinitely in size with height, and must therefore combine. Since the height, z , is the only length parameter imposed, the thermals must have a size, r , proportional to it: thus

$$z = nr \quad (1)$$

where n is a number determined by the geometry of the motion of thermals. The geometry must be independent of z , and the amalgamation of thermals must reduce the number with height so that the same fraction of a horizontal area is occupied by thermals at all heights.

The behaviour of the thermals, although they are continually amalgamating, is assumed to be described by the equations for an isolated thermal. The chief grounds for this simplification are that a thermal is a very dissipative configuration of motion and achieves its ultimate motion pattern very quickly, probably in the course of rising about one diameter. The motion which turns the thermal inside out in such a way that entrained fluid is rapidly dispersed throughout the whole thermal, even if entrained over a small part of the surface, ensures that axial symmetry is rapidly re-established after amalgamation. We therefore write

$$w = C (g B r)^{1/2} \quad (2)$$

$$B = \Delta \rho' \rho \quad (3)$$

where w is the vertical velocity. C is a constant measured by experiment. B , w , and ρ may be mean values of some particular values such as the maximum buoyancy anomaly, the rate of rise of the top and density.

In order to maintain similarity the buoyancy flux must be independent of height; otherwise a length would be introduced which would interfere. The environment of the thermals must be subsiding without local change of potential temperature, which must therefore be uniform. The convection is thus not warming the air but transporting buoyancy through it. An air mass is warmed by this type of thermal convection only when the environment is stably stratified, and in that case similarity would disappear unless the stratification varied in a unique way with height. Thus we could image a variety

252 R. S. SCORER

of thermal strengths, some of the feebler ones reaching an equilibrium level and becoming part of the environment, others being absorbed into more buoyant ones as already envisaged.

The theoretical aspects of the argument to follow do not depend on the precise form which thermal convection takes. If enough were known about plumes from infinitesimal sources in a statically unstable medium calculations could be made on the assumption that convection was composed of them. But only thermals have been sufficiently studied for a numerical result to be obtained. One reason for this is that thermals bear a closer resemblance to what is observed in the atmosphere by glider pilots and by other means, and plumes seem to be rather a feature of laboratory experiments in which the mechanisms for heating the surface are different from that for ground heating.

Thermals have another advantage over plumes or any other configuration in this analysis because we need to know the buoyancy flux produced by them as well as the momentum flux. In a plume a detailed knowledge of the correlations between vertical velocity and horizontal velocity and buoyancy would have to be known. A thermal on the other hand transfers momentum and buoyancy as if the mean values pervaded the whole thermal and it had a closed boundary which contains the transferred material whose motion is known in terms of the mean values.

Fig. 1 is a visual impression of the thermal convection we are discussing.

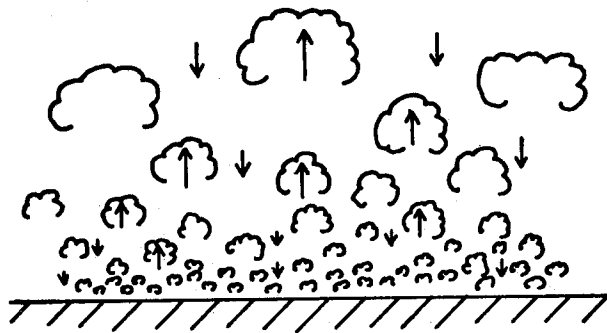


Fig. 1. When similarity prevails thermals must (a) have a size proportional to height (b) occupy the same fraction of a horizontal area at all heights. Consequently they must amalgamate during ascent so as to decrease in number. As they rise they also grow by entrainment of air of the environment, and so the rate of descent of the environment must decrease downwards, and such environment as reaches the lower levels has the same potential temperature as that higher up. The figure gives an impression of the pattern of thermals

2. The Details of the Similarity Regime of Convection by Thermals

The mean vertical velocity is assumed to be zero. This is equivalent to neglecting density variations in an isobaric surface in the equation of continuity of mass. Thus if σ is the fraction of the whole area occupied by thermals

$$\sigma w + (1 - \sigma) w_e = 0 \quad (4)$$

where w and w_e are the upward velocities of the thermals and the environment.

If $\bar{\tau}$ is the mean buoyancy (reciprocal of absolute potential temperature) at any level and τ' and τ'_e are the mean anomalies of the thermals and the environment,

$$\bar{\tau} = \sigma (\bar{\tau} - \tau') + (1 - \sigma) (\bar{\tau} - \tau'_e) \quad (5)$$

so that τ' is a positive quantity and τ'_e is negative, and

$$\sigma \tau' + (1 - \sigma) \tau'_e = 0. \quad (6)$$

For a liquid we would replace τ by ρ .

The buoyancy flux is

$$F = \sigma w \tau' + (1 - \sigma) w_e \tau'_e = \frac{\sigma}{1 - \sigma} w \tau' \quad (7)$$

by means of (4) and (6). We can express this as a function of height z above the apparent level of origin of the thermals as follows:

$$B = \tau' / \bar{\tau} \quad (8)$$

so that

$$w \tau' = C \left(g \frac{\tau'}{\bar{\tau}} z \right)^{1/2} \tau' = C (g \tau'^3 z / n \bar{\tau})^{1/2}. \quad (9)$$

Now

$$\bar{\tau} = \tau_e - \tau'_e = \tau_e + \frac{\sigma}{1 - \sigma} \tau' \quad (10)$$

so that because τ' tends to zero as z increases, $\bar{\tau}$ tends to τ_e which is the buoyancy of the subsiding environment. Since we are ignoring the region near the surface in which τ' is comparable with $\bar{\tau}$ and in which the thermals are infinitesimally small, we may put $\bar{\tau}$ equal to τ_e in (9) and obtain from (7)

$$F = \frac{\sigma C}{1 - \sigma} \left(\frac{g}{n \tau_e} \tau'^3 z \right)^{1/2}. \quad (11)$$

254 R. S. SCORER

For a flux independent of z it is therefore required that

$$\tau' \propto z^{-1/3}. \quad (12)$$

By differentiation of (10) we obtain

$$\frac{\partial \bar{\tau}}{\partial z} = \frac{\sigma}{1-\sigma} \frac{\partial \tau'}{\partial z} \quad (13)$$

and so

$$-\frac{\sigma \tau'}{1-\sigma} \bigg/ \frac{\partial \bar{\tau}}{\partial z} = -\tau' \bigg/ \frac{\partial \tau'}{\partial z} = 3z \quad (14)$$

which is a result required later.

We may also remark that the well known result that

$$\frac{\partial \bar{\tau}}{\partial z} \propto z^{-4/3} \quad (15)$$

is also obtained, and that this depends only on (a) the assumption that geometrical similarity exists, (b) the formula (2) which follows directly from that without any reference to a particular geometrical model, and (c) the assumption of buoyancy flux independent of height. It is therefore a purely mechanical result and is obtained without reference to heat. It is clear from the argument used here that it is not a valid formula close to the surface for two reasons: first, the physical mechanisms of radiation and molecular transfer which are dominant there are ignored, and secondly the Boussinesq approximation, made in obtaining (4) and again in writing τ_e for $\bar{\tau}$ in deriving (11) is not valid there.

In view of (12) we have immediately from (7) that

$$w_e \propto z^{1/3} \quad (16)$$

for F and σ independent of z . The picture of convection thus implies that the subsidence velocity of the environment decreases downwards because the subsiding air occupies the same area at all heights while the thermals are entraining some of it at every level. The upward velocity of the thermals is proportional to the same power of z , according to (4) so that they accelerate upwards. This is much more in accord with observation than the behaviour of an isolated thermal having a constant total buoyancy anomaly, for then

$$B \propto r^{-3} \quad (17)$$

and so with (2) and (1) we have

$$w \propto z^{-1} \quad (18)$$

The amalgamation of thermals thus has a most important effect. The acceleration must mean that the value of C which will be used, which is for isolated thermals, is not precisely correct for this convection, but the error is not significant in this context. The mechanisms by which a thermal approaches its limiting velocity are not like those of a normal system approaching the limit exponentially. The motion is established by the orderly operation of buoyancy forces and the region occupied by eddy motions increases if the thermal is decelerated. The configuration of the motion changes, and it is not a simple balance between an accelerating force and a brake proportional to the velocity.

3. Rise through Wind Shear

This problem was discussed at length by HALL [2], whose paper includes the main result of this one but without a full discussion of the implications of its derivation and its consequences. An isolated thermal experiences a vertical acceleration relative to its

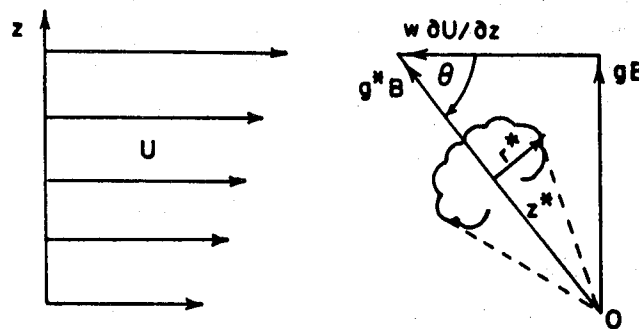


Fig. 2. Coordinates and notation for a thermal rising through wind shear. It moves as if subjected to a buoyancy g^*B which is the vector addition of the actual buoyancy gB and the relative acceleration of the environment $w \partial U / \partial z$

environment equal to gB . When it rises through wind shear, $\partial U / \partial z$, its environment is accelerated relative to it with a horizontal acceleration $w \partial U / \partial z$. The total acceleration is therefore the vector sum of these, whose magnitude we can represent by g^*B . If θ is the inclination of the axis of symmetry of the thermal to the horizontal (see Fig. 2)

$$g^*B = gB \sin \theta = w \frac{\partial U}{\partial z} / \cos \theta \quad (19)$$

$\theta = 90^\circ$ if there is no shear.

256 R. S. SCORER

The width of the inclined thermal, r^* , and, z^* , the distance from its instantaneously apparent origin in space, are related to its total inclined speed $w/\sin \Theta$ and relative horizontal velocity u by

$$\frac{w}{\sin \Theta} = \frac{u}{\cos \Theta} = C (g^* B r^*)^{1/2} = C \left(\frac{g}{\sin \Theta} B \frac{r}{\sin \Theta} \right)^{1/2} \quad (20)$$

and so

$$w = C (g B r)^{1/2} \quad (21)$$

and

$$\frac{u}{\partial U / \partial z} = \frac{w \cot \Theta}{w^{-1} g B \cot \Theta} = C^2 r \quad (22)$$

which is required later.

This part of the argument could not be sustained in such a simple form for plume convection because a bent over plume is certainly not like a vertical plume tilted over: each section of it is much more like a section of a two-dimensional thermal. Even this argument for thermals is restricted by the assumption that the environment has a single value for its horizontal velocity as far as the thermal is concerned. This means that the typical velocities due to the relative motion must be large compared with the differences in velocity due to the wind shear in the thermal's neighbourhood. Thus

$$r \frac{\partial U}{\partial z} \ll w \quad (23)$$

is a requirement.

The assumption in HALL's paper [2] that the two components of the relative acceleration can be compounded has been given some additional justification by some experiments by RICHARDS [5] on puffs. A body of fluid ejected into an otherwise stationary environment of the same density assumes a configuration of velocity which is for practical purposes identical with that of a thermal. This was a rather unexpected result because it was thought that the region of mixing in a thermal arose from buoyancy forces. A puff can be made without a mixing region in the form of a ring vortex, but if care is taken to make it initially turbulent it retains the thermal-like velocity pattern. Thus the buoyant effects represented in the vertical accelerations can be compounded with inertial effects due to the horizontal accelerations.

4. The Ratio K_M/K_H

By equating the buoyancy flux implied by the definition of K_H to the formula for the flux in (7) we obtain

$$-K_H \frac{\partial \bar{\epsilon}}{\partial z} = \frac{\sigma}{1-\sigma} w \tau' \quad (24)$$

and so

$$K_H = -\frac{\sigma}{1-\sigma} w \tau' / \frac{\partial \bar{\epsilon}}{\partial z} = 3 w z \quad (25)$$

by (14).

By the definition of U we have that if u and u_e are the horizontal velocity anomalies of the thermals and the environment,

$$U = \sigma (U - u) + (1 - \sigma) (U - u_e) \quad (26)$$

and so

$$\sigma u + (1 - \sigma) u_e = 0. \quad (27)$$

By the definition of K_M

$$-K_M \frac{\partial U}{\partial z} = -\sigma u w - (1 - \sigma) u_e w_e = -\frac{\sigma}{1-\sigma} u w \quad (28)$$

and so by means of (1) and (22) we obtain

$$K_M = \frac{\sigma}{1-\sigma} \frac{u w}{\partial U / \partial z} = \frac{\sigma}{1-\sigma} C^2 w r = \frac{\sigma}{1-\sigma} \frac{C^2}{n} w z. \quad (29)$$

Therefore

$$\frac{K_M}{K_H} = \frac{\sigma C^2}{(1-\sigma) 3 n}. \quad (30)$$

5. The Numerical Value of K_M/K_H

The argument above does not really require that there should be a very deep layer in which the similarity exists. K_M and K_H could be expressed in terms of the local value of r , and all we assume really is that the mechanics of the individual thermal, whatever sort of environment it is in, are rather like those of the similarity regime. The only factor in (30) which would be significantly altered by changing the regime is the number 3 which arises because of the law represented in (12). Convection with a buoyancy flux decreasing with height could not have a very different value, and much more uncertainty arises in estimating σ .

258 R. S. SCORER

The factors C^2 and n are those which are most characteristic of the particular convection that occurs, and these have to be obtained from experiment because there is no theoretical means of obtaining them. C represents the relationship of w to B and r and gives the rate of rise of a buoyant mass; n represents the rate of widening or mixing of the buoyant fluid as it rises: neither of these can be in error by more than a fraction of an order of magnitude.

The most complete set of experiments on thermals has been made by RICHARDS [4] and in the place of (2) he found it more consistent to write

$$w = \frac{1}{2} C_1 n^{1/2} (m B g z)^{1/2} \quad (31)$$

where the volume of the thermal is $m r^3$. Thus our C is given by

$$C = \frac{1}{2} C_1 n^{1/2} m^{1/2}. \quad (32)$$

He found that although C and n varied considerably from thermal to thermal while remaining constant for the life of each thermal, C_1 was very much more nearly the same for all thermals with a value of 0.73. C , on the other hand, ranged from about 1.7 to 7. Also m is about 3. Thus

$$\frac{C^2}{n} = \frac{1}{4} C_1^2 m = 0.4 \text{ roughly.} \quad (33)$$

Values obtained in the earlier experiments were somewhat lower than this but SAUNDERS [6] obtained values of $C = 1.5$, $n = 5$ from observations of cumulus clouds in Sweden. His larger value of n probably represents the effect of erosion of the thermals in the stably stratified environment with evaporation.

The value of σ varies quite a lot. Glider pilots find that up-currents are much stronger than the intervening down-currents, which can scarcely be detected in fair weather cumulus conditions in the environment of thermals below cloud. HARDY and OTTERSTEN [3] and others have obtained radar pictures of thermals giving $0.1 < \sigma < 0.6$. In a cloud layer σ could range from as much as 0.5 to as little as 0.01 or less in oceanic areas. Where the visible cloud occupies as much as half the area the up-currents occupy a much smaller fraction of the area. Thus we can probably say that

$$\frac{1}{3} > \sigma \quad (34)$$

and in some circumstances very small values could be found.

Ratio of Momentum and Material Vertical Eddy Transfer 259

The quantity σ enters into the formula for K_M/K_H because if σ is very small, for a given mean buoyancy gradient the buoyancy anomaly is very large: consequently a reduction to a very few intense thermals makes them each carry a lot of buoyancy but they do not carry a corresponding increase in momentum.

If we put $\sigma = 0.1$ we obtain

$$\frac{K_M}{K_H} = \frac{\sigma}{1-\sigma} \frac{C^2}{3n} = 0.013 \quad (35)$$

and we could expect values to range from about 0.1 to perhaps 10^{-3} . It appears therefore that thermals are much more efficient at transferring buoyancy (or heat) than momentum.

6. Convection by Cumulus in a Stratified Environment

The configurations of motion and buoyancy anomaly could be very similar around a cloud thermal to what we have supposed for dry ones, but because the environment is stably stratified our calculation of the heat transfer has to be altered. The estimate we have just made would be more correct if K_H were taken to represent the water vapour transfer coefficient because humidity is not far from uniform in the environment of the cumulus and the nonuniformities have a negligible affect on the motion anyway.

Near the top of a layer containing a steady amount of cumulus the continual evaporation of the clouds produces a very significant amount of downdraughts which might cause a mean upward vertical velocity in the environment as explained by FRASER [1]. This leads to an overall cooling of the layer. However the result still represents the fact that the thermals will be a very good agent for the transfer of water vapour but poor for momentum.

The importance of this result is that in parameterising the effects of cumulus in large scale numerical models it will be adequate to introduce a very large buoyancy or vapour transfer coefficient while transferring no momentum at the same time. This raises the question of how to represent the buoyancy transfer. If we made the transfer coefficient infinite we would simply put temperature gradient as soon as the cumulus appeared equal to that which cumulus convection ultimately gives rise to. If we wished to have a time lag we should express the transfer in terms of the departure of the gradient from this value, which would itself depend on whether the whole air mass became saturated or retained a constant cloud amount.

260 R. S. SCORER

The main feature of cumulus convection which renders this treatment of heat transfer inapplicable is that most of the heat transfer is by subsidence or ascent of the environment. That the clouds transfer a negligible amount of heat was demonstrated by FRASER [1]. The lapse rate of the environment is not related to the buoyancy anomaly of the thermals, and so we cannot obtain results like those for the similarity regime.

7. The Mechanism of Selective Transfer

The effect of buoyancy forces in modifying the transfer by eddies has been discussed in a limited way by SCORER [7, 8]. It is appropriate to state the ideas anew here in the light of the other arguments presented.

In order to produce a Reynolds stress the eddy motion must have its energy increased at the expense of the mean shear. It is well known that vorticity is increased by the stretching of vortex lines, but if the vortex lines of a chaotic pattern of vorticity (i.e. turbulence) are stretched by the shearing motion of the fluid on a large scale the kinetic energy of the eddy motion is only increased thereby if the vorticity is in the form of tubes rather than sheets — “spaghetti rather than lasagne”. Stretched sheets merely become thinner and the vorticity is increased merely by bringing the fluid of different velocities closer together. But stretched tubes acquire more energy of rotation. That spaghetti-like vorticity behaves like elastic strands can be demonstrated by calculating conditions under which waves can be propagated along vortex tubes. Waves cannot be propagated along a vortex sheet but disturbances remain in situ and become distorted by the redistributed velocity pattern.

The disturbances represented by the mean shear are of very low frequency, and so they are all trapped and the vortex tubes behave like elastic fibres and absorb energy when they are stretched. The motion is not reversible because the tubes are all the time distorting one another, and soon become randomly oriented again after the stretching. For shorter period large scale deformations however the eddies would introduce some visco-elastic properties into the fluid.

It is interesting that randomly chaotic vorticity, which is isotropic turbulence, initially produces no Reynolds stress, but as soon as a deformation makes it anisotropic, a continued deformation feeds “elastic” energy into the tubes.

For an incompressible inviscid fluid the vorticity equation is

$$\frac{D\omega}{Dt} = (\omega \text{ grad}) v - \frac{1}{\rho} \text{grad } \rho \times \left(g - \frac{Dv}{Dt} \right) \quad (48)$$

and in motions produced by small buoyancy the acceleration is small compared with g , so that the last term can be ignored. The

Ratio of Momentum and Material Vertical Eddy Transfer 263

first term on the right represents the advection of the vortex lines with the fluid. Clearly the vorticity produced by gravity is perpendicular to g ; and this represents the vortex ring motion characteristic of thermals. But in horizontal mean motion with a vertical gradient, horizontal vortex lines are not stretched, and so thermals cannot initially produce any Reynolds stress. After a vertical displacement has taken place the rings become inclined as indicated in Fig. 2: but in thermals the motion is being continually destroyed by smaller eddies and recreated by the buoyancy forces, so there is a tendency all the time to create horizontal vortex tubes, and no Reynolds stress.

On the other hand horizontal vortex rings are the best configuration of vorticity for transferring material, or heat or pollution or anything fixed to the material, while vertical vortex lines, which are in a good position to produce a Reynolds stress do not transfer material and are not created in a buoyancy driven eddy motion.

It is a reasonable conclusion that since in a stable stratification the horizontal vortex lines which are transferring material vertically are put into reverse by gravity, a stable stratification will inhibit material transfer. This is obvious on any picture of material transfer, but the vertically oriented vortex tubes will not be stopped by the gravity field, and so, except in so far as the general level of turbulence is lower in a stably stratified fluid anyway, the Reynolds stresses will not be affected. We can therefore expect that in this case

$$K_M/K_H > 1. \quad (49)$$

Unsteady two dimensional stable waves in a horizontally stratified fluid can transfer momentum vertically: for example the waves produced in the lee of a suddenly introduced obstacle transfer momentum from the obstacle and therefore through the fluid to a finite volume of it. These are motions which transfer momentum and no material property at all, and for which, therefore

$$K_M/K_H = \infty. \quad (50)$$

This does not justify the description of the wave motion as a form of turbulence but it does imply that momentum is of a different nature from other transferable properties in fluids. Reynolds analogy between the momentum and material transfer is not generally valid.

264 R. S. SCORER: Ratio of Momentum and Material Vertical Eddy Transfer

The propagation of momentum by waves is really of quite a different kind and can be excluded from the discussion of eddy transfer mechanisms on the ground either that it is not a diffusive motion or that it is a motion with a clearly defined scale which does not decrease with time.

References

1. FRASER, A. B.: The 'White Box': the Mean Mechanics of the Cumulus Cycle. *Quart. J. Roy. Met. Soc.* **94**, 71 (1968).
2. HALL, W. S.: The Rise of an Isolated Thermal through Wind Shear. *Quart. J. Roy. Met. Soc.* **88**, 34 (1962).
3. HARDY, K. R., and H. OTTERSTEN: Radar Investigations of Convective Patterns in the Clear Atmosphere. *J. Atmos. Sciences* (in press, 1969).
4. RICHARDS, J. M.: Experiments on the Penetration of an Interface by Buoyant Thermals. *J. Fluid. Mech.* **11**, 369 (1961).
5. RICHARDS, J. M.: Puff Motions in Unstratified Surroundings. *J. Fluid. Mech.* **21**, 97 (1965) (see p. 105).
6. SAUNDERS, P. M.: An Observational Study of Cumulus. *J. Met.* **18**, 451 (1961).
7. SCORER, R. S.: Natural Aerodynamics (pp. 128—131). London: Pergamon Press, 1958.
8. SCORER, R. S.: The Effect of Thermal Convection on Transfer Mechanics in the Atmosphere. *Int. J. Air and Water Pollution* **6**, 101 (1962).

Author's address: Dr. R. S. SCORER, Imperial College, London, S.W. 7, Great Britain.

Notes taken by:

R. E. Forbes

P. M. Caplan

HORIZONTAL MOMENTUM TRANSPORT BY THERMALS; THE POSSIBILITY OF CYCLONE GENERATION

The question being considered today is the generation of concentration of vorticity, e.g., by eddies. Normally eddies are thought to be diffusive in nature although this is not necessarily true of momentum distribution. Consider, for example, the curved path as shown in Fig. 1 with uniform velocity at A, i.e., a neutrally stable profile.

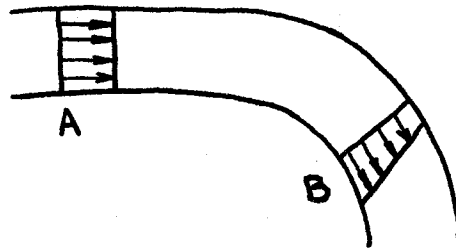


Fig. 1

At point B where the flow undergoes a turn, the speed q will have to be proportional to $\frac{1}{r}$, r being the distance measured from the center of curvature in order to have zero vorticity. That is, the flow at the inside wall will have to be faster than that at the outside wall. It will be unstable if the flow approaching the bend is already faster on the inside at the entrance to the bend. In that case, it would tend to develop radial motion, interchanging parcels and mixing them. Turning the stream to the other direction, with the velocity profile shown as in Fig. 2, the flow will then be stable, because the vorticity is in the direction as the curve.

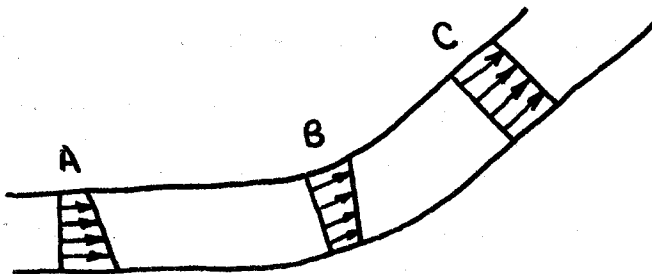


Fig. 2. Stable Configuration

(Note that the profiles are changed when the curvature changes)

Going back to the static case, consider an unstably stratified fluid in a tank, downward motion will occur spontaneously, somewhat like the dynamically unstable case of having radial motions. On the other hand, if

the tank is stably stratified, upon being mixed up continuously by interchanging the parcels vertically, one will end up with a uniform density distribution as a result of energy being put into the system (by stirring). Similarly, then, we could stir the flow in Fig. 2 at the point C where the flow is stable and the velocity at B will thus be uniform. By doing so, we go from a stable to a neutral state. The crucial point of this is that no force along the direction of the motion is exerted on the system. Otherwise the velocity profile could be determined by the force. A grid, for example, cannot be used as it would apply a force in the direction of the motion, causing therefore rather different result.

Take the case of thermal convection the cross section of which is shown in Fig. 3 below.

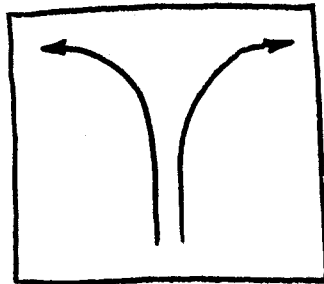


Fig. 3

In the horizontal plane as shown, the eddy motion is produced by thermal convection. When the thermal reaches a lid or very stable layer the kinetic energy developed by the vertical force will cause horizontal displacements, as in the anvil of a convection cloud. Thus, thermal convection is a means by which motion of horizontal displacement can be caused by vertical forces in a fluid which is moving horizontally, therefore, possibly altering the velocity distribution in curved motion, as all motions on the earth are. The main question to be answered is whether, in a stable curved motion, the stirring will cause the flow to go to assume the neutral state as it does in a static case. If it does, some of the consequences can be considered in the following.

To illustrate the idea, consider annular region, in which the fluid is circulating at uniform angular velocity, so that $v = r\Omega$, Ω being constant, as shown in Fig. 4 below.

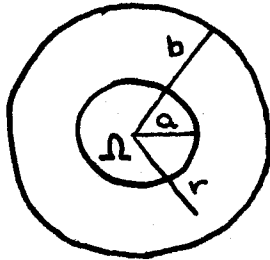


Fig. 4

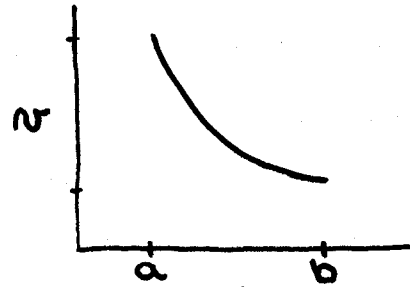


Fig. 4a

Starting with this situation, the difference of pressure between $r=a$ to $r=b$ is then

$$\Delta P_0 = P_b - P_a$$

produced by a simple solid rotation. If the fluid is now stirred up and changes into a neutral state, then

$$vr = \text{constant.}$$

If the stirring is caused by internal motion, the total angular momentum is then conserved, and that will then produce a profile like that shown in Fig. 4a. In that case, calculation based on the assumption of conservation of total angular momentum then shows,

$$\Delta P_1 = \left[\frac{1}{4} (b^2 + a^2)^2 / a^2 b^2 \right] \Delta P_0$$

If $b = na$ with n reasonably large, e.g., 10, then

$$\Delta P_1 \approx \frac{1}{4} n^2 \Delta P_0$$

In other words, the new pressure difference can be very large compared to the original one if n is very large. There is this to say, if a neutral profile could be induced by stirring, one would in fact generate a very low pressure center. Furthermore, the new state has a greater kinetic energy

than the original, and the energy must have been transferred from the eddies to the mean motion.

This fact is indeed very important. Consider a region in a tropical ocean, where a low pressure center is generated. That will then cause an adiabatic expansion of the inflowing air which continuously absorbs heat from the sea even though the sea temperature is no greater at the center. Thus, a heat source located at the low pressure center is created, which provides the means to keep hurricanes going when heat is always produced in the middle. The centrifugal force near the eye of the cyclone that one must overcome gets bigger and bigger, so that stable regime can be produced there.

The question is then does this really happen. In fact, it does not necessarily happen always. Consider a portion of a curved flow as shown in Fig. 5. Suppose the flow is stirred by placing eddies in them, e.g., the anvils in a cumulus cloud.

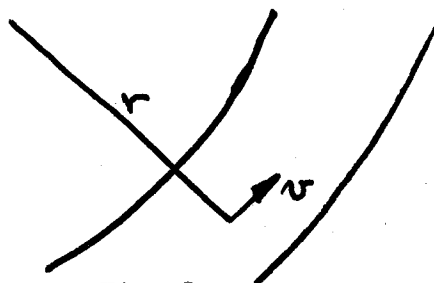


Fig. 5

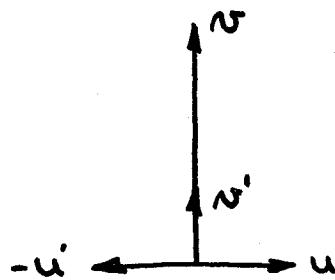


Fig. 5a

At the point r , suppose particles are projected in all directions. Assuming that for every v' projected, there are u' and $-u'$ being produced, as in Fig. 5a. In other words, v' and u' are not correlated with each other at that initial moment, i.e., $\overline{u'_0 v'_0} = 0$, where the subscript 0 is used to denote the values at the initial moment. The argument in fact is similar to the Prandtl mixing length theory that gives rise to the Reynolds stress even if $\overline{u'v'}$ started off as being zero. The aim here is to take the particle along a trajectory with no correlation at the origin and to find out whether they are correlated with each other at the end of the trajectory.

In molecular diffusion, one may imagine the particles as travelling along a straight line in between the collisions. But here, the parcels of fluids are moving under the pressure field of the environment, i.e.,

$$\frac{\partial p}{\partial r} = \frac{\rho u^2}{r}$$

To see what they do, we must consider the equations of motion

$$\frac{\partial}{\partial r} \left[\frac{1}{2} (\underline{u} + \underline{u}')^2 \right] + \frac{\rho u^2}{r} = 0 \quad \text{(energy, } \frac{\rho u^2}{r} \text{ being the pressure gradient)}$$

where $\underline{u} = (u, v)$ and $\underline{u}' = (u', v')$

$$\text{and } \underline{u} + \underline{u}' = \frac{d\underline{u}}{dt} \quad \text{(conservation of angular momentum)}$$

They merely state the balance of kinetic energy and the conservation of angular momentum respectively. The aim is to derive $u' dr$ and $v' dr$ so as to see whether u' and v' are correlated when the particle moves to the new position.

For that purpose, we have,

$$(\underline{u} + \underline{u}') \frac{\partial}{\partial r} (\underline{u} + \underline{u}') + u' \frac{\partial u'}{\partial r} + \frac{\rho u^2}{r} = 0$$

and

$$\frac{\partial}{\partial r} (\underline{u} + \underline{u}') = - \frac{d\underline{u}}{dt} = - \frac{\underline{u} + \underline{u}'}{r}$$

Thus,

$$- \frac{(\underline{u} + \underline{u}')^2}{r} + \frac{\rho u^2}{r} + u' \frac{\partial u'}{\partial r} = 0$$

and

$$u' \frac{\partial u'}{\partial r} = v' \left(\frac{2u}{r} + \frac{u'}{r} \right)$$

$$\frac{\partial v'}{\partial r} = - \left(\frac{u + u'}{r} + \frac{\partial u}{\partial r} \right) = - \left(\zeta + \frac{u'}{r} \right)$$

where

$$\zeta = \frac{\partial u}{\partial r} + \frac{u}{r}$$

is the vorticity of the mean flow. Defining also the deformation rate,

we have

$$e_{r\theta} = \frac{\partial v}{\partial r} - \frac{v}{r} = \int -\frac{2\omega}{r}$$

In the neutral state, $\int \omega = 0$ as there is no vorticity, but then, the deformation is non-zero. On the other hand, the state of no deformation, given by $e_{r\theta} = 0$, the vorticity is equal to $\frac{2\omega}{r}$. The molecular viscosity of the fluid will tend to produce the state of $e_{r\theta} = 0$ which is different from the state of zero vorticity, which the eddies are supposed to produce. There is in fact nothing new about that; for example, in the atmosphere, the molecular motion in a stratified field tends to produce an isothermal state whereas the stirring motions produce an adiabatic lapse rate, thus, there is no reason why the stirring motion and the molecular motion should produce the same thing. It is therefore the aim today to find out what the eddy motion will produce.

In this respect, we have the following Taylor series, recalling that the origin for time τ is taken to be at the moment where $\overline{u'_0 v'_0} = 0$.

$$u'v' = u'_0 v'_0 + \left[\frac{\partial}{\partial r} (u'v') \right]_0 \Delta r + \frac{1}{2} \left[\frac{\partial^2}{\partial r^2} (u'v') \right]_0 (\Delta r)^2 + O(\Delta r^3)$$

For Δr , the increment of the radial distance in time τ , then,

$$\begin{aligned} \Delta r &= \left(\frac{dr}{d\tau} \right)_0 \tau + \frac{1}{2} \left(\frac{d^2 r}{d\tau^2} \right)_0 \tau^2 + \dots \\ &= u'_0 \tau + \frac{1}{2} \left(\frac{\partial u'}{\partial \tau} \right)_0 \tau^2 + \dots \\ &= u'_0 \tau + \frac{1}{2} \left(\frac{\partial u'}{\partial r} \cdot \frac{dr}{d\tau} \right)_0 \tau^2 + \dots \\ &= u'_0 \tau + \frac{1}{2} u'_0 \left(\frac{\partial u'}{\partial r} \right)_0 \tau^2 + O(\tau^3) \end{aligned}$$

because, at t_0

$$\frac{\partial^2 r}{\partial t^2} = \frac{\partial}{\partial t} \cdot \frac{\partial r}{\partial t} = u' \frac{\partial u'}{\partial r}$$

After a simple substitution, then,

$$\begin{aligned} u'v' &= u'_0 v'_0 + \tau \left[u' \left(u' \frac{\partial v'}{\partial r} + v' \frac{\partial u'}{\partial r} \right) \right. \\ &\quad + \frac{1}{2} \tau^2 \left[v' \left(\frac{2u'}{r} + \frac{v'}{r} \right) \left(u' \frac{\partial v'}{\partial r} + v' \frac{\partial u'}{\partial r} \right) \right. \\ &\quad \left. \left. + u'^2 \left(u' \frac{\partial^2 v'}{\partial r^2} + 2 \frac{\partial u'}{\partial r} \frac{\partial v'}{\partial r} + v' \frac{\partial^2 u'}{\partial r^2} \right) \right] \right] + O(\tau^3) \end{aligned}$$

Now, since the eddies are assumed to be symmetrical about $r = \text{const}$ $\theta = \text{const}$.

$$\overline{u'_0 v'_0} = 0$$

by assumption,

$$\overline{u'v' \frac{\partial v'}{\partial r}} = -\overline{u'^2 \left(\zeta + \frac{v'}{r} \right)} = -\overline{u'^2 \zeta}$$

$$v' \left(\frac{2u'}{r} + \frac{v'}{r} \right) \left(u' \frac{\partial v'}{\partial r} + v' \frac{\partial u'}{\partial r} \right) = \left(\frac{2u'}{r} v' + v'^2 \right) \left[-u' \left(\zeta + \frac{v'}{r} \right) + \frac{v'}{u'} \left(\frac{2u'}{r} + \frac{v'}{r} \right) \right]$$

= 0 in the mean

when $u' = u'_0, v' = v'_0$ because

$$\overline{u'_0 v'_0} = \overline{v'_0{}^2 u'_0} = \overline{v'_0{}^3} = \frac{\overline{v'_0{}^3}}{\overline{u'_0}} = \frac{\overline{v'_0{}^4}}{\overline{u'_0}} = \frac{\overline{v'_0{}^5}}{\overline{u'_0}} = 0$$

Hence,

$$\overline{u'v'} = \left[-\overline{u'^2 \zeta} + \overline{v'^2 \frac{2u'}{r}} \right] \tau + O(\tau^3)$$

When the following are taken into account:

$$\begin{aligned} u'^2 u' \frac{\partial^2 v'}{\partial r^2} &= -u'^3 \left\{ \frac{\partial \zeta}{\partial r} + \frac{1}{r} \frac{\partial v'}{\partial r} - \frac{v'}{r^2} \right\} \\ &= -u'^3 \left\{ \frac{\partial \zeta}{\partial r} - \frac{\zeta}{r} - \frac{2u'}{r^2} \right\} = 0 \text{ in the mean,} \\ u'^2 \frac{\partial u'}{\partial r} \frac{\partial v'}{\partial r} &= -2u'^2 \frac{v'}{u'} \left(\frac{2u'}{r} + \frac{v'}{r} \right) \left(\zeta + \frac{v'}{r} \right) \\ &= -2u'v' \left(\frac{2u'}{r} + \frac{v'}{r} \right) \left(\zeta + \frac{v'}{r} \right) = 0 \text{ in the mean,} \end{aligned}$$

and

$$\begin{aligned} \overline{u'v'} \frac{\partial^2 \overline{u'}}{\partial r^2} = \overline{u'v'} \left\{ -\frac{v'^2}{u'^2} \left(\frac{2u'}{r} + \frac{v'}{r} \right)^2 \right. \\ \left. - \left(5 + \frac{u'}{r} \right) \left(\frac{2u'}{r} + \frac{v'}{r} \right) + v' \left(\frac{\partial}{\partial r} \frac{2u'}{r} - \frac{v'}{r} - \frac{2v'}{r^3} \right) \right\} \end{aligned}$$

= 0 in the mean

as they all involve $\overline{u'^3}$ etc. and thus no correlation by symmetry.

Calculating $\overline{u'v'}$ up to $O(r^3)$ will give, as the most important coefficient, the expression

$$\frac{4v_0^2}{3r} \left\{ \overline{u_0'^2} r - \overline{v_0'^2} \frac{2u_0}{r} \right\} r^3$$

being the ones involving the lowest order in $\overline{u'v'}$. In other words, up to this order, the major effect is that of vorticity and curvature, and hence no new phenomena are introduced. The important thing here is that the situations in which $\overline{u'v'}$ is zero depend on the relative magnitude of $\overline{u_0'^2}$ and $\overline{v_0'^2}$. The following cases illustrate the possibilities.

Case I. $\overline{u_0'^2} = \overline{v_0'^2} = q'^2$ (isotropic case)

then

$$\overline{u'v'} = -q'^2 r \epsilon_{r\theta}$$

Thus, the stress continues as long as the fluid is being deformed and will tend to produce solid rotation, as the case with molecular viscosity.

Therefore, the result of having isotropic eddies is not to produce a neutral state--with zero vorticity.

Case II. $\overline{v_0'^2} = 0$ i.e. only radial impulses.

In an unstable flow with spontaneous mixing, the result is to produce a zero vorticity state, because only then is the stress zero when $\overline{u_0'^2}$ is non zero. The eddies that are produced spontaneously in a curved flow are not the same as those in Case I. They may produce a $\overline{u'}$ but not a $\overline{v'}$, as in this case.

Then the stress is

$$\overline{u'v'} = -\overline{u'^2} \tau \zeta$$

which tends to reduce the vorticity and to make $\omega \sim \frac{\partial \omega}{\partial r}$.

In a line of cumulus along the wind, as it may be approximately in a hurricane, this mechanism may be very important in that they maintain a flow for which $\omega r = \text{constant}$. They in fact push the vorticity, and therefore the angular momentum into the middle by removing it from the region which is stirred by cumulus.

On the edge of a region with a lot of cumulus clouds that produce a large amount of horizontal mixing, one could well produce velocity discontinuities. The billow instability will make the discontinuous layer roll up causing a concentration of vorticity and a low pressure center. The center will then act as a heat source over the sea. This in fact is how hurricanes might occur, as some of the evidence from the Hong Kong Observatory suggest. Sometimes they seem not to maintain the heat source for long enough and are dissipated by randomly arranged clouds.

Case III. $\overline{u'^2} = 0$ i.e. only tangential impulses.

Then

$$\overline{u'v'} = \frac{2\omega}{r} q'^2 \tau$$

and the stress tends to make the flow straight, i.e., $r = \infty$.

Case IV. $r = \infty$, rectilinear flow.

§ is now the shear and we have the classical result of mixing length theory.

$$\overline{u'v'} = -q'^2 \tau \frac{\partial \omega}{\partial r}$$

the mixing length being $q'^2 \tau$.

The main theme that comes out here is that randomly oriented eddies tend to do the same as molecular viscosity. But unlike the latter, the effect of the pressure field may cause peculiar effects if only radial or tangential displacement is present.

To sum up, Case I can produce vorticity at the edge of a stirred region where \mathbf{q} is discontinuous. Case II can produce vorticity at the center and edges of a stirred region. While Cases III and IV do not seem specially relevant. Thus, to get concentrated vorticity, we need a sharp boundary to a region of clouds, or **2-D** lines of clouds lined up along the flow.

Notes taken by:

S. K. Chan

J. R. Travis

I. DISTRAILS AND CONTRAILS IN A STABLE ATMOSPHERE

When aircraft goes, it leaves behind lots of water in its exhaust. The formation of contrails can be shown by Figures 1a, b, c*:

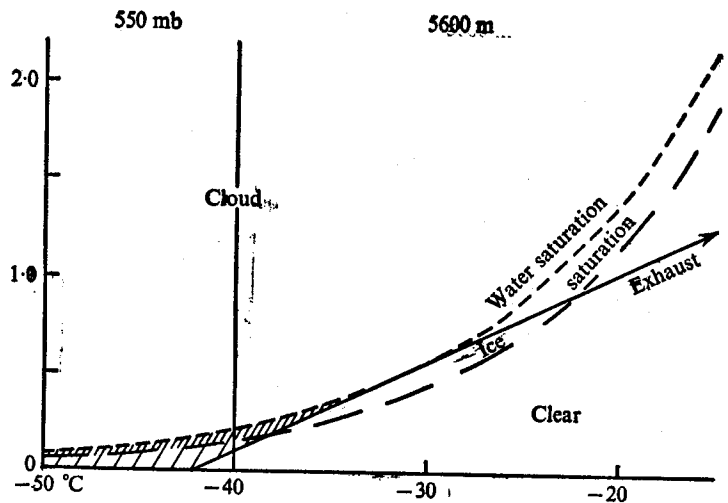


FIGURE 1a. Water and ice saturation mixing ratio curves for air at 550 mb. If the point representing the ambient air lies in the shaded region a contrail will form as the exhaust, represented by a point in the direction indicated, is diluted isobarically. If the ambient air point is in the doubly shaded region and the trail is glaciated it will persist. It will be glaciated immediately if it reaches a temperature below -40°C .

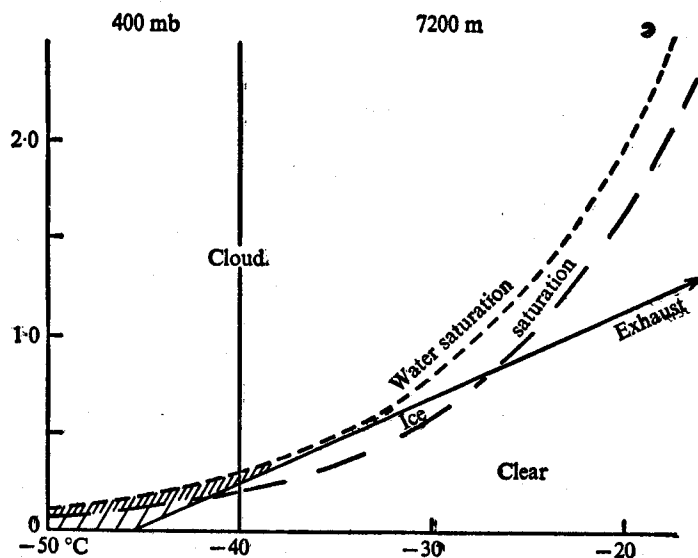


FIGURE 1b. The same as figure 1a for 400 mb.

* Reprinted from J. Fluid Mech. (1970) in press, printed in Great Britain, by R. S. Scorer and L. J. Davenport, (Figs. 1,2,3,4,9 shown in these notes as Figs. 1a,1b,1c,2,11.)

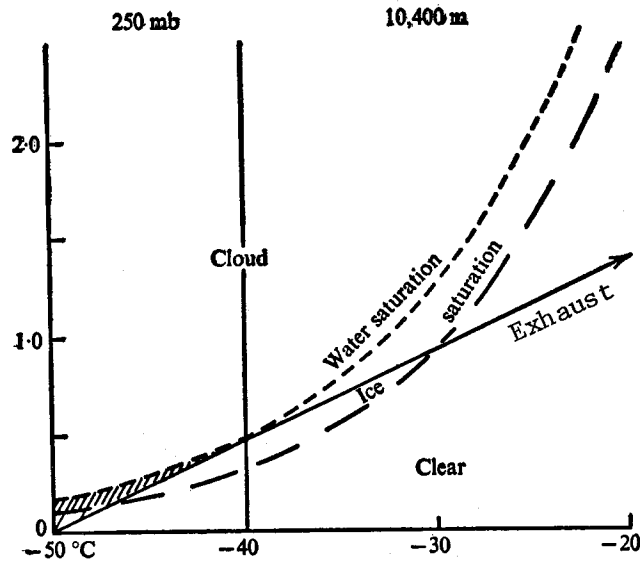


FIGURE 1c. The same as figure 1b for 250 mb.

The arrow marked 'exhaust' indicates the direction of the point representing typical aircraft exhaust. As the exhaust mixes with the air, the mixture is represented by a point on the straight line joining the points representing the ambient air and the exhaust. As the mixing proceeds, cloud will appear if water saturation is reached, which means that for a contrail to occur in previously clear air the ambient air point must lie within the shaded area below the water saturation line and above the tangent to it from the exhaust point. If the environment air is below -40°C , then the cloud will freeze and has persistence, since it will not evaporate. If the ambient air temperature is above -40°C , then whether they persist or not depends on the humidity of the environment. In that region, it can be called semi-persistent as shown in the [Fig. 2].

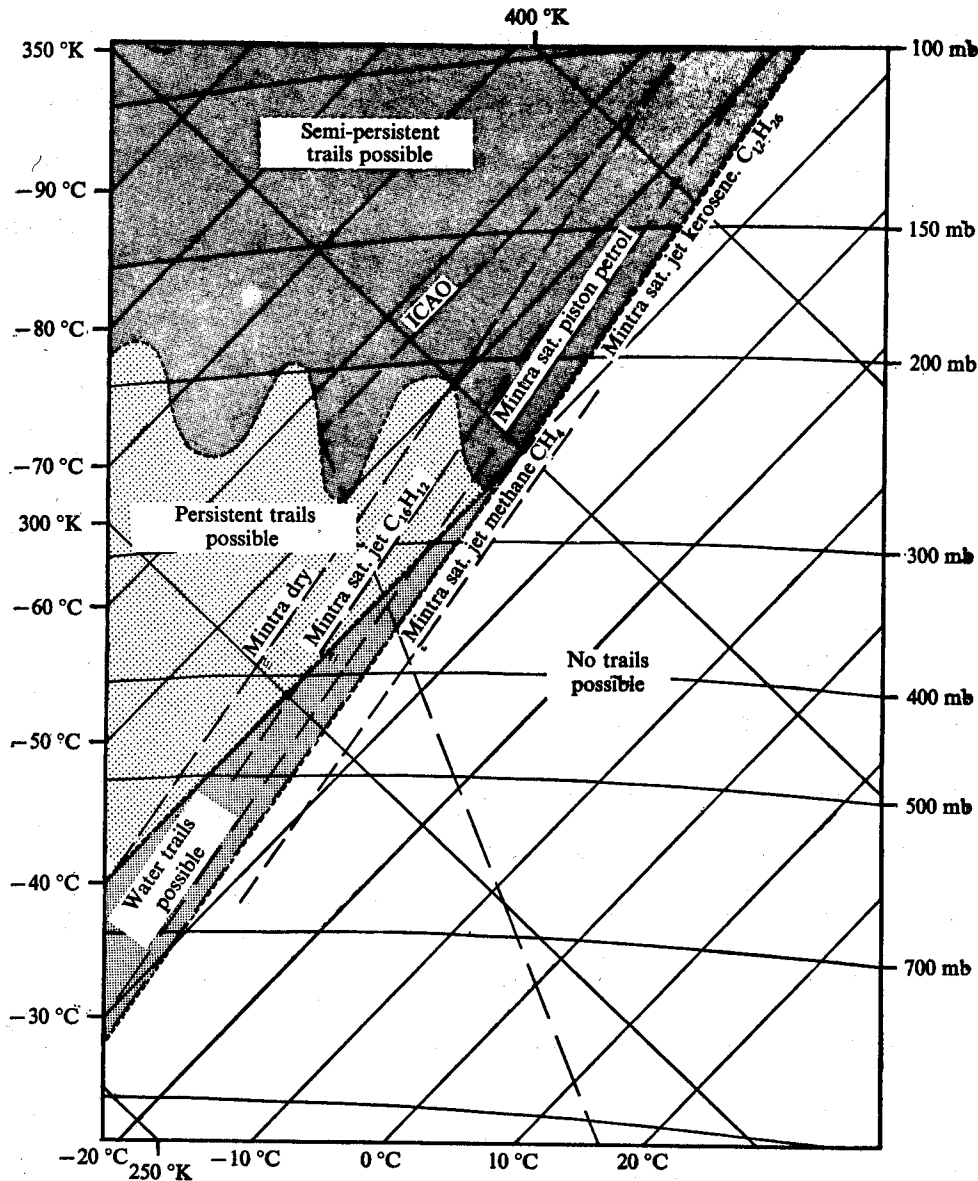
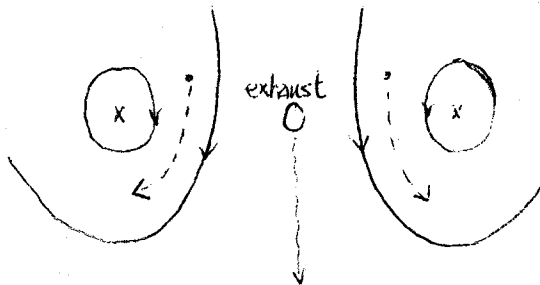


Figure 2. The conditions in the atmosphere required for condensation trail formation are shown on this T ϕ gram in which the two orthogonal coordinates are temperature (in °C) and log (potential temperature), the potential temperature being indicated in °K. The isobars are slightly curved and the diagram is drawn so that they are almost horizontal. Pressure and temperature are then used to plot a sounding of the atmosphere on the diagram: and the line marked ICAO represents the ICAO standard atmosphere, with a tropopause at about 320 mb.

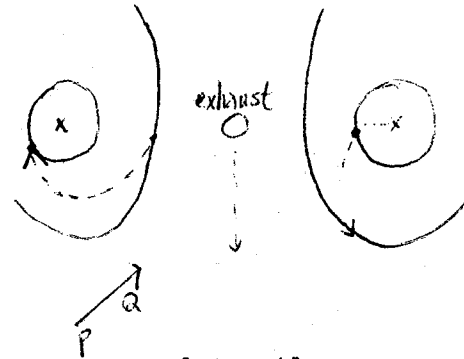
The shaded areas are where trails are possible from jet aircraft burning kerosene: they are bounded by the 'mintra' which indicates the pressure, at each temperature, below the altitude of which trails cannot be formed. The 'mintra dry' indicates the limit for an absolutely dry atmosphere.

[For a description of the T ϕ gram see, for example, Scorer, R. S., 1958: Natural Aerodynamics. Oxford: Pergamon, pp. 256-260.]

When we look at the exhaust from below, we can see two trails move apart as shown in Fig. 3. If we look at it in the direction of \vec{PQ} , then we'll see the inner particle cross the outer one in the right side vortices, but outer particle cross inner particle in the left side vortices as shown in Fig. 4.

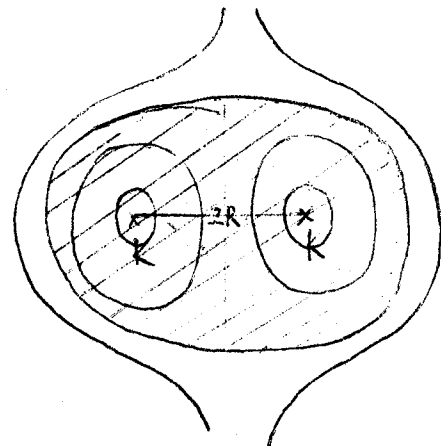


[Fig. 3]



[Fig. 4]

The streamline pattern can be shown in Fig. 5, only the air in the shaded region moves with the vortices and it is called "accompanying fluid" in which no buoyancy force appears since it has uniform density. But it acquires buoyancy when it descends through a stably stratified atmosphere.

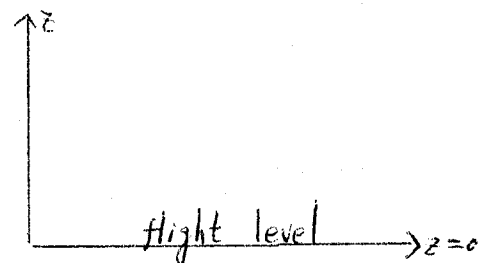


[Fig. 5]

If the circulation of the vortex pair is const. K . and their altitude is z , then the vertical velocity

$$W = \frac{dz}{dt} = - \frac{K}{4\pi R}$$

The impulse (vertical momentum) $Q = -2\pi K R$.

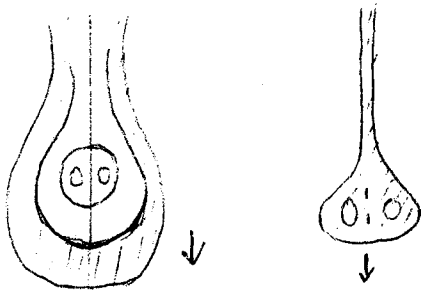


We like to know what effect the buoyancy has on the shape of the vortices. (Buoyancy against the circulation and gives the downwind motion of the entire accompanying fluid.)

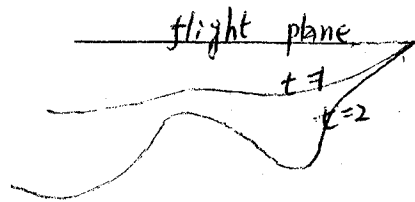
Assume the atmospheric stratification $\beta = -\frac{1}{\tau} \frac{dz}{dz}$

then $\frac{\Delta z}{\tau} = -\beta z$, where z is the vertical displacement of the trail air.

Decrease of R can give the increase of downward impulse Q and accelerate downward motion. So as the vortices go down to lower level the size decreases and it will have some detrainment and leave the environment fluid behind as shown in Fig. 6.



[Fig. 6] Fluid left behind and pair accelerate downwards.



[Fig. 7] The growing of small irregularities

Since velocity increases in the direction of displacement, it means that distortions grow unstably. Any irregularity on it will grow as it goes down as shown in Fig. 7 and all wavelengths are unstable.

The momentum equation can be written as

$$\frac{dQ}{dt} = g m R^2 \Delta f \quad \Delta f = f \frac{\Delta z}{\tau}$$

$$\therefore 2k \frac{dR}{dt} = g m R^2 \beta z$$

$$\frac{dR}{dz} = -(2\pi g m \beta / k^2) R^3 z$$

$$R = R_1 (1 + R_1^2 z^2 / h^2)^{-\frac{1}{2}}$$

$$W = W_1 (1 + R_1^2 z^2 / h^2)^{\frac{1}{2}}$$

$$h^4 = k^2 / 2\pi m g \beta$$

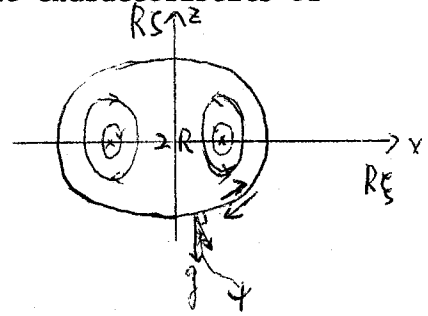
$$z = \frac{h^2}{R_1} \sinh \frac{kt}{4\pi h^2}$$

$$R = R_1 \operatorname{sech} \frac{kt}{4\pi h^2}$$

$$W = W_1 \cosh \frac{kt}{4\pi h^2}$$

So the solutions show everything depends on the characteristics of atmosphere β but not the circulation K .

On the boundary of accompanying fluid, vorticity is generated by the difference in density as shown in Fig. 8. The generation of vorticity can be expressed by



[Fig. 8]

$$\frac{D\eta}{Dt} = \frac{\Delta z}{2} (g \sin \psi - f \sin \theta), \quad (\because f \ll g)$$

$$\frac{D\eta}{Dt} = u \frac{\partial \eta}{\partial x} + w \frac{\partial \eta}{\partial z} \quad (\because f \text{ is neglected}).$$

where η is the velocity discontinuity at boundary.

Define ϕ by $\eta = (2\pi R^2 g \beta z / K) \phi$

then $\frac{\partial \phi}{\partial \xi} = \frac{w}{u g}$

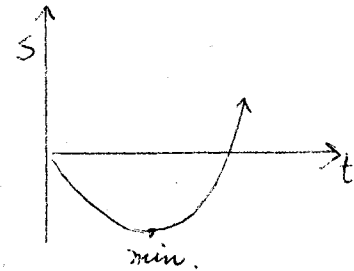
$$\frac{\partial \phi}{\partial \xi} = \frac{1}{g}$$

where $g^2 = u^2 + w^2 =$ speed of fluid on the boundary.

Let w_s vertical velocity due to vortex sheet at $\xi = s$ at stagnation

then $\frac{K}{\pi R^2 (1+s^2)} - \frac{R^2 g \beta z}{K} w_s = \frac{K}{4\pi R}$

or $\frac{3-s^2}{(1+s^2) w_s} = \frac{4\pi R^3 g \beta z}{K}$



As fluid detrained, the stagnation point moves downwards to s , fluid left behind. But vorticity at boundary increases, the size becomes less, so the stagnation point rises again after it arrives at the minimum level

s_{min} , which occurs at

$$t^* = 0.66 (m g \beta / 8 \pi)^{-\frac{1}{2}} \approx (\beta \times 10^{-3})^{-\frac{1}{2}} \text{ sec} \approx 30 \sim 100 \text{ sec}$$

$$(m \approx 1.5, \quad g = 10^3, \quad \beta \text{ in cm}^{-1})$$

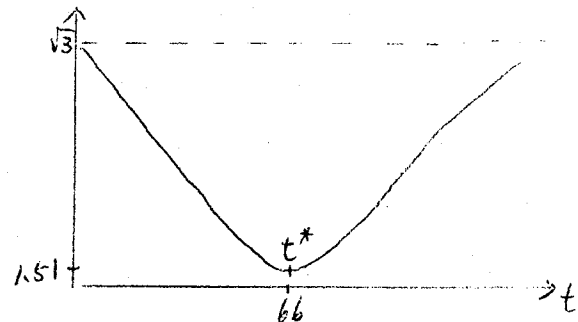
t^* depends only on β but not the characteristics of atmosphere

ζ	-1.73	-1.59	-1.05	-0.23	1.05	1.59	1.73
ϕ	0	0.75	1.66	2.50	3.76	4.66	5.42

For $R_1 = 13 m$, $K = 190 m^2 sec^{-1}$

$\beta = 2.2 \times 10^{-7} cm^{-1}$, $g = 10^3$

t^* is shown in Fig. 10.



[Fig. 10]

The form of the instability of the vortex pair

The vortex cores can be seen to 'burst' when tip contrails are present. According to (11) or (13) the vortex pair is seen to be carried downwards with a constant velocity at first, but later with an exponentially increasing velocity. This means that in the later stages, though not at first, irregularities in the original vortex pair will grow exponentially and the vortices will assume an undulated configuration as shown in figure with the width of the pair decreased

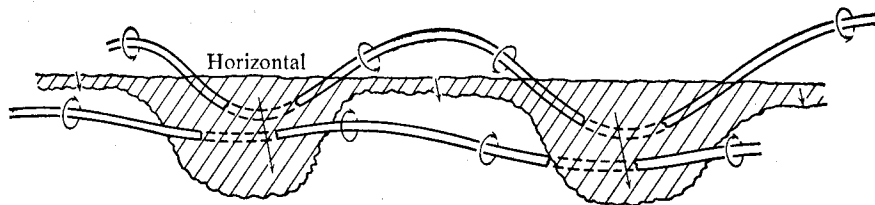


FIGURE 11. Perspective diagram of the relative positions of the cloud blobs and the burst parts of the tip vortices in the aircraft wake.

at the troughs as compared with the crests. Furthermore, because of the exponential growth, the configuration will be in a series of arches without significant regions of upward curvature. The tip trails will burst at the bottoms of the troughs. When bursting begins it will spread along the tip vortices as they descend.

If there is any cloud from a nearly centrally placed engine it will be detrained at the top if it has had time to pass round the vortices leaving a straight upper edge, while the bottom of it will be caused to descend in a series of blobs (figure 11) which correspond to where the vortices are closer together at the troughs.

Notes taken by:

Yun-Mei Chang

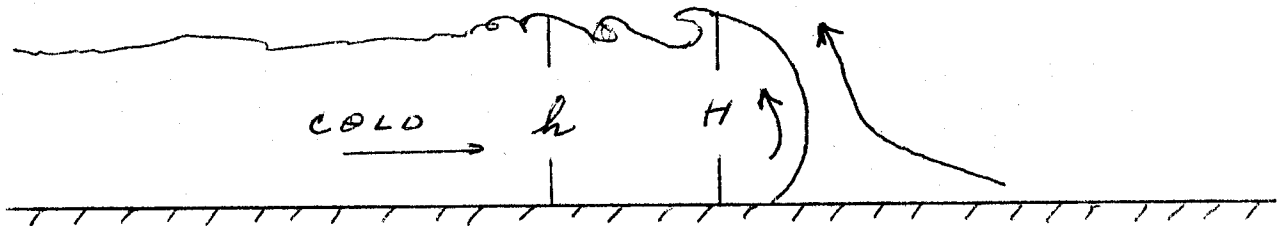
W. H. Mach

DENSITY CURRENTS, MAMMA, CELLS AND STREETS

1. Density Currents

Density currents are the movement of fluid of higher density into an area of lower density. Examples of density currents are sea breeze fronts, outflow of cold air from storms (haboobs are a particular example showing extreme properties) and some cold fronts.

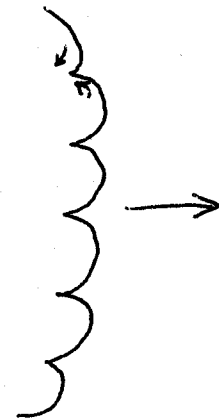
Laboratory experiments by J. E. Simpson have shown the mechanisms very clearly. Dye was inserted in fluid flow at appropriate points to demonstrate the fluid motion. The density current flow shows a characteristic pattern provided that scales are large enough that viscous effects are insignificant outside boundary layers.



Usual properties of density currents are:

- A. Maximum wind at the ground.
- B. Well developed nose with some pile up.

The leading edge shows a scalloped appearance from above. Lobes on the front enclose air in the path. The theoretical angle of the leading edge of the front according to classical hydrodynamical theory is 60° in nonviscous fluid, but surface drag affects this angle significantly.



C. An upcurrent occurs inside the denser fluid immediately behind the nose of the front.

D. The mixing region is narrow, but billows occur on the upper behind the nose, sometimes far back.

A movie of Simpson's experiments clearly demonstrated the above properties.

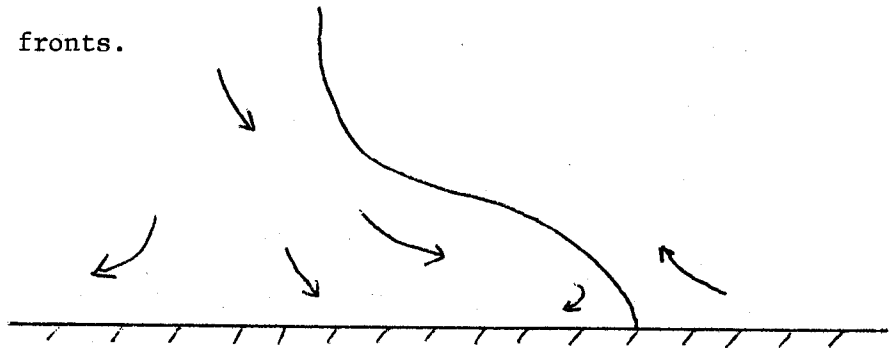
Characteristic velocity of density current fronts is $(gBh)^{\frac{1}{2}}$, assuming that the nose height and the depth of the flow are about the same. The depth of typical density currents runs from fifty to several thousand feet. Sea breezes frequently are of the order of 1000 feet in depth.

Sea breeze fronts often can be detected on radar from echoes of birds soaring in the updraft and feeding on insects carried up by it. However, radar intensity is not strongly related to frontal strength. Often cloud wisps accompany fronts. Glider pilots frequently detect fronts by differences in visibility across the fronts.

Downdrafts from
nearby showers

frequently produce
a short period of

high wind. Such downdrafts have a different structure from the density current structure discussed previously, and their variation with time is much greater.

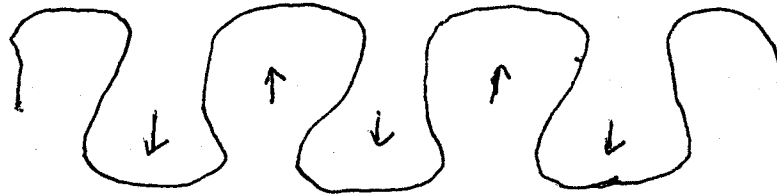


Sea breezes may inhibit convection near shorelines, with convective clouds showing up along a curve inland from the shore. Cloud lines also are observed offshore; the cause of these is not so evident, and may not be associated with density currents.

2. Mamma

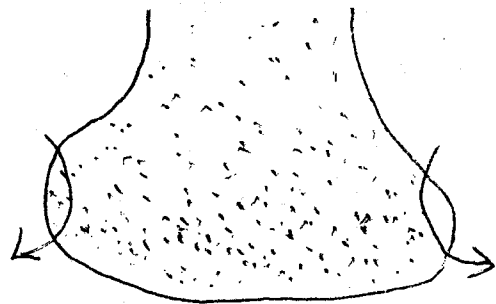
The mamma phenomenon occurs occasionally at the lower surfaces of cloud layers associated with convective clouds. For illustration, consider the lower surface of a thunderstorm anvil spreading out from the thunderstorm system. The cloud surface is adjacent to a clear air region which usually has lower mixing ratio. In a subsidence region, the cloud temperature drops along the moist adiabatic and the adjacent clear air along the dry adiabatic.

The boundary between the cloudy air and the clear air below it becomes gravitationally unstable and tends to develop a characteristic pattern called mamma.



The rising pockets of clear air may appear light when the cloud layer is thin and illuminated from above. Mamma may be considered to be negative thermals. The scale of these is generally much smaller than that of typical buoyant thermals rising from the ground, because of the small thickness of the unstable layer.

Double outlines sometimes are seen associated with mamma. Fallout precipitation creates negative buoyancy and generates a downdraft. The fallout tends to accumulate at the leading edge of the downdraft, because of the relative velocity of the downdraft and the environment. The "fallout front" may be visible as a second outline under the lower boundary of the cloud proper. The fallout front tends to spread as a negative thermal. Vorticity is generated as the front develops, and is enhanced by the greater density of fallout in the center of the front.



3. Cellular Convection

The best example of cellular convection is the sea fog. Warm air over a cold sea produces condensation of clouds in that air. The radiation surface is transferred from the sea to the cloud top which is a cold source radiating

into space and after 12-20 hrs downward convection is established. The sunlight will be absorbed by the sea, and the convection will be upside-down. Because the sea is becoming warmer than the cloud convection will begin. There will be upcurrents, but because there are no hot spots, the convection will tend to be slow. The air which has risen recently will tend to have a larger spectrum of drop sizes than that which is at the same height for a longer time, since the smaller drops will evaporate after awhile. The fog is continuous across the coastline, but there will be no convection on land because the land is also cold. In such cases the transition from land to sea can be observed in a sharp change in the quality of cloud bows and glories when the drop size spectrum changes.

The depth of the layer of sea fog is the most important parameter in determining the cell size or the spacing between upcurrents. The cells generally tend to be half as wide as their height. If the cells are flat, shear stresses will be introduced which will reduce the motion. If they are too high, up-currents and down-currents will cause stress reducing the motion. In the balance between the buoyancy forces and the eddy stresses more or less the same cell shape seems to occur every time.

4. Streets

Much of the ocean is covered by large areas of cloud streets which are produced by the influence of one length scale on another. Convection takes place mostly in cold air masses moving toward the equator; hence there is subsidence and drying out of the air which provides a mechanism for the steady state evaporation of cumulus clouds. There will be some flow between the clouds through the cloud base since there is a heat flux. An extensive sub-cloud stable layer through which thermals rise has been found to be very common. The sinking of the clouds above the stable layer provides the mechanism for heat transfer.

Subsidence does not usually occur with cumulus clouds over land. If you have a sea breeze over land (i.e., if the air mass generating cumulus is on the whole going up and doesn't have the sub-cloud stable layer), the effect is of a sea breeze from the plains toward the mountains. There are two ways of propagating things through the atmosphere. There are fast moving sound waves (usually called acoustic gravity waves) which will not produce horizontal density gradients, and there are slow moving gravity waves which provide a means for advecting mass. Sound waves move the whole atmosphere in a compression wave, but there is no lifting of the air mass. Hence the sea breeze must be propagated by gravity waves, and the time scale is such that the sea breeze is not important in the center of the United States.

The sub-cloud layer over the ocean is very important because it is always there. An air mass subsiding must have some mechanism to get through the layer at some place. The sub-cloud layer produces buoyancy and thermal-like circulation develops. Condensation generates more buoyancy and thermals get sucked through the layer at some places over the ocean. The mechanism can continue to work only if the thermals going through the layer line themselves up with the wind shear. Enough heat must be transferred going through the layer to preserve the steady state. The spacing of the streets is possibly determined by how much heat must be fed into the stable layer to maintain a steady state. Different areas of the stable layer may require different amounts of heat input to retain equilibrium, and this could be a mechanism which leads to the non-constant spacing of cloud streets.

REFERENCE:

Scorer, R. S., 1958: "The Dynamics of Mamma", Science Progress No. 181, Jan. 1958, p.75.

Notes taken by:

R. M. McGehee

J. M. Miller